Mathematical Modelling of Active Packaging Systems for Horticultural Products

A thesis presented in partial fulfilment of the requirements for the degree of
Doctor of Philosophy in Packaging Technology
at Massey University, New Zealand

Weerawate Utto
2008

ABSTRACT

Active packaging systems can offer significant advantages in preventing quality loss in horticultural products through control of microbial and/or physiological activity. By delivering and sustaining volatile active agents at effective levels in a package atmosphere, significant shelf life extension can thus be achieved. Design of these systems is complicated by the number of possible package, product, active agent and carrier combinations that can be employed and the significant interactions that may occur between these components. Mathematical modelling can be used to simplify system design and reduce the number of experimental trials required to achieve optimal active packaging systems. In this study a generalised modelling methodology was developed and validated to facilitate the design of active controlled volatile release packaging systems for horticultural products.

The modelling methodology was developed using an example system which comprised tomatoes packed under a modified atmosphere (MA; 5 % (v/v) CO_2 and 10 % (v/v) O_2) in a LDPE bag with a polymer film sealed sachet containing silica gel pre-saturated with the antifungal agent hexanal. Experimental trials showed that for this system a target sustained hexanal concentration of 40-70 ppm was required. This was shown to be (i) the minimum inhibitory concentration (MIC) for controlling *Botrytis cinerea* growing on tomatoes stored at 20°C and ~99%RH, (ii) to have only a relatively minor influence on the postharvest quality of tomatoes under these active MA conditions, and (iii) to promote only a small apparent uptake of hexanal from the atmosphere by the tomatoes.

The effective hexanal permeabilities of Tyvek®, LDPE and OPP sachet films were characterised using the isostatic method and shown to exhibit a dependence on both temperature (10 and 20°C) and concentration (over a range of 0.01-0.22 $mol \cdot m^{-3}$). Average permeabilities decreased in the order of Tyvek® > LDPE > OPP, respectively, at all temperatures at comparable hexanal partial pressures.

Hexanal sorption isotherms for silica gel at both 10 and 20ºC were determined using the gravimetric method and were reasonably well described by the Langmuir equation. The equilibrium amount adsorbed was significantly reduced at the higher temperature but the

pre-adsorption of water vapour on hexanal uptake on silica gel showed no uniform trend on the sorption characteristics suggesting that multicomponent sorption is complex.

A generalised modelling methodology was developed through conceptualising key mass transfer processes involved in these active MA packaging systems. Quantitative methods for deciding the relative importance of each process were established together with guidelines for when simplifying assumptions could be made. This information was formalised into a decision tree to allow appropriate assumptions to be made in model formulation without unacceptable loss of model accuracy. Methods to develop generalised equations from these assumptions to describe changes in the sachet, package headspace and outer bag film with respect to an active agent and MA gases were then identified.

The mathematical modelling methodology was applied to the example hexanal release active MAP tomato packaging system. For these systems there was a high initial peak in package headspace concentration during the first 24 h which declined to a quasi steady-state concentration over a period of days. The quasi steady-state headspace concentrations were generally in the MIC range and were well predicted by the model. Interactions between water vapour and silica gel may have been responsible for the relatively higher hexanal concentration at the onset of release from the Tyvek® sachet (a highly porous material). However the influence of water vapour (>95% RH in the MA bag containing tomatoes) during the quasi steady-state period appeared to be insignificant for all sachet films.

The model was successfully applied to a range of packaging configurations and storage temperatures. A lack of fit was evident between model predictions and experimental trials during the initial (unsteady-state) stages of the release pattern for both headspace vapour concentrations and adsorbed mass on the silica gel. These differences were attributed to (i) model input uncertainties, chiefly with regard to the estimated coefficients of both the Langmuir isotherm equation and film permeability, and (ii) overestimated effective permeability values predicted by extrapolation of the concentration dependence of film permeability beyond the conditions for which the permeability was measured. These results suggest improved models for the effective permeabilities of the films, quantified under a range of vapour concentrations and concentration gradients, are required for better describing fluxes across the sachet film.

Despite these limitations, the model did describe the general release pattern. The model was then used to pose a range of '*what-if*' scenarios investigating the release patterns predicted for different active packaging designs. This analysis gave useful insights into how sorption isotherm shape and package/sachet design parameters can be manipulated to achieve different volatile release platforms.

The work clearly demonstrated the importance of accurate data for permeability of volatile compounds through polymer films and for sorption of the active agent on the carrier phase. More work on characterising these systems is recommended to further improve model-based design methods for active MAP systems.

Overall the generalised methodology developed can be confidently adopted for constructing a mathematical model that provides sufficient accuracy and simplicity to be implemented for designing active packaging systems for horticultural and food products.

ACKNOWLEDGEMENTS

I wish to express my appreciation to the following who supported me and were involved in this thesis:

Associate Professor John Mawson (Chief), Associate Professor John Bronlund, and Dr. Ken Wong, for your supervison, inspiring wisdom, professional attitudes, solid confidences and allocating the financial support for experimental work on active packaging technology as part of contract no. CO4X0401 from the Foundation for Research Science & Technology (FRST), which assisted greatly in completion of this project.

Lex Dillon and Peter Wilson, NZ Hothouse Ltd. (Auckland, New Zealand) for supplying fresh tomatoes and commercial information necessary for experimental planning and for other discussions. Also staff at MG Palmerston North Ltd. for their assistance in transporting and stocking tomatoes.

Sue Nicholson, Peter Jeffery, Byron McKillop, John Edwards, John Syke, Ann-Marie Jackson, John Pedley and Garry Radford for assistance and guidance in making and/or maintaining experimental equipment. Dr. Lian-Heng Cheah (Crop and Food Research Ltd., Palmerston North , New Zealand), Dr. Narumol Matan (Walailuk University, Na Khorn Sri Thammarat, Thailand) and Jon Palmer for guidance and assistance in microbiological work. Dr. Bruce Mackay for his professional skill in statistics, and discussing statistical analyses. Yvonne Parkes, and Dianne Reilly for administrative details throughout the study.

Postgraduates at Fresh Technologies, IFNHH, Massey University, including Andrew Nevins, Usha Gaddam, Pittiporn Ounsuvan, Thammarat Pranamornkit, Jantana Suntudprom, Rattanawan Jansasithorn, and in particular Wattana Pongjaruwat, for discussing and challenging knowledge and details of postharvest and packaging technologies. Former Fresh Technologies associates including Dr. David Tanner, Mr. Tom Robertson, Dr. Maarten Hertog, Dr. Henry Sabarez, and Dr. Kate Maguire for inspiring me to studying further at the doctorate level.

Ms. Gabrielle J. Eustace (or ‘mum Gay’ my host kiwi mother; 7 Moerangi St. Palmerston North) for providing food, shelter, love and care for me and my family.Your kindness and patience are also so wonderful. Thai friends (especially Duljira, Angkana, Chanapa, Wattana, Suppanikar and Piyawan) for being kind, caring and helpful and endorsing greatness of friendship.

Professor Ian and Mrs. Blondie Warrington for love, care and assistance for all study needs and family settlement, and particularly Blondie for providing invaluable and tireless midwifery care.

The Royal Thai government for proving a full doctoral scholarship. The Faculty of Agriculture, Ubon Ratachathani University for official grant support for me to be successful as a scholarship recipient and to complete this study.

Finally, I would like to thank my wife (Grittaya) for your understanding and supports on contributions required for this project and your exceptionally good motherhood in looking after and raising our beloved daughter (Norakamol). Thanks also for my family (both the Uttos and the Chaisiwamongkols) for their support and encouragement.

Weerawate Utto **September, 2008**

Table of contents

LIST OF NOMENCLATURES

A_{film} = Film area (m^2)

A_{scfl} = Sachet film surface area (m^2)

A_{pkfl} = Packaging film surface area (m^2)

A_{fr} = Fruit surface area (m^2)

a_{exp}^{Hxl} = Coefficient of the hexanal exponential isotherm equation ($g \cdot g^{-1}$)

A_{GC}^{i} = Area of gas chromatogram peak from the injected volume of sample (area)

b_{Lgm}^{i} = Langmuir constant ($m^3 \cdot mol^{-1}$)

b_{film} = Fitted exponential coefficient of effective permeability to hexanal of the film ($m^3 \cdot mol^{-1}$)

b_{Tyvek}, b_{LDPE}, b_{OPP} = Fitted exponential coefficient of effective permeability to hexanal of Tyvek®, LDPE and OPP films, respectively ($m^3 \cdot mol^{-1}$)

$b_{Lgm,10^\circ C}^{Hxl}$, $b_{Lgm,20^\circ C}^{Hxl}$ = Langmuir coefficients at 10 and 20ºC (dimensionless), respectively

Bi = Biot number for mass transfer (dimensionless)

b_{scfl} = Fitted exponential model coefficient of effective permeability to hexanal vapour of sachet film material ($m^3 \cdot mol^{-1}$)

b_{Lgm}^{Hxl} = Langmuir constant of hexanal sorption ($m^3 \cdot mol^{-1}$)

b_{pkfl} = Fitted exponential model coefficient for effective permeability to hexanal vapour of packaging film material ($m^3 \cdot mol^{-1}$)

b_{exp}^{Hxl} = Coefficient of the hexanal exponential isotherm equation (dimensionless)

$C_{gas\ phase}$ = Equilibrium concentration in gas phase ($mol \cdot m^{-3}$)

C_{film}^{i} = Concentration of the diffusant *i* in film ($mol \cdot m^{-3}$)

ΔC_{film}^{i} = Concentration difference of diffusant *i* between the two sides of the film ($mol \cdot m^{-3}$)

C_{g}^{i} = Equilibrium vapour concentration (or pressure) of adsorbate *i* with adsorbents (gas phase, $mol \cdot m^{-3}$)

C_s^i = Equilibrium adsorbed amount of adsorbate *i* on adsorbents (solid phase, mol·g^{-1})

$C_{s,max}^i$ = Maximum adsorbed amount of adsorbate *i* on adsorbent estimated by Langmuir sorption isotherm (mol·g^{-1})

C_{inlet}^{Hxl} = Inlet hexanal concentration (mol·m^{-3})

C_{outlet}^{Hxl} = Outlet hexanal concentration (mol·m^{-3})

$C_{h,conc}^{Hxl}$, $C_{l,conc}^{Hxl}$ = Hexanal concentration at the high and low concentration side of the film, respectively (mol·m^{-3})

C_{avg}^{Hxl} = Effective mean of hexanal concentrations measured in both chambers of the permeability cell at steady-state (mol·m^{-3})

$C_{g,x\,film}^{Hxl}$ = Hexanal concentration in the gas phase which is equilibrium with film at position *x* in film material (x_{film}) (mol·m^{-3})

$C_{paper\ phase}$ = Equilibrium concentration in paper phase (mol·g^{-1})

$C_{scfl,0}^i$ = Concentration of active agent *i* in sachet film at x = 0, facing the carrier bed (mol·m^{-3})

$C_{scfl,L_{scfl}}^i$ = Concentration of active agent *i* in the sachet film at x = L_{scfl}, facing the package headspace (mol·m^{-3})

$C_{pkfl,0}^i$ = Concentration of active agent *i* in the film at x = 0, facing the package headspace (mol·m^{-3})

$C_{pkfl,L_{pkfl}}^i$ = Concentration of active agent *i* in the film at x = L_{pkfl}, facing the surrounding environment (mol·m^{-3})

$C_{fr,ext}^{O_2}$, $C_{fr,int}^{O_2}$ = Concentration of gas O_2 in external and internal fruit, respectively (mol·m^{-3})

$C_{fr}^{SO_2}$ = Concentration of SO_2 dissolved in fruit (mol·m^{-3})

$C_{fr,e}^{SO_2}$ = Equilibrium concentration representing the maximum SO_2 concentration attained in the corn (mol·m^{-3})

$C_{fr,air}^i$ = Concentration of active agent *i* surrounding fruit (mol·m^{-3})

C_{pkhs}^i = Concentration of active agent *i* in package headspace (mol·m^{-3})

$C_{g,bed}^{Hxl}$ = Equilibrium hexanal vapour concentration above the carrier bed (mol·m^{-3})

C_{pkhs}^{Hxl} = Hexanal vapour concentration in the package headspace (mol·m^{-3})

C_{sat}^{Hxl} = Saturated hexanal vapour concentration at a given temperature (mol·m^{-3})

$C_{s,bed}^{Hxl}$ = Equilibrium adsorbed amount of hexanal on the carrier bed (mol·g^{-1})

$C_{s,max}^{Hxl}$ = Maximum amount of hexanal adsorbed on the carrier estimated by the Langmuir sorption isotherm (mol·g^{-1})

C_{env}^{Hxl} = Hexanal concentration in the bulk environment surrounding the outer bag (mol·m^{-3})

$C_{g,1}^{Hxl}$, $C_{g,J+1}^{Hxl}$ = Equilibrium hexanal vapour concentration in the packaging film, at the discrete nodes $j = 1$ and $j = J + 1$, respectively (mol·m^{-3})

$C_{g,j}^{Hxl}$ = Equilibrium hexanal vapour concentration in the packaging film at discrete node $j = 2 : J$ (mol·m^{-3})

$C_{s,bed,i}^{Hxl}$ = Initial hexanal adsorbed amount of the carrier bed (mol·g^{-1})

C^{i} = Concentration of VOC *i* (mol·m^{-3})

C_{scfl}^{Hxl} = Hexanal concentration in sachet film (mol·m^{-3})

$C_{g,x_{scfl}}^{Hxl}$ = Hexanal concentration in gas phase which is in equilibrium with the sachet film material at a position *x* (x_{scfl}) (mol·m^{-3})

C_{pkhs}^{i} = Concentration of active agent *i* in package headspace (mol·m^{-3})

C_{scfl}^{i} = Concentration of active agent *i* in sachet film (mol·m^{-3})

$C_{g,bed}^{i}$ = Equilibrium concentration of active agent *i* above the carrier bed (mol·m^{-3})

$C_{s,bed}^{i}$ = Equilibrium adsorbed amount of active agent *i* on the carrier bed (mol·g^{-1})

$C_{s,bed,ini}^{i}$ = Initial value of equilibrium adsorbed amount of active agent *i* on the carrier bed (mol·g^{-1})

$C_{pkhs,ini}^{i}$ = Initial value of concentration of active agent *i* in package headspace (mol·m^{-3})

C_{pkfl}^{i} = Concentration of active agent *i* in packaging film (mol·m^{-3})

$C_{pkfl,0}^{i}$ = Concentration of active agent *i* in packaging film at $x_{pkfl} = 0$

$C^{i}_{pkfl,L_{pkfl}}$ = Concentration of active agent *i* in packaging film at $x_{pkfl} = L_{pkfl}$

C^{i}_{env} = Concentration of active agent *i* in surrounding environment ($mol \cdot m^{-3}$)

C^{MCP}_{sat} = 1-MCP saturated vapour concentration ($mol \cdot m^{-3}$)

C^{MCP}_{scfl} = 1-MCP concentration in sachet film ($mol \cdot m^{-3}$)

C^{MCP}_{pkfl} = 1-MCP concentration in packaging film ($mol \cdot m^{-3}$)

C^{MCP}_{env} = 1-MCP concentration in environment ($mol \cdot m^{-3}$)

$C^{Hxl}_{scfl,0}$ = Hexanal concentration in sachet film at position $x_{scfl} = 0$ ($mol \cdot m^{-3}$)

C^{Hxl}_{sat} = Saturated hexanal vapour concentration ($mol \cdot m^{-3}$) (i.e. 0.46 $mol \cdot m^{-3}$, at 20ºC)

$C^{Hxl}_{g,pkfl,ini}$ = Initial equilibrium concentration of hexanal vapour in packaging film ($mol \cdot m^{-3}$)

$C^{Hxl}_{g,pkfl,avg}$ = Mean equilibrium concentration of hexanal vapour in film ($mol \cdot m^{-3}$)

D = Mass diffusivity ($m^2 \cdot s^{-1}$)

D^{Hxl}_{scfl} = Hexanal mass diffusivity in the sachet film ($m^2 \cdot s^{-1}$)

d = Integration constant ($mol \cdot m^{-1} \cdot s^{-1}$)

D^{i}_{film} = Diffusivity of diffusant *i* in film ($m^2 \cdot s^{-1}$)

D^{i}_{scfl} = Mass diffusivity of active agent *i* in sachet film ($m^2 \cdot s^{-1}$)

D^{i}_{pkfl} = Mass diffusivity of active agent *i* in packaging film ($m^2 \cdot s^{-1}$)

$D^{SO_2}_{fr}$ = Effective mass diffusivity of SO_2 dissolved in fruit ($m^2 \cdot s^{-1}$)

D^{MCP}_{scfl} = Mass diffusivity of 1-MCP in sachet film ($m^2 \cdot s^{-1}$)

D^{MCP}_{pkfl} = Mass diffusivity of 1-MCP in packaging film ($m^2 \cdot s^{-1}$)

Ea = Energy of activation ($J \cdot mol^{-1}$)

F_0 = Fourier number (dimensionless)

ΔG° = Free energy ($J \cdot mol^{-1}$)

ΔH_s = Heat of solution for the permeant gas ($J \cdot mol^{-1}$)

ΔH° = Apparent enthalpy change ($J \cdot mol^{-1}$)

J_{film} = Steady-state flux across film ($mol \cdot s^{-1} \cdot m^{-2}$)

J^{i}_{film} = Steady-state diffusion flux of diffusant *i* in film ($mol \cdot m^{-2} \cdot s^{-1}$)

J_{scfl} = Steady-state flux at sachet boundary ($mol \cdot s^{-1} \cdot m^{-2}$)

K^{i}_{Lin} = Linear isotherm constant or partition coefficient of adsorbate *i* ($m^3 \cdot g^{-1}$)

K^{i}_{Frd} = Freundlich constant ($mol^{1-n_{Frd}} \cdot m^{3n_{Frd}} \cdot g^{-1}$)

$K_{paper/air}$ = Partition coefficient ($m^3 \cdot g^{-1}$)

$k^{Hxl}_{tom,reac}$ = Coefficient of reaction rate of hexanal and tomatoes ($\mu mol \cdot s^{-1} \cdot kg^{-1} \cdot (m^3 \cdot mol^{-1})^{n_{reac}}$)

k = Surface mass transfer coefficient ($m \cdot s^{-1}$)

K^{i}_{bed} = Coefficient of the linear desorption isotherm of active agent *i* for the carrier (adsorbent) bed ($m^3 \cdot g^{-1}$)

K^{MCP}_{bed} = Coefficient of linear sorption isotherm of 1-MCP for silica gel as reported by Lee (2003) ($m^3 \cdot g^{-1}$)

k^{O2}_{fr} = Fruit skin permeance to gas O_2 ($m \cdot s^{-1}$)

$k^{i}_{fr,reac}$ = Rate coefficient for the reaction of the active agent *i* and fruit ($mol \cdot s^{-1} \cdot kg^{-1} (m^3 \cdot mol^{-1})^{n_{reac}}$)

k_{mO_2} = Michaelis-Menten constant for O_2 consumption (kPa)

K^{Hxl}_{Lin} = Coefficient of the hexanal linear isotherm equation ($g \cdot g^{-1}$)

K^{i}_{GC} = Detector response or slope ($mol \cdot area^{-1}$) of standard curve of VOC *i* as shown in Figure C-1

$k^{Hxl}_{Lgmfl,1}$ = Coefficient of Langmuir relationship between hexanal vapour and LDPE film sorption ($m^3 \cdot mol^{-1}$)

$k^{Hxl}_{Lgmfl,2}$ = Coefficient of Langmuir relationship between hexanal vapour and LDPE film sorption (dimensionless)

k_{scfl} = Constant in simplified ODE (s^{-1})

L_{film} = Film thickness (m)

L_{scfl} = Sachet film material thickness (m)

L_{pkfl} = Packaging film material thickness (m)

L = Characteristic dimension of bag (m)

li = Log integral function

M_{tom} = Mass of tomatoes (kg)

M_{bed} = Mass of the carrier bed (free of the mass of active agent *i*) (g)

m = Term in series solution (given as 5 terms)

N^{i}_{film} = Steady-state rate of transfer of gas *i* across the film (mol·s^{-1})

n_{Frd} = Exponential factor ($0 < n_{Frd} < 1$) in Freundlich equation (dimensionless)

n_{reac} = Order of reaction rate (dimensionless)

N^{O2}_{fr} = Steady-state rate of transfer of gas O_2 across fruit skin (mol·s^{-1})

$n^{O_2}_{pkhs}$ = Number of oxygen moles in package headspace (mol)

$n^{CO_2}_{pkhs}$ = Number of carbon dioxide moles in package headspace (mol)

Δp^{i}_{film} = Partial pressure differential of gas *i* at both sides of film surfaces (Pa)

P^{i}_{film} = Permeability to permeant *i* of the film (mol·m·s^{-1}·m^{-2}·Pa^{-1})

$P^{i}_{film,0}$ = Fitted pre-exponential factor for permeability to permeant *i* of the film (mol·m·m^{-2}·s^{-1}·Pa^{-1})

P^{Hxl}_{film} = Effective film permeability to hexanal (mol·m·m^{-2}·s^{-1}·Pa^{-1})

$P^{Hxl}_{film,0}$ = Fitted pre-exponential factor for effective permeability to hexanal of the film (pmol·m·m^{-2}·s^{-1}·Pa^{-1})

$P^{Hxl}_{Tyvek,0}$, $P^{Hxl}_{LDPE,0}$, $P^{Hxl}_{OPP,0}$ = Fitted pre-exponential factor for effective permeability to hexanal of Tyvek®, LDPE and OPP films, respectively (pmol·m·m^{-2}·s^{-1}·Pa^{-1})

$P^{Hxl}_{scfl,0}$ = Pre-exponential factor of effective permeability to hexanal vapour of sachet film material (mol·m·m^{-2}·s^{-1}·Pa^{-1})

$P^{Hxl}_{pkfl,0}$ = Fitted pre-exponential factor for effective permeability to hexanal vapour of packaging film material (mol·m·m^{-2}·s^{-1}·Pa^{-1})

$P^{O_2}_{pkfl}$ = Film permeability to O_2 (mol·m·m^{-2}·s^{-1}·Pa^{-1})

$P^{CO_2}_{pkfl}$ = Film permeability to CO_2 (mol·m·m^{-2}·s^{-1}·Pa^{-1})

$p^{O_2}_{pkhs}$ = O_2 partial pressure in the package headspace (kPa)

$p^{O_2}_{env}$ = O_2 partial pressure in the bulk environment (kPa)

$p^{CO_2}_{env}$ = CO_2 partial pressure in the bulk environment (kPa)

$p^{CO_2}_{pkhs}$ = CO_2 partial pressure in the package headspace (kPa)

P^{i}_{scfl} = Permeability to active agent *i* of sachet film material (mol·m·m^{-2}·s^{-1}·Pa^{-1})

P^{i}_{pkfl} = Permeability to active agent *i* of packaging film material (mol·m·m^{-2}·s^{-1}·Pa^{-1})

P^{MCP}_{scfl} = Sachet film permeability to 1-MCP vapour (mol·m·m^{-2}·s^{-1}·Pa^{-1})

P^{MCP}_{pkfl} = Packaging film permeability to 1-MCP vapour (mol·m·m^{-2}·s^{-1}·Pa^{-1})

P^{Hxl}_{pkfl} = Permeability to hexanal vapour of the packaging film (m^{2}·s^{-1})

Q_{outlet} = Outgoing flowrate (m^{3}·s^{-1})

$Q^{out}_{l,conc}$ = Outlet gas flowrate from the low hexanal concentration side of the film (m^{3}·s^{-1})

R = Gas constant (8.314 J·mol^{-1}· K^{-1})

r^{Hxl}_{tom} = Apparent rates of uptakes of hexanal vapour by tomatoes (mol·s^{-1}·kg^{-1})

r_{scfl} = Rate of changes of active agent concentration in the sachet film (dimensionless)

r_{bed} = Rate of changes of active agent concentration in carrier bed (dimensionless)

r_{pkhs} = Rate of changes of active agent concentration in package headspace (dimensionless)

r_{pkfl} = Rate of changes of active agent concentration in the packaging film (dimensionless)

r^{SO2}_{fr} = Reaction rate of SO_2 and corn (mol·m^{-3}·s^{-1}) which Haros et al. (2005) assumed to follow first order kinetics

R_{fr} = Radius of fruit (assumed to be spherical) (m)

r^{i}_{fr} = Reaction rate of between active agent *i* and fruit (mol·s^{-1}·kg^{-1})

r^{i}_{pkhs} = Rate of accumulation of active agent *i* in package headspace (mol·s^{-1})

r^{Hxl}_{scfl} = Rate of hexanal permeation through the sachet film material (mol·s^{-1})

r^{Hxl}_{pkfl} = Rate of hexanal permeation through the packaging film material (mol·s^{-1})

r_{O_2} = Rate of O_2 consumption by respiration (mol·s^{-1}·kg^{-1})

$r^{max}_{O_2}$ = Maximum O_2 consumption rate (mol·kg^{-1}·s^{-1})

r_{CO_2} = Rate of respiratory CO_2 production (mol·s^{-1}·kg^{-1})

R_{pkfl} = Half thickness of film (m)

S^{i}_{film} = Solubility coefficient of gas *i* into film ($mol \cdot m^{-3} \cdot Pa^{-1}$)

$S^{i}_{film,0}$ = Fitted pre-exponential factor for solubility to permeant *i* of the film ($mol \cdot m^{-3} \cdot Pa^{-1}$)

ΔS° = Entropy ($J \cdot mol^{-1} \cdot K^{-1}$)

S^{i}_{scfl} = Sachet film solubility to active agent *i* ($mol \cdot m^{-3} \cdot Pa^{-1}$)

S^{MCP}_{scfl} = Sachet film solubility to1-MCP as reported by Lee (2003) ($mol \cdot m^{-3} \cdot Pa^{-1}$)

S^{i}_{pkfl} = Packaging film solubility to active agent *i* ($mol \cdot m^{-3} \cdot Pa^{-1}$)

S^{Hxl}_{scfl} = Sachet film solubility to hexanal ($mol \cdot m^{-3} \cdot Pa^{-1}$)

S^{MCP}_{scfl} = Sachet film solubility to 1-MCP ($mol \cdot m^{-3} \cdot Pa^{-1}$)

S^{MCP}_{pkfl} = Packaging film solubility to 1-MCP ($mol \cdot m^{-3} \cdot Pa^{-1}$)

S^{Hxl}_{pkfl} = Packaging film solubility to hexanal vapour ($mol \cdot m^{-3} \cdot Pa^{-1}$)

T_{film} = Measured film temperatures (K)

$T_{10^{\circ}C}$, $T_{20^{\circ}C}$ = Temperature (K) for 10 and 20ºC, respectively

T_{pkg} = Temperature of package (K)

t = Time (s)

V_{pkg} = Volume of package (m^3)

Vol_{inj} = Injected volume of sample (m^3)

x_{film} = Position in film (m)

x_{fr} = Position in fruit (m)

x_{pkfl} = Position in packaging film material (m)

x_{scfl} = Position in sachet film (m)

Y_{avg} = Fraction unaccomplished change of concentration (dimensionless)

Z^{Hxl}_{Lgmfl} = Fitted coefficient of Langmuir relationship for hexanal vapour sorption on LDPE film ($mol \cdot s^{-1} \cdot m^{-2}$)

LIST OF FIGURES

LIST OF TABLES

Chapter 1

INTRODUCTION

1.1 Background

The horticultural industry is very important to the New Zealand economy. Over recent years (2003-2007), exports of fresh (e.g. kiwifruit, pipfruit, asparagus, squash, onion and tomato) and processed (e.g. processed sweet corn, pea, carrot, and tomato) horticultural products increased in value from approximately $1.97 to 2.53 billion (MAF 2007). To maintain international markets and prices to sustain growers, the key focus of horticultural producers is to maintain and improve already high product quality (MAF 2007). Packaging is considered one key aspect of postharvest technology to both maintain quality and extend shelf life of horticultural products. This can be achieved through improved protection from environment conditions (e.g. light, oxygen, moisture, and contaminations) or enhancing cooling rates to minimise heat accumulation (Merts 1996; Tanner 1998), providing information through labels, and providing improved convenience (e.g. easy opening, and reclosable package) (Ahvenainen 2003). In recent years, packaging technology offers interactive management (e.g. real-time traceability) throughout the supply chain using radio frequency identification (RFID) and global positioning (GPS) tracking (Järvi-Kääriäinen 2003; Han et al. 2005).

Horticultural products, either intact or minimally processed (fresh-cut), are living tissues that continue their metabolic activities after harvest and during storage (Gil et al. 2002; Kader 2002; Lanciotti et al. 2004). Once the optimum storage temperature and relative humidity to minimise the rate of ripening and senescence are established (Thompson & Mitchell 2002), modification of the atmosphere surrounding the products is a common practice to further reduce postharvest quality changes and extend shelf life (Kader et al. 1989). However, optimal packaging atmospheres can be adversely affected by dynamic changes in temperature and relative humidity through the cool chain (Day 1989). This in turn may pose a significant risk to preservation of the product's quality because modified atmosphere packaging (MAP) relies on the interactions between the gas atmosphere, metabolic activity of the packaged produce and the properties of the packaging to achieve the desired outcomes (Zagory 1995).

For a given permeability of the packaging material, the packaged product adjusts its metabolic activity according to the concentrations of the main respiratory gases (CO_2 and O_2). If the metabolic activity increases, this will increase CO_2 production and lower O_2 availability (Kader et al. 1989). The respiration rate of horticultural products is more strongly affected by temperature than the permeability of most existing packaging films utilised in MAP. Thus even a small temperature increase can cause rapid accumulation of CO_2 and depletion of O_2 in the package (Cameron et al. 1995). Continuous decreases in the O_2 level can initiate anaerobic respiration or fermentation, which generally results in poor quality, such as off-flavour development and increased pathogenic susceptibility (Labuza & Breene 1989; Yam & Lee 1995).

To improve the efficacy of MAP, active packaging technologies have been incorporated to provide alternative interactive controls between the packaged food, package, packaging atmosphere and the environmental conditions to better achieve and retain optimal modified atmospheric conditions inside the package (Rooney 1995b; Brody 2002). In the context of horticultural products, "active" may refer to systems for control of environmental parameters such as moisture content or gas atmosphere composition, to the control of microbial growth, or the control of the physiology of the product. According to Rooney (1995b), this is mainly achieved by scavenging mechanisms, which remove one or more components from the internal environment, or desorption mechanisms, which allow the controlled release of one or more active components.

Whilst the scavenging systems are commercially available, desorption systems are less well studied and yet offer interesting possibilities for extending shelf life and quality of perishable product (Utto et al. 2005). Although a number of the desorption-based active packaging systems have been commercialised (for example sachet releasing ethanol vapour commercially sold under the trade names of Antimold Mild® and Negamold® Freund Industrial Co., Japan), generic approaches to design and optimise packages are mainly empirical or rely on proprietary information from companies.

Fundamental knowledge needed to better implement their new technology relating to packaging design of desorption-based active packaging systems is valuable. To maximise application of this knowledge it should be incorporated into a framework that would permit engineers and/or technical users to predict outcomes of a new package design for '*what-if*'

scenarios for given products in typical horticultural postharvest handling systems. To simulate and understand '*what-if*' scenarios relevant to specific new package designs, one may perform many experiments by "trial and error" testing. However this approach has the disadvantages of being costly in experimental development and time consuming, and it is difficult to transfer results obtained from one product-package-storage system to others. Alternatively, the development of predictive tools based on mathematical models, in which the key variables relevant to the new package as well as the handling system can be specified or estimated, will allow new packaging systems to be designed and screened prior to prototype testing. Development of such predictive tools will formalise the understanding of the underlying phenomena occurring in these systems, and in so doing will contribute significantly to food packaging research.

At the start of this project, the fundamental knowledge needed to construct mathematical models for the design of the such active packaging systems, were limited in availability and scope, and this research to fill these knowledge and technical gaps was justified.

1.2 Research aim

The aim of this research project was to formalise the fundamental knowledge of desorption controlled release active packaging in the form of mathematical models. These models will allow the design of systems that can dynamically deliver and sustain one or more active components at effective levels in a package atmosphere, incorporating the postharvest responses of the product and the storage conditions.

1.3 Research objectives

To achieve the research aim, the following specific objectives were set as the research milestones:

(1) To develop a conceptual model which accommodates all relevant aspect(s) of the design of active packaging systems, where the active agents can be delivered and sustained at the required level to regulate quality changes through influencing product physiology and inhibiting growth of spoilage or pathogenic microorganisms, or a combination of both.

(2) For a representative specific application (i.e. a given horticultural product and active control system), to:

(a) Develop a model active packaging system for experimental investigation of the postharvest behaviour of the selected product

(b) Determine the effective concentrations of the chosen active agent and their effects on postharvest attributes of the selected horticultural products, including microbial suppression, respiration rate and ethylene production under simulated storage condition.

(c) Identify the equilibrium and kinetic mechanisms which govern the sorption of the active agent by, and its release from, the chosen carrier material, and how key packaging and environmental factors affect the equilibrium concentration through storage.

(d) Mathematically model and experimentally validate (including assessing the limitations of the model) the distribution of the active agent within the model active packaging system, under a known storage condition.

(3) To use the developed modelling tools to investigate *what-if* scenarios to gain further insights into release patterns of the active agent for different active packaging systems.

(4) Summarise model methodology and associated input data requirements for design of packaging systems for other food and horticultural products

1.4 Structure of thesis

In Chapter 2, a review of relevant literature is presented, covering the current trends and opportunities in the development of the active packaging systems with an emphasis on horticultural products, and the basic physical phenomena from which mathematical models of active packaging system will be developed.

In Chapter 3, the active MAP system of interest, a hexanal controlled release sachet for tomatoes was experimentally studied. Effects of hexanal vapour on postharvest qualities of tomatoes such as antimicrobial activity, rates of respiratory O_2 consumption and ethylene generation, and apparent rates of hexanal uptake by tomatoes were studied.

Chapter 4 presents studies of the effective hexanal permeability of films (used as sachet materials and outer bag) and sorption isotherms for hexanal on silica gel.

Chapter 5 presents the conceptual model developed for active MAP systems. A decision tree for facilitating the selection among modelling options was also developed and utilised for modelling the hexanal-based active MAP for tomatoes. The formulations of mathematical model and its MATLAB® language codes to predict dynamic hexanal concentration in the package headspace are presented.

Chapter 6 presents results of model validations against experimentally collected data of a range of active MAP systems and discusses the model performance through sensitivity analyses considering uncertainties associated with model inputs.

Chapter 7 subsequently presents applications of the mathematical model to predict '*what-if*' scenarios of hexanal releases which were not experimentally measured and to be utilised as means to understand key mass transfer processes involving in the simulated scenarios.

Lastly, Chapter 8 presents the general discussion on the findings from the present work along with recommendations for future work to provide further insights for better understanding and optimisation of active packaging systems for horticultural products.

Chapter 2

LITERATURE REVIEW

2.1 Introduction

This review is presented in two sections. The first summarises the principles of, and recent technological advances in, active packaging systems applied to horticultural products. The second section reviews the development of mathematical models for the design of such active packaging systems.

2.2 Overview of active packaging technologies for horticultural products[1]

2.2.1 Active packaging requirements for horticultural products

Packaging can be designed to supplement other postharvest control technologies (chiefly the management of temperature and relative humidity) to maintain product quality and extend the storage shelf life (Thompson & Mitchell 2002). One widely used approach is to modify the normal atmosphere surrounding the packaged product by selectively adding or removing gaseous species. This is known as modified atmosphere packaging (MAP) and its key objective is to reduce the availability of O_2 and increase CO_2 levels to retard the respiration and related metabolic changes of fresh produce. Applications of MAP for postharvest storage of selected fresh fruits and vegetables, and the optimum levels of O_2 and CO_2 for these, are well documented (Kader et al. 1989; Thompson & Mitchell 2002; Kader & Saltveit 2003a).

In spite of it being widely commercialised, there is much evidence to show that MAP alone is unlikely to be completely effective for controlling changes in postharvest quality, particularly when these are in response to temperature and relative humidity fluctuations in the storage environment. To overcome this problem, consideration has been given to active packaging systems, which have successfully been utilised with meat, fishery and bakery products (Day 1989), to actively control the desired modified atmosphere composition with

[1] This is a summary of the comprehensive review published as Utto W, Mawson A J, Bronlund J E, & Wong K K Y (2005). Active packaging technologies for horticultural produce. *Food New Zealand* **5** 21-32. (see Appendix A)

packages of food products and/or introduce further hurdles to deterioration. One example is a system for enriching ethanol vapour in the package headspace to inhibit microorganism growth on bakery products (Smith et al. 1995). Examples of application of active packaging with an emphasis on postharvest practice are discussed in the following sections.

2.2.2 Oxygen-scavengers

Near-ambient concentration of oxygen (O_2) in the atmosphere can markedly reduce the shelf life and marketability of horticultural products (Kader & Saltveit 2003a). The use of a scavenger for absorbing part of the residual O_2 in sealed packages and the O_2 that continuously permeates through the packaging material from the external environment could potentially improve MAP of some fruit. O_2-scavengers are principally based on metallic iron powder contained within sachets and are commercially available under trade names such as Ageless® (Mitsubishi Gas Chemical Co., Ltd. Japan) and Freshilizer® (Toppan Printing, Co., Ltd. Japan). These have been used to maintain the quality and shelf life of several horticultural commodities (Hurme et al. 2002) including sliced carrots (Pospisil et al. 2001), tomato (Charles et al. 2003) and endive (Charles et al. 2005; Charles et al. 2008). However, O_2-scavengers could potentially lower the O_2 concentration inside the package to a level at which anaerobic respiration or fermentation is initiated. This will result in rapid loss of stored product quality, commonly evidenced through a loss of texture and the development of off flavours (Yearsley et al. 1996). In addition, anaerobic pathogens and spoilage organisms may thrive (Labuza & Breene 1989). This example demonstrates how a balance between O_2 transport, O_2 scavenging and O_2 consumption by the fruit must be designed into the active packaging system to achieve an optimal outcome.

2.2.3 Carbon dioxide-scavengers or emitters, and dual-active systems

Carbon dioxide (CO_2) is formed inside many food packages owing to the metabolism of the product and that of microbial contaminants. Although increasing the CO_2 level around some commodities reduces respiration, delays senescence and retards fungal growth, excessively high CO_2 levels may induce fermentative metabolism or cause physiological disorders (Kader & Saltveit 2003a). For example, whilst CO_2 enriched atmospheres (at partial pressures higher than 20 kPa) reduced the incidence of *Botrytis cinerea* on "Redglobe" table grapes, they also accelerated stem browning (Crisosto et al. 2002). Thus

both CO_2-scavengers (e.g. Ageless® E, and Fresh Lock®, Mitsubishi, Japan; also functioning as O_2 scavengers) and CO_2-emitters (e.g. Ageless® G and Vitalon® GMA, Mitsubishi, Japan; also functioning as O_2 scavenger) could be beneficial to shelf life extension for fresh fruit and vegetables, depending on the situation (Smith et al. 1995; Vermeiren et al. 2003). The so-called dual-action active packaging systems consist of either an O_2-scavenger plus a CO_2-scavenger or an O_2-scavenger and a CO_2-emitter. In one specific application of the latter, the O_2-scavenger was designed to release roughly the same amount of CO_2 as that of scavenged O_2. Iron-based powder and ascorbic acid were used as the O_2-scavenger and CO_2-emitter, respectively, however technical information such as the nature of the interaction of scavenged O_2 and ascorbic acid to release CO_2 was not published (Harima 1990). Calcium-based materials such as calcium hydroxide ($Ca(OH)_2$) are commonly utilised together with iron-based powder to scavenge both CO_2 and O_2, respectively (Smith et al. 1995). For CO_2-scavenging purposes, the use of soda lime, magnesium oxide and activated charcoal has been documented for pears (Ning et al. 1997), mushroom (Jayathunge & Illeperuma 2001), mangoes (Illeperuma & Jayasuriya 2002) and endives (Charles et al. 2005). The favoured approaches for incorporating these ingredients into an active packaging system are coatings on the packaging material surface or the inclusion of the active material in sachets.

2.2.4 Atmospheric control via temperature compensating films

One main disadvantage of conventional plastic films (e.g. low density polyethylene (LDPE)) commonly used in the horticultural industry is the mismatch between gas evolution or uptake by metabolism and gas exchange with the environment by permeation (Mannapperuma & Singh 1994; Kader & Saltveit 2003a). As respiration and fermentation rates of horticultural products are more strongly affected by temperature than is the permeability of most existing packaging films, even a small temperature increase can cause rapid accumulation of CO_2 and depletion of O_2 in the package. Research to overcome this problem has therefore focused on developing new classes of polymer films with activation energies of permeation more closely matching activation energies for respiration in order to maintain a suitable gas composition inside the modified atmosphere package (Yam & Lee 1995). Probably the most widely known temperature-responsive package materials are those using Landec's Intellipac™ membrane technology. Permeabilities to gases (chiefly O_2 and CO_2) of this polymer film are increased by structural rearrangement as the

temperature surrounding the packaged products is increased above a pre-determined temperature. By such alterations the rapid accumulation of CO_2 and depletion of O_2 in the package caused by high respiration rate in response to elevated temperatures can therefore be minimised (Clarke 2001; Paul & Clarke 2002).

2.2.5 Water vapour regulators

Accumulation of water inside packages can occur owing to continuous transpiration from and respiration of the product, and drip loss from cut tissues, as well as by condensation arising from temperature fluctuations when the equilibrium relative humidity is high. Excessive moisture may increase the risk of microbial decay since high humidity and/or the presences of droplets favour the growth of spoilage organisms (Wills et al. 1989). Adsorbent pads, for example Toppan Sheet™, (Toppan Printing Co.Ltd, Japan), Fresh-R-Pax™ (Maxwell Chase Inc., GA, USA) and DriMop® (Multisorb Technologies Inc., USA), are used commercially for products such as sliced tomato or melon, and for frozen strawberries or similar products, where drip losses on thawing detracts from market appeal (Rooney 1995a; Brody et al. 2001b). Anti-fogging films have also been utilised to cosmetically minimise the presence of droplets on the inside surface of film bags, though this does not change the amount of liquid water in the package (Rooney 1995a). Another approach to scavenging excess moisture in food packages is to intercept the moisture in the vapour phase, reducing the relative humidity in the headspace and thereby the surface-water content and water activity (a_w) of the food. This can be done by incorporating humectants (e.g. sorbitol, xylitol, sodium chloride) or desiccants (e.g. silica gel) in the packaging system within either a sachet or the film (Labuza & Breene 1989; Shirazi & Cameron 1992).

Although the reduction of excessive moisture in the package atmosphere can delay deterioration of fresh fruits and vegetables, excessively low relative humidity will cause high water loss from the commodity. Thus, a package that is able to (i) take up water vapour when the temperature drops and the relative humidity rises, and (ii) release water vapour back into the package headspace in response to low relative humidity levels, like the active fibreboard carton developed by Patterson & Joyce (1993), could be beneficial for products exposed to fluctuating conditions during storage and handling.

2.2.6 Ethylene regulators

Although many of the effects of ethylene on plants are economically positive, such as de-greening of citrus and ripening of bananas, ethylene can be detrimental to quality and marketability, in particular by stimulating postharvest softening (Zagory 1995) for a range of products such as apple (Johnston et al. 2002), plum (Menniti et al. 2004), kiwifruit (Kim et al. 2001) and avocado (Jeong et al. 2002). Active packaging systems for ethylene control can be designed for ethylene-removal and ethylene-antagonism.

The active ethylene-removal systems generally employ oxidising agents such as $KMnO_4$, titanium dioxide catalyst, or dicarboxyoctyl ester of tetrazine which are captured on adsorbent materials such as activated carbon, silica gel, alumina, and zeolite (Zagory 1995). As the surrounding ethylene is adsorbed by the adsorbent, the oxidising agents chemically oxidised the ethylene to ethylene glycol (Brody et al. 2001a) or acetaldehyde, which is further oxidised to CO_2 and water through the intermediate oxidation of acetic acid (Vermeiren et al. 2003). These active systems are currently used in sachet form, which can conveniently be placed inside the product package (Brody et al. 2001a; Day 2003; Vermeiren et al. 2003; Choehom et al. 2004). In addition, ethylene removal active systems have been developed in the form of films into which oxidising-agent adsorbents (as discussed above) or adsorbents with an affinity for ethylene such as activated carbon and zeolites, are impregnated. Trade names of ethylene scavenging films include ‘Profresh’ (E-I-A Warenhandels GmbH, Austria), BO film (Odja Shoji C., Japan), and ‘PEAKfresh’ (PEAKfresh Products Ltd., Australia) (Zagory 1995; Brody et al. 2001a; Day 2003; Vermeiren et al. 2003).

Recently Terry (2007) reported the higher ethylene scavenging capacity of a palladium (Pd)-based material (Pd-impregnated zeolite with a Pd loading of 2.5% (m/m) [*sic*]), compared to the capacities of a well-known commercial ethylene scavenger, Ethysorb® ($KMnO_4$-impregnated alumina; 5% m/m [*sic*]; Stay Fresh Ltd, London, UK). The Pd-based material advantageously maintained its scavenging capacity under a high humidity condition (tested at ~100% RH), at which the capacity of the Ethysorb® become rapidly diminished due to the water-stimulated conversion of $KMnO_4$ to manganese oxide (this being visually observed through the colour change of the scavenger from purple to brown). Terry (2007) incorporated the Pd-based materials (in a loose configuration) in containers of pre-climacteric bananas, avocadoes, and strawberries, and reported that ethylene was

effectively removed while each product's postharvest quality (i.e. skin colour and firmness) was reasonably well maintained. The ethylene removal rates appeared to depend on the amounts of the scavenging materials added. Abe & Watada (1991) utilised a Pd-chloride impregnated activated carbon to effectively remove ethylene and reduce the rate of softening of minimally processed kiwifruits and banana, and for decreasing chlorophyll loss in lightly processed spinach leaves (at 20ºC for 3 days). However its performance relative to other scavengers was not reported.

For ethylene-antagonism based control, active agents such as 1-methylcyclopropene (1-MCP) (Blankenship & Dole 2003), nitric oxide (NO) or nitrous oxide (N_2O) (Leshem & Wills 1998) have been utilised. These gases are believed to bind to ethylene receptors, thereby minimising and/or blocking subsequent binding of ethylene. This slows or delays most of ethylene accelerated metabolic processes and reduces the incidence of physiological disorders associated with ethylene (Leshem & Wills 1998; Blankenship & Dole 2003). Among these ethylene antagonists, only 1-MCP is used commercially. It is currently marketed as SmartFresh^{TM} by AgroFresh Inc. for use on fruits, vegetables and flowers such as apple, kiwifruit, avocado, tomato and roses (Blankenship & Dole 2003). There have been recent several research reports on the controlled release of 1-MCP from carriers including porous materials (Daly & Kourelis 2001; Kostansek 2003; Lee 2003; Lee et al. 2006) and polymeric films (Macnish et al. 2004; Hotchkiss et al. 2007).

2.2.7 Antimicrobial packaging

Horticultural products are rich in moisture and nutrients and can therefore serve as suitable substrates for the development of microorganisms that may be agents of foodborne illness or cause spoilage. Fresh produce may rapidly become rotten and unfit for sale and this ubiquitous problem can be encountered during harvest or postharvest operations. Active packaging is one of several approaches, which include chemical treatment, heat treatment, the use of biological antagonists and ionising radiation, that have been implemented for controlling decay and pathogen proliferation in fresh horticultural products such as strawberries, apples (Conway & Sams 1983; Conway et al. 1999; Sholberg et al. 2000; Conway et al. 2005), bell pepper (Miller et al. 1984), soy bean (Lee et al. 1998), lettuce (Moore et al. 2007), broccoli (Suzuki et al. 2004), table grapes (Kou et al. 2007), and pineapple (Wijeratnam et al. 2005).

In recent times there has been increasing public concern about the carcinogenic risks posed by several kinds of synthetic fungicide (e.g. captan and benomyl) in agricultural products and the environment (Wisniewski & Wilson 1992; Utama et al. 2002). This has stimulated increasing interest in the possible use of natural substances such as chitosan, plant extracts, essential oils and plant aroma volatiles as antimicrobial agents (Lanciotti et al. 2004; Tripathi & Dubey 2004). Natural plant aroma volatiles such as hexanal, tran-2-hexenal, ethanol, and 2-nonanone have all shown promise owing to their effective antimicrobial activities (Wilson & Wisniewski 1989), their GRAS (generally recognised as safe) status, and their degree of volatility (Mari & Guizzardi 1998). Volatility is particularly important for active packaging systems designed to promote controlled release and/or fumigation during storage and transport of food products. Among plant aroma volatiles, ethanol has been extensively used to reduce microbial decay of a range of horticultural products including table grapes (Chervin et al. 2005; Lurie et al. 2006; Romanazzi et al. 2007), fresh-cut mangoes (Plotto et al. 2006), and Chinese bayberry (Zhang et al. 2007). Applications of ethanol are increasingly reported among grapes for replacing SO_2 (as an antimicrobial agent) to avoid fruit skin bleaching. Controlled release systems emitting ethanol vapour have been commercialised through several brand names (e.g. Ethicap® and Antimold 102®; Freund Industrial Co., Ltd. Smith et al. 1995) and these are also widely used in active packaging systems for food products as diverse as bakery products (Smith et al. 1987; Daifas et al. 2000; Franke et al. 2002; Daifas et al. 2003) and broccoli (Suzuki et al. 2004).

There is also increasing research into the utilisation of other volatiles, especially aldehydes, esters and ketones such as hexanal, trans-2-hexenal, hexylacetate, nonanal and 2-nonanone, to control postharvest pathogens such as *Botrytis cinerea*, *Pencillium expansum*, and *Pichia subpelliculosa*. Products tested included raspberry (Vaughn et al. 1993), strawberry and blackberry (Archbold et al. 1997), grape (Archbold et al. 1997; Archbold et al. 1999), and apple (Song et al. 1996; Wolford 1998; Lanciotti et al. 1999; Corbo et al. 2000; Song et al. 2007). However exposure of the product to these volatile compounds has commonly been limited to fumigation scenarios and there is limited evidence of the development of active controlled release systems.

Active agents derived from plant essential oils, for example eugenol, cinnamaldehyde and thymol which are the key antimicrobial compounds in clove oil, cinnamon oil, and oregano and thymol, respectively (Davidson 2001) have also been increasingly studied and utilised in active packaging systems for horticultural products. These components have reasonable volatility (Burt 2004; Ayala-Zavala et al. 2008) and have been trialled with products such as tamarillo (Pongjaruwat 2007), sweet cherries (Serrano et al. 2005), table grapes (Valverde et al. 2005), tomatoes (Matan 2008), and Swiss chard leaves (Ponce et al. 2004). Extensive research on the applications of antimicrobial essential oils has also been reported in other food products such as bakery products (Matan et al. 2006), pasteurised milk (Gaysinsky et al. 2007), and apple juice (Friedman et al. 2004). Similarly to the plant aroma volatiles, the development of controlled release systems for these essential oil vapours are limited and generally the carriers are filter papers and/or gauzes saturated with the oil. Recently Pongjaruwat (2007) utilised polymeric film sachets containing clove-oil saturated silica gel adsorbents as the carrier to delivery eugenol vapour to the package headspace for delaying de-greening of tamarillo stems. However in this use, the active agent appeared to promote decolourisation of the skin. Thus both the positive effects on mould growth and possible detrimental effects on other quality attributes must be carefully studied and controlled to achieve the desired outcomes.

2.2.8 Other interesting trends and developments

There is a recent trend of research to investigate the synergistic effects of combinations of active agents on postharvest qualities. For example, fumigations using a mixture of 1-MCP and hexanal vapour was beneficial in delaying ethylene-induced softening and to minimise *B. cinerea* decay of the stem ends of pears during long term cold temperature storage (at -1°C for 2 to 8 months) (Spotts et al. 2007). Similarly the use of calcium chloride dip (1% w/v chlorinated water) and controlled atmosphere storage (3% O_2 and 10% CO_2) with 1-MCP treatment delayed changes of fresh-cut strawberries (firmness, skin colour, sensory perception and microbial growth), during 12 days storage period at 5°C (Aguayo et al. 2006).

Incorporation of phase change materials (PCMs) in food packaging systems has also been evaluated for providing thermal buffering to delay temperature changes of packaged horticultural product and the package headspace composition. This research has chiefly

focused on these short periods of temperature increase that may occur during shipping, especially for air transport. The PCM employed in this regard must be a material having an appropriate latent heat property by which heat energy can be stored or released. Examples of PCM are paraffin wax and butyl stearate and their latent heats are reportedly ~160-190 $J \cdot g^{-1}$ (Johnston et al. 2008), and ~123-200 $J \cdot g^{-1}$ (Feldman et al. 1986), respectively.

Recently Johnston (2008) reported the development of a PCM composite material comprising (i) a paraffin wax-based PCM commercially sold under the trade name of Rubitherm RT6 (Rubitherm Technologies GmbH, Berlin Germany), and (ii) a nano-structured calcium silicate (NCS; this is a porous and very high surface area carrier developed by Johnston et al. 2006). Those were incorporated into 'Post-It' bubble polymeric wraps and used as liners in corrugated boxes containing asparagus. Plain wraps (those not containing the PCM) and box materials (corrugated board) were reported by Johnston (2008) as providing minimal effective insulation and thermal buffering capacity. Johnston (2008) reported that the temperature of asparagus packaged in the treatment containing the PCM was maintained at 10ºC for a further ~ 5 h prior to slowly reaching equilibrium with the storage temperature which had been sharply increased from 1-2ºC to 23ºC.

2.3 Modelling active modified atmosphere packaging (Active MAP) for horticultural products

The incorporation of active packaging components such as oxygen scavengers and ethanol vapour emitters within equilibrium (or passive) modified atmosphere packaging for horticultural products can be designated as 'active' MAP, following Charles et al. (2003). To date, while the modelling of passive MAP is well developed and reported elsewhere (see Cameron et al. 1989; Mannapperuma & Singh 1994; Cameron et al. 1995; Yam & Lee 1995; Merts 1996; Talasila & Cameron 1997; Charles et al. 2003; Charles et al. 2005), studies on modelling of active MAP are limited to those of Charles et al. (2003; 2005) in which the active systems utilised were oxygen and carbon dioxide scavengers. Charles et al. (2003; 2005) utilised the principle of mass balances (of either O_2 or CO_2) applied to the packaging film (for describing the permeation process), the packaged products (utilisation or production by respiration) and the scavengers (removal).

Although controlled release active MAP systems to deliver several active agents, for example 1-MCP (Daly & Kourelis 2001; Kostansek 2003; Lee 2003; Macnish et al. 2004; Lee et al. 2006; Hotchkiss et al. 2007), ethanol (Smith et al. 1987; Suzuki et al. 2004; Chervin et al. 2005; Lurie et al. 2006; Plotto et al. 2006; Zhang et al. 2007), sulphur dioxide (Ahvenainen 2003), eugenol (Pongjaruwat 2007), and chlorine dioxide (ClO_2) (Mahovic et al. 2007), have been developed and reported, the application of mathematical models to these active MAP systems have not been investigated or analysed

The concentrations of active agents in the package atmosphere may be predicted by using a similar approach to that employed by Charles et al. (2003; 2005) as summarised above. In certain cases, paper-based packaging materials such as corrugated boxes and trays are also components of the packaging systems and the interaction of active agents with these materials also needs to be taken into account.

A detailed knowledge of the relevant transport processes is therefore essential to develop mathematical models, and includes understanding of:

1. Sorption equilibrium (relationships) between the active agent and the carrier (matrix) such as a porous adsorbent (Lee 2003; Lee et al. 2006; Mahovic et al. 2007; Pongjaruwat 2007), filter paper (Lurie et al. 2006; Plotto et al. 2006; Zhang et al. 2007), or polymeric film (Macnish et al. 2004; Hotchkiss et al. 2007). The adsorption equilibrium isotherm will influence the initial load of the agent on the carrier and so will affect the availability of the agent during the course of its release. Meanwhile, the desorption isotherm will affect the dynamics of the components release into the headspace during the storage.

2. Permeation through packaging film materials of the active agents from the carriers to the packaging headspace and from there into the surrounding environment. These processes have a major influence on the accumulation of active agent in the headspace (Song et al. 1996). The required understanding in this aspect may also extend to paper-based packaging materials, when these are components of the packaging system of interest.

3. Interactions of the active agents with each horticultural product of interest. This interaction can contribute to (i) the rate of change of postharvest quality of the

product and (ii) changes of concentrations of the active agent in the package headspace.

General principles and examples of the key mass transport processes identified above are provided in the following review sections.

2.4 Sorption isotherms of active agents

Incorporation of the controlled release systems within the passive MA package can be achieved by several techniques including surface coating of packaging films or boards, impregnating them by blending or mixing into polymeric structures of films, and enclosing them on carriers within sachets (Rooney 1995a; Han 2003; Ozdemir & Floros 2004; De Jong et al. 2005; Utto et al. 2005). Table 2-1 summarises the relative advantages and disadvantages of these various techniques and their application depends on the packaging requirements of the particular product. For example the film surface coating or impregnation method is considered suitable for films that will be used to wrap individual items e.g. individually shrink-film wrapped papaya (Singh & Rao 2005) or avocado (Yahia & Gonzalez-Aguilar 1998). Also impregnation could be suitable when a product is presented on a tray covered with a plastic film such as fresh-cut tomatoes (Artés et al. 1999). Meanwhile sachets are considered convenient to insert into current packages containing multiple items as for example, adding sachets containing O_2 scavengers into passive MAP bags for tomatoes (Charles et al. 2003) and endives (Charles et al. 2008).

Table 2-1 Comparison of different controlled release active packaging configurations (modified from Rooney 1995a; Smith et al. 1995; Han 2000; Han 2003)

Systems	Advantages	Disadvantages
Sachet	• Simple to use as they are added to the packages along with the product • Sachet can be conveniently removed from packages and discarded at the end of the storage period • Low probability that the packaging material properties will be compromised, especially physical/mechanical properties	• Consumer concerns about sachets inside the packages and possible consumer misuse of sachets, leading to concerns of 'fear of ingestion', 'spillage of sachet contents into food and adulteration of the food product', and of the 'foreign component' in the package
Adding to packaging material[1]	• Reduced risk of inadvertent ingestion, and/or misuse of active agents by consumers • No risk the sachet material spillage into packaged food • Reduction of packaging components • Minimising consumers' attitudes toward the 'foreign component' of the sachet in the package • Functionality improvement and giving new or extra functions to packaging materials e.g. oxygen scavenging, ethylene absorbing	• The addition of active ingredients to films may decrease their physical/mechanical properties, resulting in a higher failure rate during transportation, which may lead to safety and contamination concerns • Non-food grade immobilised substances may chemically detach from their fixed position and diffuse into packaged food

[1] Including spraying/coating, chemical immobilisation and blending or mixing into the polymeric structures of the films

Sachets have been extensively used in active MAP to contain carriers which are pre-equilibrated with active agents (Table 2-2). The carriers commonly are porous adsorbents such as silica gel and zeolites due to their high specific surface areas which ensures sufficient amounts of agents are available to be delivered within the desired timeframe (Lee 2003; Lee et al. 2006; Mahovic et al. 2007; Pongjaruwat 2007). As these are the most generic form of controlled release system and can be easily used with existing packaging formats, all future discussion will focus on the use of such porous adsorbents.

It is important to understand how the loading of active agents on such carriers varies under different storage conditions, especially with respect to temperature and RH. It is also necessary to characterise how the adsorbed amount then influences its release rate driven by concentration gradient differences across the active controlled release system, the package and the immediate environment.

Table 2-2 A summary of active MAP systems that can release active agents into the package headspace and their reported application for horticultural products

Active systems			Horticultural products	References
Active agent	**Carrier**	**Configurations**		
1-MCP	Silica gel	Sachet	Tomato	Lee (2003)
Ethanol	Proprietary silica gel	Sachet [a]	Broccoli	Suzuki et al. (2004)
2-nonanone	Modified cornstarch	Sachet	Raspberry, strawberry	Vaughn et al. (1993)
Eugenol	Silica gel	Sachet	Tamarillo	Pongjaruwat (2007)
Eugenol, Thymol, Menthol and Eucalyptol	Sterilised gauzes [b]	Loose	Sweet cherry	Serrano et al. (2005)
SO_2	Proprietary silica gel	Pad [c]	Grape	Mustonen (1992)
Hexanal	Paper	Wet paper pad	Sliced apple	Corbo et al. (2000)
Chlorine dioxide	Zeolite	Sachet	Tomato	Mahovic et al. (2007)

[a] Sold under the trade name Antimold Mild® (Freund Industrial Co., Ltd., Japan)

[b] Similar to those are used for first aid purposes; one agent for one gauze

[c] Sold under trade names such as UVAGAS SO_2 pad (Grapetek (Pty) Ltd., Epping, South Africa)

Sorption isotherms relate the composition of the solid phase to the equilibrium gaseous concentration surrounding the solid (Do 1998b), thus providing a method of estimating the equilibrium loading of active agent on a spcified carrier for a given temperature. The generic sorption isotherm function is given by Eq. 2-1.

$$C_s^i = f\left(C_g^i\right) \qquad \textbf{(Eq. 2-1)}$$

where

C_s^i = Equilibrium adsorbed amount of adsorbate *i* on adsorbents (solid phase, $mol \cdot g^{-1}$)

C_g^i = Equilibrium vapour concentration (or pressure) of adsorbate *i* with adsorbents (gas phase, $mol \cdot m^{-3}$)

There are several types of sorption isotherms each with a characteristic curve (Adamson 1990) such as those shown in Figure 2-1. The type of isotherm depends on the natures of both the adsorbate and adsorbent. For example, whilst moisture sorption isotherms of many

biological materials, including food products and paper-based materials, are often reported to follow the sigmoid shape (the Type II isotherm as shown in Figure 2-1; also see Blahovec 2004), those of silica gel adsorbents (Type 3A and RD, Fuji Silysia Chemical Ltd., Japan) are most commonly found to be linear (Ng et al. 2001). Furthermore, although similar types of adsorbents (e.g. activated carbon, BPL, Pittsburg Chemical Co. USA) were used, different isotherm shapes were observed for different adsorbates. N_2 adsorption yielded a linear shape for the nitrogen adsorption but a Type I shape (Figure 2-1) was observed for carbon dioxide (Valenzuela 1989).

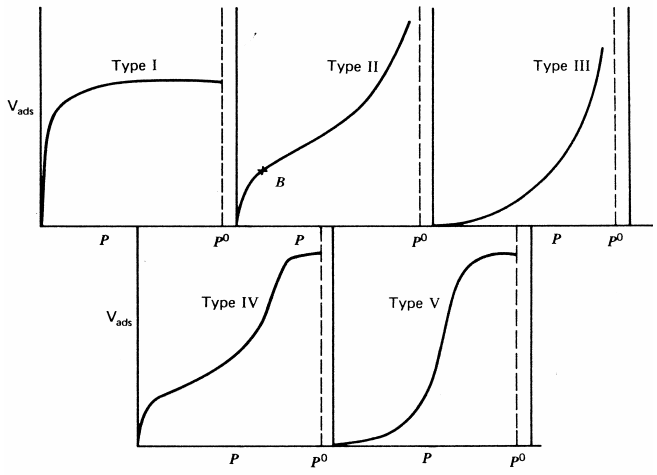

Figure 2-1 Brunauer's five types of adsorption isotherm of which V_{ads}, p, p^0 and B representing sorption extents (volume), pressure, saturated pressure, and a knee of the curve indicating a completion of a monolayer (reprinted from Adamson 1990)

Whilst isotherm data of many compounds such as ethanol and sulphur dioxide are available in the separation science literature for a range of adsorbents (see e.g. Valenzuela 1989 and Do 1998b), sorption isotherm data appropriate to other active packaging systems is relatively limited. With respect to the active release packaging systems for horticultural products, at present only sorption isotherms for 1-MCP and silica gel[2] are available. These were reported by Lee (2003), with the data collected in the pressure range of 0.1-0.8 Pa, and a temperature range of 50-80ºC (Figure 2-2).

[2] Other adsorbents tested were Tenax-TA and activated clay. However their adsorptive capacities were less than those of silica gel (Lee 2003).

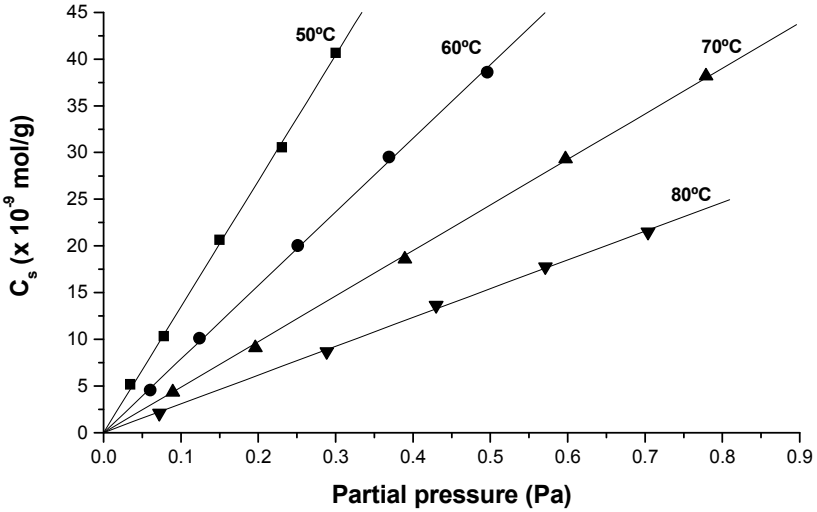

Figure 2-2 Adsorption isotherm of 1-MCP on silica gel at 50, 60, 70, and 80°C (digitally redrawn[3] from Lee 2003); lines representing the Linear adsorption isotherm model (Eq. 2-2).

1-MCP sorption isotherm for silica gel adsorbents (Lee 2003) fitted the linear isotherm model very well (Figure 2-2; Eq. 2-2). This model is referred to as Henry's law for gas adsorption and generally provides a good approximation only for systems operating at low concentration (Adamson 1990; Lee 2003).

$$C_s^i = K_{Lin}^i C_g^i \qquad \textbf{(Eq. 2-2)}$$

where

K_{Lin}^i = Linear isotherm constant or partition coefficient of adsorbate *i* ($m^3 \cdot g^{-1}$)

Given that silica gel adsorbents are important carriers in active MAP systems (refer to Table 2-2), the characteristics of sorption isotherms on silica gel of a range of compounds that could potentially be used as active agents are summarised in Table 2-3. Isotherms for N_2, CO_2, O_2 and water vapour are summarised in Valenzuela (1989).

[3] Using TechDig software (a Microsoft Windows tool for digitising data from a graphical image).

Table 2-3 Shapes and fitted equations of sorption isotherms for selected certain active agents for silica gel adsorbents [a]

Active agents	Postharvest applications [b]	Isotherm shape [c]	Fitted isotherm equations	Ref. no.[d]
Ethanol	Antimicrobial	Type I	Brunauer–Emmett–Teller (BET) for calculating monolayer coverage	[1]
SO_2	Antimicrobial	Type III	Freundlich and Dubinin-Radushkevitch-Kaganer (DRK)	[2]
Acetaldehyde	Antimicrobial	Type I	Langmuir, BET, Freundlich and the empirical model	[3]
N_2O [e]	Ethylene action inhibition	Type I	Langmuir	[4]
NO	Ethylene action inhibition	Type I	Nonlinear, not specified	[5]
Ethylene	Stimulations of quality changes e.g. de-greening	Type I	Toth and UNILAN	[6]

[a] Silica gel adsorbents were not similar among experiments. Experimental characterisation of these sorption isotherms were not purposely for applications of active packaging systems for either horticultural or other food products.

[b] Postharvest applications of active agents reported above were summarised in Utto et al. (2005), except acetaldehyde which is reported in the study of Almenar et al. (2006)

[c] referred to Figure 2-1. It should be noted that isotherm shapes of ethanol, nitric oxide and ethylene systems were similar to the Type I, however they did not reach a plateau over the concentration range tested.

[d] [1] Madeley & Sing (1959), [2] Kopac & Kocabas (2002), [3] Ghosh & Hines (1990), [4] Groen et al. (2002), [5] Solbakken & Reyerson (1959), and [6] Valenzuela (1989).

[e] Proprietary silicate-1 crystals as adsorbents

From Table 2-3, it is evident that there is a range of sorption isotherm equations available to be used for describing sorption equilibrium characteristics. These equations may be derived either theoretically (e.g. Langmuir, BET and DRK) or empirically (such as Freundlich, Toth and UNILAN) and are well documented in Adamson (1990), Tien (1994), and Do (1998b). The mathematical simplicity of the models, together with their adequacy and accuracy for expressing the data over the relevant range of concentrations and temperatures, are the main selection criteria for choosing between isotherm models (Weber 1985). The Langmuir (Eq. 2-3) and Freundlich (Eq. 2-4) models are frequently used due to their simplicity and having the ability to describe experimental results over wide concentration (or partial pressure) ranges (Geankoplis 1993a; Kopac & Kocabas 2002).

$$C_s^i = \frac{C_{s,max}^i b_{Lgm}^i C_g^i}{1 + b_{Lgm}^i C_g^i} \qquad \textbf{(Eq. 2-3)}$$

$$C_s^i = K_{Frd}^i \left(C_g^i\right)^{nFrd} \quad \textbf{(Eq. 2-4)}$$

where

$C_{s,max}^i$ = Maximum adsorbed amount of adsorbate *i* on adsorbent estimated by Langmuir sorption isotherm ($mol \cdot g^{-1}$)

b_{Lgm}^i = Langmuir constant ($m^3 \cdot mol^{-1}$)

K_{Frd}^i = Freundlich constant ($mol^{1-n_{Frd}} \cdot m^{3n_{Frd}} \cdot g^{-1}$)

n_{Frd} = Exponential factor ($0 < n_{Frd} < 1$) in Freundlich equation (dimensionless)

The Langmuir isotherm model was developed by assuming monolayer adsorption of the adsorbate onto a finite number of identical active sites on the adsorbent (Geankoplis 1993a). It is used to describe the Type I isotherm shape (Figure 2-1), typical of microporous adsorbents (with a pore diameter < 2nm) with adsorbates having molecular diameters slightly smaller than the adsorbent pore size (Gregg & Sing 1982). In contrast, the Freundlich isotherm model is an empirically derived isotherm for expressing sorption on heterogeneous surface adsorbents (Geankoplis 1993a) that offers benefits in describing a wider range of sorption systems (Weber 1985). The Freundlich model is often used to describe sorption on activated carbon adsorbents (Do 1998c, page 51).

In addition to the properties of adsorbates and adsorbents, environmental conditions can affect equilibrium sorption characteristics. Temperature and relative humidity are the key factors to consider for horticultural product storage and handling.

- **Storage temperature**

Elevated temperatures can either increase or lower the adsorption of adsorbates by adsorbents, depending on the thermodynamic properties of the system. For an exothermic system, the extent of adsorption becomes less as the temperature increases, while the converse applies for endothermic systems (Adamson 1990; Chen et al. 2007). Lee (2003) reported a lowering of 1-MCP uptake by silica gel as storage temperatures increased (see Figure 2-2).

- **Relative humidity**

Other compounds present in the gaseous phase may interact with either the adsorbate or adsorbent, or both, and may affect the equilibrium condition compared to the pure adsorbate-adsorbent system. Evidence shows that a high relative humidity can affect the

equilibrium condition by stimulating the release (desorption) of an active agent from the controlled release system. Such examples include ethanol-silica gel (Smith et al. 1995), and 1-MCP- silica gel or 1-MCP-cyclodextrin (Daly & Kourelis 2001; Kostansek 2003; Lee 2003). Weber (1985) warns that the effects of other components on the sorption isotherms of individual components may be inconclusive because the components of a mixture may (i) mutually enhance adsorption, (ii) act relatively independently, or (iii) interfere with one another. For example, Steffan & Akgerman (2001) reported noncompetitive adsorption on silica gel adsorbents (Davisil, grade 645, Aldrich Chemical Co., US) for binary adsorbate systems such as water/hexane and water/benzene because the water adsorbed onto polar sites whilst the nonpolar sites were preferred by the organic compounds.

2.5 Controlled release of active agents to the package atmosphere

Dynamic release of active agents from adsorbents occurs by desorption. Continuous uninhibited desorption might negatively affect the efficacy of the active MAP system if the active agent is rapidly depleted through its release into and transport out of the packaging system. Controlled release systems are therefore required to provide the required release pattern into the package headspace, such as ‘fumigation’ (release providing a high concentration for a limited period), ‘sustaining’ (maintaining the vapour concentration at an effective level for a required storage period), or a balance between these patterns when each might be appropriate at different times (e.g. initial release at a high concentration and then sustained release to maintain the lower concentration level). Following Han (2000), minimising the transfer of active agents from carriers using polymeric film materials is one of key approach utilised for such purposes. Examples include sachet systems or controlled release systems utilising chitosan, alginate, or soy protein films, and cyclodextrin (Han 2000).

Polymeric films are common sachet materials (Lee 2003; Mahovic et al. 2007; Pongjaruwat 2007) and the release of the active agent involves at least two mass transfer processes: (i) desorption of the agent from the adsorbent, and (ii) sorption into and diffusion through the controlling polymeric film structure (including transfer through associated boundary layers). Alternatively, carriers of the active agents and/or the active agents themselves may be directly incorporated into polymeric films. Release mechanisms

for these configurations, including desorption from the carriers into and diffusion within the film matrix, can be considered analogous to those identified above for the sachet configuration.

Knowledge and modelling principles of desorption processes and mass transfer within polymeric film will now be considered:

2.5.1 Desorption

Fundamentally the desorption process is a reversal of the adsorption process. According to Weber (1985), adsorption processes are complex and involve three main consecutive mass transport steps (Figure 2-3) including (i) bulk transport of adsorbate(s) in the fluid phase (or bulk solution), (ii) diffusion of adsorbate(s) through a boundary layer surrounding the adsorbent, and (iii) diffusion within the adsorbent to active adsorption sites (intraparticle transport). The relative importance of each step determines the sorption rate and is dependent on both the adsorbate's (e.g. chemical properties) and the adsorbent's (e.g. porosity or pore size distribution) properties.

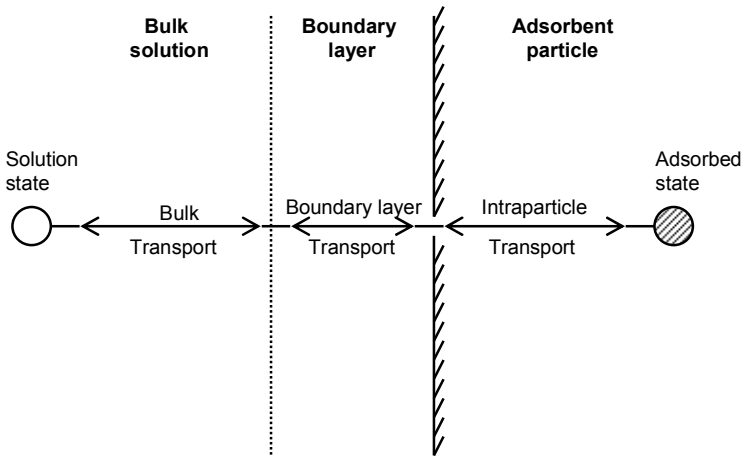

Figure 2-3 Mass transport steps during adsorption by a porous adsorbent (redrawn after Weber 1985)

Different mathematical models are cited in the separation science literature with varying degrees of complexity for describing the kinetics of sorption (and hence desorption) processes. The models can be generally classified into two groups according to the assumptions made regarding the importance of diffusion resistances within the porous adsorbents:

2.5.1.1 Models based on diffusion resistance

Models in this first group consider all diffusional resistances occurring during adsorption (as shown in Figure 2-3). For intraparticle diffusion, mass transport is modelled by considering one or a combination of pore-, surface- and Knudsen diffusion. The characteristics of each are summarised in Table 2-4. Principles and applications of these models are well documented (Geankoplis 1993b; Do 1998a; Johnson 1999; Mugge et al. 2001).

Table 2-4 Mechanisms and characteristics of intraparticle transport models (Geankoplis 1993b; Do 1998a; Johnson 1999; Mugge et al. 2001)

Mechanisms	Key characteristics
Pore diffusion	• Mean free path of molecules is small compared to the diameter of the pores • Molecule-molecule collisions mainly occur during diffusion through pores • Important intraparticle transport mode for large pore particles and at high pressures
Surface diffusion	• Diffusion of molecules along the pore wall surface in which adsorbates adsorb on the surface of the pore and migrate from one site to another through interactions between the surface and adsorbate molecules • Surface diffusion becomes important for porous particles with a relatively high surface area and at high concentrations of the adsorbate
Knudsen diffusion	• Mean free path of molecules is much larger than the pore diameters • Molecule-wall collisions occur mainly during diffusion through pores • Knudsen diffusion may be dominant for gaseous diffusion at low pressure or high temperature

Chu & Hashim (2002) suggested that although this group of models has been extensively used to describe the kinetics of sorption processes of several adsorbate-adsorbent systems, their application is limited to adsorbents having regular shapes (e.g. sphere, cylinder and slab). Implementing models for adsorbents having an irregular shape (e.g. sheet-like shape) may be mathematically cumbersome.

2.5.1.2 Models based on instantaneous mass transfer

For models in this second group, the mass transfer processes shown in Figure 2-3 are assumed to be instantaneous and an equilibrium exists between the surface and the fluid at each point inside the particle (McCabe et al. 2001). For example, Heirlings et al. (2004) assumed instantaneous equilibrium was attained between α-tocopherol in both the gas

phase and adsorbed phase on solid silica materials (α-tocopherol carriers impregnated in the film) during the release of α-tocopherol from LDPE film. However sorption isotherms of α-tocopherol in the silica materials were not reported. This second group of models are of lower complexity in comparison to the diffusional resistance type and their application is easily extended to irregularly shaped particles. However this group of models may be not suitable for systems in which kinetic processes are crucially dependent on pore mass transport, for example, some catalysis processes (Mills 1995a).

Several factors can affect the desorption process. The key factors and their effects are summarised as follows:

- **Adsorbate molecular weight**

Adsorbates with high molecular weight (MW) tend to diffuse more slowly within the adsorbent than those having lower MW. Thus, for example, methane (MW, 16 g/mol) diffuses within activated carbon adsorbents at a faster rate than carbon dioxide (MW, 44 g/mol): the gas phase diffusivities (at 20ºC) of methane and carbon dioxide are 6.98×10^{-7} and 1.26×10^{-7} $m^2 \cdot s^{-1}$, respectively (Prasetyo & Do 1998).

- **Affinity with adsorbents**

Adsorbates having stronger affinities with the adsorbent are less likely to desorb. Lee (2003) reported that desorption of 1-MCP from activated carbon adsorbents is essentially minimal. The activated carbons generally have high adsorptive capacity for organic compounds and high temperature or low pressure is technically employed to desorb the adsorbate. The further discussions on this aspect is provided by Do (1998b) and Thomas & Crittenden (1998b).

- **Storage environment**

As discussed earlier, the desorption process can be influenced by changes in storage temperature and relative humidity. The dependence of mass diffusivity on temperature is well known (e.g. see Geankoplis 1993b; Johnson 1999), while the effect of relative humidity is assumed to be due to the competition for active adsorption sites through displacement of adsorbed molecules by water vapour (Smith et al. 1987; Lee 2003). Ayala-Zavala et al. (2008) recently reviewed the potential of utilising the high relative humidity (up to 100%RH) developed in passive MA packages containing fresh-cut horticultural products as the trigger to release antimicrobial essential oils, 1-MCP and other volatile

compounds from microencapsulated cyclodextrin. However desorption caused by water vapour displacement might not occur in certain systems due to non-competitive adsorption of water vapour and other compounds on adsorbents (as discussed in section 2.4) or a strong affinity of the adsorbents for water vapour. Lee (2003) reported very low 1-MCP desorption from activated carbon adsorbents pre-saturated with 1-MCP even though the adsorbents were exposed to a high relative humidity condition (~90% RH).

2.5.2 Diffusion through mass transfer controlling polymeric film structures

Diffusion through non-perforated polymer film can be modelled using Fick's second law of diffusion (Eq. 2-5), simplified to a one-dimensional diffusion, where the local concentration within the film changes with time and position along the diffusion path in the film. Crank (1975) introduced various solutions for Eq. 2-5 with different dimensions for the diffusion matrix and boundary conditions.

$$\frac{\partial C^i_{film}}{\partial t} = D^i_{film} \frac{\partial^2 C^i_{film}}{\partial x^2_{film}} \qquad \textbf{(Eq. 2-5)}$$

where

C^i_{film} = Concentration of the diffusant *i* in film (mol·m^{-3})

D^i_{film} = Diffusivity of diffusant *i* in film (m^2·s^{-1})

x_{film} = Position in film (m)

Eq. 2-5 has been extensively used to model diffusion mass transfer within polymer film matrices into which active agents have been impregnated (mostly by direct mixing into the medium without using carriers). A summary of selected research work is provided in Table 2-5.

Table 2-5 Selected works using Fick's second law to model diffusion of active agents in polymeric materials, for controlled release applications.

Active systems [a]		Applications	Mass transfer processes	Ref. no.[b]
Agent	Matrix			
BHA, BHT	HDPE	Antioxidant film	Diffusion transfer of antioxidant from film surface to contacted oatmeal cereal	[1]
Potassium sorbate	LDPE	Antimicrobial film	Diffusion transfer of agent from film surface to contacted cheese	[2]
PEI	HDPE	Hexanal scavenging film	Hexanal vapour sorption into the aldehyde scavenger film and interaction with the agent	[3]
Lysozyme, nisin, sodium benzoate	PVOH	Antimicrobial film	Diffusion transfer of agents from film surface to contacted water	[4]
α-tocopherol, nisin	Paperboard	Antioxidant & antimicrobial material	Diffusion transfer of agents to contacted emulsion solution (a mixture of water, paraffin oil and polyoxyethylene-sorbitan)	[5]
UV stabiliser	PET	UV stabilised PET bottle	Diffusion transfer of UV stabiliser to contacted ethanol/water, isooctane and coconut oil	[6]
α-tocopherol	EVA, LDPE, and silica material	Antioxidant films	Diffusion transfer of antioxidant to contacted 95% ethanol solution	[7]
Thymol	Biodegradable zein film	Antimicrobial film	Diffusion transfer of thymol from film surface into contacted water	[8]

[a] BHA= Butylated hydroxyanisole, BHT= Butylated hydroxytoluene, HDPE = High Density Polyethylene, LDPE = Low Density Polyethylene, PEI= Polyethylene imine, PVOH = Polyvinyl Alcohol, PET = Polyethylene terephthalate, UV= ultra violet and EVA = Ethylene Vinyl acetate

[b] [1] Miltz et al. (1988), [2] Han & Floros (1998), [3] Del Nobile et al. (2002), [4] Buonocore et al. (2004), [5] Lee et al. (2004), [6] Begley et al. (2004), [7] Heirlings et al. (2004), and [8] Del Nobile et al. (2008)

At steady-state ($\partial C^{i}_{film} / \partial t = 0$), Fick's second law can be integrated to calculate the flux of diffusant across the film (Eq. 2-6). This is commonly known as Fick's first law and can be implemented to model steady-state mass transfer where there is an assumed linear relationship between diffusion flux and the concentration gradient between the two sides of the film (Robertson 1993c; Selke et al. 2004; Dury-Brun et al. 2007).

$$J^{i}_{film} = D^{i}_{film} \frac{\Delta C^{i}_{film}}{L_{film}} \quad \textbf{(Eq. 2-6)}$$

where

J^{i}_{film} = Steady-state diffusion flux of diffusant *i* in film (mol·m^{-2}·s^{-1})

L_{film} = Film thickness (m)

ΔC^{i}_{film} = Concentration difference of diffusant *i* between the two sides of the film (mol·m^{-3})

When the diffusant or permeant is a gaseous compound at sufficiently low concentrations, the concentration gradients due to concentration differences between two sides of the surface of the film can be linked to partial pressure gradients using Henry's law (similar to Eq. 2-2), by using the solubility coefficient (S^{i}_{film}) to represent the equilibrium uptake of the permeant by the packaging film (Robertson 1993c; Selke et al. 2004; Dury-Brun et al. 2007). The relationship between concentration and pressure gradient is then expressed in Eq. 2-7;

$$\Delta C^{i}_{film} = S^{i}_{film} \Delta p^{i}_{film} \quad \textbf{(Eq. 2-7)}$$

where

S^{i}_{film} = Solubility coefficient of gas *i* into film (mol·m^{-3}·Pa^{-1})

Δp^{i}_{film} = Partial pressure differential of gas *i* at both sides of film surfaces (Pa)

The generic form of steady-state gaseous permeation through a polymer film is shown in Eq. 2-8 and Eq. 2-9 as a result from combining Eq. 2-6 and Eq. 2-7. Eq. 2-9 demonstrates that the permeability is a product of diffusivity and solubility:

$$N^{i}_{film} = \frac{P^{i}_{film} A_{film} \Delta p^{i}_{film}}{L_{film}} \quad \textbf{(Eq. 2-8)}$$

where

$$P^{i}_{film} = D^{i}_{film} S^{i}_{film} \quad \textbf{(Eq. 2-9)}$$

where

N^{i}_{film} = Steady-state rate of transfer of gas *i* across the film (mol·s^{-1})

A_{film} = Film area (m^{2})

P^{i}_{film} = Permeability to permeant *i* of the film (mol·m·s^{-1}·m^{-2}·Pa^{-1})

Because of its explicit solution Eq. 2-8 has been extensively used in modelling steady-state gas permeation of O_2, CO_2, N_2 and water vapour in passive MAP systems (Merts 1996; Chen et al. 2000; Charles et al. 2003; Charles et al. 2005) and in modelling shelf life of food products, e.g. in predicting the profile of accumulation of moisture within dried food packages (Robertson 1993d; Selke et al. 2004). The permeabilities of polymeric films to individual gases (i.e. O_2, CO_2, and N_2) and VOCs can be found elsewhere including Pauly (1999) who extensively documented permeability values (as well as individual value of diffusivity and solubility) for a wide range of permeant-polymer film systems.

In most cases permeability is a constant for a polymer-permeant system at a given temperature and it is common to characterise the effect of temperature on P^{i}_{film} by Arrhenius or power law relationship. In addition to temperature, there are other factors that potentially affect permeability. These may be broadly categorised as (i) the nature of the polymer film including crystallinity, glass transition (T_g), and polymeric structural arrangement, (ii) concentration and molecular size of the permeant, and (iii) the storage environment (temperature and relative humidity). The effects of these factors have been well documented in literature (see Zobel 1982; Robertson 1993c; Piringer 2000; Selke et al. 2004), including the recent comprehensive reviews by Dury-Brun et al. (2007) and Sajilata et al. (2007) which consider the mass transfer of flavours and volatile organic compounds (VOCs) through food packaging polymer films. The effects of those factors on permeability of specific films in active packaging systems are further discussed in Chapter 4.

Song et al. (1996) studied LDPE film permeability to hexanal and hexylacetate vapour (as potential antimicrobial vapours for controlling *Penicillium expansum* and *Botrytis cinerea* inoculated on sliced apples) at 0 to 30ºC and reported their strong temperature dependence was well described by the Arrhenius relationship (Eq. 2-10).

$$P^{i}_{film} = P^{i}_{film,0}\, exp\left(\frac{-Ea}{RT_{film}}\right) \qquad \textbf{(Eq. 2-10)}$$

where:

$P^{i}_{film,0}$ = Fitted pre-exponential factor for permeability to permeant *i* of the film ($mol \cdot m \cdot m^{-2} \cdot s^{-1} \cdot Pa^{-1}$)

R = Gas constant (8.314 $J \cdot mol^{-1} \cdot K^{-1}$)

Ea = Energy of activation ($J \cdot mol^{-1}$)

T_{film} = Measured film temperatures (K)

The values of Ea for hexanal and hexylacetate were reported to be 44.6 and 23.6 $kJ \cdot mol^{-1}$, respectively, indicating that LDPE permeability to hexanal vapour is more sensitive to changes in temperature than is hexylacetate. Likewise, Wolford (1998) studied permeability to hexanal vapour of a metallocene-catalysed ethylene-hexene copolymer film (Exact^{TM} 4151) at 5 and 23ºC and reported a positive correlation between temperature and permeability. There is much literature providing information on the Arrhenius relationship for polymer films with respect to permeation by gases and vapours. For example Pauly (1999) reported LDPE permeabilities to various gases (including O_2, CO_2 and N_2) and organic vapours (e.g. acetaldehyde) across the temperature range from 0 to 74ºC.

The effects of relative humidity on permeability are relevant in active packaging systems where the polymer film will play a role in regulating the release of active agent. RH effects on film permeability depend firstly on whether the film is hydrophobic or hydrophilic in nature. Hydrophobic films such as LDPE and PP have a low affinity for water vapour, while the hydrophilic films, such as EVOH and PVOH, have a strong affinity for water vapour (Robertson 1993c; Selke et al. 2004). Lee (2003) and Lee et al. (2006) reported minimal effects of a high humidity level (90%RH) on 1-MCP release from pouches made with LDPE. In hydrophobic films, the polarity of the film may have to be taken into account when considering the effects of RH. Hydrophobic polar films, such as PET, could adsorb or interact with water vapour (another polar compound) and permeability can be affected by RH level of the surrounding environment (Nielsen et al. 1992; Sajilata et al. 2007). The permeability of hydrophilic films can be altered by water vapour and are likely to increase in high RH environments (DeLassus et al. 1988; Robertson 1993c). The utilisation of hydrophilic film materials as the controlled release layer may provide a benefit in enhancing the release of active agents in response to generation of high humidity conditions.

Several VOCs have potential to be utilised as active agents for antimicrobial control (Utto et al. 2005) and the effects of their concentration on film permeability must be taken into account in the design of active packaging systems. Film permeability to VOCs is generally concentration dependent due to the concentration dependence of both diffusivity and solubility, resulting from the plasticising action of the absorbed molecules. Plasticisation facilitates diffusion of the permeant through the polymeric structures by increasing the mobility of polymers and/or the void volume for diffusion (Zobel 1982; Robertson 1993c; Selke et al. 2004). Knowledge of the concentration dependence of VOC film permeability are extensively discussed elsewhere (Zobel 1982; Zobel 1985; DeLassus et al. 1988; Mulder 1991; Piringer 2000). However, studies of this aspect of active MAP systems for horticultural or food products are limited. In addition, DeLassus (1997) suggested that utilising VOCs with polymer film materials may require understanding the importance of the time taken to establish steady-state concentration gradients through the film. The diffusion of large molecules or those where there is a strong affinity of permeants for the polymer may slow the development of the concentration gradient and the achievement of steady-state. This delay period may even be longer than the anticipated shelf life of packaged products. The relatively slow permeation of the active agent through the polymer film layer could thus affect the level of active agent in the packaging system, such as vapour concentration in the headspace or on the outer film surface directly contacting the packaged product.

2.6 Permeation through packaging materials

2.6.1 Polymer film materials: non-perforated and perforated films

In practice, polymer films used in the horticultural industry are applied in several forms, such as bags, box liners, cling films, and pallet shrouding (Thompson & Mitchell 2002) and these can be either non-perforated or perforated. Generic approaches to modelling permeation in non-perforated packaging films were discussed in section 2.5.2.

Perforated film materials are increasingly being used as packaging for horticultural products because they provide improved gaseous permeability, particularly for oxygen thus better assuring aerobic conditions in the package (Utto 2001). A number of mathematical models are used to model mass transfer through perforated channels, where the continuous

section of the film material is assumed to be only a supportive structure for the pores and to contribute minimally to overall mass transfer (Renault et al. 1994b; Hernandez 1997; Del-Valle et al. 2004).

Several models were developed based on assumptions around the size of the pore (d) and the mean free-path of the gas molecules (λ) and the ratio of d/λ is adopted as a criterion for justifying the approach to model diffusion through the pore. Knudsen diffusion is used where d/λ <0.2, Fickian molecular diffusion is used for d/λ >20 and transitional flow for d/λ in the range of 0.2 to 20 (Hernandez 1997). Given 10^{-7}-10^{-9} m as a generic magnitude of λ (Hernandez 1997), Knudsen diffusion might be negligible in practice because pore diameters of perforated film used for horticultural products vary from 10μm (microperforation) to 17 mm (macroperforation) (Emond et al. 1991; Fishman et al. 1996; Utto 2001; Del-Valle et al. 2003; Del-Valle et al. 2004) and these typically yield d/λ values > 20. Hernandez (1997) suggested that Knudsen diffusion might become significant in regard to leakage from and integrity of packaging seals, where helium ($\lambda \approx 25\mu m$) is used as the leak detecting gas and the leaking pore diameter might be about 5μm or less.

Hernandez (1997) also observed that there might be a total pressure gradient along the diffusional path of the pore. In this case, the flow can be modelled by using Poiseuille's law rather than diffusive mass transfer. In practice, the steady-state diffusion mass transfer approach is mostly commonly used for modelling perforated film, in which the package atmosphere pressure is considered to remain equal to atmospheric pressure. This approach was utilised to model permeation of O_2, CO_2 and water vapour (Merts 1996; Del-Valle et al. 2003), and organic vapours such as methanol, ethanol, n-propanol, ethyl acetate and acetaldehyde (Del-Valle et al. 2004). In most cases model predictions were reported to agree with experimentally collected data, after adjusting the model by incorporating an empirical factor to minimise variations attributed to, for example diffusive path length (Fishman et al. 1996; Del-Valle et al. 2003; Del-Valle et al. 2004) and resistance of air to diffusion of gases (Merts 1996).

Renault et al. (1994a; 1994b) pointed out that applying Fick's law to model gas transport in air through perforations (as summarised above) may not be appropriate because its key assumptions are made with regard to permeation through the film, not the air. The Stephan-

Maxwell law, which well describes the relationships existing between fluxes and concentration gradients of gases in air, was used as an alternative modelling approach and its application was demonstrated for O_2 and CO_2 transport in a MAP system for strawberries enclosed by a microperforated film. The key assumptions of this approach were simultaneous gas diffusion and convection with negligible air resistance around the perforations. However, the model predictions only agreed with experimental data after incorporating an empirical factor to correct the reduction of diffusional area due to the resistance to gaseous diffusion in the pore volumes (Renault et al. 1994a; Renault et al. 1994b).

2.6.2 Paper-based packaging materials

In the horticultural industry, paper-based packaging materials are generally used in the format of boxes (either cardboard or corrugated) or moulded-pulp trays. Paper materials are reportedly a sink for VOCs (Triantafyllou et al. 2005), consequently knowledge of the sorption isotherms and/or partition coefficients between paper materials and specific VOCs is necessary for modelling VOC transfer to paper, and *vice versa*. The principles governing the sorption isotherm are the same as those discussed in section 2.4, where the partition coefficient ($K_{paper/air}$) Eq. 2-11 represents the partitioning of organic compounds between the paper sample and the gas atmosphere (Triantafyllou et al. 2005). It should be noted that the partition coefficient is similar to the K^i_{Lnr} of the linear isotherm (Eq. 2-2).

$$K_{paper/air} = \frac{C_{paper\ phase}}{C_{gas\ phase}} \qquad \textbf{(Eq. 2-11)}$$

where

$K_{paper/air}$ = Partition coefficient ($m^3 \cdot g^{-1}$)

$C_{paper\ phase}$ = Equilibrium concentration in paper phase ($mol \cdot g^{-1}$)

$C_{gas\ phase}$ = Equilibrium concentration in gas phase ($mol \cdot m^{-3}$)

Lee (2003) reported extremely low $K_{paper/air}$ values (≈0 [*sic*]) at 23°C for 1-MCP with filter paper, Tyvek®, and LDPE films utilised as sachet materials in a 1-MCP controlled release system. This indicated that 1-MCP effectively only resided in the gas phase and not in the solid phase.

Paper-based packaging materials can naturally release various VOCs (e.g. due to oxidative reactions of cellulose-based compounds) and the release of these into the package headspace may alter the sensory quality of packaged products (Wenzl & Lankmayr 2001). This suggests the importance of considering release of VOCs from paper materials (including sheet, cardboard or corrugated board) as a secondary 'source' for certain active agents and particularly hexanal, which is a common VOC released from paper materials (Wenzl & Lankmayr 2001).

As paper materials are porous and hydrophilic materials, moisture sorption is likely and will result in (i) increased water loss from fruit due to increasing water vapour gradients between fruit and air (Kays 1991), and (ii) reduced mechanical properties as the damp material will have inferior properties such as edge crush test strength or bending stiffness (Soroka 1995; Nevins et al. 2004; Parker et al. 2006). The equilibrium water vapour sorption of paper material can be modelled using sorption isotherms representing the equilibrium relationship between moisture content and water activity (a_w). Parker et al. (2006) extensively reviewed moisture sorption isotherms for paper and paperboard in food chain conditions (typically characterised by high relative humidities and low storage temperatures). Guggenheim-Anderson-de Boer (GAB) and the Brunauer-Emmett-Teller (BET) are the common moisture isotherm models and their application for modelling water vapour sorption in corrugated boxes and moulded pulp tray used with horticultural products are well documented (Eagleton & Marcondes 1994; Merts 1996; Tanner 1998).

2.7 Interactions of active agents and horticultural products

Active agents are designed to be delivered from the controlled release system and to interact with packaged horticultural products to achieve desired quality outcomes. Examples include 1-MCP release for inhibiting ethylene responsiveness of tomatoes (Lee 2003), eugenol for maintaining the colour of tamarillo stem (Pongjaruwat 2007) and sweet cherry (Serrano et al. 2005), SO_2 or ethanol for controlling grey mould in grapes (Mustonen 1992; Lurie et al. 2006), and ClO_2 for controlling bacterial soft rot in tomato (Mahovic et al. 2007). These interactions can however affect the activities or concentrations of active agents during the desired storage period. For example Hamilton-Kemp et al. (1996) reported metabolism of antimicrobial volatile compounds (hexanal, nonanal and hexylacetate) by strawberries which reduced their concentration in the

headspace. Nanthachai et al. (2007) recently reported 1-MCP absorption characteristics of several plants such as apple, cantaloupe, leaf lettuce and mango, where 1-MCP concentrations were exponentially reduced to different extents among the tested products. This literature highlights the importance of considering the product as a possible 'sink' for the active agents within the system.

The interactions of volatile active agent with fruit might be modelled as a gas exchange due to a concentration gradient across the skin between the internal and external atmospheres of fruit. Models based on Fick's first law (see Solomos 1987; Ben-Yehoshua & Cameron 1989) have been extensively used in this regard where, as summarised by Merts (1996), key assumptions are (i) a relatively small skin thickness compared to the radius of the organ, and (ii) the fruit internal atmosphere composition beneath the skin is considered uniform. However the assumption of uniform internal concentration may not be always accurate because metabolic consumption of O_2 may lead to an internal concentration gradient. Justifications for the assumptions therefore may be required. To do so, Merts (1996) utilised the dimensionless Biot number (Bi), which is the ratio of external to internal resistances to mass transfer across the fruit skin contributed by the surface (i.e. the effective skin permeance to O_2 and CO_2) and internal fruit properties (i.e. effective diffusivity of O_2 and CO_2 in flesh), respectively, to justify the uniformity of internal fruit concentration. Merts (1996) reported values of Bi were generally less than 0.1 where this value was suggested by Geankoplis (1993c) as a reasonable criteria to neglect (not significant if neglected) the internal mass transfer resistance.

In the same manner as modelling diffusion through film materials, Fick's second law modelling approach can be utilised where internal concentrations are likely to vary with time and position in the fruit. Several researchers have utilised this approach to model unsteady-state internal atmosphere concentrationsof , for example, O_2 and CO_2 in apple (Mannapperuma et al. 1991), sulfur dioxide in dent corns (Haros et al. 2005), and toluene and p-xylene in grapefruits (Gorna-Binkul et al. 2001). However the implementation of the unsteady-state modelling approach might be complicated in term of antimicrobial active agents because microorganisms could be an additional sink for these (Archbold et al. 1997; Corbo et al. 2000).

Alternatively, kinetic models based on n^{th}-order rates of chemical reaction could be utilised to model the interaction as a function of concentrations (and temperature). This approach is similar to those utilised to model quality changes of food products during either processing and storage (see Labuza 1982; Robertson 1993a; Earle & Earle 2003). An example of this approach is the study of Wolford (1998) of rates of hexanal consumption by sliced apples within the range of 0 to ~0.02 $mol \cdot m^{-3}$, at 5-23ºC. Compared to Fick's law modelling approaches, the use of a rate equation requires a smaller number of parameters or mass transfer coefficients and provides benefits where experimental equipment or procedures for measuring effective diffusivity within fruit flesh or the skin permeances have not been fully developed or verified.

In addition to understanding the removal of active agents through interactions with packaged products, the effects of active agents on key postharvest physiological processes (in particular respiration and ethylene production) and other quality attributes (such as colour and texture) are of importance. For example ethanol was reported to stimulate the respiration rates of tomato (Saltveit & Sharaf 1992) and potato (Rychter et al. 1979). Understanding changes in physiological properties and quality attributes in response to active agent exposure are essential as their consequences might alter the equilibrium gas compositions (especially of O_2 and CO_2) of passive MAP systems or cause loss of economic value. For example there are reports of skin discolouration of strawberries (Hamilton-Kemp et al. 1996) and sliced apples (Wolford 1998) under high concentrations of volatile compounds such as hexanal, hexylacetate and nonanal, and such exposures were reportedly phytotoxic.

2.8 Summary

This review provides an overview of active packaging systems with an emphasis on applications for horticultural products (so-called active MAP). There is a developing body of literature on active systems for delivering 1-MCP and antimicrobial plant volatiles. This is particularly true for the latter which may be more acceptable to many consumers in place of synthetic fungicides which potentially pose health risks and are viewed negatively. Extensive studies have been conducted to improve exposure and delivery techniques, chiefly for fumigation, (e.g. using mixtures of active agents to achieve additional effects), and for controlled release systems (e.g. utilising humidity or heat to trigger the release of

the active agent) for both groups of active compounds. The most technically advanced systems are those are for 1-MCP and ethanol release, however only the ethanol release systems have been commercialised.

There is very limited evidence of the use of mathematical models to generalise and design active MAP systems, even though principles of the modelling of passive MAP have been well developed and practically verified. The review has accordingly outlined principles and approaches for modelling the key mass transfer phenomena expected to occur in active MAP systems with an emphasis on controlled release systems for a volatile active agent. The implications for design of active MAP systems drawn from the review can be summarised:

1. Knowledge of interactions between the active agents (e.g. antimicrobial VOCs) and carriers (e.g. adsorbents) are required and these can be understood through characterising the sorption isotherms. Quantifying the effects of temperature and relative humidity on these isotherms will be important.

2. If polymeric films form part of the controlled release mechanism, film permeability to the active agents must be understood. Knowledge of effects of storage conditions (temperature and/or relative humidity) and concentrations of active agents on permeabilities is essential. Paper-based packaging materials may be sources of VOCs that are used as active agents due to natural release of VOCs from e.g. cellulose-based reactions.

3. The enclosed horticultural product may be a sink for the volatile compound agents and so may influence its the package headspace concentration; such interaction must therefore be modelled.

4. The active agent may affect the product's postharvest physiological response which may subsequently affect the overall MAP designs with regard to achievement of optimal O_2 and CO_2 levels for extending the product's shelf life. These effects must also be studied and quantified.

The following chapters present experimentally collected data with regard to the implications identified above, to allow development of mathematical models for design of active MAP system for horticultural products.

Chapter 3

THE EFFECTS OF ACTIVE AGENTS ON POSTHARVEST QUALITY: HEXANAL VAPOUR AND TOMATO MODEL SYSTEM

3.1 Introduction

Specific product-package systems are useful to demonstrate how appropriate conceptual models can be developed for active MAP systems. In Chapter 2, Table 2-2 summarised the common aspects of active MAP systems for horticultural products. These include (i) sachets containing active agents pre-adsorbed onto a carrier (for which silica gel adsorbents enclosed in polymer films have been commonly used), (ii) a plastic bag as the primary package enclosing the product and sachet, and (iii) an active agent which is delivered from the sachet into package headspace in such a way that its concentration is maintained at a targeted level for the duration of a pre-determined storage period. In the present work, hexanal vapour and fresh tomatoes were used as the example active MAP system to demonstrate all these aspects. The features of this system are summarised in Table 3-1.

Table 3-1 Description of working example MAP system: an Active MAP with a hexanal vapour controlled release sachet for tomatoes

Active MAP components	Description
Active agent	▪ Hexanal (antimicrobial agent) (97% G.C. grade, Sigma Chemical Co., USA)
Postharvest target	▪ *Botrytis cinerea* (a key postharvest pathogen)
Horticultural product	▪ Tomato (*Lycopersicon esculentum* Mill., cv. 'Royale')
Carrier particles	▪ Silica gel (6-12 mesh, Grade 40, Davison Chemical, Maryland, US.)
Sachet material	▪ Polymer film materials (e.g. LDPE, Oriented Polypropylene (OPP), Tyvek® and film thicknesses are 30, 20 and 173 μm, respectively)
Packaging material	▪ LDPE film material (30 μm film thickness; in heated sealed bag configuration)
Storage temperature	▪ 10 and 20°C ± 1ºC.

The application of hexanal vapour as an antimicrobial agent against a range of key postharvest pathogen such as *Botrytis cinerea*, *Monilinia fructicola*, *Alternaria alternata*, and *Colletotrichum gloeosporioides* has been tested either *in vitro* or *in vivo* for apples, strawberries, and grapes (Hamilton-Kemp et al. 1992; Song et al. 1996; Archbold et al. 1997; Archbold et al. 1999; Fan et al. 2006; Song et al. 2007). Fumigation for 6 - 48 h using hexanal ($C_6H_{12}O$) vapour has been demonstrated to successfully control growth of these postharvest pathogens (Song et al. 1996; Song et al. 2007). However there could be benefits in incorporating hexanal in active packaging systems within which spoilage control is achieved by the release of hexanal vapour at a low concentration over a long time. No studies on the effects of continuous exposure to hexanal vapour with regard to antifungal activity and postharvest physiology have been reported in the literature.

Tomato is a major horticultural product in New Zealand and worldwide. As tomatoes are available all year round in New Zealand, their use minimised experimental difficulties due to seasonal availability. Storage temperatures were controlled at 10 and 20ºC. The former represents the optimal temperature commonly utilised for long term tomato storage (Robinson et al. 1975), while the latter was selected to provide a challenging temperature for testing the *in vivo* antifungal activity of hexanal vapour and is typical of the temperature during uncontrolled (ambient) storage (*B. cinerea* is a key postharvest pathogen causing undesirable appearance and economic loss in the form of grey mould). To date there has been no information published on the antifungal effects of hexanal vapour on the pathogen-product model of *B. cinerea* and tomatoes.

The key objectives of work reported in this chapter were therefore: (1) to identify hexanal vapour concentrations that provide effective fungal control through continuous exposure; (2) to evaluate the inhibitory effects of these hexanal vapour concentrations when delivered in a single-dose system; (3) to quantify the effects of these hexanal concentrations on the physiology and quality parameters of tomatoes; and (4) to determine the rate of hexanal vapour uptake or conversion (if any) by tomatoes under ambient and modified atmosphere (MA) conditions. These factors characterise the requirements for design of active MAP systems.

The first three objectives provide insight into the antifungal activity and effects of hexanal vapours on postharvest attributes of tomatoes. The minimum inhibitory concentration (MIC) of hexanal to restrict growth of the model pathogen (*B. cinerea*) was then used as the targeted concentration level at which hexanal vapour released from the sachet into the package headspace was to be maintained and sustained throughout the desired storage period. Information on physiology and quality responses to continuous exposure to hexanal vapour is also important for packaging design and overall feasibility. For example, if the respiration rate changes due to hexanal exposure, this could modify equilibrium O_2 and CO_2 levels within the MA package. The last objective concerns packaging design, as hexanal concentration changes caused by packaged tomatoes is an important input to a mathematical model (developed in Chapter 6) that describes hexanal headspace dynamics.

In this chapter, two main sets of experiments are described. The first set was conducted to achieve objectives 1-3, while the second was designed for objective 4. It should be noted that a summary of the first set of experiments has been published in *Postharvest Biology and Technology*[4].

3.2 Antifungal activity of hexanal vapour and its effects on tomato physiology and quality

3.2.1 Materials and methods

Orange-red tomatoes (*Lycopersicon esculentum* Mill., cv. 'Royale'; hue angle (h°) = 50.9 ± 1.3) were harvested and delivered by NZ Hothouse Ltd. (Auckland, New Zealand) to Massey University, Palmerston North, New Zealand. Defect-free tomatoes of uniform size and colour were selected and equilibrated (20ºC, 24 h) before being randomly assigned to different experimental treatments. A split plot design with two replications was utilised, with types of air inside the exposure chambers (either hexanal-laden or hexanal-free) as main plots and storage times as subplots. Four consecutive experiments were performed during 2004-2005.

---

[4] Utto W, Mawson A J, & Bronlund J E (2008). Hexanal reduces infection of tomatoes by *Botrytis cinerea* whilst maintaining quality. *Postharvest Biology and Technology* **47** 434-437. (see Appendix B)

A hexanal exposure system similar to that of Gardner et al. (1990) was developed comprising a hexanal vapouriser connected to an exposure chamber (a 5 L glass desiccator) through 8 mm (internal diameter) polyvinyl chloride (PVC) tube. The inner surface of the PVC tube was disinfected using 70% (v/v) ethanol solution and left until dry at ambient conditions prior to use. The exposure chamber and the vapouriser were mounted within an incubator (20 ± 1ºC) (Figure 3-1). Hexanal vapour was generated by bubbling dry air (B.O.C. Gases, Christchurch, New Zealand Ltd) through pure liquid hexanal (97% G.C. grade, Sigma Chemical Co., USA) in 250 ml glass bubbling tubes (MF 29/3/250; QuickFit, England). The exposure chamber was humidified to ~99% RH (measured by a Tinytalk® RH meter; Gemini Data Loggers, UK) with a 60 ml sterilised water reservoir placed below the platform supporting the tomatoes.

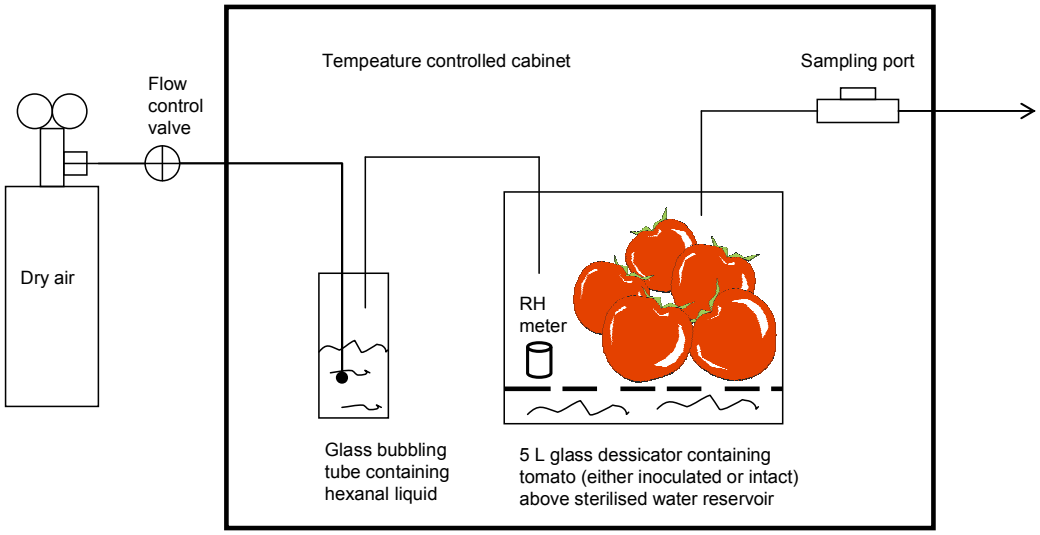

Figure 3-1 Hexanal exposure system comprising with 2 key compartments: an exposure chamber (a 5 L glass desiccators) and the 250 ml glass bubbling tubes

Hexanal vapour concentrations in the ranges of 0.21-0.63, 1.67-2.91, 4.16-6.67, 8.33-11.25 $mmol \cdot m^{-3}$ (~5-15, 40-70, 100-160 and 200-270 ppm, respectively) were achieved by adjusting the outgoing flowrates from the exposure chamber to 1-5, 8-15, 20-30 and 40-60 $ml \cdot min^{-1}$, respectively, through adjusting the control-valve (BSS4, Swagelok®, Swagelok Company, Ohio, US) connected between the dry air-reservoir and the bubbling tube. Song et al. (1966) reported effective hexanal vapour concentrations for suppressing *B. cinerea* on sliced apples at 20ºC to be in the range of 100 to 1350 ppm. Because of the commercial driven to minimise additions of food additives (including potential impact sensory quality/perception of packaged fruit and cost of additives), it was decided to initially focus

on testing low concentrations between 0 to 250 ppm. The same gas flowrates (measured using an Agilent ADM 1000 flow meter; J&W Scientific, USA) were used in the control treatments. The measured concentrations represent the effective exit (and hence headspace) values which may include any contribution of hexanal production or uptake by the tomatoes.

Two hexanal delivery systems were studied: continuous, and single-dose. The former represented an active packaging system designed to maintain a desired hexanal concentration throughout the storage period (e.g. by controlled release), while the latter represented a 'fumigation' system. Single-dose exposure was for a 2 h period at the start of the experiment, thereafter the gas flow was replaced with hexanal-free air at the same flowrate. Hexanal concentrations in the gas phase were measured by taking 0.1 ml samples using a gas-tight syringe (Hamilton Gastight®, Hamilton Co., US) through a port fitted with a Teflon-lined septum at the outlet of the exposure chamber. These samples were injected onto a gas chromatograph (GC6000 VEGA Series 2, Carlo Erba Instruments, Italy) equipped with a flame ionisation detector (FID) and a 30 m × 0.25 mm (I.D.), 0.52 μm film thickness, ZB-5 capillary column (Zebron™; Phenomenex® NZ Ltd). Operational conditions were: detector, 260ºC; inlet, 250ºC, and the column temperature was maintained at 100ºC for 30 s and then programmed to increase at 2ºC min^{-1} to 105ºC. Oxygen-free nitrogen (B.O.C. Gases New Zealand Ltd) was used as a carrier gas at a flowrate of 2 $ml \cdot min^{-1}$. The optimal spilt flow ratio was determined to be 200:1. Peak areas and retention times were recorded on an integrator (C-R6A Chromatopac Shimadzu, Japan) and compared with the response of injected standards comprising hexanal dissolved in ethyl acetate (99.5% BDH Laboratory Supplies, England). The retention time of hexanal was 2.38 ± 0.02 min. The calibration curves are presented in Appendix C. Hexanal concentrations in the exposure chamber were measured daily. For Day 0, gas samplings were performed initially after hexanal was introduced into the chamber for 30 minutes, and then every hour for 3 hours.

For each experiment, two groups of ten fruit were assigned to two different exposure chambers. One group was exposed to hexanal while the second group was flushed with air only (the 'control' group). To study the antifungal activity of hexanal vapour, each tomato was wiped with cotton pads soaked with 70% (v/v) ethanol solution to disinfect its surface and left at ambient conditions until the surface was dry. *B. cinerea* spores, which were

harvested from fungi grown on potato-dextrose agar (PDA) from spores isolated from a diseased tomato fruit, were added through the wound inoculation technique. The fruit surface was punctured in two positions to a depth of 4 mm using a glass rod of 3 mm diameter; 30 μL of a 1×10^5 spore·ml^{-1} suspension (determined using a haemocytometer; 0.1 mm, 1/400 mm^2 BS.78; Weber, England) was dropped into these holes using a pre-sterilised dropper and excess moisture was removed with a clean paper towel. The inoculated areas of the tomatoes were observed daily from outside the exposure chambers and the number of tomatoes showing fungal infection was noted and reported as a percentage of total fruit.

To study the effects of hexanal exposure on postharvest physiology and quality attributes of tomatoes, intact fresh tomatoes (i.e. fruit that were neither wounded nor ethanol- wiped) were used. Physiological and quality parameters were measured after the first day of treatment and every 3 days thereafter. For the measurement, the gas flows to the exposure chambers were stopped, the tomatoes were removed and the appropriate parameters were immediately measured.

Respiration rate and ethylene production rate of 10 individual fruit for each treatment were determined first by measuring the accumulation of CO_2 and C_2H_4 within 1 hour following Johnston et al. (2002). Skin colour was measured as hue angle (hº) using a Minolta CR200 Chromameter (Minolta Camera Co., Japan), after calibration with a standard green tile (D/0 Differential illumination, 0º viewing; light source C, Y 29.9 x 0.273 y 0.369). Three locations around the surface of individual fruit, selected at random, were measured. Fruit mass (g) was determined using a balance (0.001 g; Mettler Toledo PR1203, Switzerland) and mass loss was expressed as a percentage of the initial fresh mass. Tomato stiffness (10^6 Hz^{2}g$^{2/3}$) was assessed using a commercial acoustic firmness tester (AWETA, Nootdorp, The Netherlands) following Hertog et al. (2004a). The stiffness was measured three times around the flower end of each fruit.

The measured physiological and quality attributes were presumed to be representative of fruit inside the exposure chambers due to the short measuring period (~75-80 minutes) compared to the exposure interval. The tomatoes were returned to the chambers immediately after measurement and the gas flow was resumed.

All collected data were expressed according to the units proposed by Banks et al. (1995) and were subjected to an analysis of variance (ANOVA) using the General Linear Model (GLM). The least significant difference (LSD, $p = 0.05$) between means for multiple comparisons was calculated. Statistical Analysis Systems (SAS) software (version 8; SAS Institute, USA) was used for all statistical analyses. It should be noted that the 'Day 0' data (of 10 replicates randomly selected) appearing in the figures were not used to determine LSD values.

3.2.2 Results and discussion

Active packaging systems may be beneficial for extending the shelf life of fresh products. For example, an O_2 scavenger has been used to lower O_2 level and thus reduce the respiration rate of tomatoes (Charles et al. 2003) and ethylene absorbers have been utilised to control ethylene within the headspace of strawberry packages (Picón et al. 1993). Hexanal vapour is a natural component of tomato aroma (Stone et al. 1975) and so could be a practical tool for controlling *B. cinerea* infection on tomatoes.

Several ranges of hexanal vapour concentrations were continuously applied to tomatoes at 20ºC throughout the 7-day trial period. The concentrations were reasonably stable within 1-1.5 h after introducing hexanal vapour into the exposure chamber (Figure 3-2). The continuous application of 40-270 ppm hexanal vapour was demonstrated to be an effective antifungal treatment (Table 3-2 and Figure 3-3). This inhibition of *in vivo* growth of *B. cinerea* on tomatoes is consistent with observations for hexanal fumigation of sliced apple (Song et al. 1996), strawberries (Archbold et al. 1997), raspberries and pears (Song et al. 2007), and confirms the potential use of hexanal in active packaging systems.

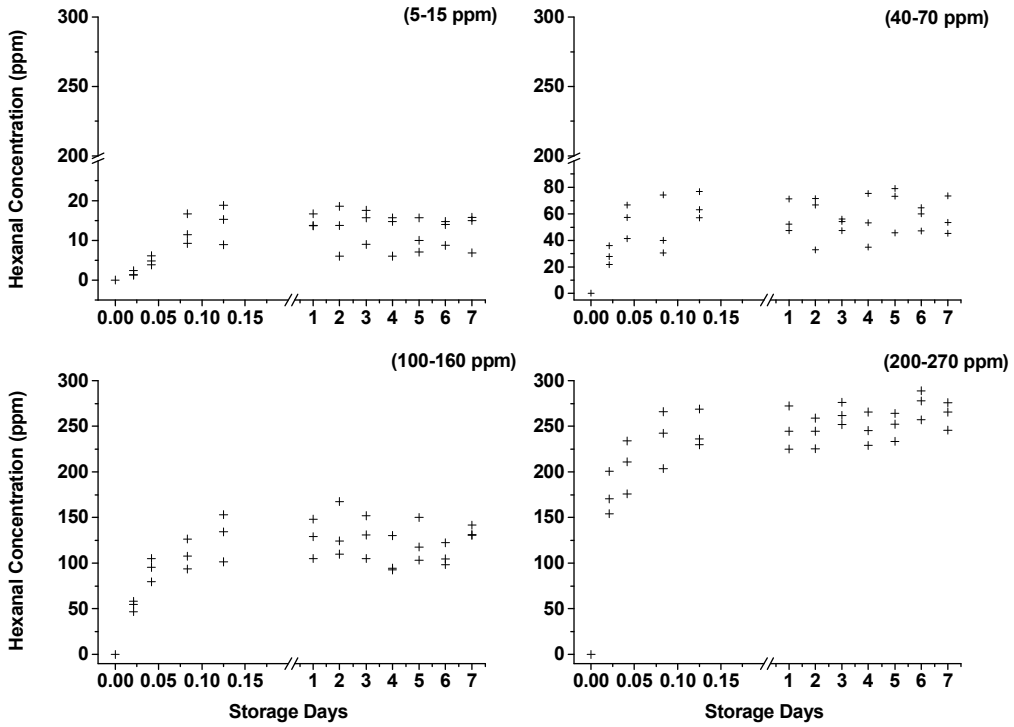

Figure 3-2 Hexanal concentrations during the continuous exposure period (3 replicates shown for each sampling time)

Table 3-2 Effect of continuous and single-dose hexanal vapour exposure on growth of *Botrytis cinerea* on wound-inoculated tomatoes. The percentages of fruit exhibiting fungal growth are represented by the symbols: –, +, ++, +++, ++++. These symbols represent 0, 10-30, 40-60, 70-90 and 100% of fruit infected, respectively.

Exposures	Concentration (ppm)	Storage Days			
		1	2	3	4 to 7
Continuous	Control	–	++	+++	++++
	5-15	–	+	+++	++++
	40-270	–	–	–	–
Single-dose	Control	–	++	++++	++++
	40-70	–	++	++++	++++
	200-270[1]	–	+	++	++++

[1] Actual percentage observed on Day 4 of 200-270 ppm single-dose treatment was about 70-90%

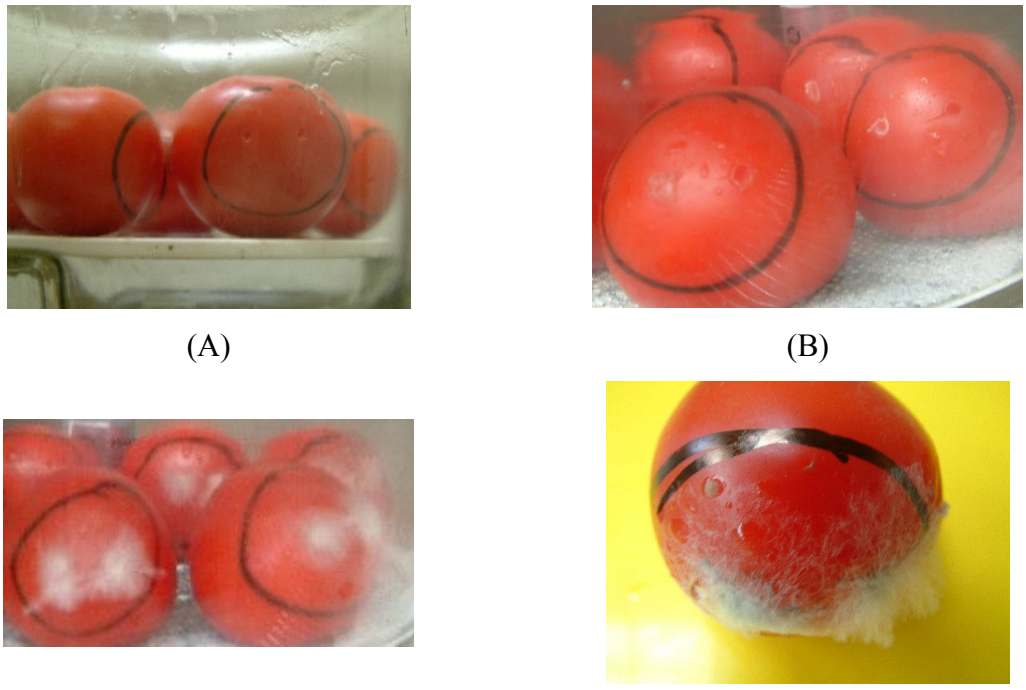

(A) (B)

(C) (D)

Figure 3-3 Tomatoes kept under different gas compositions: 40-70 ppm, at day 7 (A), 5-15 ppm on day 2 and day 4, respectively (B and C), and day 2 after leaving 40-160 ppm treated tomatoes in the ambient condition (D).

Continuous exposure provided effective inhibition under highly challenging conditions (20°C, ~99% RH) at significantly lower hexanal concentrations than required for fumigation for 12 – 48 hours (Song et al. 1996; Song et al. 2007). Single-dose treatment of tomatoes at 40-70 and 200-270 ppm for 2 h showed only limited antifungal activity. The latter treatment suppressed fungal appearance by only one day (Table 3-2), confirming a period of sustained exposure is required unless more elevated hexanal concentrations are employed.

Hexanal vapour could be either fungistatic (inhibitory) or fungicidal (lethal) to *B. cinerea*. In the present work, when hexanal vapour was replaced with hexanal-free air after the 7th day of continuous treatment, grey mould appeared within 2 days on all inoculated fruits treated with 40-160 ppm hexanal vapour (e.g. Figure 3-3D); no subsequent mould growth was found among tomatoes treated at 200-270 ppm. That higher hexanal concentrations in the air headspace appear to promote greater antifungal action is consistent with the previous reports by Song et al. (1996), Archbold et al. (1997) and Gardini et al. (1997).

At present, the mode of antifungal action of hexanal vapour is not fully understood. The mechanisms of hexanal activity against *Aspergillus niger* (*in vitro*) have been assumed to involve mass transfer processes linked to the fungal cytoplasmic membrane, e.g. partitioning into and permeation through the cell membrane (Gardini et al. 1997), which could cause alterations of cell permeability, cell membrane disruption leading to electrolytes leakages, or a deformation of membrane structure and functionality (Nychas 1995; Davidson 2001). A similar assumption was proposed for other antimicrobial volatiles and other microorganisms including (i) hexanal and trans-2-hexenal and *Pichia subpelliculosa* (*in vivo*; sliced apples) (Corbo et al. 2000), (ii) trans-2-hexenal and *Aspergillus flavus* (*in vitro*) (Gardini et al. 2001), and (iii) hexanal and *B. cinerea* and *M. fructicola* (*in vivo*; raspberries and peach in an order of pathogens) (Song et al. 2007). Further studies are required to investigate and clarify the mode of action of hexanal and other antimicrobial volatiles.

From the initial results obtained with the continuous delivery system (Table 3-2), the 40-70 ppm concentration level was designated as the MIC range. This was utilised for subsequent evaluation of the effect of continuous hexanal exposure on tomato physiology and quality. The lowest effective concentration is likely to be both more technically and economically feasible, and to be more acceptable to consumers, if applied in an active packaging system. It should be noted that this beneficial activity was demonstrated on tomatoes that were wounded, inoculated and kept at ambient temperature. These treatments represent extreme challenge conditions as opposed to the optimal temperature of 8-10ºC for storage of intact fruit (Brecht 2003) and provide further support for the use of low hexanal concentrations to prolong storage life.

The intact tomatoes showed a typical post-climacteric decline in respiration rate and ethylene generation (Figure 3-4; Atta-Aly 1992; Saltveit & Sharaf 1992). Continuous exposure to hexanal vapour at 40-70 ppm at 20 ºC increased the respiration rate by ~ 50% compared to the control during the storage period (Figure 3-4), however ethylene production was significantly higher only on the first day of storage (Figure 3-4). The mechanism for this stimulation of metabolism might be explained by the reduction of aldehydes to alcohols (i.e. hexanal reduction to hexanol) by the alcohol oxidoreductase system (Stone et al. 1975; Longhurst et al. 1990). Such enzymatic transformations of aldehydes have been reported for other products including strawberries (Hamilton-Kemp et

al. 1996) and apple (De Pooter et al. 1983), although differences in the response among cultivars have also been noted (Hamilton-Kemp et al. 1996; Song et al. 1996; Archbold et al. 1997).

Ethanol vapour was reported to stimulate respiration rate and ethylene production in tomato (Saltveit & Sharaf 1992) and respiration rate in potato (Rychter et al. 1979). According to Rychter et al. (1979), ethanol may trigger respiration intermediates, or enter the respiratory pathway as a substrate. It is possible that the hexanal vapour applied to tomatoes in this study were absorbed and transformed to hexanol, which in turn stimulated respiration in a manner similar to that of ethanol.

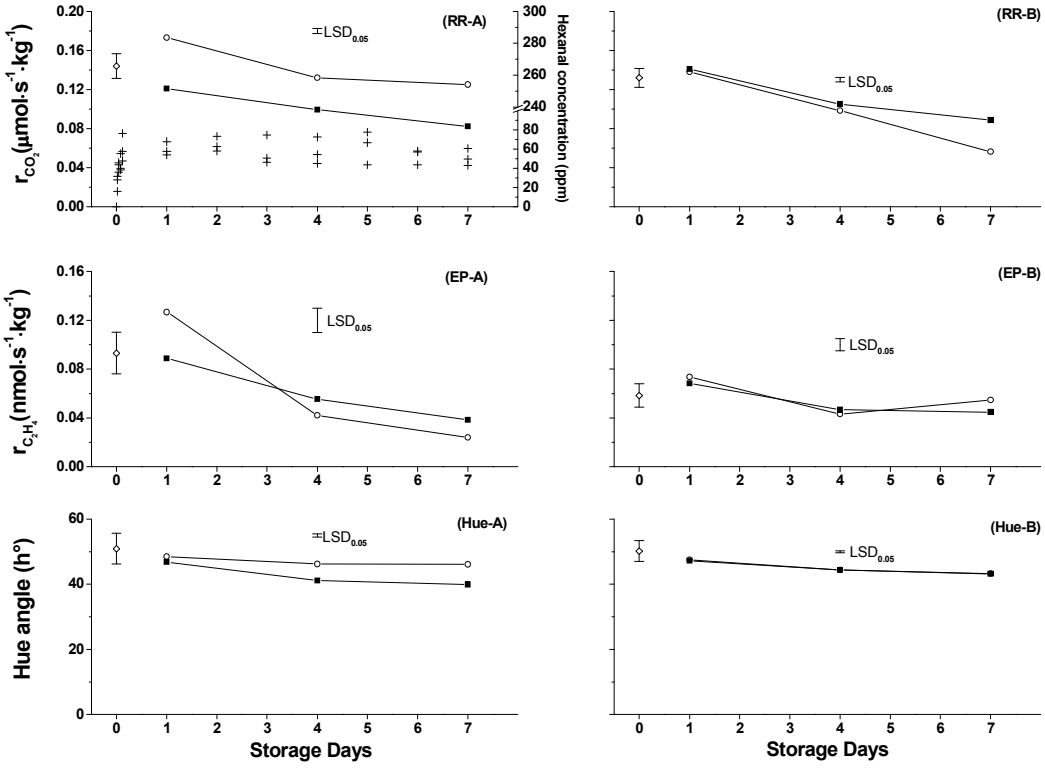

Figure 3-4 Respiration (RR), ethylene production (EP), and hue angle (Hue) of tomatoes exposed to hexanal vapour through continuous (40-70 ppm) (A) or single dose (200-270 ppm) (B) delivery systems. The symbols (◊), (o), and (■) represent average results (10 replicates) obtained from day 0, hexanal-treated tomatoes, and control treatments, respectively. Error bars at day 0 represent standard deviation from the mean. Hexanal concentrations in the exposure chamber during the storage period were represented by the symbol (+) in the RR-A graph (3 replicates shown for each sampling time)

Ethylene production rates could similarly be expected to be stimulated by hexanal if the aldehyde is transferred to the alcohol. This inference is justified by the experimental result reported by Saltveit & Sharaf (1992), in which ethylene production rates of pink tomatoes were increased for a short period after treatment with ethanol vapour and then gradually declined. Such a result was consistent with the findings in the present work (Figure 3-4). According to Beaulieu & Saltveit (1997), the observed trend could be accounted for by both vapour concentrations and fruit maturity.

Hexanol vapour was detected in the headspace above hexanal treated apples (Song et al. 1996) and strawberries (Hamilton-Kemp et al. 1996; Archbold et al. 1997) but respiration rates and ethylene production were not measured in these studies. In the present work, hexanol was not detected. Understanding these metabolic responses to hexanal exposure is important as an increased respiration rate will influence the equilibrium gas composition when modified atmosphere packaging (MAP) forms part of the active packaging system.

In spite of the noticeable hexanal effects on respiration rates and ethylene generation, there were no consequential effects of hexanal exposure in either system on stiffness throughout the storage period, which appeared stable in the range of 3.44-3.99 10^6 Hz^2 $g^{2/3}$, or on mass loss, which was observed to be less than 0.60%.

Skin colour is considered one of main quality attributes influencing consumer preferences for tomatoes (Grierson & Kader 1986). During the marketing period, continuous ripening and maturity produces a redder skin colour (presenting as low hº values) due to the accumulation of red pigments (principally lycopene; Davies & Hobson 1981). The tomatoes continuously-exposed to hexanal reddened more slowly during treatment (Figure 3-4) but ripened normally when removed to ambient storage (Figure 3-5) and their final skin colour was similar to those of the control (~35-40 h° values, after 7 days). Ethanol vapour was reported to inhibit the development of red pigment in tomatoes (Saltveit & Sharaf 1992) and it is assumed that hexanal or a product arising from hexanal conversion may act in a similar manner.

Figure 3-5 Comparison of skin colours after 7 days storage of tomatoes kept in hexanal-free air (top row) or continuously exposed to hexanal (bottom row)

In contrast to the continuous exposure technique, no significant effects of the hexanal single-dose treatment on physiology and quality attributes were apparent (Figure 3-4). Despite the effects of hexanal noted above, the quality parameter values obtained from this study were all similar to typical values reported in the literature for untreated tomatoes stored in air under comparable temperatures (18-20ºC) (Table 3-3). It may be concluded that hexanal treated tomatoes behave similarly to those not treated with hexanal and that the inclusion of hexanal in an active packaging system potentially offers the benefit of greater shelf life through reduction of postharvest rots without other detrimental effects.

Table 3-3 Comparison of postharvest physiology and quality attributes of tomatoes between data of the present work (cv. 'Royale'; measured at 20°C) and those of estimates from previously published data

Physiology/ quality attribute	The present work [a]		Published values			
	Control	Treated fruit	Data reported	Temperature (°C)	Cultivars	Ref. no.[b]
r_{CO_2} (μmol·s^{-1}·kg^{-1})	0.08-0.09	0.06-0.13	0.08	20	'Durinta'	[1]
			0.26	20	'Castlemart'	[2]
			0.15-0.27	20	'Pearson'	[3]
			0.25	20	Not specified [c]	[4]
			0.19	20	'Eurocross BB'	[5]
$r_{C_2H_4}$ (nmol·s^{-1}·kg^{-1})	0.04-0.05	0.02-0.05	0.03	20	'Capello'	[6]
			0.04		'Aromata'	[7]
			0.01-0.11	20	Not specified	[8]
			0.11	20	Not specified	[3]
Final colour (h°)	39.87-44.96	45.06-46.15	40-50	18	'Tradiro', 'Style', 'Quest'	[9]
Stiffness (10^6 Hz^{2}g$^{2/3}$)	3.44-3.98	3.76-3.99	5.18	22.6	'Tradiro'	[10]
			4.66	20	'DRW 3450'	[11]
Weight loss (%)	0.22-0.54	0.25-0.58	1.08	20	'Rupali'	[12]
			7	20	'Eurocross BB'	[5]

[a]Data was those were reported on day 7th of the storage period. Treated fruits include both the 'Continuous' and 'Single-dose' treatments

[b] [1] Artes et al. (1998), [2] Saltveit & Sharaf (1992), [3] Hardenburg et al. (1986), [4] Kader & Saltveit (2003b), [5] Robinson et al. (1975), [6] Gouble et al. (1995), [7] de Wild et al. (2005), [8] Kader (1992), [9] Hertog et al. (2004b), [10] Hertog et al. (2004a), [11] Schotte et al. (1999), [12] Thiagu et al. (1991)

[c] Not specified cultivar, but generally referred to ripening tomatoes

3.3 Apparent rate of uptake of hexanal vapour by tomatoes

Interactions between horticultural products and volatile organic compounds may involve enzymatic consumption (i.e. catabolism of the active molecules), partitioning (adsorption) within the skin or flesh, and/or production (e.g. release of the volatile compound), as discussed in Chapter 2. Although the MIC identified in the previous section could be the net result of these various processes, the complexity of possible effects meant that we did not attempt to distinguish between these, and did not attempt to identify one or more specific process dominating interactions, but instead determined the overall change in concentration that may occur through these interactions. Rates of changes of hexanal

concentrations by exposed tomatoes may thus be holistically represented by the apparent uptake rate (designated as r_{tom}^{Hxl}).

3.3.1 Materials and methods

The apparent rate of uptake of hexanal vapour by tomatoes (r_{tom}^{Hxl}) at storage temperatures of 10 and 20ºC was determined using procedures similar to those of Wolford (1998). The continuous flow-through exposure system employed was similar to that previously used in section 3.2.1. The use of a stainless steel permeability cell (described in Chapter 4), rather than the glass desiccator, provided greater security against leaks of hexanal vapour from the headspace which may cause overestimation of the apparent uptake rate. The exposure chamber and a hexanal vapouriser were mounted within a temperature controlled cabinet. Inside the exposure chamber, four tomato fruit (~100-120 g per fruit) were placed in one layer on the wire-stainless steel stand above a ~50 ml reservoir of distilled water to humidify the exposure headspace. The inlet hexanal vapour concentrations are shown in Table 4-1. From preliminary studies, it was found that steady outflow concentrations were achieved 1-1.5 h after introducing the hexanal and these levels were reasonably well maintained throughout the 24-hour exposure period. To ensure uniform concentrations, the gas samples (3 replicates) at both inlet and outlet ports were taken after the tomatoes had been exposed to hexanal for 3 h. Hexanal concentrations were quantified using the gas chromatography technique previously described. Fresh tomatoes were used in each experiment and these, and the experimental apparatus, were equilibrated at the appropriate storage temperature for 24 h prior to starting the tests.

Apparent uptake rates of hexanal in tomato were estimated by concentration differences between the inlet and outlet hexanal flows, following Wolford (1998) as shown in Eq. 3-1;

$$r_{tom}^{Hxl} = \frac{Q_{outlet}\left(C_{inlet}^{Hxl} - C_{outlet}^{Hxl}\right)}{M_{tom}} \qquad \textbf{(Eq. 3-1)}$$

where

r_{tom}^{Hxl} = Apparent rates of uptakes of hexanal vapour by tomatoes ($mol \cdot s^{-1} \cdot kg^{-1}$)

Q_{outlet} = Outgoing flowrate ($m^3 \cdot s^{-1}$)

C_{inlet}^{Hxl} = Inlet hexanal concentration ($mol \cdot m^{-3}$)

C_{outlet}^{Hxl} = Outlet hexanal concentration ($mol \cdot m^{-3}$)

M_{tom} = Mass of tomatoes (kg)

3.3.2 Results and discussion

Values of r_{tom}^{Hxl} were found to depend on both storage temperature and hexanal inlet concentration (Figure 3-6), and the variation (represented by data scattering) in r_{tom}^{Hxl} increased with increasing storage temperature and inlet concentrations. It can reasonably be assumed that changes of hexanal vapour concentration by tomatoes will involve transport of hexanal vapour across tomato cuticles. The exponential increase of r_{tom}^{Hxl} values with concentration (Figure 3-6) appeared similar to the response of film permeability to hexanal (Chapter 4), and offers support to this hypothesis.

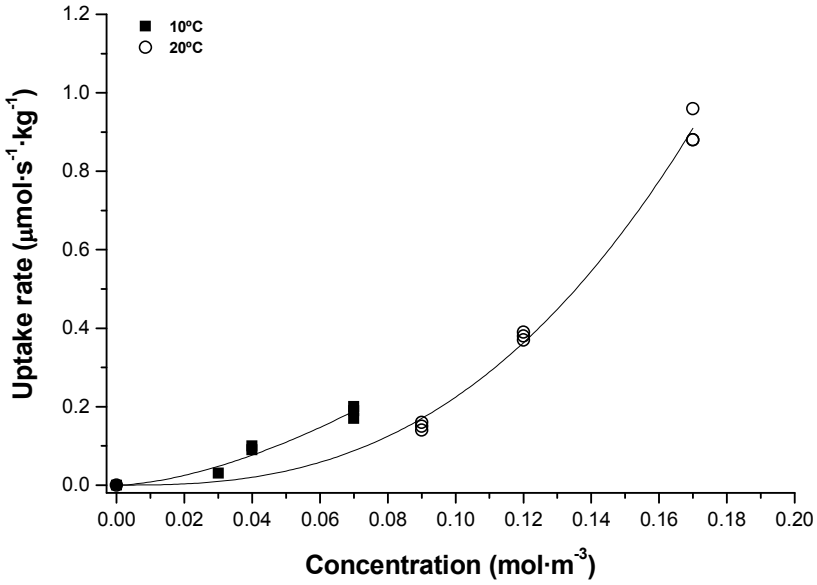

Figure 3-6 Effects of temperature and concentration on apparent uptake rates of hexanal by tomatoes at 10 and 20ºC (3 replicates for individual treatments shown for each sampling time). Solid lines were fitted by nonlinear regression using Eq. 3-2; referred to Table 3-4 for model coefficients.

Del-Valle et al. (2004) compared the permeance of tomato cuticle to urea (applied as a fertiliser) and water (Knoche et al. 1994) to a range of polymer films and suggested that skin permeance was comparable to that of an 11 μm polyethylene terepthalate (PET) film (according to the databases of the Plastic Design Library (PDL) on permeability and other

film properties of plastics and elastomers; Del-Valle et al. 2004). However there appears to be little other data on the transport properties of tomato skin for volatile organic compounds. According to Riederer (2006), the cuticle is a natural structure of which cutin and wax are key components, and it covers the epidermis of tomato skin to function in gas exchange and provision of mechanical strength. Schreiber et al. (1996) suggested that mass transport between the plant and surrounding environment, e.g. uptake of volatile compounds and loss of water from the interior of the plant structural body, are strongly dependent on the transport properties of the cuticle. Schreiber et al. (1996) also described that uptake of organic compounds through cuticles involved two key processes, which are (i) surface adsorption leading to the dissolution of solutes in the cuticle, and (ii) diffusion across the cuticle layers. These processes are also those governing mass transport across polymer films (Zobel 1982; Robertson 1993c).

Most commonly, the rate of reaction is positively correlated with temperature (Labuza 1982; Robertson 1993a; Earle & Earle 2003). As the value of r_{tom}^{Hxl} at a given concentration decreases as the temperature increases (from 10 to 20ºC), this implies, based on discussions in section 4.2.2, that sorption and diffusion processes relating to hexanal transport across the tomato cuticle are more important than the catabolism or conversion of hexanal by the tomatoes.

Because the purpose of this experimental work was to identify the overall (or effective) rate of hexanal concentration change with regard to the exposed tomatoes, a model to describe the relationship between the uptake rate and hexanal concentration was essential. Eq. 3-2 is commonly used to describe the dependence of reaction rate on concentration through identification of the apparent order of reaction (Labuza 1982; Robertson 1993a; Earle & Earle 2003). This model was implemented to describe the concentration dependence of the apparent rates of hexanal uptake where the sorption and diffusion processes of hexanal across the tomato cuticles were considered the rate limiting step in hexanal uptake. The fitting of Eq. 3-2 to r_{tom}^{Hxl} data using the nonlinear regression package (Origin 5.0; Microcal Origin Inc., US) are illustrated in Figure 3-6. The estimated model coefficients are given in Table 3-4.

$$r_{tom}^{Hxl} = k_{tom,reac}^{Hxl}\left(C_{inlet}^{Hxl}\right)^{n_{reac}} \quad \textbf{(Eq. 3-2)}$$

where

$k_{tom,reac}^{Hxl}$ = Coefficient of reaction rate of hexanal and tomatoes ($\mu mol \cdot s^{-1} \cdot kg^{-1} \cdot (m^3 \cdot mol^{-1})^{n_{reac}}$)

n_{reac} = Order of reaction rate (dimensionless)

Table 3-4 Parameter estimates and standard errors (SE) [a] resulting from nonlinear regression analysis of apparent rates of hexanal uptakes by tomatoes at 10 and 20ºC

Temperatures (ºC)	$k_{tom,reac}^{Hxl}$ (SE)	n_{reac} (SE)	n [b]
10	14.0 (52.7)	1.62 (11.8)	10
20	97.5 (20.5)	2.64 (4.3)	10

[a] The standard errors (SE) are expressed as a percentage, relative to the estimated values.

[b] n is the number of observations

The apparent order of r_{tom}^{Hxl} was approximately 1.6 and 2.6 for the 10 and 20ºC experiments, respectively (Table 3-4). Orders of reaction greater than unity are rare in reactions during food processing and preservation (e.g. see the discussion by Labuza 1982, Robertson 1993a and Earle & Earle 2003), but this may reflect that more than one process, i.e. both sorption and diffusion, and reaction, were being represented.

There is no literature data on hexanal uptake by any tomato cultivar. However, Wolford (1998) reported hexanal consumption rates of sliced 'Golden Delicious' apple (designated as r_{apple}^{Hxl}) in which consumption rates were reported to be the result of metabolism and enzymatic transformation of hexanal vapour. A comparison between r_{tom}^{Hxl} and r_{apple}^{Hxl} is illustrated in Figure 3-7. Wolford (1998) also observed a concentration dependence of r_{apple}^{Hxl}, although the effect of temperature on the rate was unclear (Figure 3-7). Wolford proposed the latter could be due to (i) the enzymatic reactions that are responsible for consumption not being temperature sensitive, (ii) the trial temperatures being too low to obtain significant effects, and (iii) potentially large variability (inherent to biological systems) between fruit responses across the range of these experimental temperatures. Only the latter seems most reasonable. Values of r_{apple}^{Hxl} increased more rapidly than r_{tom}^{Hxl} as

the hexanal concentration increased from ~0.001 to ~0.020 mol·m^{-3} and the differences observed are presumably due to physical and physiological differences between the sliced apple and tomato, particularly the fact that slicing the apple would provide a greater exposure of underlying tissues as compared to the intact tomato skin in the experiments performed in the present work. Minimally processed products tend to be more perishable than intact products because of their higher biological activity, which is elevated by the stresses caused by the processing techniques (Gil et al. 2002; Lanciotti et al. 2004).

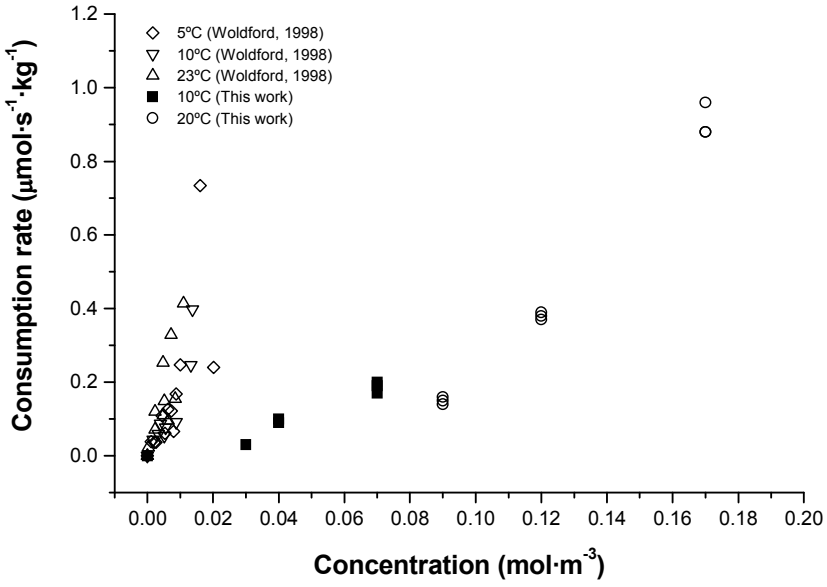

Figure 3-7 Hexanal consumption rates by sliced 'Golden Delicious' apples, at 5-23ºC (redrawn from Wolford 1998), and their comparisons to apparent uptake rates by tomatoes measured in the present work

Neglecting storage temperatures, Wolford (1998) described r_{apple}^{Hxl} dependence on concentration with an overall linear equation. However the reported R^2 and standard error (SE; expressed as a percentage relative to the estimated slope value) were ~0.51 and 66%, respectively, indicating that the linear regression model did not well represent all values of r_{apple}^{Hxl}. By fitting a nonlinear model (Eq. 3-2) to all r_{apple}^{Hxl} data, the apparent order of reaction was found to be 1.67 with R^2 and SE of ~0.72 and 14%, respectively (calculation not shown). This suggests that a nonlinear model is more suitable to describe the concentration dependence of r_{apple}^{Hxl} and r_{tom}^{Hxl}. The high variation in hexanal uptake rates measured in both tomatoes and sliced apples indicated large uncertainties that could be attributed to the

natural biological variation commonly observed in quantifying physiological parameters for horticultural products (see the discussion by Hertog et al. 2004b). Further studies are required to understand the hexanal interaction at a molecular level and determine how it influences physiological and antimicrobial activities (as discussed earlier).

The C-6 volatile compounds including hexanal, *cis*-3-hexenal, *trans*-2-hexenal and hexanol are important compounds contributing to tomato aroma (Ruiz et al. 2005) and it was partly for this reason that hexanal was selected for this study. These compounds are abundantly generated through the lipoxygenase oxidation of linoleic and linolenic acid during tissue disruption (Vick & Zimmerman 1987; Ruiz et al. 2005) and are presumably involved in the defence system in plants (Song et al. 1996). The aldehydes may also be physiologically converted to alcohol by tomatoes through the alcohol oxidoreductase system (Stone et al. 1975; Longhurst et al. 1990). Subsequent conversion of the alcohols to other aroma volatiles may also occur through enzymatic systems such as the alcohol acetyltranferase system (Stone et al. 1975; Longhurst et al. 1990).

Enzymatic conversion of hexanal to hexanol and hexylacetate was reported for apples (De Pooter et al. 1983; Song et al. 1996; Wolford 1998; Fan et al. 2006; Song et al. 2007), and strawberries (Hamilton-Kemp et al. 1996); similar patterns of conversions have also been reported for other aldehydes (Hamilton-Kemp et al. 1996). These compounds could be detected in the headspace of these previous hexanal exposure systems. In contrast, hexanal-treated tomatoes in the present work did not yield measurable amounts of products of enzymatic conversion of hexanal. It is uncertain why such hexanal reaction products could not be measured in the headspace, even though these (via injection of standard liquid solutions) could be detected by the current gas chromatography system used when injected separately at low concentrations (Appendix C).

Hexanol and hexylacetate, among others, were measurable in several studies conducted to identify aroma volatile compounds of tomatoes (Buttery et al. 1987; Maul et al. 2000; Boukobza & Taylor 2002; Krumbein et al. 2004), but these were measured from macerated or homogenate samples. Bailén et al. (2006) also noted they could not detecte hexanal and its conversion products using the direct sampling method of the headspace surrounding tomatoes packaged in MAP bags, while other volatiles e.g. heptane, nonanal, octana-1-ol and cyclopentanone were detectable.

Phytotoxicity is also another potential issue to address in application of natural volatiles in postharvest system. Archbold et al. (1997) reported phytotoxicity, evidenced by discolouration, loss of tissue turgidity and shape, and the presence of exudates, among strawberries at both 2ºC and 22ºC when exposed to volatiles generated through the inclusion of 10-60 μl (middle range) and 100-600 μl (high range) liquid volume of, for example, hexanal, (E)-2-hexenal (or trans-2-hexenal), hexylacetate, nonanal, 2-nonanone, 3-hexanone and ethyl butyrate. However, there were no symptoms of phytotoxicity in strawberries exposed to vapours generated with 2-12 μl (low range) of these compounds. Wolford (1998) reported phytotoxicity as a red tint in the apple peel when sliced apples were exposed to saturated hexanal vapour concentration at 23ºC. These observations support the proposition made in the present work that exposure to, and uptake of aldehyde compounds induces a stress response in horticultural products, which was evident in our work is an example elevated respiration rate and delayed reddening. However, if appropriately low exposure dosages are used, this stress needs not adversely affect the quality of the fruit.

3.4 Effects of modified atmosphere conditions on apparent rate of hexanal uptake by tomatoes

As active packaging systems may include multiple hurdles against microbial deterioration, such as temperature control, releases of antifungal gases and generation of a modified atmosphere (MA), it was necessary to determine if a passive MA surrounding the tomatoes could affect the apparent hexanal uptake rate. Additional experiments were therefore performed to investigate such effects. From preliminary studies, the equilibrium MA condition in the headspace of a common LDPE bag (30 μm thickness; 250 × 250 mm size) at 20ºC, was ~5% CO_2 and ~10% O_2 (as reported later in Chapter 6). These MA conditions were selected for the work described in the following subsections.

3.4.1 Experimental settings

The experimental set-up and operation were the same as those described in section 3.3. However the gas compositions flowing into the exposure chamber were varied as summarised in Table 3-5.

Table 3-5 Gas streams introduced to the exposure chamber (as experimental treatments)

Treatment code	Description
HxlMA	Flow of hexanal vapour generated by MA air (~5% CO_2 and ~10% O_2)
HxlDA	Flow of hexanal vapour generated by dry air
MA	Flow of MA air
DA	Flow of dry air

The gas atmosphere of ~5% CO_2 and ~10% O_2 (N_2 balance) was controlled during the storage period following Yearsley et al. (1996), where the desired atmospheric composition was generated by mixing O_2-free N_2 (B.O.C. Gases New Zealand Ltd) and CO_2 (B.O.C. Gases, Christchurch, New Zealand Ltd) with dry air (B.O.C. Gases, Christchurch, New Zealand Ltd). The gas flow was controlled by two-stage regulators and precision needle valves (Nupro S series, Nupro Co., Willoughby, Ohio, US).

As too high a hexanal concentration could cause stress to the fruit, a moderate inlet concentration of 0.12-0.13 mol·m^{-3} (~2880-3120 ppm) (reported in Table 4-1) was chosen and the steady-state outlet concentration level (observed in experiments conducted in section 3.3) was in the MIC range. The experiments were conducted at 20°C and hexanal concentrations at the inlet and outlet of the exposure chamber (3 replicates) were measured at 3, 6, 24, 32, and 48 hours. The 48 hour experimental timeframe was chosen based on the results obtained from the mathematical models developed (refer Chapter 5 and 6). These indicated that significant effects of hexanal uptake processes on accumulation of hexanal in the package atmosphere could be observed within the first 48 hours of the 7 day storage period.

In addition to hexanal concentration measurement, other postharvest quality parameters were measured. Mass loss and colour changes (h° values) were measured as described in section 3.2, at the beginning (t = 0 h) and end of the experimental period (t = 48 h). Respiration rates (r_{CO_2}) were measured inside the flow-through system at 3, 6, 24, 31 and 48 h and was estimated using Eq. 3-1, which required measured values for (i) the difference in concentration of CO_2 between the inlet and outlet of the exposure chamber (measured using the gas analyser as described in section 3.2), (ii) gas flow rate, and (iii) fruit mass.

3.4.2 Results and discussion

There were no apparent effects of the MA condition on r_{tom}^{Hxl} as shown in Figure 3-8 when the outlet hexanal concentrations were in the MIC range (Figure 3-9). Values of r_{tom}^{Hxl} measured in both HxlMA and HxlDA (Table 3-5) treatments were in the range of 0.29-0.35 μmol·s^{-1}·kg^{-1} (Figure 3-8), which were consistent to those reported in Figure 3-6. The apparent rates of hexanal uptake reached a quasi steady-state within 3 hours (Figure 3-8), and none of the expected products of enzymatic conversion of hexanal vapour were measurable in either the MA or dry air outflow streams.

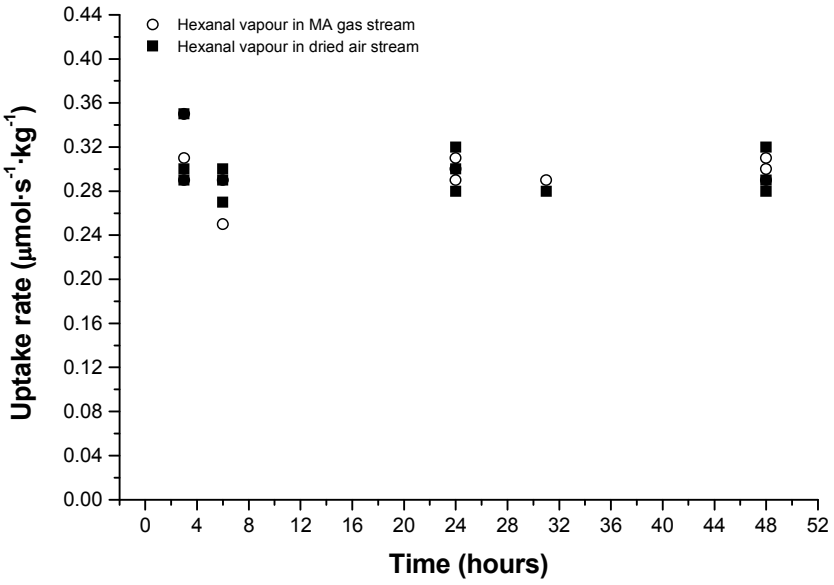

Figure 3-8 Effects of modified atmosphere conditions on apparent hexanal uptake rates of tomatoes (3 replicates for individual treatments shown for each sampling time)

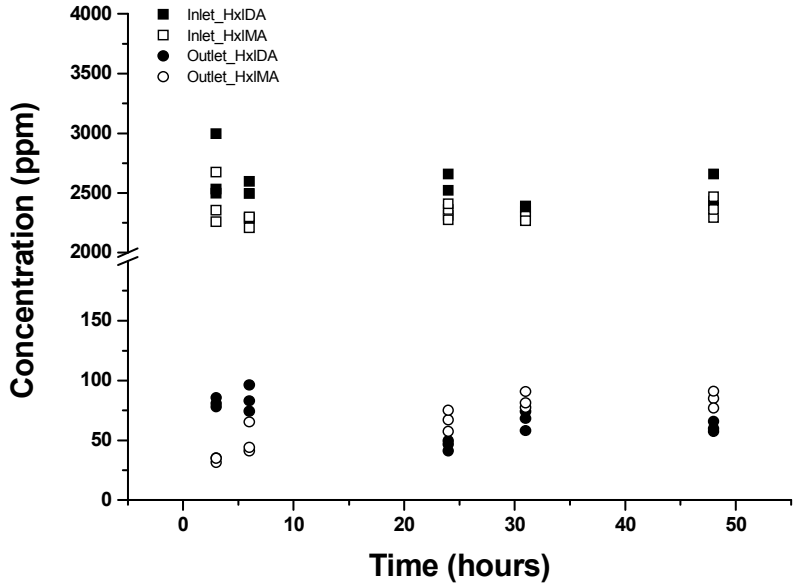

Figure 3-9 Inlet and outlet hexanal concentrations measured during experiments on the effects of modified atmosphere (MA) conditions on apparent hexanal uptake rates of tomatoes (3 replicates for individual treatments shown for each sampling time).

It was found that the gas atmosphere had a minimal effect on hue angle (hº), which appeared stable in the range of ~38.8- 42.6, or on mass loss, which was observed to be less than 0.42%. The effect of continuous hexanal exposure on hº values differed from those reported in section 3.2. This is most likely due to the tomatoes used in this experiment being redder (and hence more mature) than those in the earlier study (hº value in this experiment was ~44 compared to 47-56 in the earlier experiment). Possibly differences in cultivars used may also have influenced the fruit behaviour (P. Wilson, 2007, Pers. comm.: NZ Hothouse, New Zealand).

The r_{CO_2} values under 5% CO_2 and 10% O_2 MA conditions were lower than those in air as expected (Figure 3-10) and the values obtained appear comparable to the values for 'Maêva' and 'Trust' cultivars as reported by Hertog et al. (1998) at 18 and 23°C.

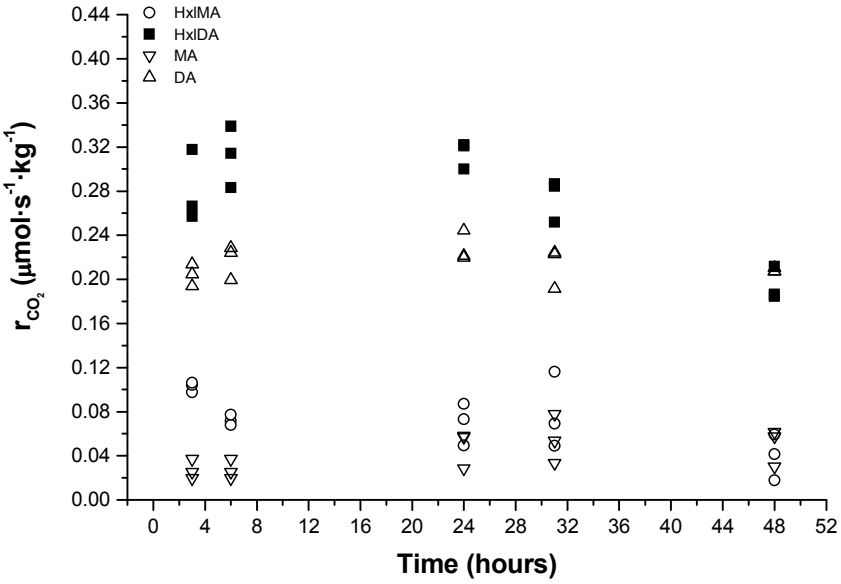

Figure 3-10 Respiration rates of tomatoes at 20ºC measured at different treatments (3 replicates of individual treatments shown for each sampling time)

It should be noted that r_{CO_2} values for the dry air (DA) treatment measured in this experiment were higher than those reported in section 3.2. Values of r_{CO_2} measured on 'Day 0' in this current work and in section 3.2 were 0.21 ± 0.04 [5] (Figure 3-10) and 0.14 ± 0.01 μmol·s^{-1}·kg^{-1}, respectively. The difference was about 1.5-fold. Although there were differences in the magnitude of the respiration rates reported in this experiment and in section 3.2, the pattern of stimulation of r_{CO_2} due to hexanal exposure appeared similar. However in this experiment, stimulation of r_{CO_2} by hexanal vapour only persisted for about 24 hours, and during this time r_{CO_2} measured under air (HxlDA) and MA (HxlMA) conditions were increased by ~25% and ~50%, respectively (Figure 3-10). After 24 hours, r_{CO_2} values measured in the HxlDA treatment continuously declined and were not different to values measured in air (DA) by 32-48 h. This contrasts with data reported in section 3.2, where hexanal stimulation of r_{CO_2} was continuously observed during the 7 day-storage period and r_{CO_2} was increased by ~50% compared to those of non-treated

[5] Presented values as average ± standard deviation; 10 replicates; the measuring method was the static method as described in section 3.2.

fruit. Such differences may be due to differences in maturity and/or cultivar, as noted above.

3.5 Summary

The results of these various trials suggest it should be possible to develop an active packaging system to increase storage life of tomatoes or other products subjected to *Botrytis* rots through sustained release of low concentration of hexanal. The MIC concentration of hexanal vapour was 40-70 ppm for suppressing grey mould appearance on wound-inoculated tomatoes during continuous exposure over a 7-day storage period at 20°C and ~99% RH. When applying this MIC, respiration and ethylene production rates of intact tomatoes were stimulated by hexanal exposure and the reddening of skin colour was slightly retarded, but there was no change to firmness of tomatoes stored at the light red stages. More mature tomatoes exhibited a temporary increase in respiration rates of ~25%, but no other quality changes were noted. Under a MA condition (~5% CO_2 and ~10% O_2) the respiration rates was systematically depressed and the tomatoes appeared to be less affected by hexanal exposure.

Hexanal uptake rates exhibited an exponential relationship with hexanal vapour concentrations. The relationship could be reasonably described by an apparent order of reaction of ~1.6-2.6. Because the relationship between uptake rates and hexanal concentration and storage temperature appeared to mimic those observed for polymer film permeability to hexanal vapour (discussed in Chapter 4), this suggests hexanal sorption and diffusion across the tomato cuticle may play an important role in hexanal concentration changes induced by tomatoes.

Overall, these studies of the biological components of an active packaging system confirm the antifungal activity of hexanal vapour and provide insights into its influence on packaged tomatoes. These results, taken together with other positive results from other crops, support the feasibility and utility of incorporating a hexanal controlled release system into passive MA packages of horticultural products. Active MAP design to achieve these goals requires matching the rate of uptake from the fruit with the desorption of the hexanal vapour from the carrier particles and the transport of the vapour through the outer

polymer films. These properties and their incorporation in mathematical models are considered in the following chapters.

Chapter 4

EVALUATING THE PHYSICO-CHEMICAL PROPERTIES OF HEXANAL VAPOUR AND SILICA GEL ADSORBENTS FOR ACTIVE PACKAGING APPLICATIONS

4.1 Introduction

This chapter describes experiments conducted to determine the key physico-chemical properties of hexanal vapour and silica gel relevant to active packaging systems. These include the permeability of polymer films to hexanal vapour and hexanal sorption isotherms for the selected silica gel adsorbent. These parameters are required in order to design novel packaging systems such as the hexanal active MAP system for tomatoes outlined in Chapter 3 and are required inputs into comprehensive mathematical models describing such systems.

4.2 Determination of effective film permeability to hexanal vapour

As previously discussed in Chapter 2, Fick's first law (Eq. 2-8) is commonly applied to model steady-state gas permeation through polymer films utilised in MAP for food products, including fresh fruit and vegetables. The flux across the film, which is assumed to be constant with time, is a product of film permeability and the concentration gradient of the active compound established between the two surfaces of the film. The permeability values are usually presumed to be concentration independent, implying the absence of interactions between the permeant and the polymeric film (Rogers 1985; Robertson 1993c; Selke et al. 2004). When interactions between the permeant and film are likely to occur, as between water vapour and hydrophilic films (such as cellulose and EVOH), or between organic vapours and polyolefin films (such as LDPE and PP) (Robertson 1993c; Sajilata et al. 2007), the assumption of concentration independence of mass transfer coefficients may not be valid and must be tested.

Hernandez-Munoz (1998; 1999) suggested that mass transport of vapour permeants (including hexanal, hexanol, ethyl carproate, d-limonene, phenylethanol and *n*-decane) through polymer films could reasonably be considered concentration independent at concentrations giving a vapour activity (or relative vapour pressure) of around 0.1 or less,

as is commonly the case in flavour scalping. Because the silica gels to be used as carriers of hexanal should (at least initially) be saturated with liquid hexanal to give a sachet headspace in which the hexanal vapour activity is ≈1.0, the mass transport of hexanal through the polymer sachet film can reasonably be expected to be concentration-dependent. To date, there appears to be no literature data on the concentration-dependence of hexanal permeability for any polymer film. The available data are generally reported as, or assumed to be concentration-independent (Leufven & Stollman 1992; Johansson & Leufven 1994; Song et al. 1996). Addressing this knowledge gap is therefore a key objective of the present work.

According to Robertson (1993c), the overall mass transfer rate of a concentration-dependent system can be defined by the Transmission Rate (TR) of the material. TR is practically measured as the molar or mass flowrate of gaseous compound passing through a barrier (assuming constant concentrations on each side), once the barrier has reached equilibrium with the compound. The attainment of equilibrium is thermodynamically the result of (i) solubilisation of the compound into the film (absorption or partitioning) and (ii) diffusion to minimise the chemical potential (represented by the concentration) gradient across the film (Rogers 1985). By definition, TR is the 'effective' value of the steady-state flux (the so-called 'effective permeability') across the film, where the processes of sorption and diffusion within the permeating medium, as well as the interactions between permeant and the medium, are taken into account.

In most examples of passive MAP for horticultural products, the transient (unsteady-state) period typically occurs within the first one or two days of storage (Yam & Lee 1995). For long storage of products, steady-state mass transfer processes are therefore more important (Yam & Lee 1995). The active MAP systems designed in the present work were intended for products to be stored for at least 7 days and very likely much longer. As a key objective of the present work was to maintain and sustain the hexanal headspace concentration at the MIC level, the mass transfer processes at steady-state were the key focus. Song et al. (1996) mentioned that LDPE used at storage temperatures of 5 to 30°C is a poor barrier to hexanal vapour. Furthermore Leufven & Stollman (1992) reported that the average timeframe for achieving steady-state flux of hexanal through LLDPE, HDPE and EVOH at 25°C was only about 4 hours. Hence, steady-state permeation through the polymer films

utilised in the present work was expected to be achieved within a relatively short timeframe compared to the shelf life of the tomatoes or other horticultural products.

Based on Fick's first law (Eq. 2-8) the permeability coefficient is calculated by dividing the thickness-corrected steady-state flux by the difference in the partial pressure of the permeant across the polymer film. Thus, the effective permeability can be calculated from the TR values based on initial film thickness when the vapour partial pressure gradient between both film surfaces is known.

4.2.1 Experimental procedures

Several techniques can be utilised for permeability measurements and these have been extensively reviewed by Felder & Huvard (1980). In the present work, the 'isostatic method' was used due to its simplicity and well developed equipment (Merts 1996; Chen et al. 2000). According to Robertson (1993c), the isostatic method utilises a partial pressure difference (the 'pressure gradient') of the test compound across the film as the driving force for permeation. The total pressure on both sides of the film is assumed equal. The partial pressure gradient must be kept constant during the experimental period and this can be done by sweeping one side of the film continuously with the test vapour whilst sweeping an inert gas on the other side into which the test gas diffuses. At selected time intervals, concentrations of the feed and permeant streams are determined and the transmission rate is monitored until the steady-state condition is reached.

Isostatic equipment similar to that described by Merts (1996) was utilised in the present work. A stainless-steel circular permeability cell (I.D. 18 cm) consisting of two chambers separated from each other by the film sample was used (Figure 4-1); the headspace volumes of the lower and upper chambers were ~380 and ~760 ml, respectively.

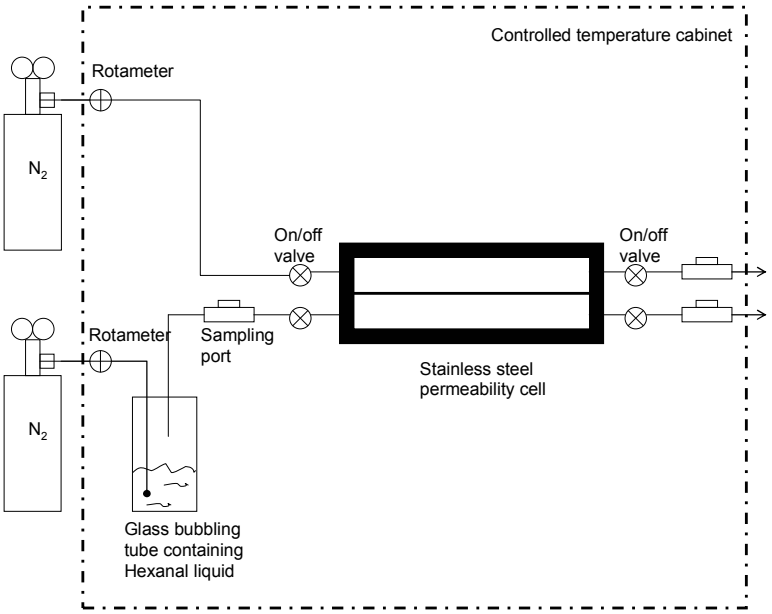

(A)

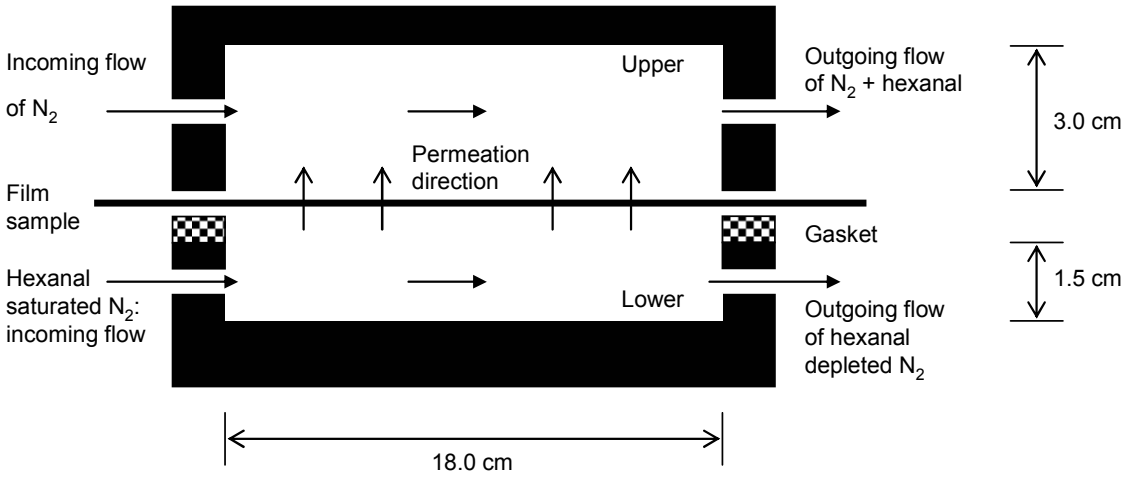

(B)

Figure 4-1 Experimental set-up for measurement of film permeability to hexanal vapour (A) and cross section of stainless steel permeability cell (B) (modified from Merts 1996)

The film was held horizontal on a stainless steel stand during the experiment. A gasket (O.D. 24 cm and I.D. 18 cm) made from a general purpose silicone septa sheet (30 × 30 cm; New Zealand Alltech Inc., Albany, New Zealand) was placed on the mounted film to provide a gas-tight seal between the two chambers. The entry and exit ports fitted into opposite sides of both halves of the permeability cell allowed a continuous gas flow to be passed through each chamber. The permeability cell was sealed by means of a screw-press mounted over the cell. In replicated preliminary studies, a decrease of only 4% in hexanal

concentration (data not shown) was observed over 48 hours when gas samples were sealed inside the permeability cell. This indicated that the permeability cell was tightly sealed and any effects of adsorption by the gasket on changes in hexanal concentration could reasonably be neglected when operating in flow-through mode.

A N_2 stream saturated with hexanal vapour was generated by a liquid-bubbling system similar to that described in Chapter 3. The hexanal vapour concentrations were achieved by adjusting the flow rate through the vapouriser measured using a rotameter (Alborg VA flowmeter 150 mm; Associated Process Controls Ltd., Auckland, New Zealand) connected between a N_2 supply cylinder and the vapouriser (Table 4-1). Outflow rates were measured with a digital gas flow meter (Agilent ADM 1000; J&W Scientific, US). Gas samples of 0.1-ml were taken from a stainless steel T-port, where one branch was fitted with a Teflon septum; one side of the joint was connected to the outlet of the vapouriser and the other was connected with a ~2 m long stainless steel tube (6 mm OD) leading hexanal vapour to either a fumehood or the permeability cell. Hexanal concentrations were quantified using the gas chromatographic procedures described in Chapter 3.

Table 4-1 Hexanal vapour concentrations and carrier gas flowrates delivered to the permeability cell.

Temperature (ºC)	Inlet concentration ranges ($mol \cdot m^{-3}$)	Flow rates of carrier (N_2) introduced to vapouriser ($ml \cdot min^{-1}$)
10	0.02-0.03 [a,b]	15-20
	0.03-0.04 [a,b]	25-30
	0.05-0.06 [a,b]	40-45
20	0.01-0.05[a]	2-5
	0.09-0.10 [a,b]	10-15
	0.12-0.13 [a,b]	20-25
	0.17-0.18 [a,b]	30-35
	0.19-0.20	40-45
	0.22-0.24	50-55

[a] These concentrations were employed for OPP and Tyvek®, while all concentrations were employed for LDPE. The selection of concentrations and flow rates was made following initial experiments on LDPE at 20ºC. It was found that at least three concentration levels were required to describe concentration-dependent permeability.

[b] These concentrations were used in experiments on rates of hexanal consumption by tomatoes (Chapter 3)

Once a constant concentration (Table 4-1) was achieved, hexanal vapour was directly delivered to the permeability cell by connecting the stainless steel tube to the inlet port of the bottom compartment of the cell via stainless steel connections (Swagelok®, Swagelok

Company, Ohio, US). Meanwhile the hexanal-free N_2 flow (controlled at 20-22 ml·min^{-1}) was passed through the upper chamber to maintain the partial pressure gradient across the film material.

It should be noted that hexanal vapour was not humidified as was described by Song et al. (1996) and Johansson & Leufven (1994). This decision was made as the hexanal saturated gas phase within a sachet was expected to be dry for most of the period of interest. Also the literature suggested minimal effects of water vapour on mass transfer of organic volatiles across hydrophobic non-polar films, including LDPE, OPP and Tyvek®, as well as negligible interactions of water vapour with such films. For example DeLassus et al. (1988) reported no effects of RH on the permeation of trans-2-hexenal vapour through Saran® film (vinylidene chloride copolymer).

The times required for achieving steady-state concentrations on both sides of the permeability cell at 10 and 20°C were less than ~8 and ~3.5 hours, respectively[6]. To ensure uniform concentrations in the chambers, the period prior to taking gaseous samples at 10 and 20ºC was set at 10 and 6 hours, respectively. At that time and afterwards, replicate gas samples (0.1 ml) were taken through a port fitted with a Teflon-lined septum fitted to both chambers using a gas-tight syringe (Hamilton Gastight®, Hamilton Co., US). Typically the sampling period was approximately 25-30 minutes.

New film samples were used for each concentration and temperature. Films and all other experimental equipment were equilibrated at the trial temperature for 24 hours before starting the tests. The experimental apparatus was kept in a controlled temperature cabinet (set point ± 1ºC).

The effective hexanal vapour permeabilities of three polymer films were measured. The films used were Low Density Polyethylene (LDPE) (30 μm; Propak Supplies, Palmerston North, New Zealand), Oriented Polypropylene (OPP) (20μm; Huhtamaki, New Lynn, New Zealand), and Tyvek® (173 μm; Type 10, Dupont, Wilmington, US). These three films are commonly used in MAP systems for food and horticultural products. Tyvek® is also

[6] Preliminary experiments were performed using OPP films which have the lowest permeabilities to hexanal vapour

commonly used for making sachets, such as those containing O_2 scavengers, C_2H_4 absorbers and desiccants, due to its porosity and durability to both liquid water and a range of chemicals, including ethyl acetate, formaldehyde and glycerol (Marotta 1997; Anonymous 2004).

The effective film permeability was estimated using Eq. 4-1:

$$P_{film}^{Hxl} = \frac{Q_{l,conc}^{out} \cdot C_{l,conc}^{Hxl} \cdot L_{film}}{A_{film}\left(C_{h,conc}^{Hxl} - C_{l,conc}^{Hxl}\right) \cdot R \cdot T_{film}} \qquad \textbf{(Eq. 4-1)}$$

where

P_{film}^{Hxl} = Effective film permeability to hexanal (mol·m·m^{-2}·s^{-1}·Pa^{-1})

$Q_{l,conc}^{out}$ = Outlet gas flowrate from the low hexanal concentration side of the film (m^3·s^{-1})

$C_{h,conc}^{Hxl}$, $C_{l,conc}^{Hxl}$ = Hexanal concentration at the high and low concentration side of the film, respectively (mol·m^{-3})

4.2.2 Results and discussion, part I : Overall effective permeability and concentration dependent characteristics

The effective hexanal permeability of LDPE (P_{LDPE}^{Hxl}), OPP (P_{OPP}^{Hxl}) and Tyvek® (P_{Tyvek}^{Hxl}) are illustrated as functions of the mean hexanal vapour concentration across the film in Figure 4-2. In all experiments both surfaces of the tested film were exposed to different concentrations of hexanal vapour. As the differences in hexanal vapour concentration were always relatively small in these experiments (with the feed typically ≤ 1.5-fold the permeate side concentration), it was assumed that an arithmetic average was be a reasonable basis on which to express the permeability. However up to 10-fold difference was observed for in the case of OPP; the implications of this are discussed later in this section.

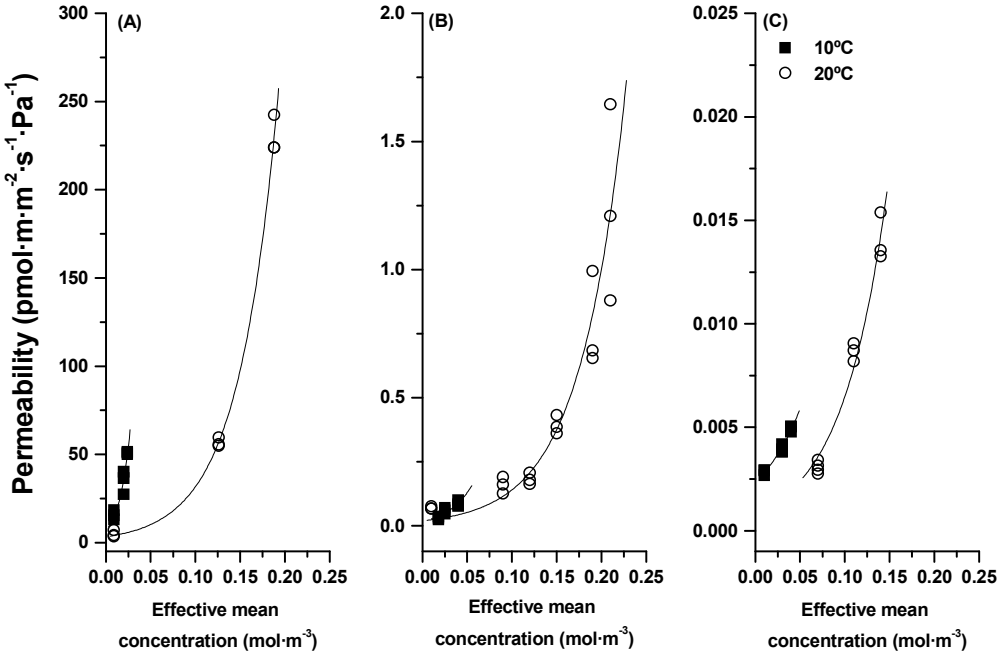

Figure 4-2 Effective permeability to hexanal of Tyvek® (A), LDPE (B) and OPP (C) measured at 10 and 20°C. (Three replicates are shown for each concentration difference tested). The solid lines were fitted using nonlinear regression (Eq. 4-3). Note a different y-axis scale was chosen for each graph to better represent the data.

Considered at the similar average concentration of 0.12-0.13 mol·m^{-3} at 20ºC, P_{Tyvek}^{Hxl} was about 300 and 6,000-fold higher than the values of P_{LDPE}^{Hxl} and P_{OPP}^{Hxl}, respectively. The value of P_{LDPE}^{Hxl} at 0.12-0.13 mol·m^{-3} and 20°C was therefore ~20-fold higher than the equivalent value of P_{OPP}^{Hxl}. The same order of permeability, $P_{Tyvek}^{Hxl} > P_{LDPE}^{Hxl} > P_{OPP}^{Hxl}$, was also observed at 10ºC, with P_{Tyvek}^{Hxl} values at 0.02-0.03 mol·m^{-3} being more than 250 times higher than those of the LDPE and OPP films.

At a given temperature, all the effective film permeabilities increased exponentially with increasing concentration (Figure 4-2). At 10ºC, permeability to hexanal vapour of all films increased by 2.5 to 4-fold as hexanal vapour concentrations increased from ~0.02 to ~0.05 mol·m^{-3}. At 20ºC, as the concentrations increased from ~0.01 to ~0.24 mol·m^{-3}, increases of P_{Tyvek}^{Hxl}, P_{LDPE}^{Hxl}, and P_{OPP}^{Hxl} were approximately 62-, 24-, and 3-fold, respectively. Similar exponential relationships between permeability (or permeance) and concentration were

reported in other systems, including ethyl acetate, toluene, d-limonene, α-pinene and methyl-ethyl-ketone in OPP films (Huang & Giacin 1998), and benzene, hexane and cyclohexane in LDPE and polyether-block-amide (PEBA-4033PE) membranes (Friess et al. 2004). Many further examples of the concentration dependence of mass transfer through polymer films or membranes can be found in literature (Rogers et al. 1962; Zobel 1982; Rogers 1985; Mulder 1991; Piringer 2000).

In Figure 4-2, it can be observed that the permeability for a given film at 10ºC appeared higher than that at 20ºC for comparable hexanal concentrations. This could be explained by the dominance of the sorption process in permeation of hexanal across the film. According to Robertson (1993c), sorption of readily condensable volatiles (including hexanal) by the polymer film tends to be thermodynamically favoured at lower temperatures and the relationship between solubility and temperature can be described by an Arrhenius-type equation (Eq. 4-2).

$$S^{i}_{film} = S^{i}_{film,0}\ exp\left(-\Delta H_s \,/\, RT_{film}\right) \qquad \textbf{(Eq. 4-2)}$$

where

S^{i}_{film} = Film solubility to permeant *i* ($mol \cdot m^{-3} \cdot Pa^{-1}$)

$S^{i}_{film,0}$ = Fitted pre-exponential factor for solubility to permeant *i* of the film ($mol \cdot m^{-3} \cdot Pa^{-1}$)

ΔH_s = Heat of solution for the permeant gas ($J \cdot mol^{-1}$)

At higher concentrations, the diffusion process should be facilitated by the increased plasticisation due to sorbed hexanal molecules. Leufven & Stollman (1992) similarly reported the dominance of sorption processes in permeation of hexanal and other aldehydes, including butanal, pentanal, and heptanal through PP, PVC, LLDPE and EVA/PE/EVA films. The permeability values showed a generally decreasing trend as temperature increased from 5-75ºC.

An empirical exponential relationship (Eq. 4-3) was used to describe permeability as a function of the concentration of hexanal vapour as shown in Figure 4-2. This exponential modelling approach has been successfully utilised in other studies to describe concentration dependence of diffusivity of benzyl acetate, 2-methoxyphenol and d-limonene in OPP film (Zobel 1982) and dichloromethane in PP film (D'Aniello et al.

2000). The parameters estimated for hexanal vapour permeability (using Origin 5.0 Nonlinear regression package; Microcal Origin Inc. US) are shown in Table 4-2.

$$P_{film}^{Hxl} = P_{film,0}^{Hxl}\, exp\left(C_{avg}^{Hxl} \cdot b_{film}\right) \qquad \textbf{(Eq. 4-3)}$$

where

$P_{film,0}^{Hxl}$ = Fitted pre-exponential factor for effective permeability to hexanal of the film (pmol·m·m^{-2}·s^{-1}·Pa^{-1})

C_{avg}^{Hxl} = Effective mean of hexanal concentrations measured in both chambers of the permeability cell at steady-state (mol·m^{-3})

b_{film} = Fitted exponential coefficient of effective permeability to hexanal of the film (m^{3}·mol^{-1})

Table 4-2 Parameter estimates and standard errors (SE) resulting from nonlinear regression analysis of permeability to hexanal vapours of Tyvek®, LDPE, and OPP films, measured at 10 and 20ºC

Temperature (ºC)	Tyvek®			LDPE			OPP		
	$P_{Tyvek,0}^{Hxl}$ (SE) [a]	b_{Tyvek} (SE)	n [b]	$P_{LDPE,0}^{Hxl}$ (SE)	b_{LDPE} (SE)	n	$P_{OPP,0}^{Hxl}$ (SE)	b_{OPP} (SE)	n
10	7.06 (22.6)	81.6 (12.4)	9	0.02 (27.1)	38.5 (20.2)	9	0.002 (4.3)	18.7 (7.0)	9
20	3.33 (18.1)	22.5 (4.3)	9	0.02 (56.2)	19.6 (14.2)	18	0.001 (20.0)	19.7 (7.8)	9

[a] The standard errors (SE) are expressed as a percentage relative to the estimated values. The nonlinear regressions were performed using the Nonlinear Regression package of Origin 5.0 (Microcal Software Inc., US).

[b] *n* is the number of observations.

where

$P_{Tyvek,0}^{Hxl}$, $P_{LDPE,0}^{Hxl}$, $P_{OPP,0}^{Hxl}$ = Fitted pre-exponential factor for effective permeability to hexanal of Tyvek®, LDPE and OPP films, respectively (pmol·m·m^{-2}·s^{-1}·Pa^{-1})

b_{Tyvek}, b_{LDPE}, b_{OPP} = Fitted exponential coefficient of effective permeability to hexanal of Tyvek®, LDPE and OPP films, respectively (m^{3}·mol^{-1})

Although results from the exponential model predictions show reasonable agreement with the experimental data, high uncertainty (represented by the SE values) can be observed, noticeably for $P_{LDPE,0}^{Hxl}$ measured at 20ºC (Table 4-2). Variations observed in permeability coefficients may be assumed to be due to interactions between hexanal vapour and polymer films, causing concentration dependence of mass transfer processes. Robertson (1993c) suggested that permeation of organic vapours through polymer films was complicated by mass transfer processes due to the concentration dependence of both solubility and diffusivity.

Because effective permeability in the present work was determined based on Fick's first law, it is interesting to investigate the relationship between hexanal concentration and position within the film, which is commonly assumed to be linear (Robertson 1993c). According to Selke et al. (2004), this assumption is suitable for a system at low permeant concentrations, for which permeability is generally assumed to have a low (or no) concentration dependence. To demonstrate the effects of permeant concentration on the within-film concentration gradients, a mathematical model (Eq. 4-4) was developed to describe the relationship of hexanal concentration with film position. Details of the mathematical model derivation and solution are provided in Appendix D.2.1.

$$\frac{x_{film}}{L_{film}} = \frac{exp\left(C_{h,conc}^{Hxl} \cdot b_{film}\right) - exp\left(C_{g,x_{film}}^{Hxl} \cdot b_{film}\right)}{exp\left(C_{h,conc}^{Hxl} \cdot b_{film}\right) - exp\left(C_{l,conc}^{Hxl} \cdot b_{film}\right)} \qquad \textbf{(Eq. 4-4)}$$

where

$C_{g,x_{film}}^{Hxl}$ = Hexanal concentration in the gas phase which is equilibrium with film at position x in film material (x_{film}) (mol·m^{-3})

x_{film} = Position in film material (m)

In the experimental trials, high concentration gradients were observed between film surfaces for the OPP film as expected due to its relatively low permeability to hexanal vapour. The effect of high and low surface permeant concentrations ($C_{h,conc}^{Hxl}$ and $C_{l,conc}^{Hxl}$ selected from the experimental data at 20ºC as 0.264 and 0.025 mol·m^{-3}, respectively) on the predicted steady-state concentration gradients for OPP films are illustrated in Figure 4-3. A nonlinear concentration gradient is apparent for OPP (Figure 4-3) such that a very rapid decrease in predicted concentration occurs in a relatively thin layer of the film

adjacent to the low concentration side. A similar nonlinear gradient in OPP film at 10ºC is predicted for the lower feed side concentration ($C_{h,conc}^{Hxl}$ and $C_{l,conc}^{Hxl}$ as 0.07 and 0.005 mol·m^{-3}, respectively) (Figure 4-3). DeLassus & Jenkins (1986) similarly reported that the greatest partial pressure changes during permeation of d-limonene (from orange juice) across multilayer-films having the same thickness occurred within the layer having the lowest permeability.

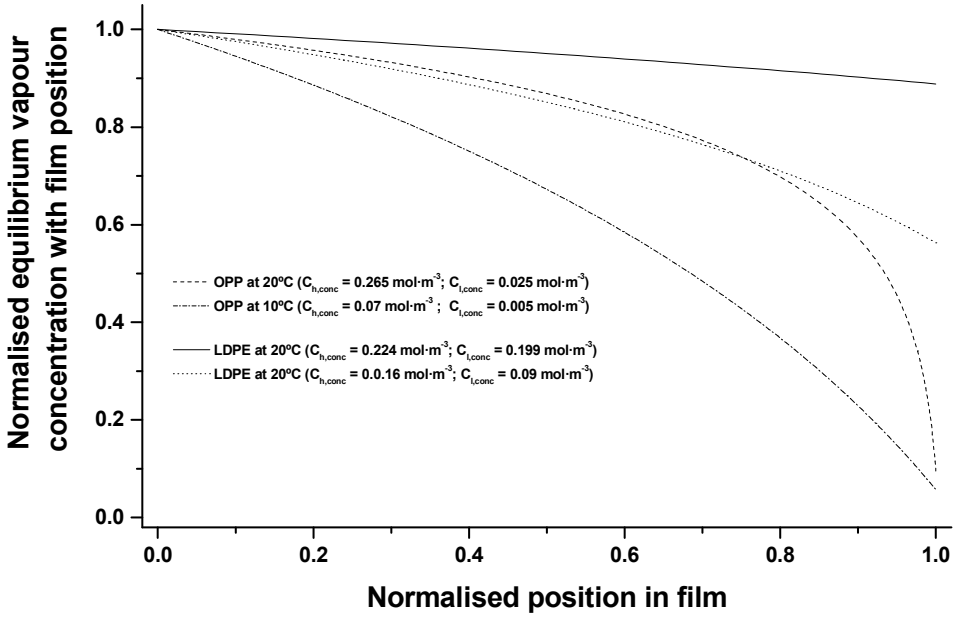

Figure 4-3 Steady-state concentration gradients predicted using Eq. 4-4 for conditions when large (as a case of OPP film; dashed and dashed-dotted line) and small and moderate (as a case of LDPE film; solid and dotted lines, respectively) concentration gradients. On the x-axis, x= 0 represents the film surface facing the high hexanal concentration ($C_{h,conc}^{Hxl}$) and x = 1 the film surface facing against the low concentration ($C_{l,conc}^{Hxl}$).

By implementing Eq. 4-4 for LDPE film (with $C_{h,conc}^{Hxl}$ and $C_{l,conc}^{Hxl}$ equal to 0.224 and 0.199 mol·m^{-3}, respectively; 20ºC), a more linear steady-state concentration gradient was observed (Figure 4-3). When the difference between feed and downstream concentrations becomes greater (e.g. $C_{h,conc}^{Hxl}$ and $C_{l,conc}^{Hxl}$ of 0.16 and 0.09 mol·m^{-3}, respectively, at 20ºC; the largest gradient observed in the LDPE experiments), only a slight deviation from the linear gradient is noticeable. The high porosity and permeability properties of the Tyvek® film are confirmed by the small differences of steady-state concentrations at both sides of the

films (≤ 9%) and a nearly-horizontal and linear concentration gradient can then be expected.

The predictions obtained using Eq. 4-4 support the assumption that a linear and small internal (within film) concentration gradient occurs in systems with low permeant concentrations and low concentration gradients between the chambers. This analysis supports that the use of an arithmetic average to characterise the influence of hexanal vapour concentration on permeability is reasonable, particularly for Tyvek® and LDPE films.

The results (Figure 4-3) also demonstrate that when large vapour concentration differences occur across a film (such as may be expected in the first stages of volatile release from a sachet), the assumption of a linear gradient to estimate the mass transfer rate across the film (e.g. using Fick's first law as shown in Eq. 2-8) may not be appropriate and the flux may be underestimated. In this case (when the exponential dependency of permeability to concentration applies; Eq. 4-3), Eq. 4-5 is suggested to be more suitable to predict the hexanal flux across the film. Eq. 4-5 was derived based on the fact that the steady-state flux at any point in the film is the same even though the local hexanal concentration and hence permeability will vary. The derivation of this equation is given in Appendix D.2.2.

$$J_{film} = \frac{P_{film,0}^{Hxl} RT_{film}}{b_{film} L_{film}} \left(exp\left(C_{h,conc}^{Hxl} \cdot b_{film} \right) - exp\left(C_{l,conc}^{Hxl} \cdot b_{film} \right) \right) \quad \textbf{(Eq. 4-5)}$$

where

J_{film} = Steady-state flux across film (mol·s^{-1}· m^{-2})

Comparisons of fluxes across a LDPE film calculated using Eq. 2-8 and Eq. 4-5 are shown in Table 4-4. It can be seen that no significant differences in predicted steady-state fluxes occur at low hexanal concentration differences across the film such as scenarios 1 to 4. When the concentrations difference between both sides of the film become greater (as shown by scenarios 5 and 6), Eq. 2-8 estimates the flux to be much lower than Eq. 4-5 does. For this reason, Eq. 4-5 is expected to be more suitable equation to describe hexanal release from a sachet.

Table 4-4 Comparison of hexanal steady-state flux across LDPE film calculated using Eq. 2-8 and Eq. 4-5.

Illustrative scenarios	$C_{h,conc}^{Hxl}$ (mol·m^{-3})	$C_{l,conc}^{Hxl}$ (mol·m^{-3})	Flux calculated using Eq. 2-8 (mol·m^{-2}·s^{-1}) [a]	Flux calculated using Eq. 4-5 (mol·m^{-2}·s^{-1}) [a]	Relative ratio
1 [b]	0.01	0.003	1.21×10^{-8}	1.21×10^{-8}	1.00
2 [b]	0.20	0.17	2.28×10^{-6}	2.33×10^{-6}	1.02
3 [b]	0.22	0.19	2.58×10^{-6}	2.61×10^{-6}	1.01
5 [c]	0.46	0.00	6.75×10^{-5}	6.85×10^{-4}	10.15
6 [d]	0.23	0.002	3.56×10^{-6}	7.39×10^{-6}	2.08

[a] LDPE film of 30μm thickness and the coefficients of effective permeability utilised in both equations were those estimated for 20ºC as shown in Table 4-2.

[b] Actual values of both $C_{h,conc}^{Hxl}$ and $C_{l,conc}^{Hxl}$ obtained in experiments

[c] A scenario representing the onset of hexanal release from the sachet in which concentrations in the sachet headspace and package were assumed equal to the saturated hexanal concentration at 20ºC and zero, respectively.

[d] A scenario representing the situation when the hexanal concentration in the package headspace attains the MIC level (40 ppm; 0.002 mol·m^{-3}) and that in the sachet headspace is a half of the saturated hexanal concentration at 20ºC.

4.2.3 Results and discussion, part II: Comparison of experimentally measured permeabilities with published data

In this section, the measured hexanal permeabilities in LDPE, OPP and Tyvek® are compared to data available in the literature. Storage temperatures (which also influence glass transition behaviour (T_g) in addition to the effects on sorption and diffusion processes), relative humidity, and concentration dependence are key factors among others, potentially affecting film permeability to volatile organic compounds (VOCs) (Robertson 1993c; Brandsch & Piringer 2000; Piringer 2000; Selke et al. 2004; Dury-Brun et al. 2007).

4.2.3.1 Tyvek® film

The high values of P_{Tyvek}^{Hxl} obtained in the present work (Figure 4-2) were unsurprising given the known porous structure of Tyvek® (Marotta 1997; Anonymous 2004). Although there is no reported information on Tyvek® permeability to hexanal vapour, its permeability to other volatile organic compounds (VOCs) has been studied in regard to construction and building materials (Yang et al. 2005). These data are summarised in Table 4-3.

Table 4-3 Estimated permeability to various VOCs of Tyvek® building materials measured at 23ºC (modified from Yang et al. 2005) [a]

Organic vapours	Initial concentration in material ($mol \cdot m^{-3}$)	P^{i}_{Tyvek} ($pmol \cdot m \cdot m^{-2} \cdot s^{-1} \cdot Pa^{-1}$) [b]
Undecane	3.18×10^{-4}	4.98
2-pentyl-furan	2.32×10^{-4}	3.02
1-octen-3ol	2.95×10^{-3}	10.83

[a] The technique employed by Yang et al. (2005) is described as headspace analyses in which the tested sample was placed in a small sealed chamber. Levels of the compound accumulating in the headspace were then dynamically analysed until a steady-state was attained

[b] Permeability was estimated from reported partition coefficients (K^{i}_{Tyvek}, dimensionless; $S^{i}_{Tyvek} = K^{i}_{Tyvek} \big/ RT_{Tyvek}$, $mol \cdot m^{-3} \cdot Pa^{-1}$), and diffusivity (D^{i}_{Tyvek}, $m^2 \cdot s^{-1}$) of test compounds, through the relationship: $P^{i}_{Tyvek} = D^{i}_{Tyvek} \times S^{i}_{Tyvek}$.

When considered at the same concentrations as reported in Table 4-3, the magnitudes of permeability to hexanal vapour of Tyvek® (P^{Hxl}_{Tyvek}) predicted by Eq. 4-3, (~3.35 $pmol \cdot m \cdot m^{-2} \cdot s^{-1} \cdot Pa^{-1}$) appears comparable to those of undecane and 2-pentyl-furan, but nearly 3-fold (at ~3.56 $pmol \cdot m \cdot m^{-2} \cdot s^{-1} \cdot Pa^{-1}$) lower than that reported for 1-octen-3ol. Tyvek® has been recently reported as a suitable material for making sachets containing active systems that release volatile compounds, such as eugenol volatiles for maintaining colour of tamarillo stem (Pongjaruwat 2007) and chlorine dioxide for suppressing growth of *Erwinia carotovora* subsp. *carotovora* (the pathogen causing bacterial soft rot) inoculated on tomato (Mahovic et al. 2007). However, the permeabilities of Tyvek® to either eugenol or chlorine dioxide were not reported by the authors.

4.2.3.2 OPP film

Whilst there is no information reported on P^{Hxl}_{OPP}, the permeabilities of PP film to hexanal (designated as P^{Hxl}_{PP}) and other aldehydes quantified in the range of 5-75°C were reported by Leufven & Stollman (1992) as shown in Table 4-4. OPP film is a modification of PP through an orientation technique (by stretching the film to cause molecular realignment) that improves the film properties with regard to crystallinity, barrier behaviour and strength

(Selke et al. 2004). The reported values of P_{OPP}^{Hxl} are consistently much lower than those of P_{PP}^{Hxl} (Table 4-4), indicating that OPP is a better barrier to hexanal than PP film.

The permeability of OPP films to other VOCs is also summarised in Table 4-4. The concentration and temperature dependency of OPP film permeability found in the present study is confirmed by results reported by Huang & Giacin (1998), Zobel (1982) and Liu et al. (1991) for a range of VOCs. Also, the magnitude of effective OPP permeability to hexanal vapour quantified in the present work was in line with that of OPP permeability to other VOCs (Table 4-4).

Liu et al. (1991) reported that RH affected permeability of PVDC-coated OPP to toluene. Significant influences of RH were reported for toluene with concentrations in the range of 0.0016-0.0024 mol·m^{-3}, where the permeability at 21ºC increased as the RH increased from 0% (dry condition) to 86%. However the effect of varying RH was minimal at higher toluene concentrations (0.0033 mol·m^{-3}). Liu et al. (1991) postulated that the RH effects resulted from water vapour interactions with unidentified hydrophilic surfactants incorporated in the PVDC coating resin. These interactions were proposed to occur concurrently with those between toluene and PVDC contributing to a relaxation in the molecular structures of the PVDC coating and yielding a high toluene concentration dependency of the permeability values. Because OPP and PVDC films have relatively low solubility for water vapour but relatively high solubility for toluene, this could also be the reason for there being no RH effect on permeation at high toluene concentrations, where the effects of water vapour-surfactant interactions on structural relaxation of the OPP polymer could be outweighed by the interactions between toluene and PVDC. At a given relative humidity, Liu et al. (1991) reported the strong toluene concentration dependent permeability of OPP films. Overall, at high toluene concentrations and in the absence of a hydrophilic surfactant, RH effect appears not to be a significant factor.

Table 4-4 Comparison of permeability of OPP and PP films to hexanal and other selected volatile organic compounds (VOCs)

Ref. no. [a]	Film type	Compound	Temp (ºC)	Concentration level (Conc.; mol·m^{-3})	RH level (%)	Permeability (pmol·m·m^{-2}·s^{-1}·Pa^{-1})	Reported significant dependence of permeability [b]		
							Temp.	Conc.	RH
[1]	OPP	Hexanal	10	0.01, 0.03, & 0.04	No	0.003, 0.004, & 0.005 [c]	Yes	Yes	n/a
	OPP		20	0.07, 0.11, & 0.14	"	0.003, 0.010, & 0.014 [c]	"	"	"
[2]	PP	Hexanal	5-75	0.001-0.20 [d]	"	0.02-0.04	Yes	n/a	n/a
		Butanal	"	0.01-0.12 [d]	"	0.01-0.025	"	"	"
		Pentanal	"	0.01-0.5 [d]	"	0.005-0.04	"	"	"
		Heptanal	"	0.0004-0.06 [d]	"	0.005-0.07	"	"	"
[3]	OPP [e]	Ethyl acetate	30	0.44, 0.98, & 1.91	"	0.0002, 0.0003, & 0.01 [c]	Yes	Yes	n/a
			40	0.43, 0.95, & 1.85	"	0.0007, 0.0008, & 0.015 [c]	"	"	"
			50	0.42, 0.92, & 1.79	"	0.0017, 0.0018, & 0.0195 [c]	"	"	"
		d-Limonene	40	0.014, 0.028, & 0.05	"	0.002, 0.008, & 0.012 [c]	"	"	"
			50	0.013, 0.027, & 0.053	"	0.004, 0.019, & 0.024 [c]	"	"	"
			60	0.013, 0.026, & 0.052	"	0.009, 0.034, & 0.042 [c]	"	"	"
[4]	B-OPP [f]	Benzyl acetate	25	0.0002, 0.0006, 0.002, & 0.004 [g]	"	0.02, 0.019, 0.03, & 0.04 [c]	n/a	Yes	n/a
		2-methoxy-phenol	"	0.0001, 0.0008, 0.0013, 0.0016, 0.0017, 0.003, & 0.006 [g]	"	0.0128, 0.0133, 0.0128, 0.016, 0.017, 0.017, & 0.020 [c]	"	"	"
		d-Limonene	"	0.0014, & 0.06 [g]	"	0.003, & 0.05 [c]	"	"	"
[5]	B-OPP [f,h]	Ethanol	25	0.09	"	0.0003	n/a	n/a	n/a
		Methanol	"	0.17	"	0.0009	"	"	"
		Menthol	"	0.002	"	0.009	"	"	"
		Propanal	"	0.12	"	0.0004	"	"	"
[6]	OPP [i]	Toluene	21	0.0016	56 & 86	0.00001, & 0.015 [j]	n/a	Yes	Yes
				0.0024	0, 56 & 86	0.0004, 0.003, & 0.015 [j]	"	"	"
				0.0033	"	7.56, 7.24, & 7.94 [j]	"	"	No

[a] [1] The present work, [2] Leufven & Stollman (1992), [3] Huang & Giacin (1998), [4] Zobel (1982), [5] Zobel (1985), and [6] Liu et al. (1991)

[b] "n/a" = not available information, 'Temp.' = temperature, and 'Conc.' = concentration.

[c] Permeability values were reported in the order of concentrations shown in the 'concentration level' column.

[d] Concentrations used in experiments were reported as 'a range of concentration', instead of specific values for individual measured permeability.

[e] There are also reports on OPP permeability to toluene, methyl-ethylketone, and α-pinene; the trends of these were similar to those shown in Table 4-4.

[f] BOPP represents a biaxially-OPP with co-extruded surface layer (SCB30).

[g] Reported as vapour concentration gradient between two surfaces of a tested film.

[h] There are also reports on B-OPP permeability to a range of VOCs, such as acetic acid, decane, ethane, guaiacol, heptyl acetate and xylene.

[i] Two-side-PVDC-coated OPP.

[j] Permeability values were reported in the order of relative humidities shown in the 'RH level (%)' column.

Both P_{PP}^{Hxl} and P_{OPP}^{Hxl} show a positive trend of temperature dependence in the range of 5 to 25ºC (Table 4-4). However Leufven & Stollman (1992) reported that P_{PP}^{Hxl} values decreased by nearly 50% as the temperature increased from 25 to 75ºC and noted a similar

temperature dependence for PP permeability to each of butanal, pentanal, and heptanal. They suggested that this discontinuous nature of temperature dependence may be due to a reduced sorption of the VOC as the temperature increased, which in turn reduced the overall permeability (as earlier discussed in section 4.2.2).

In general, values of P_{OPP}^{Hxl} were approximately 10-fold lower than those of P_{PP}^{Hxl} over a range of 5 to 25ºC (Table 4-4). As noted, this suggests that the OPP film provides a better barrier to hexanal permeation, as could be expected from the improved barrier properties resulting from the orientation technique. The key contributor to the superior barrier property to hexanal transfer of OPP films is expected to be the increase in crystallinity. The crystallinities of OPP and PP films are reportedly about 80% (Willige et al. 2002) and 39% (Charara et al. 1992), respectively. Regions of high crystallinity are considered impermeable, thus creating longer diffusion paths and reducing the area for permeation, so retarding diffusion processes (Giacin 1987; Dury-Brun et al. 2007). The effects of crystallinity on mass transfer processes across polymer film materials have been well studied, e.g. for toluene and N-heptane in PE (Lutzow et al. 1999), dichloromethane in PP (D'Aniello et al. 2000), and various flavour compounds in PET, polycarbonate (PC), and polyethylene naphthalate (PEN) (Willige et al. 2002).

Willige et al. (2002) reported that OPP film (30μm film thickness; 0.916 g·cm^{-3} film density) minimally absorbed hexanal (less than 0.1 mmol·m^{-2} [*sic*]) and other flavour compounds, such as linalool, octanol, and limonene at 4ºC because this temperature is close to OPP's glass transition temperature (T_g) of -5 to 0ºC. The glass transition temperature is a measure of the mobility of the polymeric chain and is considered a key factor among others (such as polymeric composition and surface treatments) that could affect the rate of permeation processes (Brandsch & Piringer 2000; Selke et al. 2004). A film kept at a temperature close to or lower than its T_g is likely to have a higher proportion of the glassy and hard structures in which free rotation of polymers is restricted and the free volume for diffusion is subsequently reduced. Therefore, diffusion is expected to proceed at a slower rate. As the temperature increases above T_g, there is a rearrangement of polymeric molecules toward the so-called rubbery state, where faster diffusion and hence quicker attainment of equilibrium can occur. Table 4-5 summarises T_g values of a range of polymer films for food packaging applications.

Table 4-5 Summary of T_g values of a range of polymer films for food packaging applications (modified from Brandsch & Piringer 2000; Willige et al. 2002; Selke et al. 2004)

Polymer film [a]	Glass transition temperature (T_g ; ºC)
LDPE, LLDPE, HDPE [b]	-120 to -22
Non oriented PP (PP)	-22 to -12
OPP	-5 to 0
PS	74 to 105
PVC	90
PVDC	-17
PET	70-83
EVOH	55 to 70
PVOH	85
PEN	78 to 120
PC	120 to 150
PVAC	28-31

[a] LDPE = Low Density Polyethylene, LLDPE = Linear Low Density Polyethylene, HDPE = High Density Polyethylene, PP = Polypropylene, OPP = Oriented Polypropylene, PS = Polystyrene, PVC = Polyvinyl chloride, PVDC = Polyvinylidene chloride, EVOH = Ethylene Vinyl Alcohol, PVOH= Polyvinyl Alcohol, PEN = Polyethylene naphthalate, PC = Polycarbonate, and PVAC = Polyvinyl Acetate.

[b] Data documented by Selke et al. (2004) and Brandsch & Piringer (2000) for all of these PE-based films were considered greatly different, and these are -120 and -30 ± 5, respectively.

From Table 4-5, it can be inferred that at ambient temperature (i.e. 20°C), LDPE film has more polymeric chains in the rubbery state than films such as PET and EVOH, suggesting the barrier properties to gas and vapour permeation of these latter films will also be better than those of LDPE film.

4.2.3.3 LDPE film

At present, the only literature available on P_{LDPE}^{Hxl} is the report by Song et al. (1996) (Table 4-6). However there are also reports of permeability to hexanal vapour of other films in the polyethylene family, for example HDPE, LLDPE, EVOH and multi-layer films such as EVA/PE/EVA (Table 4-6). For LDPE, Song et al. (1996) reported that the temperature dependence of P_{LDPE}^{Hxl} for 0 to 30°C was well described by the Arrhenius relationship (Eq. 2-10) (also discussed in section 2.5.2). Predicted permeabilities to hexanal vapour at 10 and 20 °C using Eq. 2-10 (~0.025 and 0.047 pmol·m·m^{-2}·s^{-1}·Pa^{-1}, for 10 and 20 °C, respectively) are reasonably comparable to data identified in the present work (Table 4-6;

assuming minimal effects of concentration dependence, as also discussed later in this section), if the coefficients of the Arrhenius model identified by the nonlinear regression of permeability values reported by Song et al. (1996) are used (i.e. the Arrhenius model fitted pre-exponential factor for permeability to hexanal vapour ($P_{LDPE,0}^{Hxl}$) and energy of activation (Ea) of 5.35×10^{-6} mol·m·m^{-2}·s^{-1}·Pa^{-1}and 45.20 kJ·mol^{-1}, respectively). The trends of temperature dependence of P_{LDPE}^{Hxl} in the present work were also consistent with those reported by Song et al. (1996). The temperature dependence of other polymer films to hexanal and other compounds reported in the literature is summarised in Table 4-6.

P_{LDPE}^{Hxl} values measured at 10 and 20°C in the present work were comparable to those reported by Song et al. (1996), although concentrations 10-fold different were utilised (Table 4-6). According to Eq. 4-3 and coefficients reported in Table 4-2, the predicted values for P_{LDPE}^{Hxl} at 10 and 20°C at the concentrations of 0.002-0.003 mol·m^{-3} examined by Song et al. (1996) were approximately 0.019 and 0.020 pmol·m·m^{-2}·s^{-1}·Pa^{-1}, respectively. These are lower but not markedly so than the values reported by Song et al. (1996) of 0.03 and 0.05 pmol·m·m^{-2}·s^{-1}·Pa^{-1}, respectively. These data suggests that P_{LDPE}^{Hxl} can reasonably be modelled as concentration independent over the low concentration range of 0.002-0.02 mol·m^{-3}.

Table 4-6 Comparison of permeability of LDPE and other polyethylene family films to hexanal and other selected volatile organic compounds (VOCs)

Ref. no. [a]	Film type	Compound	Temp (ºC)	Concentration level (Conc.; mol·m^{-3})	RH level (%)	Permeability (pmol·m·m^{-2}·s^{-1}·Pa^{-1})	Reported significant dependence of permeability [b]		
							Temp.	Conc.	RH
[1]	LDPE	Hexanal	10	0.02, 0.03, & 0.04	No	0.03, 0.06, & 0.09 [c]	Yes	Yes	n/a
			20	0.01, 0.09, 0.12, 0.15, 0.19, & 0.21	"	0.07, 0.16, 0.18, 0.39, 0.78, & 1.24 [c]	"	"	"
[2]	LDPE	Hexanal	0-30	0.002-0.003 [d]	Humidified [e]	0.01-0.09	Yes	n/a	n/a
[3]	LLDPE [f]	Hexanal	5-75	0.001-0.2 [d]	No	0.02-0.05	Yes	n/a	n/a
	EVA/PE/EVA [f]		"	"	"	0.02-0.03	"	"	"
	EVA/PP/EVA [f]		"	"	"	0.01-0.05	"	"	"
[4]	LLDPE [g]	Hexanal	25	0.001-0.2 [d]	20-82	0.01- 0.03	n/a	n/a	Yes
	HDPE		"	"	"	0.01-0.03	"	"	"
	EVOH		"	"	"	4.0×10^{-5}-0.01	"	"	"
[5]	Exact ™ 4151 [h]	Hexanal	5	0.030	No	2.30×10^{-5}	Yes	Yes	n/a
	Exact ™ 4151		25	0.033 & 0.034	"	4.60 - & 8.10- $\times 10^{-5}$ [c]	"	"	"
[6]	LDPE	trans-2-hexenal	28	0.003, 0.005, 0.008, & 0.01	No	0.119, 0.118, 0.155, & 0.120 [c]	n/a	No	n/a
	EVOH		45	0.005	0 & 90	0.00003, & 0.002 [i]	Yes	n/a	Yes
			75	0.005	0 & 90	0.0002, & 0.01 [i]	"	"	"
	Saran ®		75	0.005	0 & 90	0.00045, & 0.00043 [i]	n/a	n/a	No
[7]	HDPE [j]	Ethyl acetate	30	0.44, 0.97, & 1.90	No	0.004, 0.010, & 0.013 [c]	Yes	Yes	n/a
			40	0.43, 0.95, & 1.85	"	0.008, 0.013, & 0.017 [c]	"	"	"
			50	0.41, 0.92, & 1.79	"	0.012, 0.015, & 0.022 [c]	"	"	"

[a] Reference numbers refer to [1] The present work, [2] Song et al. (1996), [3] Leufven & Stollman (1992), [4] Johansson & Leufven (1994), [5] Wolford (1998), [6] DeLassus et al. (1988), and [7] Huang & Giacin (1998), respectively. Polymer abbreviations: EVA, PE, EVOH, and Saran® represent ethylene vinyl acetate, polyethylene, ethylene vinyl alcohol, and commercial name of polyvinylidene chloride copolymer, respectively.

[b] "n/a" = not available information, "Temp." = temperature, and "Conc." = concentration.

[c] Permeability values were reported in the order of concentrations shown in the 'concentration level' column.

[d] Concentrations used in experiments were reported as 'a range of concentration', instead of specific values for individual measured permeability.

[e] No reported actual value but described as 'humidified'.

[f] There were also reports on permeability of these films to butanal, pentanal, and heptanal. Temperature effects on these permeability have similar trends as reported for hexanal in Table 4-6.

[g] There were also reports on permeability of these films to butanal, pentanal, heptanal, octanal and decanal. The effect of RH on permeability of these were similar to those reported for hexanal in Table 4-6.

[h] Metallocene catalysed ethylene-hexene copolymer, (Exxon Chemical, US).

[i] Permeability values were reported in the order of relative humidities shown in the 'RH level (%)' column.

[j] There were also reports on HDPE permeability to toluene, d-limonene, methyl-ethylketone, and α-pinene. Concentration and temperature effects on permeability show similar trends to those reported for hexanal in Table 4-6.

From Table 4-6, measured P_{LDPE}^{Hxl} values tended to be higher than hexanal permeability of LLDPE, HDPE, multilayer film (i.e. EVA/PP/EVA and EVA/PE/EVA), and metallocene polymer films. The good barrier to gas and vapour transfer of HDPE films is evidenced

through its low permeability to ethyl acetate, toluene, d-limonene, methyl-ethylketone, and α-pinene, however the permeability to these compounds was reported to be concentration and temperature dependent (Huang & Giacin 1998) (Table 4-6). Selke et al. (2004) suggested that multilayer film materials commonly provide improved barrier properties compared to single layer films and this is supported by the low permeability to hexanal of the multilayer films reported by Leufven & Stollman (1992) (Table 4-6). According to Selke et al. (2004), metallocene polymers generally have more uniform and controlled molecular weight distribution, resulting in improved film properties as gas and vapour barriers. Wolford (1998) reported metallocene-LDPE film had an excellent barrier to hexanal vapour. These low permeability films may suit applications where a slow controlled release of hexanal is required.

Although values of T_g for LDPE, LLDPE, and HDPE are in a similar range (Table 4-5), the better barrier properties of LLDPE and HDPE compared to those of LDPE may be explained by differences of crystallinity and structural arrangement. LLDPE is a modified form of LDPE having regular and linear short molecular branches (Robertson 1993c). Although some properties of LLDPE are similar to those of LDPE, such as density (Selke et al. 2004), LLDPE tends to have improved mechanical and barrier properties. Crystallinity of LLDPE can vary between 45-88% (Zhu et al. 1999; Willige et al. 2002), and is higher than that of LDPE which varies from 20 to 62% (Zhu et al. 1999). The better hexanal barrier property of HDPE than LDPE could be the result of both (i) the higher density of HDPE (940-965 kg·m^{-3} for HDPE, 915 to 939 kg·m^{-3} for LDPE) and (ii) the more linear polymer structure of HDPE than LDPE (in which the molecular arrangement is highly branched). Furthermore HDPE has up to 90% crystallinity (Robertson 1993c). Other improved properties of HDPE include stiffness, tensile and bursting strength, and chemical resistance (Robertson 1993c; Selke et al. 2004).

Although Song et al. (1996) humidified their hexanal vapour, the reported values of P_{LDPE}^{Hxl} were comparable to those quantified in the present work (Table 4-6) when considered at 0.02 mol·m^{-3}, where minimal concentration dependence of P_{LDPE}^{Hxl} was reasonably justified (as discussed earlier). These results suggest there was insignificant influence of water vapour on hexanal permeation through LDPE film, as was expected in line with the general trend for organic vapour permeation through hydrophobic nonpolar films such as LDPE,

HDPE, and OPP (Rogers et al. 1962; Karel 1975; Rogers 1985; DeLassus et al. 1988). The similarities between literature data and results obtained from the present work provide some confidence in the information obtained on P_{LDPE}^{Hxl}. In contrast to such general trends, Johansson & Leufven (1994) reported the significant effects of relative humidity on hexanal permeability of LLDPE (P_{LLDPE}^{Hxl}) and HDPE (P_{HDPE}^{Hxl}) films at 25°C (Table 4-6), although the trend was unclear. Whilst P_{LLDPE}^{Hxl} and P_{HDPE}^{Hxl} values increased ~3.5-fold as RH increased from 20 to 52%, these values decreased ~1.5-fold as the RH was further increased from 52 to 82%. Johansson & Leufven (1994) also reported similar RH effects on permeability of LLDPE and HDPE to other aldehydes including butanal, pentanal, heptanal, octanal and decanal. They assumed that the effects of RH were due to the plasticising effects of sorbed water vapour, even though the solubility of water vapour in hydrophobic nonpolar films is low. As RH increased from 20 to 52%, greater amounts of water vapour were assumed to be absorbed by LLDPE film (Johansson & Leufven 1994). Johansson & Leufven (1994) speculated that sorbed molecules then facilitate diffusion of organic permeant through increasing free volume within the polymeric structure, however the plasticizing effects were presumably suppressed as the RH further increased because more sorbed water molecules potentially competed with other permeants for the available spaces. This could result in decreasing permeability values at higher relative humidity levels.

At present there is limited information on RH effects on P_{LLDPE}^{Hxl} and P_{HDPE}^{Hxl} to compare with the results reported by Johansson & Leufven (1994). Information on P_{LLDPE}^{Hxl} was reported by Leufven & Stollman (1992) but in this case the hexanal vapour was not humidified (Table 4-6). P_{LLDPE}^{Hxl} values reported by Leufven & Stollman (1992) appear ~10-fold higher than the corresponding values reported by Johansson & Leufven (1994), even though the LLDPE films tested and experimental methodologies were similar. However, differences in results among these studies were not discussed or explained. Furthermore, although a range of conditions (i.e. 0.001-0.2 mol·m^{-3}; 5-75ºC) were employed in determining permeability, neither the actual concentrations corresponding to individual values of permeability nor the exact concentration dependence were reported. The effects of concentration dependence may be assumed to be an important factor contributing to the apparent differences of P_{LLDPE}^{Hxl} values. Further studies are therefore required to elucidate

RH effects on P_{LLDPE}^{Hxl} and these experiments must be made across a range of hexanal concentrations and concentration differences.

The insignificant effect of water vapour on permeation of hexanal through hydrophobic nonpolar polymer films is also implied from the work of DeLassus et al. (1988) on film permeation of trans-2-hexenal ($C_6H_{10}O$) (Table 4-6). This compound is another important C_6-aldehyde compound from plant materials (Hamilton-Kemp et al. 1996) and chemically, trans-2-hexenal has an aliphatic chemical structure close to hexanal. DeLassus et al. (1988) reported no effect of an RH close to 90% at 75ºC on permeability of Vinylidene Chloride (VDC) copolymer films to trans-2-hexenal (at fixed concentration at 0.005 mol·m^{-3}). However a clear influence of RH on EVOH permeability to trans-2-hexenal was reported, where permeability increased nearly 60-fold as RH increased from 0 to 90%. In addition to investigating RH effects, DeLassus et al. (1988) also studied the effects of concentration of trans-2-hexenal (0.003-0.01 mol·m^{-3}) on LDPE permeability, and reported reasonably constant permeability values over this concentration range (Table 4-6).

For hydrophilic polar film materials such as EVOH and cellophane, RH of the surrounding environment could affect film permeability to gaseous and volatile compounds (Robertson 1993c). Significant effects of water vapour on permeation of hexanal and other aldehyde compounds through EVOH film were reported by Johansson & Leufven (1994) (Table 4-6), where EVOH permeability increased ~250 fold as the surrounding humidity increased from 20 to 82%.

4.2.3.4 Concluding remarks from the comparison of experimental and literature data

Overall the permeabilities to hexanal vapour of Tyvek®, OPP and LDPE films quantified in the present work appear reasonable, and particularly, the magnitudes of OPP and LDPE permeabilities are in a line with literature data. This provides some confidence in the experimental data to be used in the subsequently developed mathematical models.

4.3 Determination of hexanal sorption isotherms for silica gel adsorbents

The equilibrium distribution between the adsorbed volatile agent on the carrier and the in the vapour headspace above the adsorbent is a key parameter in the design of an active packaging system. It is this equilibrium that controls the magnitude of the driving force for

volatile transfer out of the sachet. As discussed in the literature review, sorption isotherms vary with the properties of the adsorbent and adsorbate comprising the system as well as with environmental conditions such as temperature and relative humidity. There is no reported data for the sorption isotherm of hexanal on silica gel or other major porous adsorbents (e.g. activated carbon) making it necessary to experimentally determine the isotherm and how this was influenced by storage conditions.

4.3.1 Approaches for determining sorption isotherms

Methods for obtaining sorption isotherms for gaseous species on porous particles have been described by many researchers (Apostolopoulos 1985; Belmabkhout et al. 2004; Thielmann 2004). In general the methods utilise one of three basic approaches:

- *Gravimetric*: direct measurement of weight changes of samples which have been equilibrated at a constant temperature at different partial pressures of the vapour of interest (Belmabkhout et al. 2004).
- *Volumetric*: an indirect measurement of the mass adsorbed, determined by a mass balance over the gas phase, through application of the equation of state before and after equilibrium conditions are attained (Belmabkhout et al. 2004).
- *Inverse Gas Chromatography (IGC)*: a method which employs porous particles packed in a column as the stationary phase (as in gas chromatography), into which a known gaseous mobile phase (specified by composition and flow rate) is directed. Sorption characteristics are quantified through chromatographic responses (i.e. peak height and area) (Apostolopoulos & Gilbert 1983; Apostolopoulos 1985; Gilbert 1993). The IGC technique provides the key benefit of identifying equilibrium conditions at relatively low partial pressure (known as the Henry's law isotherm range) and the required length of the experimental period is considerably shorter than the other two techniques (Thielmann 2004).

Whilst attempts to conduct sorption experiments using both IGC and volumetric methods were made, these were limited by a number of practical problems (see discussion in Appendix E.1 to E.4). The gravimetric measurement approach was therefore principally used in the present work.

4.3.2 Experimental procedures

A gravimetric method used was similar to that reported by Nerín & Asensio (2004) and Triantafyllou et al. (2005) for determining sorption characteristics of organic vapour for paper materials. One gram samples of silica gel adsorbent (6-12 mesh, grade 40, Davison Chemical, Maryland, US) of precisely measured mass were placed in glass vials (20 ml, New Zealand Alltech Inc., Albany, New Zealand). Silica gel grade 40 was chosen due to its wide use as a common desiccant; all samples were dried for 12 hours at 110ºC and equilibrated to the experimental temperatures for 8 hours (over silica gel in a desiccator) prior to commencing the experiments. The properties of the silica gel are summarised in Table 4-7.

Table 4-7 General properties of silica gel grade 40

Properties (Units)	Values
Particle diameter (mm) [a]	1.70-3.35
Pore diameter (nm) [a, b]	~ 2.2
Apparent particle density ($kg \cdot m^{-3}$) [a]	2100
Specific surface area ($m^2 \cdot g^{-1}$) [c]	664

[a] Information provided by the manufacturer.

[b] Note that the hexanal molecular diameter is ~0.7 nm (Banerjee et al. 2005), which is smaller than the pore diameter of the silica gel. Therefore silica gel is able to accommodate hexanal molecules.

[c] Information provided by an independent study conducted by the Victoria University of Wellington, Wellington, New Zealand (J. Grindrod, Pers. Comm., 2006).

The vials were sealed with aluminium caps lined with Teflon-coated septa (Alltech Inc., Auckland, New Zealand). Different volumes of pure GC grade hexanal liquid (50 μL to 0.5 ml) were injected into a series of vials. The liquid was carefully introduced onto the wall of the vial using a Microliter™ syringe (Carlo Erba, Instruments, Italy) to avoid direct contact of liquid droplets with the silica gel. These droplets flowed downward slowly and appeared to quickly evaporate into the gas phase. All vials were kept in temperature controlled cabinets at 10 and 20ºC ± 2°C. After leaving the vials at 20ºC for two weeks, or at 10ºC for one month, hexanal partial pressures in the vial headspaces were determined using gas chromatography (as described in Chapter 3), while the corresponding uptakes of hexanal were quantified by weighing the silica gel samples. These were transferred from the vials into stainless steel cups, immediately covered with lids and weighed on a Mettler analytical balance (0.001g Mettler Toledo PR5003, Switzerland).

In addition to the vial testing system, air-tight glass desiccators (~1 L) containing hexanal liquid were used for characterising sorption under saturated conditions (p/p_s =1) at both 10 and 20ºC. A perforated ceramic plate was used to hold the sample above the pure hexanal liquid. Two gram samples of silica gel (in a stainless steel cup) were placed inside the desiccators and allowed to equilibrate. The desiccators were kept in the same storage environments as those used for vials. The samples were covered so as to be air-tight during weighing to ensure no gains or losses of masses occurred. The samples were weighed periodically over six weeks until a constant mass was reached. Samples were returned to the sealed containers immediately after weighing. Sample masses were stable after either one month or two weeks storage at 10 and 20°C, respectively.

4.3.3 Preliminary validation of the gravimetric sorption method

Since there is no report of sorption isotherms of hexanal on silica gel, verification of the gravimetric sorption method described earlier was performed against published data for acetaldehyde (Ghosh & Hines 1990) and ethanol (Madeley & Sing 1959). Isotherms for these volatiles was reportedly determined by a gravimetric method using quartz-spring-type microbalances[7] and the silica gel adsorbents used were comparable to those used in the present work (in respect of specific surface area, pore size and particle diameter).

Volumes of the acetaldehyde or ethanol injected into the vials corresponded to published uptake data. For example, to achieve 0.19 $g \cdot g^{-1}$ ethanol uptake by silica gel as reported by Madeley & Sing (1959), one gram of silica gel was put into a vial, into which 0.24 ml of ethanol liquid (density of 0.79 $g \cdot ml^{-1}$; ≥99.8% GC grade, Riedel-de Haën supplied by Sigma Aldrich, New Zealand) was then injected. This volume was allowed to totally evaporate. The resultant uptake should correspond to $p/p_s \cong 0.36$ at 25ºC (note the mass of ethanol vapour in the air phase will be very much smaller than that adsorbed on the silica gel). After leaving the vials at 14ºC for 1 month (for acetaldehyde) and 25ºC for 2 weeks (for ethanol), headspace vapour partial pressure and equilibrium uptake were quantified. The gas chromatography settings for measuring acetaldehyde and ethanol samples are provided in Appendix C.

---

[7] As hexanal vapour potentially causes serious damage to the weighing sensor of a microbalance, hexanal sorption isotherms quantified in this manner have high experimental cost (P. Attwool, Pers. Comm. 2006; Surface Measurement System, London, UK).

The adsorption isotherms obtained for the test compounds are plotted together with literature data in Figure 4-4. Reasonable agreement with the literature data was found; the minor deviations evident for ethanol may be due to differences in the specific surface area of the silica gels used in the study of Madeley & Sing (1959) and the present work, which were ~613 and 664 $m^2 \cdot g^{-1}$, respectively. For acetaldehyde sorption data, the silica gel adsorbents utilised in the study of Ghosh & Hines (1990) were similar to those used in the present work and the sorption isotherms were in good agreement. These results provided confidence in the implementation of the gravimetric approach for quantifying hexanal sorption isotherms for silica gel adsorbents.

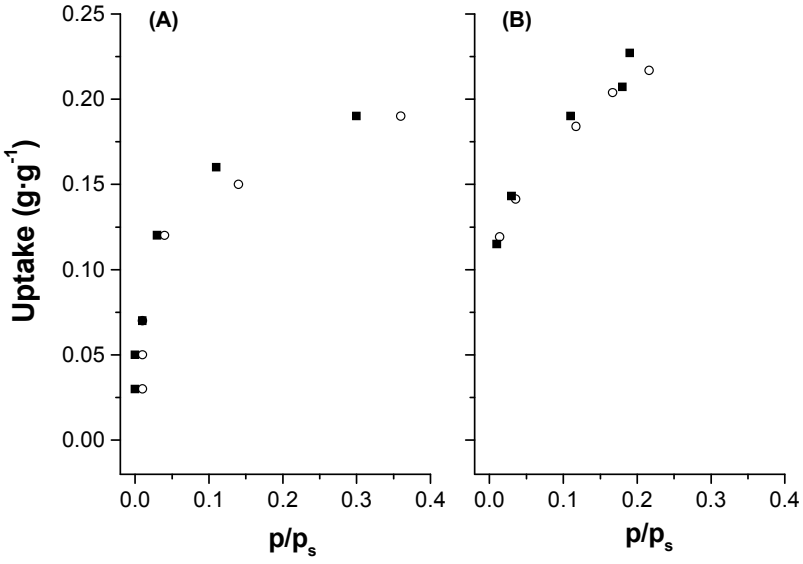

Figure 4-4 Comparison of sorption isotherms for ethanol and acetaldehyde measured using the gravimetric sorption method used for silica gel adsorbents for experimental (■) and literature data (o) reported for ethanol by Madeley & Sing (1959) (A) and acetaldehyde by Ghosh & Hines (1990) (B). Experimental data were collected at the same temperatures as the reported data, namely 25°C for ethanol and 14°C for acetaldehyde.

4.3.4 Hexanal sorption isotherms for silica gel adsorbents

Hexanal sorption isotherms for silica gel adsorbents at 10 and 20ºC are shown in Figure 4-5 [8]. The effect of temperature on sorption behaviour was quite marked with the adsorption uptake measured at 10ºC being significantly higher than that at 20ºC. These findings are consistent with the thermodynamic fundamentals of adsorption (Weber 1985), which is an exothermic process and the spontaneity of which is expected to decrease as the temperature of the system increases (note this is discussed further in section 6.4.4). For example, Lee (2003) reported a continuous decline in uptake of 1-MCP by silica gel as the temperature was raised from 50 to 80ºC. Similarly Ng et al. (2001) reported a decrease in water vapour adsorption on silica gel when the temperature was increased from 30 to 65ºC.

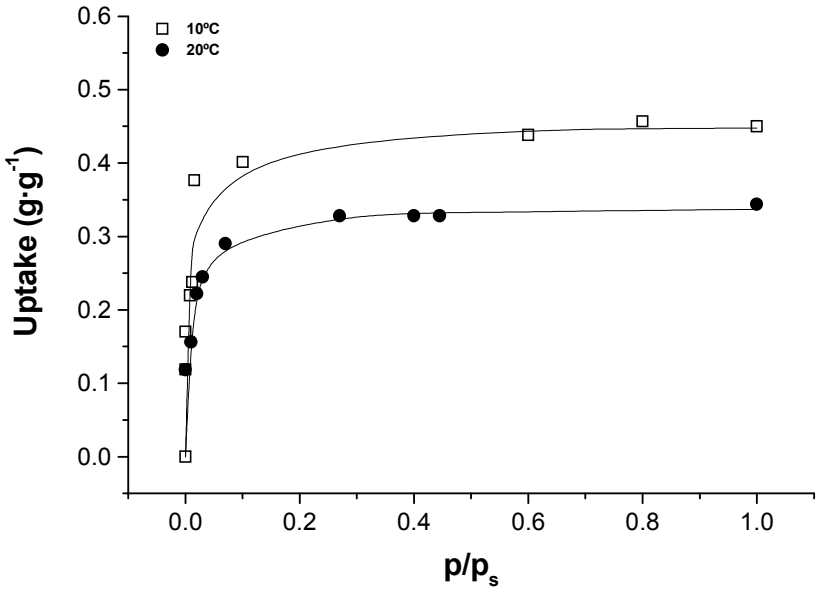

Figure 4-5 Hexanal sorption isotherms for silica gel grade 40 at 10 and 20ºC measured using a gravimetric sorption approach. Solid lines were fitted using the Langmuir isotherm model Eq. 2-3.

The hexanal sorption isotherms showed Type I or Langmuir behaviour (Figure 4-5). Sorption on adsorbents having similar absorbate and pore dimensions (the latter no more than a few molecular diameters of the former) tend to give a Type I isotherm as uptake is

[8] The same sorption isotherms expressed in molar terms ($mol \cdot g^{-1}$ and $mol^{1} \cdot m^{-3}$ as units for uptake and hexanal vapour concentration, respectively) are shown in Appendix E.6 and the Langmuir model estimated coefficients were for those used within the mathematical models.

limited to a monolayer on the pore walls (Gregg & Sing 1982; Thomas & Crittenden 1998b). When the pore diameters of microporous adsorbents are considerably smaller, the adsorption potential field of neighbouring walls overlaps (Gregg & Sing 1982; Adamson 1990) and sorption occurs rapidly at low partial pressure. In Figure 4-5, hexanal sorption is essentially completed at $p/p_s \approx 0.3$ and this confirms the Type I sorption behaviour of hexanal sorption by silica gel for which the ratio of pore to molecular diameters (refer to Table 4-7) was ≈ 3.

Type I adsorption isotherms generally have a limited extent of hysteresis upon desorption because capillary condensation, which is one of main factors contributing to hysteresis, is likely to be absent in narrow pores (Adamson 1990). Ghosh & Hines (1990) reported Type I sorption isotherms for acetaldehyde, propionaldehyde and butyraldehyde, at 9-35ºC on silica gel grade 40. Although hysteresis loops were reported during desorption of these compounds, the extent of hysteresis became very small as the number of carbon atoms in the compounds increased from 2 to 4. Based on such a finding, no significant hysteresis was expected in the desorption of hexanal (C_6) and this was confirmed using a volumetric sorption method (Autosorb-1; Quantachrome Instruments, US) conducted by an independent testing laboratory (Appendix E.4). For this reason, no further experiments on hexanal desorption were performed.

The Langmuir isotherm model was fitted to both sets of sorption isotherm data, as shown in Figure 4-5, yielding the model coefficients given in Table 4-8. The Langmuir model showed a reasonably good fit with experimentally collected data and is the model of choice for describing Type I sorption data because of its simplicity and practicality (Thomas & Crittenden 1998b). However, high variation was observed in the estimation model coefficients; in particular the b_{Lgm}^{Hxl} values have standard errors in the range of 40-52% of the mean.

Table 4-8 Parameter estimates and standard errors (SE) from nonlinear regression analysis of hexanal sorption isotherm data for silica gel grade 40 at 10 and 20ºC

Temperature (ºC)	$C_{s,max}^{Hxl}$ (SE) [a] **(g·g^{-1})**	b_{Lgm}^{Hxl} (SE) **(dimensionless)**	n [b]
10	0.45 (9.6)	136 (51.9)	10
20	0.34 (7.0)	87 (40.4)	10

[a] The standard errors (SE) is expressed as a percentage of the estimated value. The nonlinear regressions were conducted using the Nonlinear Regression package of Origin 5.0 (Microcal Software Inc.)

[b] n is the number of observations.

As discussed earlier, gas uptake could occur and approach saturation at relatively low pressures for systems having a Type I sorption isotherm. When the condition is favourable for adsorption (e.g. at lower temperatures), b_{Lgm}^{Hxl}, which represents the affinity between the surface and adsorbate, is expected to be high. In such cases, estimates of b_{Lgm}^{Hxl} can be very sensitive to the accuracy of concentration measurement at these low partial pressures. In contrast, the variation in estimates for $C_{s,max}^{Hxl}$ was smaller because it is relatively insensitive to partial pressure in the gas phase.

The estimated values for $C_{s,max}^{Hxl}$ and b_{Lgm}^{Hxl} from the nonlinear regression method (Table 4-8) were relatively close to those given by linear regression using the optimal reparameterisation of the Langmuir equation as described by Ratkowsky (1990). The maximum difference of coefficients estimated by the nonlinear and linear regression approaches for $C_{s,max}^{Hxl}$ and b_{Lgm}^{Hxl} was < 1% and < 16%, respectively. The highest difference was observed for the estimates of b_{Lgm}^{Hxl} at 10ºC, while the difference between estimated values of b_{Lgm}^{Hxl} at 20ºC was less than 6% (Appendix E.5).

The b_{Lgm}^{Hxl} and $C_{s,max}^{Hxl}$ values estimated in the current experiment (Table 4-8) reasonably agree with corresponding values (Table 4-9) estimated using nonlinear regression for (i) literature data on sorption of a range of VOCs for silica gel adsorbents (for comparable silica gel properties such as particle size and specific surface area, and experimental temperatures in the range of 9-30°C) and (ii) preliminary experimental data of ethanol and acetaldehyde sorption isotherms for silica gel reported in section 4.3.3. Similar trends were also observed in the uncertainty associated with estimates of b_{Lgm}^{i} and $C_{s,max}^{i}$. For all cases,

standard errors associated with b^i_{Lgm} values were large, at up to 56% of the mean (Table 4-9). Considering these points, the estimated coefficients of the Langmuir equation for hexanal sorption on silica gel appear reasonable and provide confidence for their implementation as model inputs in subsequent work.

Table 4-9 Parameters of the Langmuir model equation estimated using nonlinear regression for literature data on sorption of a range of VOCs for silica gel adsorbents

VOCs	Temperature (°C)	Studied range of relative pressure (p/p_s)	$C^i_{s,max}$ (SE) [a] (g·g^{-1})	b^i_{Lgm} (SE) [a] (dimensionless)
Acetaldehyde [b]	14	0.003 - 0.42	0.23 (4.0)	55.39 (21.1)
		0.01 - 0.19 [c]	0.22 (5.2) [c]	83.89 (27.9) [c]
	25	0.001- 0.15	0.23 (4.0) [d]	42.21 (11.1) [d]
Propionaldehyde [b]	9	0.01 - 0.45	0.22 (1.9)	105.41 (15.7)
	24	0.01 - 0.32	0.20 (2.1)	103.68 (15.6)
Butyraldehyde [b]	15	0.007 - 0.56	0.22 (2.5)	141.98 (26.2)
	26	0.02 - 0.34	0.21 (1.6)	86.42 (13.5)
Ethanol [e]	25	0.01 - 0.36	0.19 (7.7)	34.41 (25.1)
		0 - 0.30 [c]	0.19 (13.8) [c]	52.39 (56.7) [c]
Acetylene [f]	25	0.0001- 0.01	0.06 (6.5)	221.25 (15.3)
Ethylene [f]	25	0.0003 - 0.02	0.06 (2.9)	49.23 (4.7)
Heptane [f]	30	0.001- 0.95	0.25 (1.4)	22.62 (6.5)
Propane [f]	25	0.001- 0.11	0.13 (4.6)	10.23 (8.0)
Propylene [f]	25	0.001 - 0.09	0.12 (3.3)	34.71 (8.2)

[a] Estimated $C^i_{s,max}$ and b^i_{Lgm} represent the maximum adsorbed phase concentration of substance *i* (g·g^{-1}) and Langmuir constant for sorption of substance *i* (dimensionless), respectively. Values in parentheses are standard errors (SE) expressed as a percentage of the estimated values.

[b] Estimated values of isotherm data for (single component) sorption of acetaldehyde, propionaldehyde and butyraldehyde on silica gel grade 40 (reported by Ghosh & Hines 1990) .

[c] Estimated values of isotherm data for sorption of acetaldehyde and ethanol on silica gel grade 40 presented in section 4.3.3 (primary validations of sorption isotherms). There were certain ethanol vapour concentration that were too low to be measured by the current gas chromatographic settings. These were then reported as zero (i.e. also shown in Figure 4-4).

[d] Nonlinear regression analysis by fixing value of $C^i_{s,max}$ to be equal to that of estimated value at 14ºC, to obtain reasonable convergence of model prediction results and literature data.

[e] Estimated values of isotherm data for ethanol for silica gel adsorbents (reported by Madeley & Sing 1959) for which the reported silica gel were comparable to those used in the present work (also see section 4.3.3).

[f] Estimated values of isotherm data for acetylene, ethylene, heptane, propane and propylene (extensively collected and reported by Valenzuela 1989) in which silica gel adsorbents for these VOCs are referred to as Grade PA 400 or refrigeration grade (750 m^2·g^{-1}; 8-20 mesh; Davison Chemical, Co. Baltimore, US).

To gain further insight into hexanal adsorption processes the following key thermodynamic parameters were calculated based on the fitted isotherms for hexanal on silica gel (Figure 4-5 and Table 4-8): free energy (ΔG°), apparent enthalpy change (ΔH°), and entropy (ΔS°). These parameters were calculated based on the adsorption coefficient (b_{Lgm}^{Hxl}) and the following thermodynamic functions (Eq. 4-6 to Eq. 4-8; Adamson 1990; Chen et al. 2007):

$$\Delta G^\circ = -RT \ln b_{Lgm}^{Hxl} \quad \textbf{(Eq. 4-6)}$$

$$\Delta H^\circ = -\left(R \frac{\left(\ln b_{Lgm,10^\circ C}^{Hxl} - \ln b_{Lgm,20^\circ C}^{Hxl} \right)}{\left(\frac{1}{T_{10^\circ C}} - \frac{1}{T_{20^\circ C}} \right)} \right) \quad \textbf{(Eq. 4-7)}$$

Entropy (ΔS°) was calculated from the relationship between ΔG° and ΔH°, given by Eq. 4-8.

$$\Delta G^\circ = \Delta H^\circ - T\Delta S^\circ \quad \textbf{(Eq. 4-8)}$$

where

$b_{Lgm,10^\circ C}^{Hxl}$, $b_{Lgm,20^\circ C}^{Hxl}$	=	Langmuir coefficients at 10 and 20ºC (dimensionless), respectively
ΔG°	=	Free energy (J·mol^{-1})
ΔH°	=	Apparent enthalpy change (J·mol^{-1})
ΔS°	=	Entropy (J·mol^{-1}·K^{-1})
$T_{10^\circ C}$, $T_{20^\circ C}$	=	Temperature (K) for 10 and 20ºC, respectively

Derived parameters are reported in Table 4-10. The negative values of ΔH° confirm that the adsorption process was exothermic as expected. The absolute values of ΔH° calculated for hexanal sorption processes were in the typical range of ΔH° values for physical adsorption (6 to 84 kJ·mol^{-1}; see Adamson 1990, page 595). The exothermic property of the adsorption process was also supported by the negative values of ΔG°, which became less negative with increasing temperature, although the extent of change of ΔG° was small. In contrast, values of $T\Delta S^\circ$ become more negative with increasing temperature, but the small change suggests that increasing temperature from 10 to 20°C slightly limits hexanal sorption on silica gel. Similar trends and magnitudes of estimated values for these

thermodynamic parameters for sorptions of other VOCs on silica gel (Table 4-9) were observed. For example ΔH° for butyraldehyde-silica gel system when the temperature was increased from 15 and 26 °C was ~35 kJ·mol^{-1} and ΔG° was about -12 and -11 kJ·mol^{-1}.

Table 4-10 Apparent thermodynamic parameters for hexanal sorption onto silica gel adsorbents at 10 and 20°C

Temperature (°C)	ΔH° **(kJ·mol^{-1})**	$T\Delta S^{\circ}$ **(kJ·mol^{-1})**	ΔG° **(kJ·mol^{-1})**
10	-30	-19	-11
20	-30	-20	-10

4.3.5 Determinations of the effects of relative humidity on hexanal sorption

Active system to be used inside a package containing horticultural products may be exposed to high relative humidity (> 90% RH). Water vapour may affect hexanal sorption onto or from silica gel adsorbents, due to silica gel's high water vapour sorption capacity. Because of this, experiments to identify possible effects of RH on hexanal sorption isotherm for silica gel (as used in the previous section) were undertaken.

The experimental methods employed were similar to those utilised in section 4.3.2, except the silica gel adsorbents were first equilibrated at three different relative humidity conditions: 60, 80 and 90% RH. Stainless steel cups containing 1 gram of dry silica gel were placed inside sealed plastic containers containing the appropriate glycerol-water solution to achieve the required RH and allowed to equilibrate for over a month at 20ºC. The glycerol-water solutions were prepared according to Forney & Brandl (1992). After equilibration, the silica gel samples were transferred into vials, then sealed, and randomly assigned to be tested at 10 or 20ºC. Known volumes of hexanal liquid were injected into the vials to achieve uptake in the range of 0.22-0.30 g·g^{-1} (2 replicates). This range was chosen to minimise condensation of hexanal vapour (which was previously noted near the maximum adsorption capacity). After leaving the vials for 1 month and two weeks at 10 and 20ºC, respectively, the hexanal concentrations in the headspace and the increased mass of silica gel were quantified (using methods as described in the previous section). Experimental results are summarised in Table 4-11.

Table 4-11 Experimental results on the effects of RH on hexanal sorption isotherm for silica gel adsorbents

Temp. (ºC)	Uptake of dried silica gels [a]			Uptake under varing relative humidity environment								
				60% RH			80% RH			90% RH		
	Uptake ($g \cdot g^{-1}$)	p/p_s	Cond.[c]	Uptake ($g \cdot g^{-1}$) [b]	p/p_s	Cond.	Uptake ($g \cdot g^{-1}$)	p/p_s	Cond.	Uptake ($g \cdot g^{-1}$)	p/p_s	Cond.
10	0.22	0.01	-	0.21	0.68	+	0.22	0.63	+++	0.21	0.73	+++
	0.24	0.01	-	0.24	0.71	+	0.23	0.79	+++	0.24	n/a [d]	+++
	0.38	0.02	-	0.38	0.59	++	0.38	n/a	+++	0.37	n/a	+++
20	0.22	0.02	-	0.22	0.42	+	0.23	0.42	+++	0.27	0.31	+++
	0.24	0.03	-	0.23	0.28	+	0.24	n/a	+++	0.23	n/a	+++
	0.29	0.07	-	0.30	0.26	++	0.31	n/a	+++	0.29	n/a	+++

[a] Data from Figure 4-5

[b] Data for uptake and p/p_s were average of two replicates. Sorption is based on net dried weight of silica gels which underwent pre-saturation at various relative humidity levels

[c] Cond. stands for 'Condensation level', where symbols '+', '++', and '+++' represent condensation observed 'only at septum surface', 'at septum and one side of vial walls', and 'at septum and on both sides of vial walls', respectively.

[d] n/a stands for 'not available' data for p/p_s because of errors were apparent in the chromatographic results corresponding to extremely high partial pressures.

In all cases, there was visual evidence of liquid condensation in the vials although the measured relative vapour pressure of both hexanal (p/p_s) and water were (or were expected to be) lower than 1. This suggests that the condensate may be mostly water displaced from the silica gel by the hexanal vapour. For example the calculated hexanal mass (~6×10^{-5} g; at p/p_s = 0.07, refer to Table 4-11) at 20ºC in vial headspace (20 ml) was ~5-fold lower than water vapour mass (~3×10^{-4}g assumed 100% RH; note this number also indicates only a very small amounts of water vapour were required to saturate the vial headspace compared to the amount adsorbed on dried gel at 20ºC for 60, 80 and 90% RH which were estimated from experimental data as ~0.32, 0.36 and 0.38 $g \cdot g^{-1}$, respectively). Furthermore there was a high variability of relative hexanal vapour pressure and no obvious pattern to the trend in concentration even for the case where the lowest amount of condensation was observed (i.e. 60% RH). It would appear that the adsorption system is complex and in such cases it becomes difficult to determine sorption correctly because hexanal vapour may be present in all phases, namely the liquid (condensate), gas (headspace) and solid (silica gel). For example a higher apparent hexanal uptake value at 20ºC and 90%RH than that measured for dried silica gel may be the result of hexanal being present both on the silica gel and in the condensate (note the hexanal solubility in water ~0.02 $g \cdot ml^{-1}$ Covarrubias-Cervantes et al. 2005).

Zhou et al.(2006) reported complex trends in respect to influences of pre-adsorption of water on methane sorptions for silica gel (grade 60; ~8nm pore diameter and ~316 $m^2 \cdot g^{-1}$ specific area) quantified using the volumetric method at 2ºC and methane partial pressure of 0 to ~11 MPa. While methane uptakes by silica gel having intermediate water contents (0.7 to 1.17 water ratios; the weight ratio of water to dry gel) were reportedly higher than those by dried silica gel, especially when the partial pressure exceeded ~3 MPa, very low sorption extents were reported among such wetted silica gels. For low and high water contents (0.61 and 1.3 water ratios, respectively), methane uptakes by dried silica gel were significantly higher than those of the wetted gel (for a given partial pressure). Similar trends with regard to pre-adsorbed water were reported by Zhou et al.(2002) for methane sorption on activated carbon adsorbents (carbonised coconut shell based) quantified under similar experimental conditions to these mentioned above for the methane-silica gel system. Insights or mechanisms underlying the complex isotherm characteristics reported for methane- and silica gel and activated carbon systems have not been well developed, however Zhou et al.(2002) and Zhou et al.(2006) postulated that these could be the results of for example (i) partition of methane with water available on the gel (adsorbed) and/or between adsorbent particles (free liquid), or (ii) changes of adsorbent pore structures after exposed to water, among other mechanisms.

The general agreement of hexanal uptake values measured for both dried and humidified silica gel (Table 4-11) could be assumed to result from small amounts of free water on the adsorbent surface. In all samples small amounts of condensate formed on the inner surfaces of the vial septum. It is not possible to rule out that some liquid could be picked up during gas sampling and if so, hexanal dissolved in this condensate might significantly increase the peak height obtained in GC measurement, thus indicating an unduly high apparent headspace concentrations (Table 4-11). Better temperature and pressure controlled systems may be required for further investigation of such complex systems. Possibly a quartz-spring type microbalance could be considered for such work providing protection from absorption by hexanal vapour could somehow be assured.

Although high relative humidity conditions are expected in MA packaging systems for horticultural products, the utilisation of nonperforated hydrophobic polymeric films such as OPP and LDPE as sachet materials would minimise moisture contact with the active

agent absorbent. In spite of high driving force of water vapour across the sachet (the atmosphere around the horticultural product will approach saturation in the package headspace while the RH will be very low in the sachet headspace), the estimated rate of water vapour across the LDPE sachet (given the sachet surface area as 0.003 m^2) is over 10-fold lower than that across LDPE film bag (given bag surface area as 0.125 m^2 and RH in bag and environment as ~95 and ~60%, respectively). In this case, water vapour permeation across the sachet film can reasonably be presumed negligible. It should be noted that the sizes of sachet and bag used above were later extensively used in Chapter 5 and 6. In contrast, Tyvek® is highly porous material and high water vapour transmission across the sachet may occur. Based on experimental results, while it is apparent that there is likely to be some hexanal-water vapour interaction, these effects are unlikely to influence hexanal uptake by silica gel. For this reason no further work on these interactions was carried out in this work.

4.4 Summary

The permeability in polymer film and adsorption isotherms of hexanal vapour were determined. Polymer film permeability to hexanal vapour showed a strong dependence on hexanal vapour concentrations (at concentrations above ~0.02 $mol \cdot m^{-3}$) and storage temperature. Hexanal permeability of LDPE measured in the present work (considered at low vapour concentrations) was comparable in magnitude to the literature for hexanal and other organic vapours and suggests that the isostatic measurement can provide reasonable estimates of permeability.

To date, the concentration dependent permeability to hexanal vapour of films utilised in MAP systems have not previously been reported. The findings obtained in the present work thus contribute to knowledge of permeation of VOCs through polymer films. By comparing results of the present work to relevant literature, it was hypothesised that permeability to hexanal may be affected by the level of crystallinity and T_g of film polymers in addition to concentration and storage temperature. Although the effects of RH on film permeability to certain aldehydes (including hexanal) and toluene were reported elsewhere, mechanisms underlying such effects require further study. Permeability values to hexanal vapour of OPP films were lowest while those of Tyvek® were highest of the films tested. Tyvek® material is therefore more appropriate for active packaging systems

that require rapid transfer of the active agent between the sachet and the package atmosphere or for CO_2 and C_2H_4 scavenging systems. In contrast, OPP films will be more suitable when a slow release pattern is required. The magnitude of LDPE permeability lies between these two extremes, but is nearer to OPP.

Hexanal sorption isotherms for silica gel adsorbents show a Type I sorption pattern. The isotherm data were fitted well by the Langmuir isotherm equation, although there was a relatively high SE associated with estimated b_{Lgm}^{Hxl} values. The experimental variation is considered inherent to the method, due to the rapid and large extent of hexanal adsorption at very low vapour phase concentrations. The isotherms appear consistent with literature data for sorption of other VOCs for silica gel, such as acetaldehyde, butryraldehyde ethanol, and heptane. Findings obtained in the present work contribute to the limited knowledge on equilibrium sorption data with respect to controlled release active packaging systems.

The adsorption behaviour became complex and more difficult to measure correctly when condensates was present when silica gel was pre-equilibrated at high RH values. However when using nonperforated hydrophobic polymeric films such as OPP and LDPE as sachet materials, minimal water vapour transmission into the sachet is expected. The water vapour transfer across Tyvek® in contrast may be high due to highly porous property of Tyvek®. However there was evidence of minimal effects of water vapour adsorption by silica gel on hexanal uptake and the validity of this assumption will be further discussed in Chapter 6, along with results of model predictions and empirical data of hexanal release in active MAP system with LDPE, OPP and Tyvek® as sachet materials.

Chapter 5

DEVELOPMENT OF CONCEPTUAL AND MATHEMATICAL MODELS FOR ACTIVE MAP OF HORTICULTURAL PRODUCTS

5.1 Introduction

This chapter presents a general conceptual model which can accommodate a range of designs of active MAP systems, i.e. a model that can accommodate different active agents, the carriers of these agents, and different packaging films, of differing physical sizes, for a range of horticultural products. To maintain generality, the conceptual model was based on those fundamental principles and concepts drawn from the literature review (Chapter 2) which influence equilibrium and mass transfer behaviour in respect of these alternative system components.

To develop the conceptual model, key mass transfer processes must be identified. Suitable equations and assumptions can then be implemented to generate a mathematical model of the overall system. However, modelling all of the identified processes can be a time-consuming, difficult and (often) unnecessary task. Therefore simplifying assumptions were sought where these could be justified based on relevant theories or literature data. It is preferrable if this simplification is carried out using quantitative criteria, preferably based on dimensionless numbers (e.g. the Biot number) or ratios of these. Development of such criteria was initially conducted using relevant information reported for active packaging systems employing, chiefly, 1-MCP (due to the extensive available information, as discussed in Chapter 2) and other active agents such as ethanol and acetaldehyde. A full model was then implemented for the hexanal/tomato active MAP system outlined in Chapter 3 to demonstrate its application to a specific system.

The key objectives of the work presented in this chapter were to:

(1) Identify all physico-chemical processes and properties relevant to the design and evaluation of active MAP systems that release the active agent into the package headspace.

(2) Identify possible simplifications and the requirements for these to be applied without unacceptable loss of model accuracy.

(3) Develop a comprehensive decision tree to assist in model formulation for a range of practical active packaging scenarios.

(4) Formulate and validate a mathematical model for the test system of hexanal release from silica gel in sachets enclosed with LDPE-packaged tomatoes

5.2 Conceptual model of an active MAP system for horticultural products

For the active MA package of interest (as identified in Chapter 3), the physical situation to be modelled is illustrated in Figure 5-1;

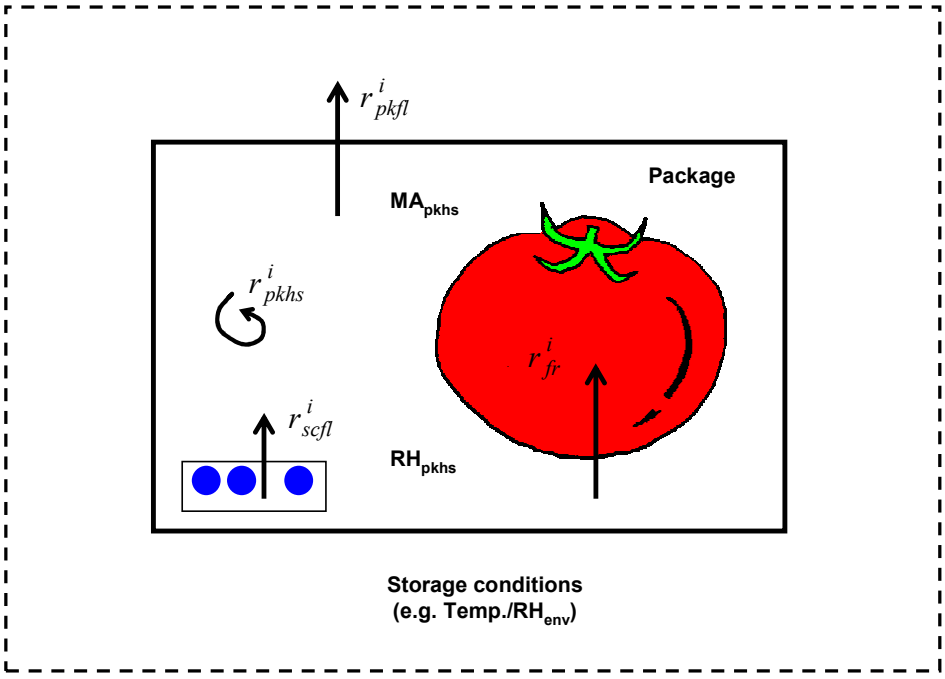

Figure 5-1 Mass transfer processes for release of volatiles gaseous components in an active MAP system with enclosed sachet and a horticultural product (subscripts: $pkhs$, $pkfl$, $scfl$, env and fr represent package headspace, packaging film, sachet film, environment and fruit, respectively; superscript i represents active agent i; MA and RH represent modified atmosphere and relative humidity, respectively)

The physical basis of the model (Figure 5-1) can be summarised as:

- A flexible non-perforated polymer film material is the primary package of the active packaging system (corrugated liner paperboard typically comprises the secondary packaging; this is not taken into account of design in the present work).

- The package is exposed to external storage and distribution conditions of which temperature and relative humidity (RH) are the most important. Over a long storage period (e.g. 7 days or more), the package will equilibrate with respect to temperature, given a reasonably constant storage temperature.
- Horticultural products continue their physiological processes after harvest and packaging. The rate depends on the prevailing temperature and composition of package atmosphere (chiefly O_2, CO_2, N_2 and possibly C_2H_4) and RH. These activities might also vary with time as the product senescences. External factors, principally the storage temperature and outer film permeability influence accumulation of these gases and water vapour in the package headspace. For long storage periods and constant storage temperature environment, the gas composition and RH inside the package headspace will attain a (quasi) steady-state.
- The controlled release system is separated from the internal package environment by the sachet material. The active agent is carried on porous adsorbent, desorbs from this into the sachet atmosphere, and then crosses the sachet film into the package headspace.
- Mass transfer of an active agent *i* occurs through the sachet film, 'into' (is 'taken up' by) the fruit, or passes through the packaging film. These rates are represented by r^i_{scfl} (mol·s^{-1}), r^i_{fr} (mol·s^{-1}; relative to fruit mass), and r^i_{pkfl} (mol·s^{-1}), respectively. The dynamic balance of these rates determines the net rate of accumulation of the active agent in the package headspace (r^i_{pkhs} ; mol·s^{-1}).

The overall mass balance for describing accumulation of an active agent in the headspace can be represented by Eq. 5-1.

$$\begin{pmatrix} Rate\ of\ active\ agent \\ accumulation\ in \\ package\ headspace \\ \left(r^i_{pkhs}\right) \end{pmatrix} = \begin{pmatrix} Rate\ of\ active\ agent \\ delivered\ from\ controlled \\ release\ saceht\left(r^i_{scfl}\right) \end{pmatrix} - \begin{pmatrix} Rate\ of\ active\ agent \\ permeation\ through \\ packaging\ material \\ \left(r^i_{pkfl}\right) \end{pmatrix} - \begin{pmatrix} Apparent\ rate\ of \\ uptake\ of\ active\ agent \\ from\ interaction \\ with\ product\left(r^i_{fr}\right) \end{pmatrix}$$

(Eq. 5-1)

5.3 Assumptions for conceptual model development

There are two levels of assumptions made for the conceptual model: 'primary' and 'secondary'. The primary assumptions are relevant to the overall characteristics of packaging systems regardless of the nature of the mass transfer processes occurring. They are specific to: (1) ideal gas behaviour, (2) thermal equilibrium, (3) constant package volume, (4) one-dimensional mass transfer and (5) uniform concentrations of active agents in package headspace. The secondary assumptions relate to the specific mass transfer processes occurring within the packaging system. The relative importance of these processes can be justified using either a theoretical or an empirical approach to minimise the complexity of the subsequently developed mathematical model. The key assumptions at both levels are discussed in the following subsections.

5.4 Primary (P) level assumptions

5.4.1 Assumption P1: The gas phase of the active packaging system can be considered as ideal

This assumption is considered reasonable at low pressures and concentrations and is generally adopted in modelling passive MAP for horticultural products (e.g. Yam & Lee 1995; Merts 1996; Chen et al. 2000). The ranges of effective or required concentrations of active agents for active MAP system have generally been reported to be in the order of parts per million (ppm; $\mu L \cdot L^{-1}$), for example 240-250 ppm (at 23ºC) for hexanal suppression of *B. cinerea* growth on sliced apples (Song et al. 1996), and 1-100 ppm (at 20ºC) as an effective concentration for 1-MCP to minimise ethylene action on kiwifruit (Kim et al. 2001). In Chapter 3, the MIC of hexanal vapour for control of *B. cinerea* growth on tomatoes was determined to be 40-70 ppm. Such concentrations are very low and it is reasonable to assume ideal gas behaviour for these compounds.

5.4.2 Assumption P2: All model compartments are in local thermal equilibrium

The assumption of thermal equilibrium is realistic for long storage and individual packages in a constant temperature environment, however it may not be true for larger scale packs such as pallets or containers. Because the model active packaging system developed in the present work was a retail or individual package with a shelf life of at least 7 days, the assumption of thermal equilibrium between the packaging environment and the packaging

system was deemed reasonable over this time frame. For situations where larger or grouped packaging formats are utilised, the temperatures of individual packages (e.g. at the centre of a pallet stack) can be predicted separately, e.g. by using the mathematical model developed by Tanner (1998).

5.4.3 Assumption P3: Mass transfer of the active agent from the sachet can be modelled in 1-dimension

This assumption was made to simplify the complexity of the mathematical model describing mass transfer processes in the active packaging system. Several mathematical models reported in the literature to describe cooling and drying processes (e.g. Tanner 1998; Meas 2006) were developed based on this 1-dimensional transport assumption and were reportedly sufficient to describe the key mass transfer processes. According to Cleland et al. (1994), to ensure 1-dimensional heat transfer, the dimension(s) for which transport is not considered must be at least three times greater than the dimension of interest. Pongjaruwat (2007) (Table 2-2) used sachets of 40 × 50 mm and the depth was determined by the diameter of silica gel (1-3 mm). Sachets of comparable dimensions were used in the present work. Given the sachet is typically only one particle layer deep, the lengths of both sides of the sachet are substantially more than 3 times of the thickness and 1-dimensional transport of hexanal vapour from the sachet can be reasonably assumed.

5.4.4 Assumption P4: Uniform concentrations of active agents in the package headspace

The likelihood of gaseous concentration gradients resulting from mass transfer processes is principally identified by a quantitative comparison of external and internal resistances to gas transfer. This is often represented by a dimensionless group known as the Biot number (Bi; Eq. 5-2). The assumption that the concentration is uniform within a phase is reasonably accurate when $Bi < 0.1$ (Geankoplis 1993c).

$$Bi = \frac{kL}{D} \qquad \textbf{(Eq. 5-2)}$$

where

Bi = Biot number for mass transfer (dimensionless)

D = Mass diffusivity ($m^2 \cdot s^{-1}$)

k = Surface mass transfer coefficient ($m \cdot s^{-1}$)

L = Characteristic dimension of bag (m)

The calculation of Bi numbers for selected volatile active agents contained on sachets within a LDPE bag (e.g. as described by Charles et al. 2003) are summarised in Table 5-1. All Bi values were substantially less than 0.1. This implies that the external resistance (contributed by the polymer film barrier) is much larger than the diffusive resistance of active agent(s) in the package atmosphere. A uniform concentration of active agents in the package headspace can thus be reasonably presumed. By using a similar approach for O_2, CO_2, N_2 and water vapour[9], Bi values for these gases were also found to be < 0.1 (calculations not shown). In practice, the assumption of uniform concentration of gaseous compounds in the package headspace is commonly made in most MAP systems (e.g. Emond et al. 1991; Cameron et al. 1995; Song et al. 2002; Charles et al. 2003; Charles et al. 2005).

Table 5-1 Estimated Bi values for diffusion of certain active agents in the package headspace

Active agents	Temperature (ºC)	D [a] ($m^2 \cdot s^{-1}$)	k [b] ($m \cdot s^{-1}$)	Bi [c]
1-MCP [d]	23	1.02×10^{-5}	5.33×10^{-7} [d]	7.32×10^{-4}
Hexanal [e]	20	7.60×10^{-6}	3.90×10^{-6} [e]	7.19×10^{-3}
Ethanol [f]	21	1.24×10^{-5}	6.88×10^{-8} [f]	7.77×10^{-5}
Acetaldehyde [f]	21	1.29×10^{-5}	6.07×10^{-7} [f]	6.59×10^{-4}

[a] Approximate mass diffusivity in air (package headspace) estimated using the correlation proposed by Fuller, Schettler, and Giddings (Johnson 1999).

[b] Permeability to active agents of LDPE film having a thickness of 25 μm.

[c] The characteristic length (L) of a bag was ~0.015 m and identified as a ratio of volume to area (Geankoplis 1993c), where bag volume and bag surface area were ~2 L and ~0.14 m^2, respectively. These figures were estimated from those reported by Charles et al. (2003) from the study of retail size MAP (LDPE bag) containing an oxygen absorber and tomatoes.

[d] Permeability reported by Lee (2003)

[e] Permeability reported by Song et al. (1996)

[f] Permeability reported by Pauly (1999)

[9] Data on LDPE film permeability and mass diffusivity are presented by Pauly (1999) and Johnson (1999), respectively.

In this work the mean hexanal vapour permeabilities for LDPE (section 4.2.2), were 4.62×10^{-6}, and 3.83×10^{-5} $m \cdot s^{-1}$ at 10 and 20ºC respectively. From these the calculated Bi values were 9.05×10^{-3} and 7.06×10^{-2}, respectively. It is therefore also reasonable to assume uniform headspace concentrations of hexanal vapour in the model active MAP systems for tomatoes.

5.4.5 Assumption P5: Negligible contribution of active agent accumulation to changes in package volume and total pressure

This assumption is justified considering the low effective concentrations of the active agent required to be achieved in the package headspace, as mentioned in section 5.4.1. The effective concentrations are significantly lower than those of other gases in the MAP system (e.g. 2-5% CO_2 and 1-10% O_2 are typical), and it is reasonable to assume these low concentrations within the package headspace will have minimal influence on the total package volume and pressure.

Dynamic volume changes of MA packages made from the flexible polymer films are nevertheless observed (e.g. Merts 1996; Talasila & Cameron 1997). These occur chiefly as a result of respiration and gaseous permeation through the sealed polymer package. For example in cases where the oxygen consumption is not balanced by mass transfer through the packaging film, a positive N_2 concentration gradient can be created resulting in N_2 permeation out of the package. The net flux of gases could then cause a reduction of the package volume until (i) the system reaches the steady-state (Mannapperuma et al. 1989; Talasila & Cameron 1997), or (ii) no further reduction in volume is possible due to the physical constraint provided by the packaged product (Merts 1996).

The alternative to modelling volume change is to assume a constant volume during the storage period (e.g. Lee et al. 1991; Charles et al. 2003). Model predictions based on constant package volume were reported to agree well with experimentally collected data, in particular once the steady-state condition developed in the package headspace. In these cases, the package volumes commonly reported in the literature were those measured by either water displacement (Charles et al. 2003; Moyls 2004) or by dilution of a known inert gas such as ethane (Lee et al. 1991). These measurements were usually conducted at the

end of the experimental period or after the attainment of the steady-state conditions. In addition, time independence of density (i.e. for determining fruit volume) and rates of physiological activities (e.g. respiration rate, and transpiration rate) of packaged horticultural products are commonly assumed during storage period. For MAP for tomatoes (e.g. Cameron et al. 1989; Tanner 1998; Charles et al. 2003), a similar assumption has been made to simplify modelling O_2 consumption by the fruit and this simplification was reported as reasonable.

In the present work, the concentration of active agent in the package headspace is the major focus as these are to be controlled within the MIC range to achieve the desired quality outcomes. Assuming a constant package volume is therefore the most conservative approach in achieving the effective level of the active agent, as any decrease in total volume would most likely increase the actual concentration of the volatile agent. Note, density of 'Royale' tomatoes was also assumed constant during the storage period (i.e. 7-14 days) and appear reasonable given the low mass loss expected and measured (e.g. < 0.60% mass loss as reported in section 3.2.2).

5.5 Secondary level assumptions

Referring to Figure 5-1, the net accumulation of active agent in the package headspace depends on the relative contributions of the identified individual mass transfer rates. The key mass transfer mechanisms and how they are modelled in order to predict the package headspace depends on the nature of each of the active agent, packaging material(s) and product. For example, mass transfer across the sachet film material (r^i_{scfl}) can be modelled by assuming either steady-state mass transfer (based on Fick's first law), where the dynamics and capacity of uptake by the film itself are neglected, or the dynamic approach (based on Fick's second law) where the concentration of active agent in the film changes with both time and position. The former approach is appropriate for transport of active agents which have low affinities with the film, while the latter might be suitable for compounds which interact with the film material. From an understanding of the various modelling options and their significance, opportunities and constraints for simplifying the mathematical models can be identified. Some of the more important aspects are discussed in the following sections.

5.5.1 Modelling of controlled release sachet systems (r^{i}_{scfl})

5.5.1.1 Modelling mass transfer within the active agent carrier

Carriers can be considered as either a (i) an entire bed of carrier materials (a homogeneous mass), or (ii) individual carrier particles. Of most interest for model development is the uniformity of active agent concentration in each of these structural compositions. The quantitative criterion adopted to determine this is the Bi value. The key internal and external resistances for the bed and/or particles may be defined as shown in Table 5-2 and conceptualised as illustrated in Figure 5-2.

Table 5-2 Internal and external resistances according to bed and particles in sachet systems

Considered level	Conceptualisation	Level of uniformity	Resistance to gas transfer	
			Internal	External
Bed	An entire bed of porous particles encasing in the sachet	Concentration surrounding the bed (sachet headspace)	Diffusion through bed	Permeation through sachet film
Particles	Individual particles in a bed	Concentration within the particles	Diffusion within particles	Diffusion through boundary film surrounding particle

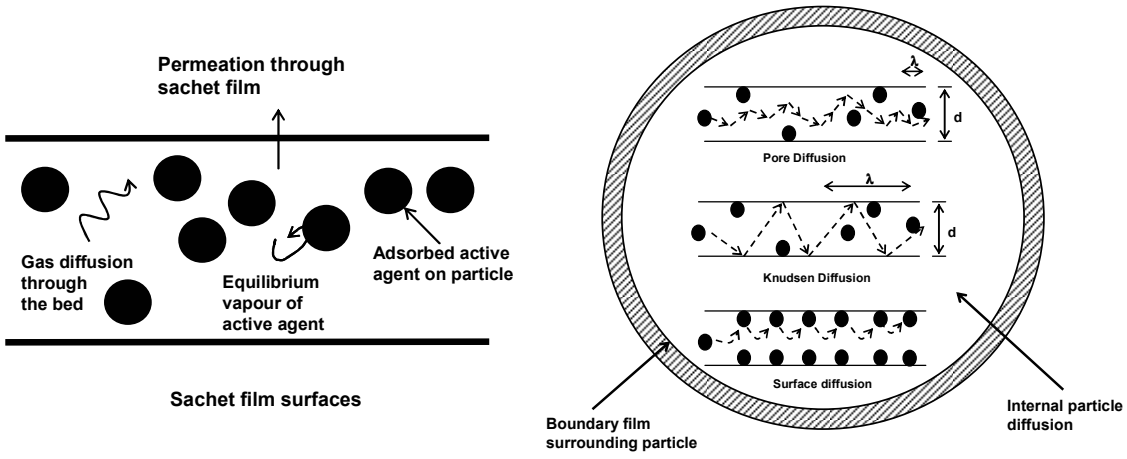

Figure 5-2 Conceptualisations of internal and external resistances of an entire bed of porous particles encasing in the sachet (A) and individual particles (B; modified from Weber 1985; Do 1998a where 'λ' and 'd' symbols represent mean free path of active agent in the gas phase and diameter of pore inside the particle, respectively).

Case 1: Bi **value of carrier bed (** Bi^{i}_{bed} **) < 0.1**

According to Geankoplis (1993c), at low Biot numbers, the rate of diffusion within the bed is high in comparison with transport through the film. In this case it can reasonably be assumed that the active agent concentration in the bed is uniform and concentration gradients occurring through the bed or within the particles are negligible. Also, only the equilibrium relationship between the active agent and solid adsorbent are required and this can be described by sorption isotherms.

Case 2: Bi^{i}_{bed} **> 0.1, but** Bi^{i}_{ptcl} **< 0.1**

For Bi^{i}_{bed} values > 0.1 the concentration gradient within the bed becomes significant and has to be taken into account in modelling the release of the active agent from the sachet. In addition, there could be significant concentration gradients within each particle due to intraparticle diffusion mass transfer that may have to be quantified through the Bi values for the particles (Bi^{i}_{ptcl}). For $Bi^{i}_{ptcl} < 0.1$, the concentration gradient within the particles can reasonably be assumed to be negligible (Geankoplis 1993c) and only that across the bed is therefore significant.

The modes of diffusion through the bed (Figure 5-3) may be classified into two groups (Bronlund 1997), including: (i) particulate surface diffusion, which can occur where a thin film (free liquid) of saturated active agent is available on the carriers or (ii) gas phase diffusion. The latter occurs when there is minimal free liquid and the active agent diffuses across the bed through voids available between particles. Equilibrium between the diffusant (active agent) and solid is assumed to occur instantaneously at the surface of the solid (following McCabe et al. 2001).

A **B**

Figure 5-3 Conceptualisation of diffusional modes within the bed (given negligible concentration gradient within particles): Particle surface diffusion, where the magenta rings represent thin films through which diffusion occur (A), and gas phase diffusion within voids available between particle (B).

Case 3: Both values of Bi^i_{bed} and Bi^i_{ptcl} > 0.1

In this situation the concentration gradients across the bed and within the particles are significant. Diffusional modes across the bed could be those discussed in the previous subsection. For the individual particles, intraparticular diffusion must be modelled and this may occur by pore, surface, Knudsen or mixed diffusional modes (Figure 5-2 and as discussed in section 2.5.1.1). Following Do (1998a), equilibrium conditions within the particle are commonly assumed to occur instantaneously and all phases within the particles are in local equilibrium with the adsorbates.

Identification of Bi^i_{bed} and Bi^i_{ptcl} for hexanal vapour in controlled release sachets

Calculations of Bi^i_{bed} for controlled release sachets were made for LDPE, OPP and Tyvek® films for which the permeability data were the average values of those quantified in section 4.2.2; a summary of the Bi^i_{bed} calculations is shown in Appendix F.1 (Table F-1). The estimated Bi^i_{bed} values of LDPE and OPP sachet systems are very much lower than 0.1 at both 10 and 20ºC (with magnitudes of 10^{-2} to 10^{-4}). However the values of Tyvek® system were ~0.2 and 0.5 at 10 and 20ºC, respectively (Table F-1). The assumption of uniform concentration in sachet headspace (or throughout the bed) may be valid only in LDPE and OPP systems. For the Tyvek® sachet, the concentration gradient across the bed may become significant. Because the estimates of Bi^i_{bed} values (for all films) were based on the average permeability values, the very high permeability values at high concentrations (such as the Tyvek® permeability at 20ºC of ~2.25×10^{-10} pmol·m·m^{-2}·s^{-1}·Pa^{-1} at ~0.22 mol·m^{-3}) were taken into account. In practice, such high concentrations should only occur in the headspace of the sachet prior to it being exposed to the package headspace ($t \leq 0$) (further discussed in Chapter 6). During storage of product following the initial period (~24 h), it can be reasonably assumed that hexanal vapour concentration in the sachet headspace will be much lower, hence the permeability value and Bi^i_{bed} will be lower (and $Bi^i_{bed} << 0.1$), so the assumption of uniform hexanal concentration is then expected to be valid.

5.5.1.2 Modelling mass transfer across the sachet film material

Most active agents are organic vapours and these could potentially interact or have strong affinities with packaging components, particularly nonpolar polymer films such as LDPE

and OPP. In this situation unsteady-state models (Fick's second law) might be the most practical approach to describe mass transfer because concentrations of diffusant are then dependent on both time and position within the film (Robertson 1993c; Beu 2000; Piringer 2000).

As the sachet film separates the carrier bed and the package headspace, it is possible to compare relative rates of concentration change in the film with those of the headspace and carrier bed. If the rate of change within the film is much faster than that in the other components, the sachet film is likely to be at equilibrium with the active agent and a steady-state concentration gradient across the film should be expected. Fick's first law can then be employed.

To select between these scenarios, a quantitative criterion for comparing magnitudes of rates of concentration changes in the carrier bed, sachet film and package headspace is required. This can be achieved through scaling analysis. Scaling analysis involves formulating dimensionless differential equations describing the rates of change of two or more parameters of interest and then identifying dimensionless parameters that can be used to compare them. Following Krantz (2007) (page 153-158), Eq. 5-3 and Eq. 5-4 were developed to allow comparison of the rates of change of concentration in the sachet film, the packaging headspace and the sachet interior (the derivations are shown in Appendix F.2.1). These equations were developed for a system where the adsorption isotherm for the vapour-carrier system is linear and the sachet releases adsorbent through a film into a package headspace. While the adsorption isotherm behaviour may be more complex than this scenario in potential systems of interest (as in the hexanal-silica gel system) it does serve as a useful approximation to be used for assessing the importance of sachet film adsorption rates.

$$\frac{r_{scfl}}{r_{bed}} = \frac{K^{i}_{bed} M_{bed}}{L_{scfl} S^{i}_{scfl} A_{scfl} RT_{pkg}} \cdot \frac{C^{i}_{scfl,0}}{\left(C^{i}_{scfl,0} - C^{i}_{scfl,L_{scfl}} \right)} \qquad \textbf{(Eq. 5-3)}$$

$$\frac{r_{scfl}}{r_{pkhs}} = \frac{V_{pkg}}{L_{scfl} S^{i}_{scfl} A_{scfl} RT_{pkg}} \cdot \frac{C^{i}_{scfl,0}}{\left(C^{i}_{scfl,0} - C^{i}_{scfl,L_{scfl}} \right)} \qquad \textbf{(Eq. 5-4)}$$

where

r_{scfl} = Rate of changes of active agent concentration in the sachet film (dimensionless)

r_{bed} = Rate of changes of active agent concentration in carrier bed (dimensionless)

r_{pkhs} = Rate of changes of active agent concentration in package headspace (dimensionless)

L_{scfl} = Sachet film material thickness (m)

S^{i}_{scfl} = Sachet film solubility to active agent *i* ($mol \cdot m^{-3} \cdot Pa^{-1}$)

A_{scfl} = Sachet film surface area (m^2)

K^{i}_{bed} = Coefficient of the linear desorption isotherm of active agent *i* for the carrier (adsorbent) bed ($m^3 \cdot g^{-1}$)

M_{bed} = Mass of the carrier bed (free of the mass of active agent *i*) (g)

$C^{i}_{scfl,0}$ = Concentration of active agent *i* in sachet film at x = 0, facing the carrier bed ($mol \cdot m^{-3}$)

$C^{i}_{scfl,L_{scfl}}$ = Concentration of active agent *i* in the sachet film at x = L_{scfl}, facing the package headspace ($mol \cdot m^{-3}$)

V_{pkg} = Volume of package (m^3)

T_{pkg} = Temperature of package (K)

On the right hand side (RHS) of Eq. 5-3 and Eq. 5-4 there are two terms. The first term of both equations represents the 'relative system capacity' of the carrier bed and package headspace, respectively, with respect to that of the sachet film. The second term in the equations is essentially the dimensionless initial driving force between the two surfaces of the sachet film and will vary from 0 to 1. At the onset of the release of active agent from the sachet to the package headspace, the driving force ratio can reasonably be assumed to be unity because the active agent should initially be absent from the package atmosphere.

The relative rate of change is subsequently dependent on the relative system capacity (Eq. 5-3 and Eq. 5-4). For future reference, the first term of Eq. 5-3 and Eq. 5-4 are referred as the ratio of carrier bed capacity to sachet film capacity (denoted as $CR_{bed/scfl}$) and the ratio of package headspace capacity to that of the sachet film (denoted as $CR_{pkhs/scfl}$),

respectively. If these ratios are large then it means that the rate of change in the sachet film is fast compared with the rate of change in the bed or package headspace. It would normally be expected that $CR_{bed/scfl}$ should have a large magnitude because the capacity of adsorbents to retain active agents is expected to be much higher than that of the thin film.

Data chiefly based on physico-chemical properties of 1-MCP reported by Lee (2003) was used to illustrate the application of scaling analysis. The reasons for this are two-fold: firstly, the development of an active package to release 1-MCP for suppressing ethylene action of tomatoes is an important milestone in the development of active packaging systems (Utto et al. 2005; Nanthachai et al. 2007). Secondly, and most importantly, because 1-MCP does not interact with common polymer films (e.g. LDPE) and the steady-state approach is commonly used for modelling mass transfer across the films (Lee 2003), it is valuable to explore when the unsteady-state modelling approach should be implemented by increasing the LDPE film affinity with 1-MCP.

For the 1-MCP and LDPE sachet system (Lee 2003) (Table 5-3), $CR_{bed/scfl}$ is ~1900 and $CR_{pkhs/scfl}$ ~1500. This suggests that the rates of change in the sachet film are much higher than those in both the carrier bed and package headspace and steady-state mass transfer in the sachet film can reasonably be assumed.

Table 5-3 Input data of 1-MCP active packaging system (at 23°C; following Lee 2003) for illustrating scaling analyses

Input data	Units	Values
L_{scfl} [a]	m	25×10^{-6}
S_{scfl}^{MCP} [a]	$mol \cdot m^{-3} \cdot Pa^{-1}$	0.0043
K_{bed}^{MCP} [a]	$m^3 \cdot g^{-1}$	0.0015
A_{scfl} [b]	m^2	0.003
V_{pkhs} [b]	m^3	0.0012
M_{bed} [b]	g	1

[a] Reported by Lee (2003) where LDPE as the sachet film material and silica gel as 1-MCP carrier

[b] Arbitrarily chosen. These values were in the range of the retail package size, and these were used extensively in mathematical simulations and physical model development (see Chapter 6)

where

S_{scfl}^{MCP} = Sachet film solubility to1-MCP as reported by Lee (2003) ($mol \cdot m^{-3} \cdot Pa^{-1}$)

K_{bed}^{MCP} = Coefficient of linear sorption isotherm of 1-MCP for silica gel as reported by Lee (2003) ($m^3 \cdot g^{-1}$)

However when the capacities of the film and other system components become comparable, the assumption of steady-state mass transfer may not be valid and that of dynamic mass transfer (unsteady-state) may become significant. To illustrate this, simulations were performed to demonstrate the influences of 1-MCP transport across the LDPE sachet film, either (i) steady-state (Fick's first law) or (ii) dynamic (Fick's second law), on accumulation of 1-MCP within a completely sealed package headspace (i.e. for a film acting as a barrier to 1-MCP, such as a foil bag). The two modelling approaches employ ordinary differential equations (ODEs) and partial differential equations (PDEs), respectively. Derivation of the mathematical models is provided in Appendix F.3.1.

When the PDE modelling approach is implemented, the initial and boundary conditions must be also justified. Prior to the release of the active agent, the sachet and packaging films may be assumed free of active agent ($C_{scfl}^{MCP} = C_{pkfl}^{MCP} = 0$; where C_{scfl}^{MCP} and C_{pkfl}^{MCP} = concentration of 1-MCP in the sachet film and packaging film, respectively). However this assumption requires further consideration for the sachet film material. The assumption $C_{scfl}^{MCP} = 0$ is probably only valid when the sachet is freshly made, i.e. if the sachet is first formed, filled with the carrier pre-saturated with the active agent, and then immediately sealed and placed into the outer bags. However if the sachet is pre-made and stored for sometime prior to being added to the package, the sachet film material should be assumed to be in equilibrium with the sachet headspace concentration of the active agent. In the latter case, a barrier to the release of the active agent (e.g. in the form of multilayer films or a surface coating) must be employed to prevent depletion of the active ingredient from the sachet (see Rooney 1995a).

The 1st kind of boundary condition was used for the PDE model where the surface concentration was assumed to be in equilibrium with the concentration of active agent surrounding the film. Concentrations were specified for (i) the gas phase surrounding the

carrier bed (sachet headspace) and (ii) the package headspace. This boundary condition is the most simple because only the partition coefficient (the film solubility to 1-MCP) is required to describe the equilibrium condition between the film and the surrounding gas. The 1st kind of boundary condition is extensively used in mathematical model development in this chapter.

The solubility of the active agent in the film is a key parameter contributing to $CR_{pkhs/scfl}$ that will vary depending on which type of the polymer film is used for the sachet. Solubility values of the sachet film were varied by factors of 10 to provide a range of $CR_{pkhs/scfl}$ values (from its original value of ~1500; provided constant values of other inputs were maintained as shown in Table 5-3) during individual PDE mathematical simulations. Figure 5-4 illustrates the resulting hexanal accumulation in the package headspace, comparing PDE results to those of the steady-state model.

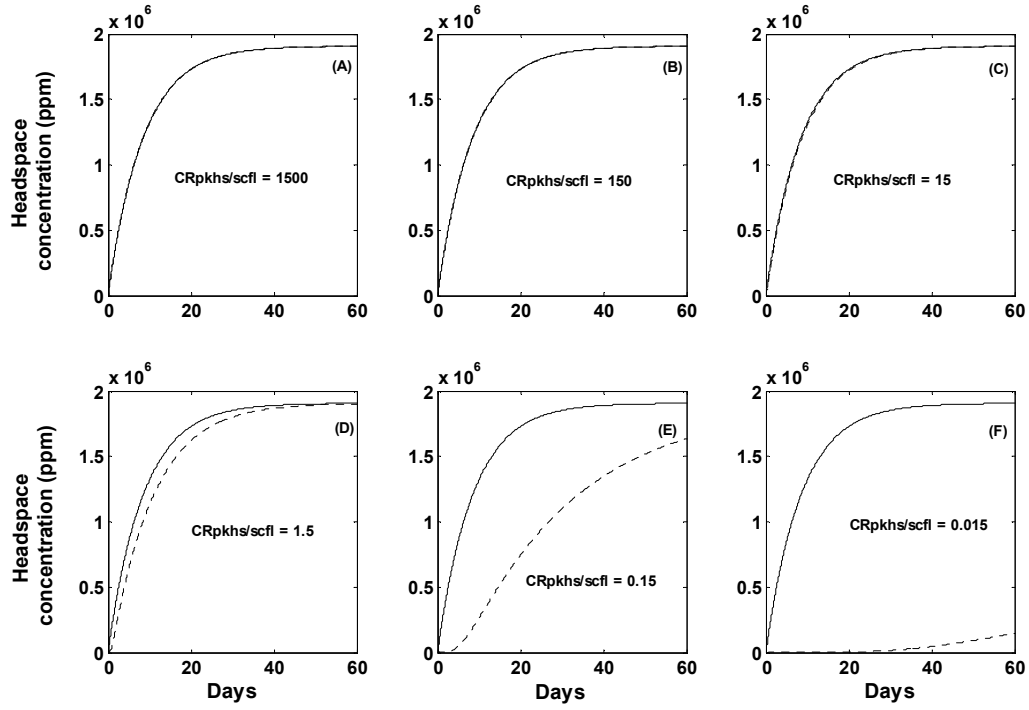

Figure 5-4 Simulations of 1-MCP accumulation in the package headspace as predicted by steady-state and PDE (with the 1st kind of boundary condition) models, represented by solid and dotted lines, respectively. $CR_{pkhs/scfl}$ was varied by changing S_{scfl}^{MCP} values.

The differences between the 1-MCP concentrations in the headspace predicted by the steady- and unsteady-state models become greater as the value of $CR_{pkhs/scfl}$ becomes smaller (i.e. as values of solubility are increased; Figure 5-4). From these simulations, it appears the capacity of the package headspace (i.e. the headspace volume) should be ≥ 2-fold higher than that of the sachet film (i.e. the sachet film volume; Figure 5-4D) in order to reasonably ignore unsteady-state mass transfer in the sachet film. For $CR_{pkhs/scfl}$ values ≤ 2 (Figure 5-4D to F), unsteady-state (Fick's second law) modelling better describes mass transport across the sachet film.

For the hexanal active MAP system, calculated values of $CR_{bed/scfl}$ and $CR_{pkhs/scfl}$ for all sachet film materials (considered at both 10 and 20ºC) were ~ 35-550 and 2-33, respectively (Appendix F.4). As these are ≥ 2 it is reasonable to assume that rate of concentration change in the sachet film will be higher than those in the carrier bed and package headspace. Mass transfer of hexanal vapour across the sachet films can therefore be reasonably modelled assuming steady-state mass transfer.

5.5.2 Modelling packaging film material (r^{i}_{pkfl})

Mass transfer processes across the outer packaging film can be examined in a similar manner to those employed for the sachet film material (section 5.5.1). In this case the relative rate of change of hexanal concentration in the packaging film compared to the package headspace can be used as the quantitative criteria, as expressed in Eq. 5-5. This scaling analysis was based on a constant partial pressure of adsorbent within the sachet being released into the headspace through the film. A derivation of Eq. 5-5 is provided in Appendix F.2.2. The first term in Eq. 5-5 is the ratio of the capacity of the package headspace for holding adsorbent to that of the packaging film, denoted as $CR_{pkhs/pkfl}$.

$$\frac{r_{pkfl}}{r_{pkhs}} = \frac{V_{pkg}}{L_{pkfl} S^{i}_{pkfl} A_{pkfl} R T_{pkg}} \frac{C^{i}_{pkfl,0}}{\left(C^{i}_{pkfl,0} - C^{i}_{pkfl,L_{pkfl}}\right)} \qquad \textbf{(Eq. 5-5)}$$

where

r_{pkfl} = Rate of changes of active agent concentration in the packaging film (dimensionless)

L_{pkfl} = Packaging film material thickness (m)

S^{i}_{pkfl} = Packaging film solubility to active agent *i* (mol·m^{-3}·Pa^{-1})

A_{pkfl} = Packaging film surface area (m^2)

$C^{i}_{pkfl,0}$ = Concentration of active agent *i* in the film at x = 0, facing the package headspace (mol·m^{-3})

$C^{i}_{pkfl,L_{pkfl}}$ = Concentration of active agent *i* in the film at x = L_{pkfl}, facing the surrounding environment (mol·m^{-3})

Given A_{pkfl} = 0.125 m^2 and other parameters in Eq. 5-5 as given in Table 5-3, $CR_{pkhs/pkfl}$ for the 1-MCP system is ~36, suggesting that the rate of adsorption by the packaging film is fast compared with the changes within the package headspace. As before a steady-state model for the loss of 1-MCP from the package headspace is appropriate. To demonstrate this, mathematical simulations of a PDE-based model to calculate the transients in the packaging film (with the 1st kind of boundary condition) were compared with values from a steady-state simulation of 1-MCP loss through the packaging film in terms of their effect on package headspace concentration (Appendix F.3.2). The 1-MCP solubility was again varied by factors of 10 to vary $CR_{pkhs/pkfl}$ from its initial value ~36 for each consecutive simulation. Figure 5-5 illustrates the simulation results.

It was evident that the deviation in 1-MCP concentration between the models becomes greater as the value of $CR_{pkhs/pkfl}$ becomes smaller due to increases in the film solubility. From the simulation results, the value of $CR_{pkhs/pkfl}$ should be ≥ 1 (Figure 5-5C) in order to reasonably neglect unsteady-state mass transfer in the packaging film.

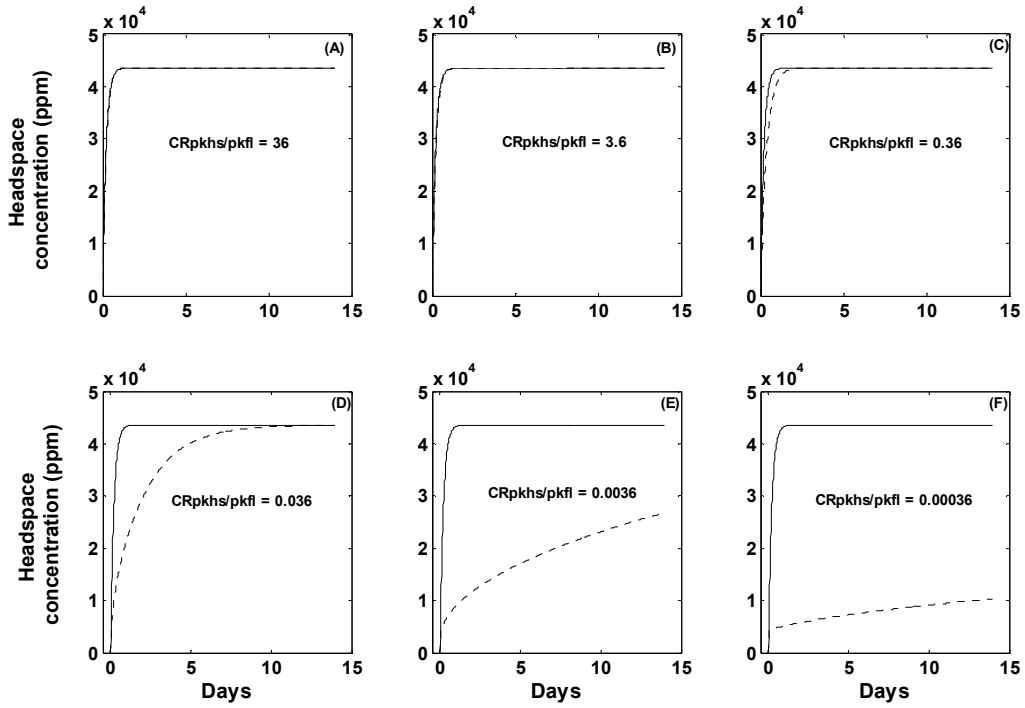

Figure 5-5 Simulations of 1-MCP accumulation in the package headspace as predicted by steady-state and PDE (with the 1st kind of boundary condition) models, represented by solid and dotted lines, respectively. $CR_{pkhs/pkfl}$ was varied by changing S_{pkfl}^{MCP} values.

A range of organic compounds, such as aldehydes and esters, have been applied in active packaging systems (see Chapter 2) and these are documented to have high solubility or affinity with common packaging films such as LDPE (Piringer 2000; Dury-Brun et al. 2007). Therefore, approaches utilised for modelling the mass transfer across the packaging film of the active agents must be carefully justified and the scaling quantitative criteria can be implemented for this purpose.

For a hexanal-based active MAP system, calculated values of $CR_{pkhs/pkfl}$ for LDPE sachet film materials at both 10 and 20ºC are 0.31 and 0.17, respectively (as shown in Appendix F.4). As these are less than 1 (Figure 5-5C), this suggests hexanal concentration changes in the packaging film are likely to be slower than those in the package headspace and therefore a PDE modelling approach is more appropriate for describing hexanal mass transport across the packaging film.

5.5.3 Modelling the active agent interaction with the product (r_{fr}^{i})

From Chapter 2, the generic approaches for modelling interactions between the active agent and the packaged horticultural product are (i) adsorption by and diffusion within the product and/or (ii) removal by reaction. Diffusion was modelled as the uptake of the active agent from the surrounding environment into the product and its transfer by diffusion, possibly to active sites where a reaction occurred. Modes of diffusion can be either steady- or unsteady-state. The choice between these could be justified by the apparent Bi value (designated as Bi_{fr}^{i}) to identify the likelihood of significant concentration gradients within the internal product according to the relative external and internal resistances, represented by the skin permeance to the active agent and mass diffusivity of the active agent in the flesh of fruit, respectively (as discussed in section 2.7).

When $Bi_{fr}^{i} < 0.1$, the steady-state mass transfer model can be reasonably used to describe diffusion of the active agent. Whilst the steady-state diffusion model is reported to describe gas exchange and, in particular, the respiration rate (Solomos 1987; Ben-Yehoshua & Cameron 1989; Merts 1996), its application to active packaging systems is limited. The generic equation for this approach is shown in Eq. 5-6 for the example of O_2 consumption by respiration. The respiration rate can be modelled using several approaches, either theoretical or empirical as documented by Fonseca et al. (2002a) and Hertog et al. (1998), among others and this is later discussed in section 5.7.4.

$$N_{fr}^{O_2} = k_{fr}^{O_2} A_{fr} \left(C_{fr,ext}^{O_2} - C_{fr,int}^{O_2} \right) \qquad \textbf{(Eq. 5-6)}$$

where

N_{fr}^{O2} = Steady-state rate of transfer of gas O_2 across fruit skin ($mol \cdot s^{-1}$)

k_{fr}^{O2} = Fruit skin permeance to gas O_2 ($m \cdot s^{-1}$)

A_{fr} = Fruit surface area (m^2)

$C_{fr,ext}^{O2}, C_{fr,int}^{O2}$ = Concentration of gas O_2 in external and internal fruit, respectively ($mol \cdot m^{-3}$)

When $Bi_{fr}^{i} > 0.1$, the unsteady-state model should be used to describe diffusion within the fruit. Haros et al. (2005) modelled diffusion of sulphur dioxide (SO_2) in dent corn during steeping using an unsteady-state modelling approach in which the interaction between SO_2

and corn was modelled as a first order kinetic reaction. As SO_2 is extensively used in the horticultural industry, e.g. for antimicrobial fumigations of grapes (Mustonen 1992), the modelling approach utilised by Haros et al. (2005) provides valuable insights. The expression of SO_2 unsteady-state diffusion and the reaction rate(s) with fruit are given by Eq. 5-7. Haros et al. (2005) utilised the boundary conditions (Eq. 5-9 to Eq. 5-10) suggested by Crank (1975) for mass transfer coupled with reaction for modelling interactions between the active agent and fruit.

$$\frac{\partial C_{fr}^{SO2}}{\partial t} = D_{fr}^{SO2} \frac{\partial^2 C_{fr}^{SO2}}{\partial x_{fr}^2} - r_{fr}^{SO2} \qquad \textbf{(Eq. 5-7)}$$

Initial and boundary conditions were as follows:

$$t = 0 \qquad C_{fr}^{SO2} = 0 \qquad 0 \le x_{fr} \le R_{fr} \qquad \textbf{(Eq. 5-8)}$$

$$t > 0 \qquad \partial C_{fr}^{SO2} \big/ \partial x_{fr} = 0 \qquad x_{fr} = 0 \qquad \textbf{(Eq. 5-9)}$$

$$t > 0 \qquad C_{fr}^{SO2} = C_{fr,e}^{SO2} \qquad x_{fr} = R_{fr} \qquad \textbf{(Eq. 5-10)}$$

where

C_{fr}^{SO2} = Concentration of SO_2 dissolved in fruit ($mol \cdot m^{-3}$)

D_{fr}^{SO2} = Effective mass diffusivity of SO_2 dissolved in fruit ($m^2 \cdot s^{-1}$)

x_{fr} = Position in fruit (m)

r_{fr}^{SO2} = Reaction rate of SO_2 and corn ($mol \cdot m^{-3} \cdot s^{-1}$) which Haros et al. (2005) assumed to follow first order kinetics

$C_{fr,e}^{SO2}$ = Equilibrium concentration representing the maximum SO_2 concentration attained in the corn ($mol \cdot m^{-3}$)

R_{fr} = Radius of fruit (assumed to be spherical) (m)

As an alternative to diffusion models, interactions between the active agent and product could be modelled as a general n^{th}-order reaction rate (similar to the second term of Eq. 5-7) (Labuza 1982; Robertson 1993a; Earle & Earle 2003). The generic expression of this model is shown in Eq. 5-11.

$$r^{i}_{fr} = k^{i}_{fr,reac}\left(C^{i}_{fr,air}\right)^{n_{reac}} \quad \textbf{(Eq. 5-11)}$$

where

r^{i}_{fr} = Reaction rate of between active agent *i* and fruit ($mol \cdot s^{-1} \cdot kg^{-1}$)

$k^{i}_{fr,reac}$ = Rate coefficient for the reaction of the active agent *i* and fruit ($mol \cdot s^{-1} \cdot kg^{-1}\ (m^3 \cdot mol^{-1})^{n_{reac}}$)

$C^{i}_{fr,air}$ = Concentration of active agent *i* surrounding fruit ($mol \cdot m^{-3}$)

In the literature, the justifications used for selection between the diffusion-based and the reaction-based modelling approaches are unclear. These appear arbitrary and are mainly based on the quality of fit and/or the simplicity of the model e.g. see discussions on respiration rate modelling by Fonseca et al.(2002a) and Fonseca et al.(2002b). The reaction-based modelling approach could simplify the complexity of mathematical models and the requirements for model inputs (such as mass diffusivity or partition coefficients) compared to the diffusion-based modelling approach. In Chapter 3 (section 3.4.2), the reaction-based modelling approach was utilised to describe the apparent rate of hexanal uptake by tomatoes because of its simplicity and for the purposes for comparing model results obtained from the present work to those reported by Wolford (1998).

5.5.4 Modelling accumulation in the package headspace (r^{i}_{pkhs})

Eq. 5-12 is the equation describing the rate of volatile accumulation in the package headspace (r^{i}_{pkhs}), which is the left hand side term of Eq. 5-1 :

$$\begin{pmatrix} Rate\ of \\ accumulation \end{pmatrix} = \begin{pmatrix} system \\ capacity \end{pmatrix} \times \begin{pmatrix} Rate\ of\ change \\ in\ concentration \\ with\ time \end{pmatrix} \quad \textbf{(Eq. 5-12)}$$

The system capacity of the package headspace is assumed to be its net volume (V_{pkg}; after subtracting the volume of fruit and any other packaging elements) which is assumed constant (section 5.4.5). The rate of accumulation can then be expressed as Eq. 5-13.

$$r^{i}_{pkhs} = V_{pkg} \times \frac{dC^{i}_{pkhs}}{dt} \quad \textbf{(Eq. 5-13)}$$

where

r^{i}_{pkhs} = Rate of accumulation of active agent *i* in package headspace (mol·s^{-1})

C^{i}_{pkhs} = Concentration of active agent *i* in package headspace (mol·m^{-3})

In modelling packaging films (Figure 5-5), it was evident that lowering the $CR_{pkhs/pkfl}$ value (by increasing the of film solubility) could affect accumulation of the active agent in the package headspace. In this case, the higher the solubility (given the same permeability), the greater the error in ignoring the transients due to film uptake. This is expected because a longer timeframe is required for the system having a high solubility value to achieve equilibrium. For such a case, the PDE model becomes appropriate for modelling mass transfer through the packaging film.

However if the $CR_{pkhs/pkfl}$ is high, the loss of active agent from the film can be modelled assuming steady-state conditions in the film. If this is done there is an implicit assumption that a steady-state active agent profile is reached instantaneously through the packaging film (i.e. the film reaches equilibrium with the permeant). In this case a factor in addition to the package volume (V_{pkg}) is required to account for system capacity of the film. This factor may be termed the Outer Film Sorption Capacity ($OFSC$). Because ambient gases (N_2, CO_2, and O_2) have low solubilities in common polymer films such as LDPE, the $OFSC$ values for these gases can reasonably be assumed negligible and only V_{pkg} is required in modelling the accumulations of these gases in MA packaging (as discussed in section 5.4.5).

For the case where the $OFSC$ becomes important (when the film has a high affinity for active agent), then it must be included with V_{pkg} and this will effectively slow the rate of change in the package headspace. At low concentrations of the active agent in the package headspace, the $OFSC$ may be calculated as the product of packaging film volume (V_{pkfl}) and concentration of active agent in the film, where the latter may be estimated following Henry's law (as discussed in 5.5.1.2). Given a reasonably linear concentration gradient through the film, an arithmetic average of the active agent vapour concentrations either side of the film (i.e. an average of C^{i}_{pkhs} and C^{i}_{env} where C^{i}_{env} represents concentration of active agent *i* in environment surrounding the bag) can be used to calculate the film

concentration. Typically the C^{i}_{env} value is zero, so the rate of accumulation described by the ODE model is then expressed as shown in Eq. 5-14.

$$r^{i}_{pkhs} = \left(V_{pkg} + \frac{V_{pkfl} S^{i}_{pkfl} RT_{pkg}}{2} \right) \times \frac{dC^{i}_{pkhs}}{dt} \qquad \textbf{(Eq. 5-14)}$$

Because the estimated values of $CR_{pkhs/pkfl}$ of the hexanal active MAP system (reported in section 5.5.2) were lower than 1 and utilisation of the PDE modelling approach for the package film was justified, the system capacity used in Eq. 5-12 was just the volume of the package headspace.

5.6 A comprehensive decision tree for the design of active packaging system for horticultural products

Figure 5-6 illustrates a comprehensive decision tree developed for the various scenarios considered in the previous sections for the design of active packaging systems with release of an active agent from sachets. The modelling options for the mass transfer processes for each key component of the active package are provided, as are the criteria for justifying the selection between these options.

In certain circumstances there may be uncertain criteria because of the complex nature of the mass transfer processes as, for example, when a reaction occurs between the active agent(s) and packaged fruit. The word '*Assumption*' is used in the decision tree to represent these uncertain criteria. It should be noted that the instantaneous equilibrium sorption condition between an active agent and solid particle, which is described by the sorption isotherm model, was applied in all modelling approaches following Do (1998a) and McCabe et al. (2001). The modelling decisions applied for the hexanal active MAP system as drawn from the previous discussion are shown as red lines in the decision tree (Figure 5-6).

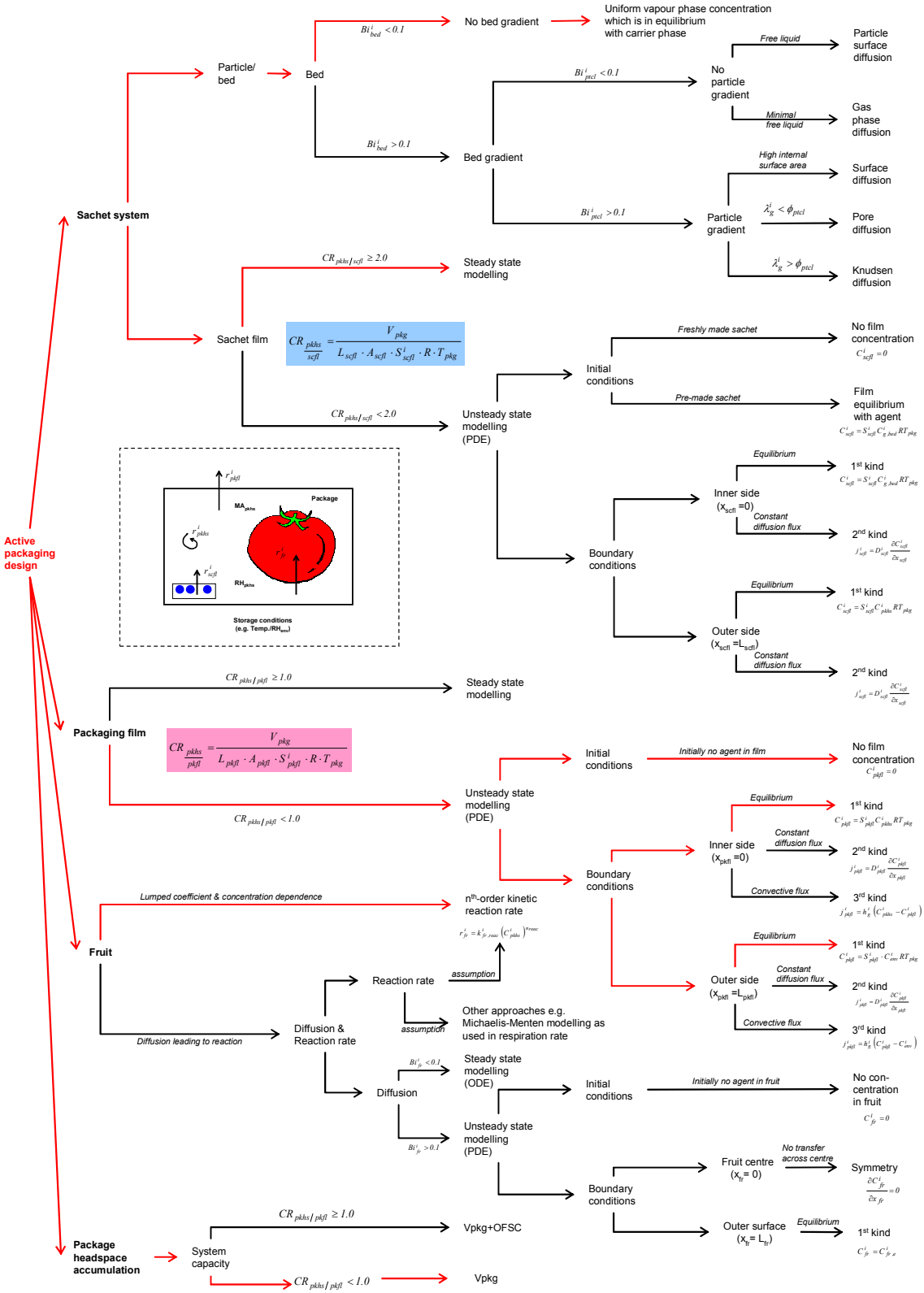

Figure 5-6 A comprehensive decision tree for design of active packaging systems for horticultural products. The modelling options employed for hexanal based active MAP for tomatoes are identified by red lines (see over for nomenclatures).

Abbreviations and symbols appearing in Figure 5-6 are defined as followings:

Symbols/ Abbreviations		Descriptions
Bi^{i}_{bed}	=	Biot value of active agent *i* with respect to the sachet carrier bed (dimensionless)
Bi^{i}_{ptcl}	=	Biot value of active agent *i* with respect to particles in the sachet (dimensionless)
Bi^{i}_{fr}	=	Biot value of active agent *i* with respect to fruit (dimensionless)
C^{i}_{scfl}	=	Concentration of active agent *i* in the sachet film material ($mol \cdot m^{-3}$)
C^{i}_{pkfl}	=	Concentration of active agent *i* in the packaging film material ($mol \cdot m^{-3}$)
$C^{i}_{g,bed}$	=	Equilibrium vapour concentration of active agent *i* of solid bed ($mol \cdot m^{-3}$)
C^{i}_{pkhs}	=	Concentration of active agent *i* in the package headspace ($mol \cdot m^{-3}$)
C^{i}_{fr}	=	Concentration of active agent *i* in the fruit ($mol \cdot m^{-3}$)
$C^{i}_{fr,e}$	=	Equilibrium concentration representing the maximum concentration of active agent *i* that the fruit can attain ($mol \cdot m^{-3}$)
C^{i}_{env}	=	Concentration of active agent *i* in surrounding environment ($mol \cdot m^{-3}$)
$CR_{pkhs/scfl}$	=	A ratio of capacity of package headspace to that of the sachet film (dimensionless)
$CR_{pkhs/pkfl}$	=	A ratio of capacity of package headspace to that of the packaging film (dimensionless)
D^{i}_{scfl}	=	Diffusivity of active agent *i* in sachet film material ($m^2 \cdot s^{-1}$)
D^{i}_{pkfl}	=	Diffusivity of active agent *i* in packaging film material ($m^2 \cdot s^{-1}$)
h^{i}_{g}	=	Convective mass transfer coefficient ($m \cdot s^{-1}$)
j^{i}_{scfl}	=	Constant diffusion flux of active agent *i* to or from sachet film material ($mol \cdot s^{-1} \cdot m^{-2}$)
j^{i}_{pkfl}	=	Constant diffusion flux of active agent *i* to or from packaging film material ($mol \cdot s^{-1} \cdot m^{-2}$)

Symbols/ Abbreviations		Descriptions
$k^{i}_{fr,reac}$	=	Reaction rate coefficient of active agent *i* and fruit ($mol \cdot s^{-1} \cdot kg^{-1}$ ($m^3 \cdot mol^{-1}$) $^{n_{reac}}$)
L_{scfl}, L_{pkfl}, L_{fr}	=	Describing the outer surfaces of sachet film, packaging film and fruit, respectively
n_{reac}	=	Order of reaction rate (dimensionless)
$OFSC$	=	Outer Film Sorption Capacity (mol)
ODE	=	Ordinary Differential Equation
PDE	=	Partial Differential Equation
R	=	Gas constant ($8.314\ J \cdot mol^{-1} \cdot K^{-1}$)
r^{i}_{fr}	=	Reaction rate between active agent *i* and fruit ($mol \cdot s^{-1}$)
S^{i}_{pkfl}	=	Packaging film solubility to active agent *i* ($mol \cdot m^{-3} \cdot Pa^{-1}$)
S^{i}_{scfl}	=	Sachet film solubility to active agent *i* ($mol \cdot m^{-3} \cdot Pa^{-1}$)
T_{pkg}	=	Temperature of package (K)
V_{pkg}	=	Package volume (m^3)
x_{scfl}	=	Position in the sachet film material (m)
x_{pkfl}	=	Position in the packaging film material (m)
x_{fr}	=	Position in the fruit (m)
λ^{i}_{g}	=	Mean free path of active agent *i* in the gas phase (m)
ϕ_{ptcl}	=	Diameter of pore inside the particle (m)

5.7 Mathematical model formulation for the Hexanal/Silica gel/Tomato active MAP system

According to the overall balance equation (Eq. 5-1), individual components were converted into the following mathematical equations.

5.7.1 Rate of hexanal release from sachet

Because $CR_{pkhs/scfl} \geq 2$ (section 5.5.1.2), it is appropriate to neglect the dynamics of adsorption in the sachet film and instead model hexanal release as a steady-state one-dimensional flux across the sachet film material. From the discussion in section 4.2.2, it is apparent that the assumption of a linear concentration gradient through the film Eq. 2-8 may lead to an underestimation of flux where a significant difference of concentration exists between the two sides of the film. This is likely to be the case for the initial stages of hexanal release from a sachet into the package headspace. In such as case, the alternative equation (Eq. 4-5) may be more appropriate and therefore this was utilised to describe the steady-state mass transfer rate of hexanal vapour across the sachet film as shown in Eq.5-15. The derivation of Eq. 5-15 is described in Appendix D.1.

$$r_{scfl}^{Hxl} = \frac{P_{scfl,0}^{Hxl} A_{scfl} RT_{pkg}}{L_{scfl} b_{scfl}} \left(exp\left(C_{g,bed}^{Hxl} \cdot b_{scfl} \right) - exp\left(C_{pkhs}^{Hxl} \cdot b_{scfl} \right) \right) \quad for\ t > 0; \qquad \textbf{(Eq. 5-15)}$$

and $for\ t = 0;\ C_{g,bed}^{Hxl} = C_{sat}^{Hxl}$

where

r_{scfl}^{Hxl} = Rate of hexanal permeation through the sachet film material (mol·s^{-1})

$P_{scfl,0}^{Hxl}$ = Pre-exponential factor of effective permeability to hexanal vapour of sachet film material (mol·m·m^{-2}·s^{-1}·Pa^{-1})

b_{scfl} = Fitted exponential model coefficient of effective permeability to hexanal vapour of sachet film material (m^{3}·mol^{-1})

$C_{g,bed}^{Hxl}$ = Equilibrium hexanal vapour concentration above the carrier bed (mol·m^{-3})

C_{pkhs}^{Hxl} = Hexanal vapour concentration in the package headspace (mol·m^{-3})

C_{sat}^{Hxl} = Saturated hexanal vapour concentration at a given temperature (mol·m^{-3})

The value of $C_{g,bed}^{Hxl}$ is varied according to the amount of adsorbed hexanal remaining in the carrier bed ($C_{s,bed}^{Hxl}$). The relationship between these parameters is described using the Langmuir sorption isotherm (Eq. 5-16) which was rearranged from its original form (Eq. 2-3) that described $C_{s,bed}^{Hxl}$ as a function of $C_{g,bed}^{Hxl}$. The rearrangement represents the actual situation where the amount of hexanal adsorbed on the silica gel decreases after the onset of release.

$$C_{g,bed}^{Hxl} = \frac{C_{s,bed}^{Hxl}}{b_{Lgm}^{Hxl} \cdot \left(C_{s,max}^{Hxl} - C_{s,bed}^{Hxl}\right)} \quad \textbf{(Eq. 5-16)}$$

where

$C_{s,bed}^{Hxl}$ = Equilibrium adsorbed amount of hexanal on the carrier bed (mol·g^{-1})

$C_{s,max}^{Hxl}$ = Maximum amount of hexanal adsorbed on the carrier estimated by the Langmuir sorption isotherm (mol·g^{-1})

b_{Lgm}^{Hxl} = Langmuir constant of hexanal sorption (m^3·mol^{-1})

From Eq. 5-16, it can be inferred that changes to $C_{s,bed}^{Hxl}$ will directly affect $C_{g,bed}^{Hxl}$, which in turn influences the concentration gradient across the sachet film. For this reason the depletion of hexanal from the adsorbent particles was modelled where the rate of change in the bed is equal to the loss through the sachet film. The rate of change of $C_{s,bed}^{Hxl}$ could be defined as shown in Eq. 5-17;

$$M_{bed} \frac{\partial C_{s,bed}^{Hxl}}{\partial t} = -\frac{P_{scfl,0}^{Hxl} A_{scfl} RT_{pkg}}{L_{scfl} b_{scfl}} \left(exp\left(C_{g,bed}^{Hxl} \cdot b_{scfl}\right) - exp\left(C_{pkhs}^{Hxl} \cdot b_{scfl}\right)\right) \quad \textbf{(Eq. 5-17)}$$

$for\ t > 0$;

and $for\ t = 0;\ C_{s,bed}^{Hxl} = C_{s,max}^{Hxl}$

5.7.2 Rate of hexanal transfer across the packaging film material

As described above, as $CR_{pkhs/pkfl} \leq 1$ (actually ~0.36; section 5.5.2) this means the dynamics of the packaging film are not fast enough to assume equilibrium with the package headspace. As such the rate of hexanal transfer from the headspace to the surrounding environment through the packaging film material was defined using Fick's second law for diffusion in one-dimension (Eq. 5-18). The solubility and permeability values were based on local hexanal concentrations in the film. The derivation of Eq. 5-18

is shown in Appendix D.1. Solutions of Eq. 5-18 were obtained numerically by using an explicit finite difference scheme described later in this chapter.

$$\frac{\partial C_{g,x_{pkfl}}^{Hxl}}{\partial t} = \frac{\partial}{\partial x_{pkfl}} \left(P_{pkfl,0}^{Hxl} RT_{pkg} \exp\left(C_{g,x_{pkfl}}^{Hxl} \cdot b_{pkfl}\right) \frac{\partial C_{g,x_{pkfl}}^{Hxl}}{\partial x_{pkfl}} \right) \quad \textbf{(Eq. 5-18)}$$

The initial (Eq. 5-19) and boundary conditions (for the 1st kind of boundary condition; Eq. 5-20 and Eq. 5-21) are given as:

$$C_{g,x_{pkfl}}^{Hxl} = 0 \qquad for\ t = 0\ and\ 0 < x_{pkfl} < L_{pkfl} \quad \textbf{(Eq. 5-19)}$$

$$C_{g,x_{pkfl}}^{Hxl} = C_{pkhs}^{Hxl} \qquad for\ t > 0\ and\ x_{pkfl} = 0 \quad \textbf{(Eq. 5-20)}$$

$$C_{g,x_{pkfl}}^{Hxl} = C_{env}^{Hxl} \qquad for\ t > 0\ and\ x_{pkfl} = L_{pkfl} \quad \textbf{(Eq. 5-21)}$$

where

$C_{g,x_{pkfl}}^{Hxl}$ = Hexanal concentration in the gas phase that is in equilibrium with the packaging film material at a position x (x_{pkfl}) (mol·m^{-3})

$P_{pkfl,0}^{Hxl}$ = Fitted pre-exponential factor for effective permeability to hexanal vapour of packaging film material (mol·m·m^{-2}·s^{-1}·Pa^{-1})

b_{pkfl} = Fitted exponential model coefficient for effective permeability to hexanal vapour of packaging film material (m^3·mol^{-1})

x_{pkfl} = Position in packaging film material (m)

C_{env}^{Hxl} = Hexanal concentration in the bulk environment surrounding the outer bag (mol·m^{-3})

The rate of hexanal loss from the package headspace to the packaging film (at $x_{pkfl} = 0$; film surface facing against package headspace) can be described as Eq. 5-22.

$$r_{pkfl}^{Hxl} = P_{pkfl,0}^{Hxl} A_{scfl} RT_{pkg} \exp\left(C_{g,x_{pkfl}}^{Hxl} \cdot b_{pkfl} \right) \frac{\partial C_{g,x_{pkfl}}^{Hxl}}{\partial x_{pkfl}} \quad \textbf{(Eq. 5-22)}$$

$for\ t > 0\ and\ x_{pkfl} = 0$

where

r_{pkfl}^{Hxl} = Rate of hexanal permeation through the packaging film material (mol·s^{-1})

5.7.3 Apparent rate of hexanal uptake by tomatoes

The nth order reaction equation was used to mathematically describe hexanal uptake by the tomatoes using the data collected in section 3.3. The apparent rate of hexanal uptake by tomatoes is given by Eq. 5-23:

$$r_{tom}^{Hxl} = k_{tom,reac}^{Hxl} \left(C_{pkhs}^{Hxl}\right)^{n\,reac} M_{tom} \qquad for\ t > 0 \qquad \textbf{(Eq. 5-23)}$$

5.7.4 Rate of accumulation of CO_2 and O_2 in package headspace (passive MAP)

As mentioned in Chapter 2, modelling CO_2 and O_2 in the passive MAP system has been well studied and verified. Equations describing rates of accumulation of CO_2 and O_2 were developed similarly to those reported elsewhere (Cameron et al. 1995; Yam & Lee 1995; Merts 1996; Charles et al. 2003).

The ordinary differential equation (ODE) for describing accumulation of O_2 in the package headspace was expressed as in Eq. 5-24.

$$\frac{dn_{pkhs}^{O_2}}{dt} = \frac{P_{pkfl}^{O_2} A_{pkfl}}{L_{pkfl}} \left(p_{env}^{O_2} - p_{pkhs}^{O_2}\right) - r_{O_2} M_{tom}, \quad for\ t > 0; \qquad \textbf{(Eq. 5-24)}$$

$$for\ t = 0;\ p_{pkhs}^{O_2} = 21\ kPa$$

where

$n_{pkhs}^{O_2}$ = Number of oxygen moles in package headspace (mol)

P_{pkfl}^{O2} = Film permeability to O_2 (mol·m·m^{-2}·s^{-1}·Pa^{-1})

$p_{pkhs}^{O_2}$ = O_2 partial pressure in the package headspace (kPa)

$p_{env}^{O_2}$ = O_2 partial pressure in the bulk environment (kPa)

r_{O_2} = Rate of O_2 consumption by respiration (mol·s^{-1}·kg^{-1})

The respiration rate of packaged produce (r_{O_2}) was mathematically modelled as Eq. 5-25 following Talasila & Cameron (1997) and others.

$$r_{O_2} = \frac{r_{O_2}^{max} p_{pkhs}^{O_2}}{k_{mO_2} + p_{pkhs}^{O_2}} \qquad \textbf{(Eq. 5-25)}$$

where

$r_{O_2}^{max}$ = Maximum O_2 consumption rate (mol·kg^{-1}·s^{-1})

k_{mO_2} = Michaelis-Menten constant for O_2 consumption (kPa)

The ordinary differential equation (ODE) for describing accumulation of CO_2 in the package headspace was expressed as Eq. 5-26.

$$\frac{dn_{pkhs}^{CO_2}}{dt} = r_{CO_2} M_{tom} - \frac{P_{pkfl}^{CO_2} A_{pkfl}}{L_{pkfl}} \left(p_{pkhs}^{CO_2} - p_{env}^{CO_2} \right), \quad for\ t > 0\ ; \qquad \textbf{(Eq. 5-26)}$$

$$for\ t = 0;\ p_{pkhs}^{CO_2} = 0.03\ kPa$$

where

$n_{pkhs}^{CO_2}$ = Number of carbon dioxide moles in package headspace (mol)

P_{pkfl}^{CO2} = Film permeability to CO_2 ($mol \cdot m \cdot m^{-2} \cdot s^{-1} \cdot Pa^{-1}$)

$p_{env}^{CO_2}$ = CO_2 partial pressure in the bulk environment (kPa)

$p_{pkhs}^{CO_2}$ = CO_2 partial pressure in the package headspace (kPa)

r_{CO_2} = Rate of respiratory CO_2 production ($mol \cdot s^{-1} \cdot kg^{-1}$)

The r_{CO_2} was estimated from Eq. 5-27 following Talasila & Cameron (1997), where the respiration quotient (RQ) represents the ratio of rate of CO_2 production to that of O_2 consumption. Under oxidative respiration condition RQ is commonly assumed to be unity and this assumption was adopted here.

$$r_{CO_2} = RQ \times r_{O_2} \qquad \textbf{(Eq. 5-27)}$$

5.8 Numerical solution of overall transport model

5.8.1 MATLAB solver for numerical solutions

The modelled system utilises simultaneous ODEs for the sachet and headspace systems and PDEs for the outer packaging film. Beu (2000) noted that for diffusion of VOCs in polymer films with concentration dependent properties, analytical solutions become mathematically cumbersome and numerical methods are useful alternatives and preferred. In addition some algebraic equations used in the model were nonlinear, especially the Langmuir sorption isotherm model. Because of these complexities, the model was solved numerically.

The PDE describing active agent transfer through the outer packaging film was converted into a series of ODE using explicit finite difference techniques. These ODE's, together with the ODE's for the sachet and package headspace, were then solved together in MATLAB® (version 6.5 The Mathworks Inc, Natick, Mass. U.S.A) using the *ode23s* solver function. A default value of 0.001 for relative tolerance of integration error (known as 'RelTol') was used for the simulations. The *ode23s* solver was chosen due to the stiff nature of the differential equations. Moler (2003) explain that stiff sets of differential equations are those when the solutions being sought for some are varying slowly, while nearby solutions are being rapidly solved. In such a case, the numerical method must take small steps to obtain satisfactory results within the designated tolerance and a longer computational time is required to obtain results compared to non-stiff equations. The stiff nature of the differential equations arises here due to the relatively rapid changes of concentration in other package components compared to those in the packaging film.

Initially the numerical method was solved using *ode45*, which is a general purpose and more accurate solver used for MATLAB® applications. Although a much long computational time was required by *ode45* than *ode23s*, results obtained from both solvers were found to be in good agreement. Because of this, *ode23s* was utilised extensively in all subsequent mathematical simulations in the present study. It should be noted that ODEs describing accumulation of O_2 and CO_2 were numerically solved with approximate initial conditions using the *ode45* solver because of the non-stiff nature of their solutions (i.e. the permeation of O_2 and CO_2 across the packaging film was modelled using the steady-state approach).

5.8.2 Finite difference solutions for PDE models

5.8.2.1 Explicit finite different scheme

To numerically solve the PDEs, the explicit finite different scheme was implemented as this is one of the most common and simple, yet effective, numerical methods for solving unsteady-state problems in heat conduction and diffusion mass transfer for systems having regular geometry (Mills 1995b). In this case the packaging film material can be considered as an infinite slab and applications of finite differences for numerical solutions of unsteady-state diffusion mass transfer processes in polymer films are well documented by

Beu (2000). Therefore an explicit finite different scheme was implemented to solve unsteady-state diffusion mass transfer of hexanal in the packaging film material.

5.8.2.2 The grid and finite difference approximations

The finite difference grid used for the packaging film with all node designations is shown in Figure 5-7. The film thickness (L_{pkfl}) was equally divided into J space steps of Δx_{pkfl} and the concentration within each node was considered uniform. This resulted in $J+1$ nodes where the numbering of nodes starts from $j=1$ at the left boundary (facing the package headspace) to $j=J+1$ at the right surface (facing the storage environment).

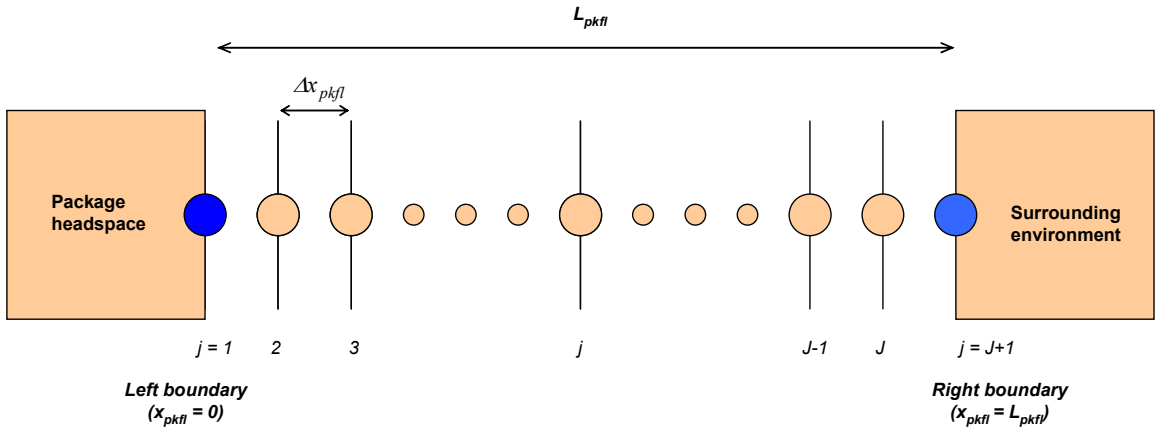

Figure 5-7 Finite difference grid for packaging film

5.8.2.3 ODE equations for film nodes

After the grid was formed, finite-difference approximations were made to approximate derivatives of the function between two discrete points using the expanded Taylor series in such a way that the partial differential equation was converted to an ODE. Approximations were performed at every node throughout the discretised matrix, therefore a series of ODEs for describing hexanal diffusion within the packaging film were derived and mathematically expressed as follows.

5.8.2.3.1 For surfaces of the film (nodes j = 1 and j = J +1)

For j = 1 ($x_{pkfl}=0$) and j = J +1 ($x_{pkfl}=L_{pkfl}$) the ODEs, which were subject to the 1st kind of boundary condition (refer to Eq. 5-28 and Eq. 5-29), were designated as:

$$\frac{\partial C_{g,1}^{Hxl}}{\partial t} = 0 \; ; \; for \; j = 1 \; \text{and} \; for \; t > 0 \qquad \textbf{(Eq. 5-28)}$$

$$\frac{\partial C_{g,J+1}^{Hxl}}{\partial t} = 0 \; ; \; for \; j = J+1 \; \text{and} \; for \; t > 0 \qquad \textbf{(Eq. 5-29)}$$

where

$C_{g,1}^{Hxl}$, $C_{g,J+1}^{Hxl}$ = Equilibrium hexanal vapour concentration in the packaging film, at the discrete nodes $j = 1$ and $j = J+1$, respectively (mol·m^{-3})

It should be noted that hexanal vapour concentrations at nodes j = 1 and j = J+1 were presumed to always be equal to the concentrations in the headspace (C_{pkhs}^{Hxl}) and environment (C_{env}^{Hxl}), respectively.

5.8.2.3.2 For internal film (nodes j = 2 : J)

For nodes j = 2: J (any x_{pkfl}), ODEs were defined as:

$$\frac{\partial C_{g,j}^{Hxl}}{\partial t} = \frac{P_{pkfl,0}^{Hxl} RT_{pkg}}{\Delta x_{pkfl} \cdot \Delta x_{pkfl}} \left(exp\left(\left(\frac{C_{g,j-1}^{Hxl} + C_{g,j}^{Hxl}}{2} \right) \cdot b_{pkfl} \right) \cdot \left(C_{g,j-1}^{Hxl} - C_{g,j}^{Hxl} \right) - exp\left(\left(\frac{C_{g,j}^{Hxl} + C_{g,j+1}^{Hxl}}{2} \right) \cdot b_{pkfl} \right) \cdot \left(C_{g,j}^{Hxl} - C_{g,j+1}^{Hxl} \right) \right)$$

$for \; j = 2 : J$ and $for \; t > 0$

(Eq. 5-30)

where

$C_{g,j}^{Hxl}$ = Equilibrium hexanal vapour concentration in the packaging film at discrete node $j = 2 : J$ (mol·m^{-3})

Because film permeability to hexanal vapour is concentration dependent, values of permeability at individual nodes were not constant or necessarily similar to each other. In this case, Beu (2000) suggested that an average mass transfer coefficient at the neighbouring nodes can be considered as a reasonable and convenient approximation. Following this, an arithmetic average value of permeability between the two nodes of interest was adopted, as expressed in the exponential term of Eq. 5-30.

5.8.3 The global mathematical model

The global mathematical model describing (i) the accumulation of hexanal in the package headspace, (ii) equilibrium hexanal vapour concentration in the film and (iii) equilibrium amount of hexanal on the solid phase (silica gel) was expressed as follows.

- **Rate of accumulation of hexanal concentration in the package headspace**

$$V_{pkg}\frac{\partial C_{pkhs}^{Hxl}}{\partial t}=\frac{P_{scfl,0}^{Hxl}A_{scfl}RT_{pkg}}{L_{scfl}b_{scfl}}\left(exp\left(C_{g,bed}^{Hxl}\cdot b_{scfl}\right)-exp\left(C_{pkhs}^{Hxl}\cdot b_{scfl}\right)\right)-\frac{P_{pkfl,0}^{Hxl}A_{pkfl}RT_{pkg}}{\Delta x_{pkfl}}exp\left(\left(\frac{C_{g,1}^{Hxl}+C_{g,2}^{Hxl}}{2}\right)\cdot b_{pkfl}\right)\cdot\left(C_{g,1}^{Hxl}-C_{g,2}^{Hxl}\right)-k_{reac}^{Hxl}\left(C_{pkhs}^{Hxl}\right)^{nreac}M_{tom} \quad \textbf{(Eq. 5-31)}$$

$for\ t>0$; and $for\ t=0;\ C_{g,bed}^{Hxl}=C_{sat}^{Hxl}\ ;\ C_{pkhs}^{Hxl}=0$

- **Rate of changes of equilibrium hexanal vapour concentration in the film**

$for\ node\ j=1$ $\quad \frac{\partial C_{g,1}^{Hxl}}{\partial t}=0 \quad for\ t>0$; and $for\ t=0;C_{g,1}^{Hxl}=C_{pkhs}^{Hxl}$ **(Eq. 5-32)**

$for\ node\ j=J+1$ $\quad \frac{\partial C_{g,j+1}^{Hxl}}{\partial t}=0 \quad for\ t>0$; and $for\ t=0;C_{g,J+1}^{Hxl}=C_{env}^{Hxl}$ **(Eq. 5-33)**

$for\ node\ j=2:J$

$$\frac{\partial C_{g,j}^{Hxl}}{\partial t}=\frac{P_{pkfl,0}^{Hxl}RT_{pkg}}{\Delta x_{pkfl}\cdot\Delta x_{pkfl}}\left(\begin{array}{l}exp\left(\left(\frac{C_{g,j-1}^{Hxl}+C_{g,j}^{Hxl}}{2}\right)\cdot b_{pkfl}\right)\cdot\left(C_{g,j-1}^{Hxl}-C_{g,j}^{Hxl}\right)\\-exp\left(\left(\frac{C_{g,j}^{Hxl}+C_{g,j+1}^{Hxl}}{2}\right)\cdot b_{pkfl}\right)\cdot\left(C_{g,j}^{Hxl}-C_{g,j+1}^{Hxl}\right)\end{array}\right) \quad \textbf{(Eq. 5-34)}$$

$for\ t>0$;and $for\ t=0;C_{g,2:J}^{Hxl}=0$

- **Rate of change of hexanal on the silica gel**

$$M_{bed}\frac{\partial C_{s,bed}^{Hxl}}{\partial t}=-\frac{P_{scfl,0}^{Hxl}A_{scfl}RT_{pkg}}{L_{scfl}b_{scfl}}\left(exp\left(C_{g,bed}^{Hxl}\cdot b_{scfl}\right)-exp\left(C_{pkhs}^{Hxl}\cdot b_{scfl}\right)\right) \quad \textbf{(Eq. 5-35)}$$

$for\ t>0$; and $for\ t=0;C_{s,bed}^{Hxl}=C_{s,max}^{Hxl}$

5.8.4 MATLAB® language codes

The formulated ODEs for the finite difference grid of the packaging film together with the ODEs for the sachet and apparent hexanal uptake by the tomatoes were transformed to MATLAB® code to solve the model. This code is shown in Appendix G.1. The codes for the ODEs describing CO_2 and O_2 accumulation were presented in MATLAB® code as shown in Appendix G.2.

5.8.5 Model checking: Checks against analytical solutions and numerical error checking

Prior to proceeding to validation or making other uses of the mathematical models, model accuracy must be checked. Errors in models may be present and these could be arised from, for example, numerical errors in the chosen solution methods or mistakes in algebraic calculation or programming routines. To check mathematical accuracy, one may compare results obtained from the mathematical models developed against those obtained from existing solutions which have already been validated. As mentioned earlier, there are complexities in the nature of mathematical models for describing mass transport in an active packaging system, thus direct comparison to analytical solutions is difficult. However, mathematical models can be simplified in order to compare numerical predictions and analytical results.

Checking of numerical errors was conducted for the PDE and its explicit finite difference solution. To form the finite difference scheme, both time and space in the film were discretised by dividing the continua into a series of nodes (or space-steps) and time-steps. Bronlund (1997) suggested that whilst making the size of time and space steps approach zero could closely represent the system of interest, this will prolong computational times and potentially cause errors associated with the calculated results. From error analyses of discrete time and space, no significant differences in package headspace concentration of hexanal vapour were found (maximum difference of 6×10^{-6} mol·m^{-3}) when the number of space steps in the film was doubled from 10 to 20. Also there were no significant errors introduced when the default value of 'RelTol' (1E-3) in the *ode23s* solver was changed to 1E-4 (maximum difference of 1×10^{-6} mol·m^{-3}), suggesting the ode solver was keeping the time step controlled to minimise numerical error. For all future simulations of the mathematical model, 10 space steps and the default value of 'ReTol' were used.

After checking for numerical errors as discussed above, numerical solutions of the PDE for simplified cases where (i) there was a negligible concentration dependence of permeability in the packaging film and (ii) constant hexanal concentrations on both sides of the film, were compared with analytical solutions as illustrated in Appendix G.3. There was good agreement between results of both solutions and this suggested the term utilised for describing diffusion through the packaging film had been correctly implemented in the model.

Checking of numerical errors for ODE models was also conducted. To do so, input data were set to extreme or constant values, including (i) no hexanal transfer out of the package, (ii) constant hexanal vapour concentration in the sachet, (iii) no hexanal uptake by tomatoes, and (iv) concentration-independent film permeability. The numerical solutions were then compared with analytical solutions and showed good agreement (Appendix G.4). This indicated that the term employed for describing permeation across the sachet film had been correctly implemented in the model.

ODEs for predicting O_2 and CO_2 in passive MAP systems have been well verified against both experimentally collected data (Charles et al. 2003; Charles et al. 2005) and analytical solutions (Merts 1996). Therefore model checking for these ODEs was not conducted.

5.9 Summary

This chapter has outlined the development of an overall conceptual model to describe key mass transfer processes of an important category of active packaging system for horticultural products. A decision tree was developed for facilitating the choice of model according to the selection of individual key model components. This was initially developed based on information for 1-MCP release systems and was then implemented for the active MAP system of interest. The most appropriate options for modelling a hexanal active MAP system for tomatoes were selected utilising the criteria for simplification provided in the decision tree. The application of the model is illustrated and discussed in the following chapters.

Chapter 6

MATHEMATICAL MODEL VALIDATION

6.1 Introduction

In this chapter, the mathematical models developed in Chapter 5 were validated against experimental data collected from active MA packages (based on LDPE film bags) for which key components, such as the characteristics of the hexanal controlled release sachet and presence or absence of tomatoes, were varied to provide a range of packaging scenarios. The accuracy of the model predictions and assumptions underlying the developed model (as identified by the decision tree; Figure 5-6) were investigated and are discussed along with the validation results.

6.2 Experiments used in validating the mathematical models

To get a better understanding of the performance of the mathematical models, validation was performed by comparing the model output with data obtained from a series of experiments which involved combinations of several active packaging design variables, including the sachet loading, ratio of sachet to bag area, storage temperature, and presence or absence of tomatoes in the package. Table 6-1 summarises the different active MA packages developed for this work.

Experiments were carried out using varying masses (1.5 – 4.5 g) of silica gel (initially saturated with hexanal vapour) pre-packaged in sachets. The method of preparing the pre-saturated silica gel samples is presented in Appendix H.1. The 50 × 60 mm and 50 × 30 mm sachets (excluding the seal area) were constructed by using aluminium foil laminate film[10] (Propak Supplies, Palmerston North, New Zealand) on the bottom of the sachets, while the top film was made of either LDPE, Tyvek® or OPP film. The foil ensured that all hexanal release occurred through the upper sachet film which was in uninhibited contact

[10] This film is a composite of LDPE film and aluminium sheet. The effects of the LDPE laminate on hexanal concentrations within the bed or permeation from the sachet were presumed to be negligible as the aluminium layer should be a near absolute barrier to hexanal transport. Information on the high barrier properties of aluminium or aluminium-composite film to gas and volatile compounds is provided by Robertson (1993b).

with the package headspace. The sachets containing silica gel saturated with hexanal were then packed into LDPE bags (as the primary package) together with either tomato fruit (6 tomatoes, with an approximate volume of 600 ml) or a sealed glass container of equivalent volume (Figure 6-1). At least 3 replicates were tested for each individual model package.

Table 6-1 Details of the active MA packages employed in the validation trials (all used a LDPE outer bag)

ID.	Sachet films	Dried silica gel weights (g)			Sachet dimensions (mm)		Packaged items [a]		Storage temperature (°C)		Storage period (days)	
		1.5	3.0	4.5	50 × 60	50 × 30	Jars	Fruit	10	20	7	14
LD1	LDPE	√			√		√	√		√	√	
LD2			√		√		√	√		√	√	
LD3				√	√		√	√		√	√	
LD4			√		√		√	√	√			√
LD5		√				√	√			√	√	
LD6		√			√ + 2 [b]		√			√	√	
LD7 [c]		√			√							
OP1	OPP	√			√		√	√		√	√	
OP2			√		√		√	√	√			√
TY1	Tyvek®	√			√		√	√		√	√	
TY2			√		√		√	√	√			√

[a] The sealed glass jar was inert to hexanal and had an volume equivalent to 6 tomatoes, which was the number of fruit generally used in the present work. RH levels in bags containing tomatoes were >95% RH as randomly measured by a Tinytalk® RH meter; Gemini Data Loggers, UK.

[b] Two sachets were packaged into one bag; usually there was only one sachet per bag.

[c] This system comprised only the sachet containing silica gel saturated with hexanal. No package or other items were included. This package model was used to determine the rate of release of hexanal from the silica gel in the sachet under conditions of maximum driving force.

(A)

(B)

Figure 6-1 Examples of active MA package containing tomatoes (A) or a sealed glass container (B)

At the end of the trial period, the volume of each package was measured by the water displacement method, modified from that of Mohsenin (1986), where the whole bag was immersed to calculate the free volume inside the package. The free volume (V_{pkg} ; ≈ 1.2 L) was calculated as the difference between the volume of the package and that of the tomatoes (or the equivalent inert volume). The volume of tomatoes was calculated from the measured mass using the density of 'Royale' tomato (~990 kg·m^{-3}). This was calculated from known fruit masses and volumes where the latter were experimentally quantified following Mohsenin (1986). The tomato density determined in the present work is comparable to that reported elsewhere for example 962 kg·m^{-3} (Tanner 1998) and 986-1025 kg·m^{-3} (Adedeji et al. 2006).

The tested active packages were stored at either 10 or 20°C. For the 10ºC samples, the total storage period was 14 days and this was divided into 3 intervals: (i) storage at 10ºC for 7 days (day 0-7), (ii) transfer to 20ºC for 5 days (day 8-12), and (iii) return to storage at 10ºC for 2 days (day 13-14). The 20ºC samples were kept for periods of up to 7 days at the constant temperature. All components of the model packages were kept at the trial temperature for at least 24 hours prior to establishment of the experiment.

Regular measurements were made to quantify the hexanal concentration in the package headspace. Gas was sampled from all replicates of each active package system. The headspace sample was drawn directly through the plastic bag. The pinholes created by inserting the syringe were immediately sealed using aluminium tape. The aluminium foil layer of this tape provides a high barrier to both the physiological gases (O_2, CO_2, C_2H_4, and H_2O) and hexanal vapour (Robertson 1993b). The patch size (~2 × 2 cm) was also small relative to the overall surface area and its interference with gas permeation through the bag could be ignored[11]. Furthermore, the adhesive applied on the bottom side of the aluminium tape was (in preliminary trials) found to have a negligible effect on hexanal concentration in the package headspace.

[11] The maximum area of the tape on one bag was less than 5.4% of total bag surface area (0.125 cm^2), given 17 (for the case of 14 days storage period; at 10ºC) as the maximum number of samples taken from any one bag.

6.3 Model input data and sensitivity analysis

The physical dimensions and physico-chemical properties of the active packages used in the experiments were required as inputs to the mathematical models. Most characteristics were experimentally determined as reported in Chapter 3 and 4, and these model input data are summarised in Table 6-2.

Table 6-2 Summary of system inputs used for mathematical model validation

Symbol	Units	Descriptions	Values used
A_{scfl}	m^2	Sachet film surface area	0.0015 and 0.003 for sachets of 50 × 30 and 50 × 60 mm, respectively (Table 6-1)
V_{pkg}	m^3	Free volume in package	0.0012
R	$J \cdot mol^{-1} \cdot K^{-1}$	Gas constant	8.314
T_{pkg}	K	Package temperature	283.15 and 293.15
L_{scfl}	m	Sachet film thickness	20×10^{-6}, 30×10^{-6}, and 173×10^{-6}, for OPP, LDPE, and Tyvek® film, respectively [a]
A_{pkfl}	m^2	Package film surface area	0.125 (250 × 250 mm package size; excluding seal area)
L_{pkfl}	m	Thickness of LDPE outer packaging film	30×10^{-6} [a]
C_{env}^{Hxl}	$mol \cdot m^{-3}$	Hexanal concentration in an environment surrounding the package	0
b_{Lgm}^{Hxl}	$m^3 \cdot mol^{-1}$	Langmuir isotherm model coefficients	Values reported in Table 4-9
$C_{s,max}^{Hxl}$	$mol \cdot g^{-1}$	Maximum hexanal uptake estimated by Langmuir model	Values reported in Table 4-9
M_{bed}	g	Mass of dried silica gel	1.5, 3.0, and 4.5
M_{tom}	g	Mass of tomatoes packed in the bag	600 (average combined mass of 6 tomatoes)
r_{tom}^{Hxl}	$mol \cdot s^{-1} \cdot kg^{-1}$	Apparent rate of hexanal uptake by tomatoes	Values reported in Table 3-4
P_i^{Hxl}	$mol \cdot m \cdot m^{-2} \cdot s^{-1} \cdot Pa^{-1}$	Effective hexanal permeability of film *i* (LDPE, Tyvek®, and OPP)	Values reported in Table 4-2
J		Numbers of discrete spaces for the finite difference numerical solution of the PDE describing mass transfer through packaging films	10

[a] Film thicknesses of samples were randomly measured using a micrometer (0-25mm; Mitutoyo Corporation, Japan) and were in reasonable agreement with the commercial specifications.

By their nature, the model inputs are subject to variations that might influence the model predictions and overall model performance. To identify how significant this uncertainty might be, sensitivity analyses of the model outputs (but principally the hexanal headspace

concentration) with regard to selected model inputs were performed. Results obtained from these sensitivity analyses can also yield information on the relative importance of measuring the inputs more or less accurately (Tanner 1998). Among the model inputs, the key parameters chosen for sensitivity analyses were A_{scfl}, V_{pkg}, L_{scfl}, A_{pkfl}, L_{pkfl}, b_{Lgm}^{Hxl}, $C_{s,max}^{Hxl}$, r_{tom}^{Hxl}, and P_i^{Hxl}. These were chosen based on the high likelihood of variations occurring during their measurement or between different packaging systems in practical operation. The extents of variation evaluated for each individual input are summarised in Table 6-3.

Table 6-3 Range of key model inputs and the justification of their use in sensitivity analyses

Inputs	Variations made	Justifications
A_{scfl}, A_{pkfl}	± 4% for dimensions of length and width of sachet and bag	• This variation represents likely inaccuracies arising from sealing, i.e. ± 2 mm deviation from the expected 5 cm length
L_{scfl}, L_{pkfl}	± 20%	• It is commonly known that thickness measured at individual points on the same polymer film sample differ (Piringer 2000). The highest variations of film thickness in this study were observed in Tyvek®, which varied by ~20%. Such an extent of variation was considered to be the extreme and was utilised with all films.
V_{pkg}	± 10%	• As the package volume was determined using a system similar to the displacement platform-scale apparatus described by Mohsenin (1986), inaccuracies could occur in the reading of the weight of water displaced after immersing the whole bag, which might not stay completely still due to buoyancy force. Because a 3-decimal balance (0.001 g Mettler Toledo PR1203, Switzerland) was used, inaccuracies at the 2nd and 3rd decimal places were likely. Based on this, 10% variation of reading water displacement and hence in volume, appeared reasonable.
b_{Lgm}^{Hxl}, $C_{s,max}^{Hxl}$	% SE reported in Table 4-9	• As this data was obtained from nonlinear regression of experimentally collected data, the estimated standard errors relative to the mean was used as the measure of uncertainty.
r_{tom}^{Hxl}	% SE reported in Table 3-4	"
P_i^{Hxl}	% SE reported in Table 4-2	"

6.4 Experimental results and discussion of model performance

Comparisons of experimentally collected data and model predictions are presented and discussed in the following sections, together with the sensitivity analyses.

6.4.1 Effects of sachet loading on the package headspace hexanal concentration

This discussion of model performance firstly focuses on model packages containing a sealed glass jar; thereafter model predictions of the effects of packaged tomatoes on the accumulation of hexanal in the package headspace are discussed. The tested active MA packages selected for study in this section were LD1, LD2, and LD3 (Table 6-1).

6.4.1.1 Model predictions for packages containing sealed glass jars

The effect of increasing silica gel loadings on hexanal release and accumulation in the package headspace can be seen in Figure 6-2A together with the model predictions. As expected, these data show that including higher masses of hexanal-saturated silica gel in the sachet produced higher initial peaks in headspace hexanal concentration. However the quasi steady-state concentrations achieved after this initial release were similar and in the range of the MIC (40-70 ppm; determined in Chapter 3) for all model packages.

The model predictions were in partial agreement with the experimental data and in particular, the model predicted overall trend and the quasi steady-state concentration quite well. A lack of fit was noticeable during the unsteady-state region (especially within the initial 12 h of the storage period, as shown in Figure 6-2B), although the model predicted the correct trend of hexanal release. The model predicted higher and earlier peaks than actually observed.

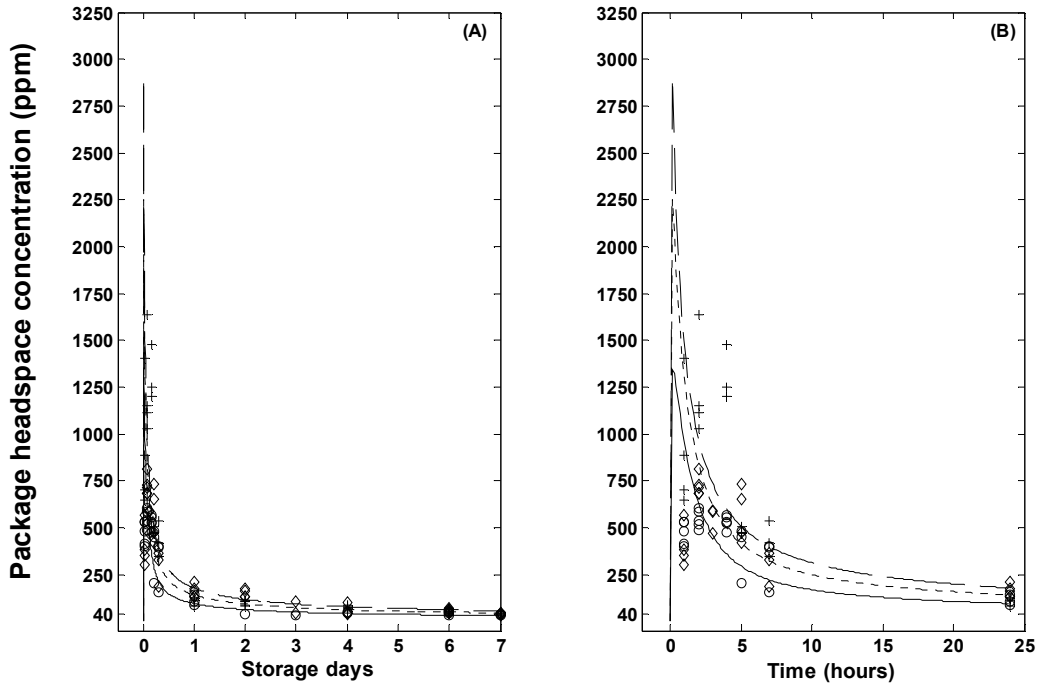

Figure 6-2 Effects of sachet gel loading on hexanal concentration in the headspace of package (C_{pkhs}^{Hxl}) containing an inert sealed glass jar, stored at 20°C. Experimental data (at least 3 replicates shown for each sampling time) of 1.5, 3.0 and 4.5 g loadings are represented by o, ◊ and + symbols, respectively, for a storage period of 7 days (A), and for the same data expanded to look at the first 24 h (B). Model predictions for each gel mass are shown through solid, dotted and dashed lines, respectively.

The release pattern of hexanal from the sachet was significantly influenced by the shape of the isotherm for hexanal adsorption on silica gel adsorbents, which was assumed identical for the adsorption and desorption isotherms (section 4.3.2). After a sachet was placed into the package with a negligible concentration of hexanal vapour at $t = 0$, there was initially a large driving force for hexanal release through the sachet film. Because of the Type I isotherm shape (reported in Figure 4-5), as the amount of absorbed hexanal on the silica gel ($C_{s,bed}^{Hxl}$) decreased slightly (Figure 6-3), the equilibrium vapour concentration above or within the bed ($C_{g,bed}^{Hxl}$; also the concentration in the sachet headspace) and hence the driving force for transfer out of the sachet, decreased dramatically (Figure 6-3). This resulted in a rapid initial release from the sachet, followed by a prolonged period of slow release (Figure 6-2 and Figure 6-3). Based on these results, it can be seen that the shape of the hexanal sorption isotherm should be highly influential on the pattern of hexanal release

from the sachet. This indicates that different release behaviour may be able to be achieved by appropriate selection of the carrier substrate.

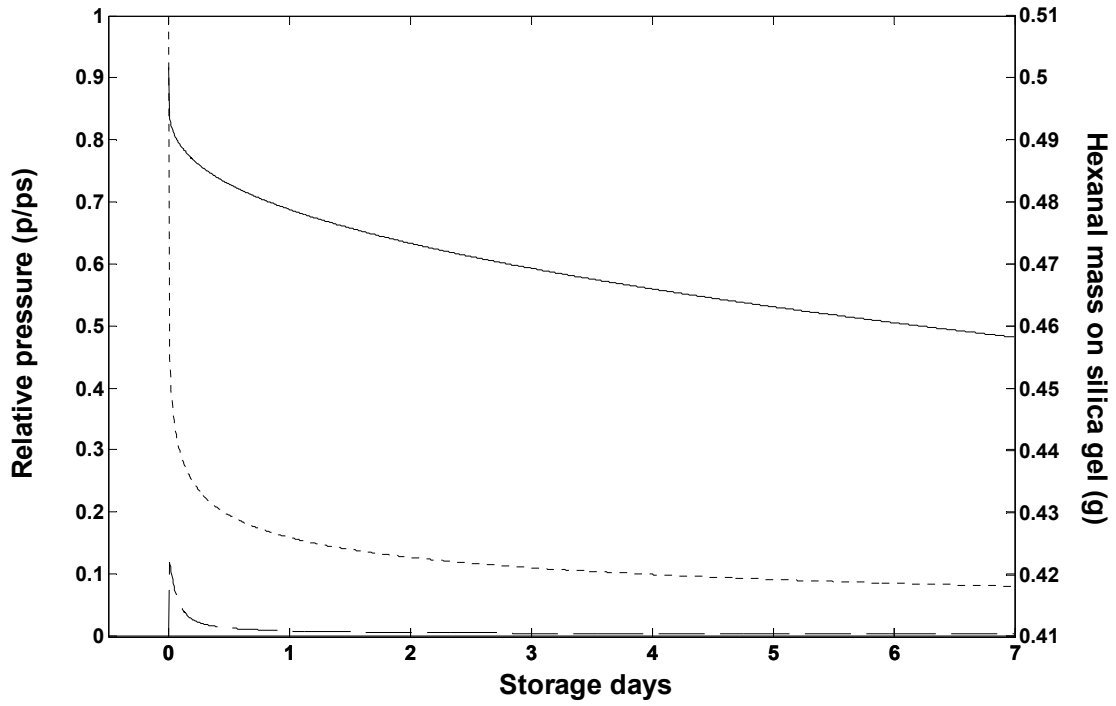

Figure 6-3 Model predictions of hexanal partial relative pressures (p/p_s) in the package headspace (dashed line) and sachet headspace (dotted line), and the hexanal mass remaining on the silica gel (solid line) for the LD1 system (1.5 g dried silica gel; Table 6-1).

From Figure 6-2 it can be seen that the higher the sachet loading, the higher the initial release peak is. This is explained by differences of system capacity in the sachet, which are in proportion to the mass of dry silica gel. According to Levenspiel (1972), the extent of change is a function of the reciprocal of system capacity (hence the silica gel mass), therefore the reduction of $C_{g,bed}^{Hxl}$ was slowest at the 4.5 g loading. This causes the slowest change of concentration gradient across the sachet film after the onset of release resulting in the highest initial peak and slowest depletion of hexanal from the package headspace (C_{pkhs}^{Hxl}). The extents of change of $C_{g,bed}^{Hxl}$ with different loadings as predicted by the model for all packaging systems are shown in Figure 6-4; note that the quasi steady-state condition values of for all systems were broadly comparable.

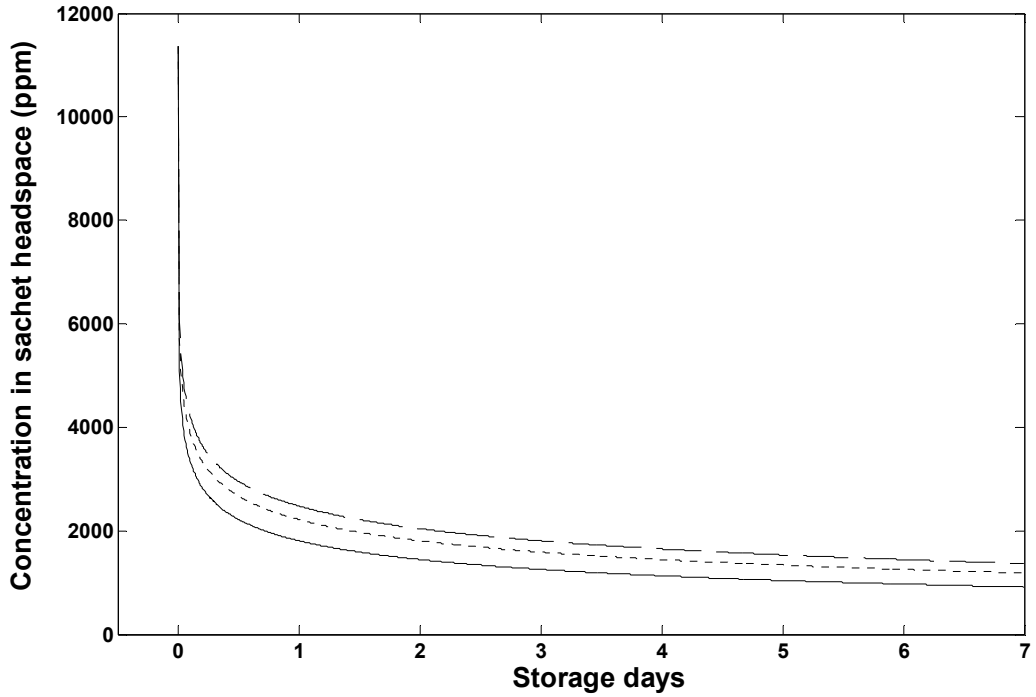

Figure 6-4 Sachet headspace concentration ($C_{g,bed}^{Hxl}$) predicted for hexanal saturated initial dried silica gel masses of 1.5, 3.0 and 4.5 g (represented by solid, dotted and dashed lines, respectively).

The relationship between $C_{g,bed}^{Hxl}$ and C_{pkhs}^{Hxl} at the steady-state condition can be mathematically represented using the generic mass balance shown in Eq. 6-1.

$$\frac{P_{pkfl}^{Hxl} A_{pkfl}}{L_{pkfl}} \left(C_{pkhs}^{Hxl} - C_{env}^{Hxl}\right) RT_{pkg} = \frac{P_{scfl}^{Hxl} A_{scfl}}{L_{scfl}} \left(C_{g,bed}^{Hxl} - C_{pkhs}^{Hxl}\right) RT_{pkg} \qquad \textbf{(Eq. 6-1)}$$

Given the special case where $C_{env}^{Hxl} = 0$, $P_{pkfl}^{Hxl} = P_{scfl}^{Hxl}$, $L_{pkfl} = L_{scfl}$, constant value of T_{pkg}, and $A_{scfl} / A_{pkfl} = \omega_A$, (Eq. 6-1) becomes Eq. 6-2.

$$C_{pkhs}^{Hxl} = C_{g,bed}^{Hxl} \frac{\omega_A}{(1+\omega_A)} \qquad \textbf{(Eq. 6-2)}$$

where

ω_A = Ratio of sachet to bag area

From Eq. 6-2, it can be seen that C_{pkhs}^{Hxl} is dependent on both $C_{g,bed}^{Hxl}$ and the ratio of sachet to bag area (ω_A). Given slight differences in the calculated $C_{g,bed}^{Hxl}$ and the same ω_A value

(≈0.024), it can be inferred from Eq. 6-2 that the quasi steady-state values of C_{pkhs}^{Hxl} for all packages will be comparable. This behaviour is well predicted by the model (Figure 6-2A).

Suzuki et al. (2004) reported a linear relationship between the mass of active carriers (3-12g gross mass of ethanol on a proprietary silica gel) and the peak concentrations and accumulation patterns of ethanol vapour (Figure 6-5A) delivered from Antimold Mild® controlled release sachets (Freundlich Co. Ltd., Japan) into the headspaces of perforated PE bags (size 18 × 28 cm; with 2 holes of 5 mm diameter on both sides of a bag) containing broccoli branchlets (*Brassica oleracea* L. var. *Italica*), when kept at 20ºC for 5 days. The highest peak release (~3.6 ppm) and quasi steady-state ethanol concentration was reported for the 12g-treatment. Likewise Smith et al. (1987) reported higher peaks of ethanol vapour released from the Ethicap® type E_4 (representing 4g gross mass of ethanol and proprietary silica gel; Freundlich Co. Ltd., Japan) compared to those from the type E_1 (1g gross mass) (Figure 6-5B), in the headspace of a high ethanol vapour barrier pouch (size 20 × 20 cm) containing a_w-adjusted PDA agar to simulate the effects of a_w (a_w 0.85 to 0.99) on ethanol release and re-absorption to agar at 25ºC for 16 days. Information reported by Suzuki et al. (2004) and Smith et al. (1987) on effects of sachet loadings on peak releases in the package headspace support the findings reported earlier in this section.

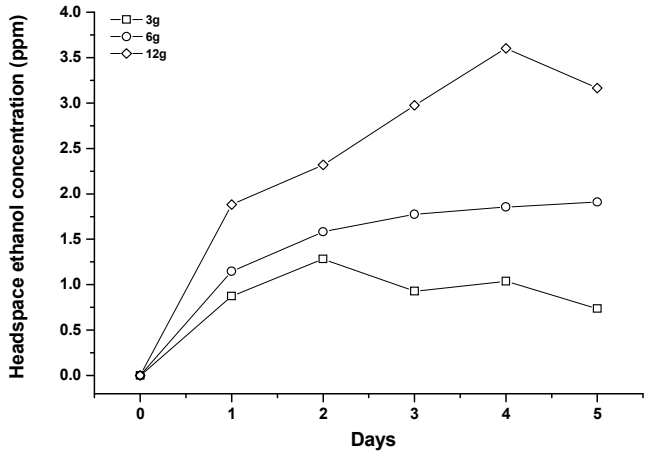

(A)

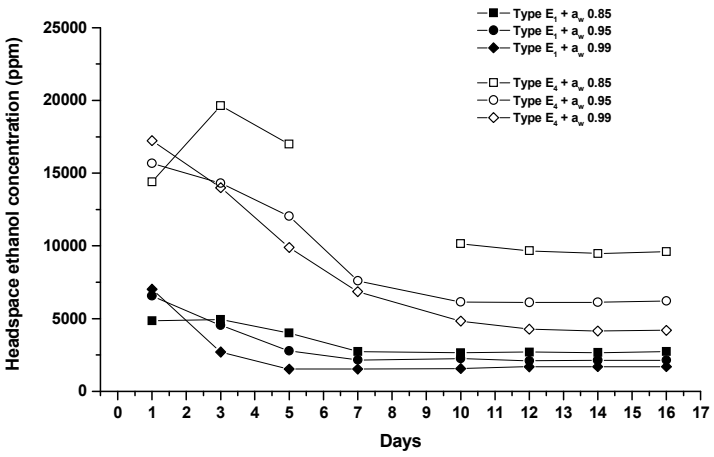

(B)

Figure 6-5 Changes in ethanol concentration in the atmosphere of perforated polyethylene bags packed with broccoli branchets (digitally redrawn from Suzuki et al. 2004) (A), or above a_w-adjusted PDA plates, packaged with Ethicap® type E_1 and E_4 in high ethanol barrier pouch (digitally redrawn from Smith et al. 1987; note data on the 7th day of E_4 + a_w 0.85 was not reported) (B).

It is worth noting that the general release pattern of ethanol reported by Smith et al. (1987) is similar to that of hexanal observed in the present work. The quasi steady-state concentrations of ethanol were attained after the initial release peaks, suggesting a similar Langmuir type isotherm. This is true of sorption of ethanol by silica gel as reported by Madeley & Sing (1959) (as discussed in section 4.3.4) but there is no available information on ethanol sorption isotherms for Ethicap® (Smith et al. 1987) or Antimold Mild® (Suzuki

et al. 2004). Furthermore the slower attainment of the quasi steady-state concentration suggests different permeability behaviour of ethanol through packaging materials used by Smith et al. (1987) and Suzuki et al. (2004) compared to that of hexanal vapour through LDPE bag.

In Figure 6-2B, differences between the model predictions and experimental data in the initial release phase are apparent. The model shows essentially instantaneous release compared to ~2-3 h to attain the peak concentrations observed in the experiments. In Figure 6-5A and B, Suzuki et al. (2004) and Smith et al. (1987) reported release peaks after one day, however data on headspace concentrations prior to these peaks were not reported. Because the model predictions of unsteady-state hexanal headspace concentrations are both overestimated (especially at 1 h) and underestimated (e.g. at 4 h as in the case of the LD3 system) (Figure 6-2B), a sensitivity analysis was carried out to investigate influences of model inputs (as shown in Table 6-3) on model predictions. The resulting predictions for the 4.5 g sachet loading system were chosen as an example and are shown in Table 6-4.

Table 6-4 Examples of model sensitivity to input variables for the system having a LDPE sachet with 4.5 g loading (LD3; Table 6-1). Experimental data are shown as o symbols.

Parameter varied	Experimental data and model predictions
A_{scfl} where • A_{scfl} = 0.0030 (control; solid line) • A_{scfl} = 0.0032 (dotted line) • A_{scfl} = 0.0028 (dashed line)	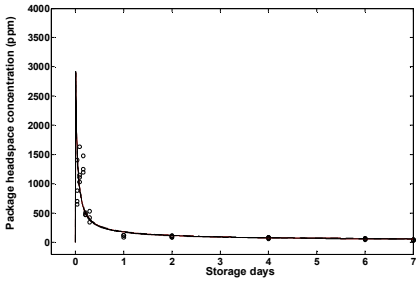
A_{pkfl} where • A_{pkfl} = 0.125 (control; solid line) • A_{pkfl} = 0.135 (dotted line) • A_{pkfl} = 0.115 (dashed line)	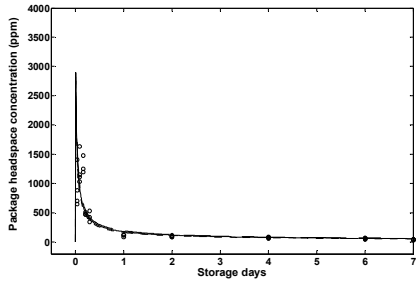
L_{scfl} where • $L_{scfl} = 30 \times 10^{-6}$ (control; solid line) • $L_{scfl} = 36 \times 10^{-6}$ (dotted line) • $L_{scfl} = 24 \times 10^{-6}$ (dashed line)	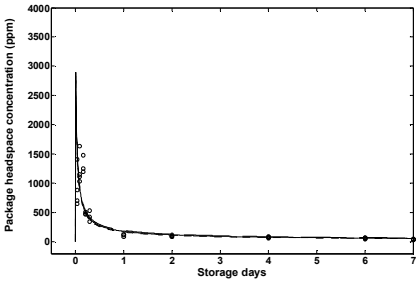
L_{pkfl} where • $L_{pkfl} = 30 \times 10^{-6}$ (control; solid line) • $L_{pkfl} = 36 \times 10^{-6}$ (dotted line) • $L_{pkfl} = 24 \times 10^{-6}$ (dashed line)	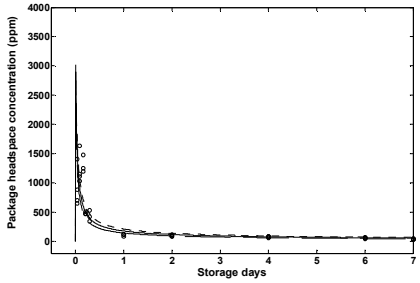
V_{pkg} where • V_{pkg} = 0.0012 (control; solid line) • V_{pkg} = 0.0013 (dotted line) • V_{pkg} = 0.0011 (dashed line)	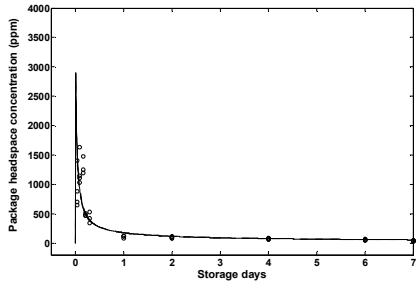

Table 6-4 Examples of model sensitivity to input variables for the system having a LDPE sachet with 4.5 g loading experiment (LD3; Table 6-1). Experimental data are shown as o symbols (continued).

Parameter	Experimental data and model predictions
$C_{s,max}^{Hxl}$ where • $C_{s,max}^{Hxl}$ = 0.00334 (control; solid line) • $C_{s,max}^{Hxl}$ = 0.00357 (dotted line) • $C_{s,max}^{Hxl}$ = 0.00311 (dashed line)	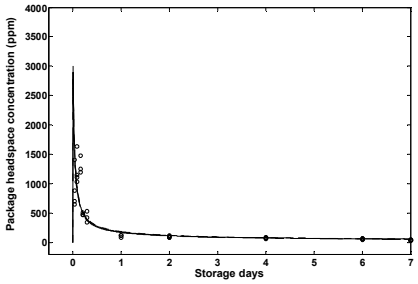
b_{Lgm}^{Hxl} where • b_{Lgm}^{Hxl} = 281.070 (control; solid line) • b_{Lgm}^{Hxl} = 394.536 (dotted line) • b_{Lgm}^{Hxl} = 167.601 (dashed line)	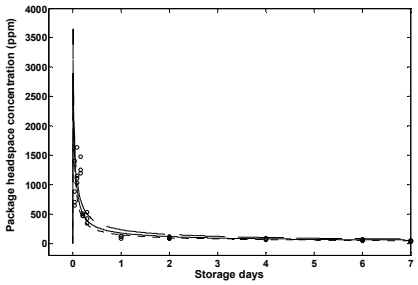
$P_{LDPE,0}^{Hxk}$, b_{LDPE} (sachet film; given fixed values of these for outer packaging film) where • $P_{LDPE,0}^{Hxk}$ = 1.97 × 10^{-14}, b_{LDPE} = 19.65 (control; solid line) • $P_{LDPE,0}^{Hxk}$ =3.12 × 10^{-14}, b_{LDPE} = 22.44 (dotted line) • $P_{LDPE,0}^{Hxk}$ = 8.77 × 10^{-15}, b_{LDPE} = 16.85 (dashed line)	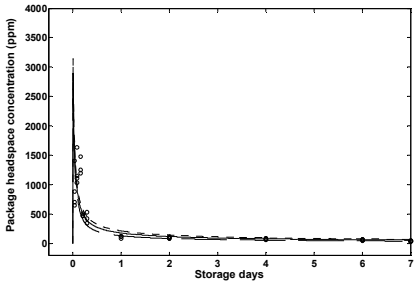
$P_{LDPE,0}^{Hxk}$, b_{LDPE} (outer packaging film; given fixed values of these for sachet film) where • $P_{LDPE,0}^{Hxk}$ = 1.97 × 10^{-14}, b_{LDPE} = 19.65 (control; solid line) • $P_{LDPE,0}^{Hxk}$ =3.12 × 10^{-14}, b_{LDPE} = 22.44 (dotted line) • $P_{LDPE,0}^{Hxk}$ = 8.77 × 10^{-15}, b_{LDPE} = 16.85 (dashed line)	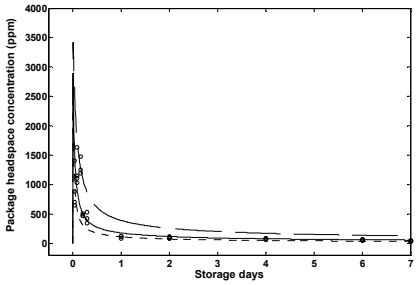

The model predictions are only slightly sensitive to variations in A_{scfl}, V_{pkg}, L_{scfl} and A_{pkfl} (Table 6-4). The slight changes in predicted values, in particular of the unsteady-state concentrations following variation to V_{pkg}, might be explained by the fact that the extent of variation was too low to obtain significant effects. For example the predicted values only

deviate noticeably when V_{pkg} is varied at least by 200% (data not shown). However such a large variation is not practical in the real situation. Thus the sensitivity analysis suggests that the effects of variations in these inputs on the model predictions can reasonably be assumed negligible and it also indicates no further effort is required to improve existing practices to quantify these parameters.

Moderate sensitivity of the predictions, particularly during the unsteady-state period, were observed as a consequence of varying values of the packaging film thickness (L_{pkfl}) (Table 6-4). Because mass transfer of hexanal through the package film was modelled using the PDE approach, varying the thickness would significantly affect the diffusion path of hexanal molecules through the film. Model predictions were slightly sensitive to the maximum hexanal adsorption on the silica gel ($C_{s,max}^{Hxl}$) and quite sensitive to variations of the Langmuir equation coefficient (b_{Lgm}^{Hxl})(Table 6-4) and, in particular, the permeability of LDPE film (P_{LDPE}^{Hxk}) which was used as both sachet and outer bag material. The model prediction results were highly sensitive to P_{LDPE}^{Hxk} variation of the outer bag, when using a constant value of P_{LDPE}^{Hxk} for the sachet material (Table 6-4). The intention in varying film thickness and permeability was to demonstrate the effects of varying film permeance (which is given by the ratio of permeability to film thickness; changing one or both parameters could then affect the overall permeance value) which reflects changes in mass transfer properties of the film, such as swelling (which is likely to increase film thickness and then permeability; Piringer 2000) or other interactions that occur between VOCs and polymers. According to Robertson (1993c), interaction between permeants and polymers can lead to complex mass transfer behaviour.

As discussed in Chapter 4, b_{Lgm}^{Hxl} is subject to uncertainty associated with the fitting of the isotherm by nonlinear regression. The lower sensitivity of model predictions to variation in P_{LDPE}^{Hxk} values for the sachet film compared to that of outer bag suggest that rate of change of concentration at the sachet film tends to be faster than that at the outer (packaging) film. The findings also support the discussion in Chapter 5 proposing that changes of concentrations for the sachet film were relatively faster than to those within the package headspace and carrier bed. Overall the high sensitivity of predicting hexanal headspace concentrations due to b_{Lgm}^{Hxl} and P_{LDPE}^{Hxk} (Table 6-4) highlights the need for improve

techniques for estimating these data. However, the results of the sensitivity analysis do suggest that sorption isotherm data obtained from the gravimetric method and permeability data obtained from the isostatic method were sensible and can reasonably well describe equilibrium behaviour of hexanal for silica gel adsorbents and LDPE permeability to hexanal vapour, respectively.

Although the sensitivity analysis illustrates the influence of input values on model predictions, it is still uncertain why the model overestimated the headspace concentrations measured in the first few hours, while the concentrations measured later (within the initial 24 h timeframe) were reasonably well predicted by the model when the uncertainties of these inputs, especially those of b_{Lgm}^{Hxl}, P_{LDPE}^{Hxk} and L_{pkfl}, were taken into account.

6.4.1.2 Model predictions for packages containing tomatoes

In this section, the influence of including tomatoes on the package headspace concentration is examined because it was evident in Chapter 3 that tomatoes contribute to reducing the hexanal concentration through their apparent hexanal uptake. Furthermore the distribution of hexanal vapour between the various packaging components was investigated using the model to obtain insights into the relative contribution of the different hexanal transport processes to hexanal accumulation in the package headspace. Because tomatoes were packaged in a non-perforated bag, MA conditions developed and the dynamics of this was also modelled.

In Figure 6-6 it is evident that the peak height during the initial release of hexanal, regardless of sachet loading, was attenuated to a marked degree by the presence of tomatoes compared to when an inert equivalent volume was present. There are literature reports of hexanal uptake by apples (Song et al. 1996; Wolford 1998) and strawberries (Hamilton-Kemp et al. 1996) and this new data confirms hexanal uptake by tomatoes from the headspace. Because the apparent uptake rate of hexanal by tomatoes (r_{tom}^{Hxl}) had an exponential relationship with the hexanal concentration, the attenuation of hexanal concentration was most obvious during the establishment phase with the 4.5 g sachet loading system.

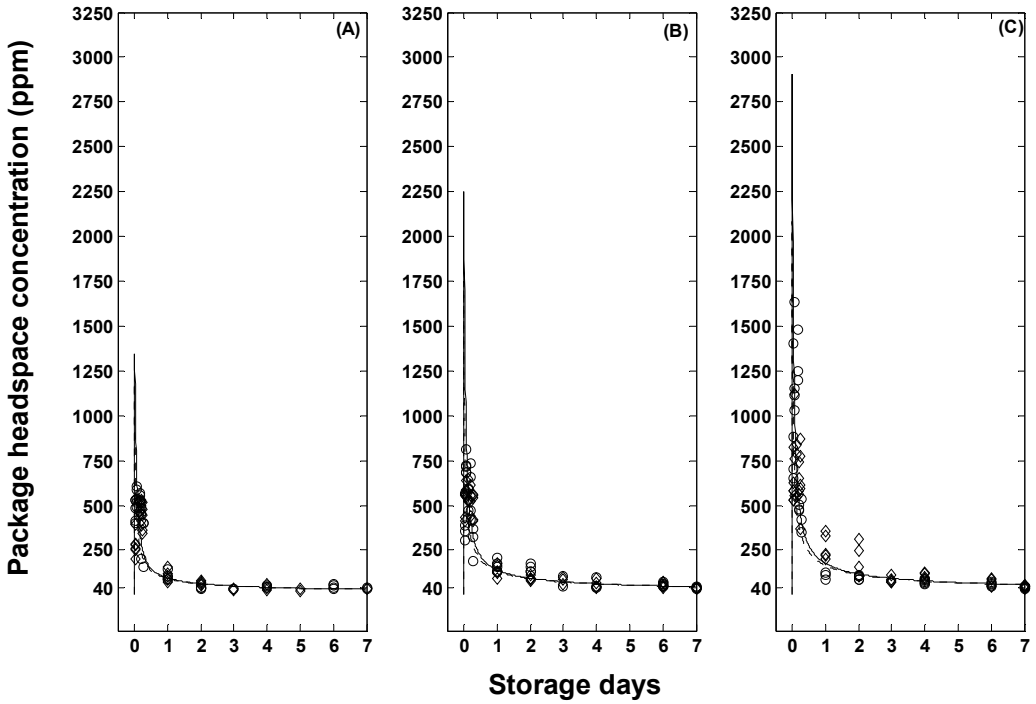

Figure 6-6 Effects of sachet loading on hexanal accumulation in the headspace of package containing tomatoes kept at 20°C. Experimental data (at least 3 replicates shown for each sampling time) for loadings of 1.5, 3.0 and 4.5 g are shown in (A), (B) and (C), respectively, where headspace hexanal concentrations of packages containing either a sealed jar (o; as previously reported) or and tomatoes (◊) are compared, for which prediction results were represented by solid and dotted lines, respectively.

Once again the mathematical model provided a reasonable fit with the experimentally collected data with regard to the overall trend and especially for the quasi steady-state concentration (Figure 6-6). However although the overall pattern was predicted, a distinct lack of fit was observed for the unsteady-state concentrations, which exhibited a similar pattern to that discussed in the previous section. In all cases, the quasi steady-state concentration was maintained at the MIC level (40-70 ppm) and should prove effective for suppressing growth caused by *B. cinerea*, as discussed in Chapter 3. Overall the release behaviour of the model active package could be exploited to achieve both an initial fumigation followed by long term control via provision of hexanal at the MIC level.

A sensitivity analysis of the model predictions for active packages containing tomatoes was carried out. As found in the previous section, only variations of L_{pkfl}, b_{Lgm}^{Hxl}, and P_{LDPE}^{Hxl}

appeared to affect model predictions. Therefore the sensitivity analysis focused on these parameters, in addition to r_{tom}^{Hxl}. The resulting predictions for the 4.5 g sachet loading are shown in the Appendix H.2 (Table H-1). The model predictions were most sensitive to variations in L_{pkfl}, b_{Lgm}^{Hxl}, and P_{LDPE}^{Hxl} (of both sachet and outer packaging films), and were not sensitive to r_{tom}^{Hxl}. With regard to b_{Lgm}^{Hxl}, and P_{LDPE}^{Hxl}, the results of the sensitivity analysis again confirmed the need for better techniques for estimating these values.

The similar quasi steady-state concentrations of all tested active MA packages, regardless of the type of package contents (tomatoes or an inert seal jar), can be explained by the relatively high rate of hexanal permeation across the package film compared to the rate of hexanal uptake by tomatoes. Figure 6-7 illustrates the differences in the mass of hexanal lost through the packaging film and that utilised by the tomatoes as predicted by the model (using LD1; Table 6-1 as an example). At the end of the experimental period, the amounts of hexanal mass permeating through the packaging film were more than 8-fold higher than those consumed through uptake processes. The hexanal mass associated with the tomatoes appeared constant within ~24 hours after the initial release of hexanal, while the amount of hexanal mass crossing the film steadily increased with storage duration. The constant mass uptake by tomatoes presumably results from the concentration dependent characteristics of r_{tom}^{Hxl}. As headspace hexanal concentrations rapidly decreased and stabilised at the low quasi steady-state concentration range, r_{tom}^{Hxl} then became very low.

The model simulations, as shown in Figure 6-7, suggest that hexanal accumulation in the package headspace is chiefly governed by the transfer processes across the packaging film, in addition to release of hexanal vapour from the sachet, rather than being governed by uptake by the tomatoes (r_{tom}^{Hxl}). For this simulation, the hexanal mass in the package headspace was calculated at ~0.005 g on day 7 which is very low compared with both the mass transferred through the outer packaging film and utilised by the tomatoes. Figure 6-7 also illustrates that only ~8.7% of the hexanal mass on silica gel was removed during the 7-day period. This is consistent with the shape of the Langmuir sorption isotherm as discussed in the previous section (but is undesirable from economic and environmental viewpoints).

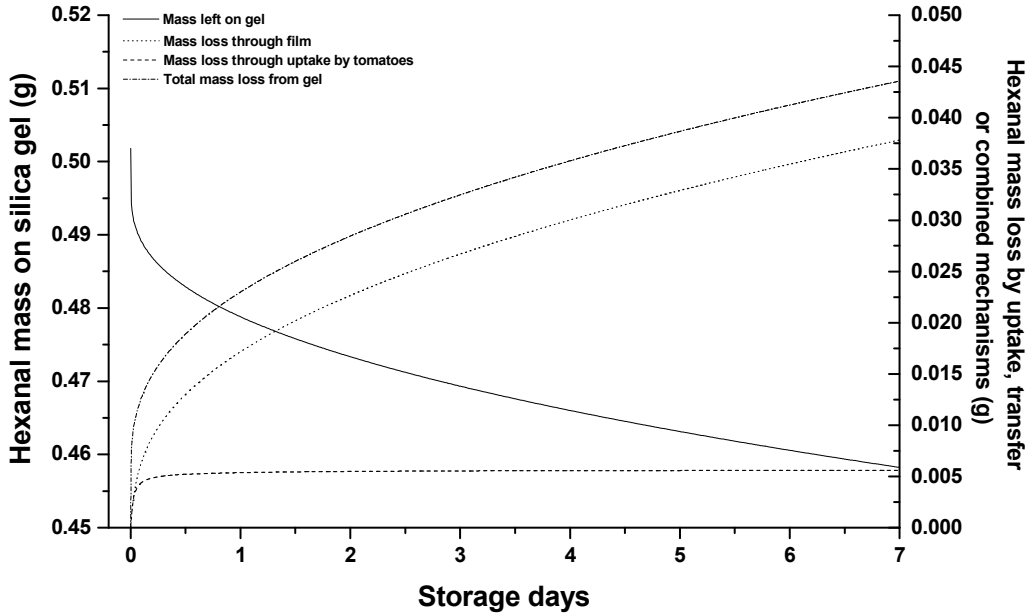

Figure 6-7 Simulations of hexanal mass remaining on silica gel due to hexanal release from the sachet to the package headspace (LHS y-axis) and the hexanal mass transferred through the packaging film or taken up by tomatoes (RHS y-axis). All simulations were based on LD1 active packaging system containing tomatoes and 1.5g dried silica gel as the hexanal carrier (Table 6-1).

Upon completion of this simulation, an overall mass balance was carried out. This was conducted by considering the amount of hexanal left on the silica gel, in the package headspace, and the integrated rates of hexanal mass transfer over the film or uptake by the tomatoes; the mass associated with the sachet film due to the steady-state permeation was ignored along with the mass in the sachet headspace. The overall balance agreed with the amount initially present (within acceptable rounding error) indicating that the hexanal mass was appropriately conserved during the simulation. Similar mass balance calculations were conducted across other active packaging systems and in all cases the hexanal masses were conserved during the simulations as expected.

The model predictions for the MA conditions (Figure 6-8) showed reasonably good agreement (the LD1 system; Table 6-1 was chosen for this example).This was especially noteworthy given that certain model inputs such as the Michaelis-Menten constants were obtained from relevant literature (Talasila & Cameron 1997, Hertog et al. 1998, Chen et al.

2000; also see Appendix G.2.3). Agreement was best for the quasi steady-state MA conditions and the gaseous atmospheres developed in the active packaging systems in the present study were reasonably comparable to those reported by Charles et al. (2003) for an O_2 scavenger-active MAP system for storage of tomatoes at 20ºC (~6-7% O_2 and ~5% CO_2 in LDPE bag containing ~840-860g intact tomatoes).

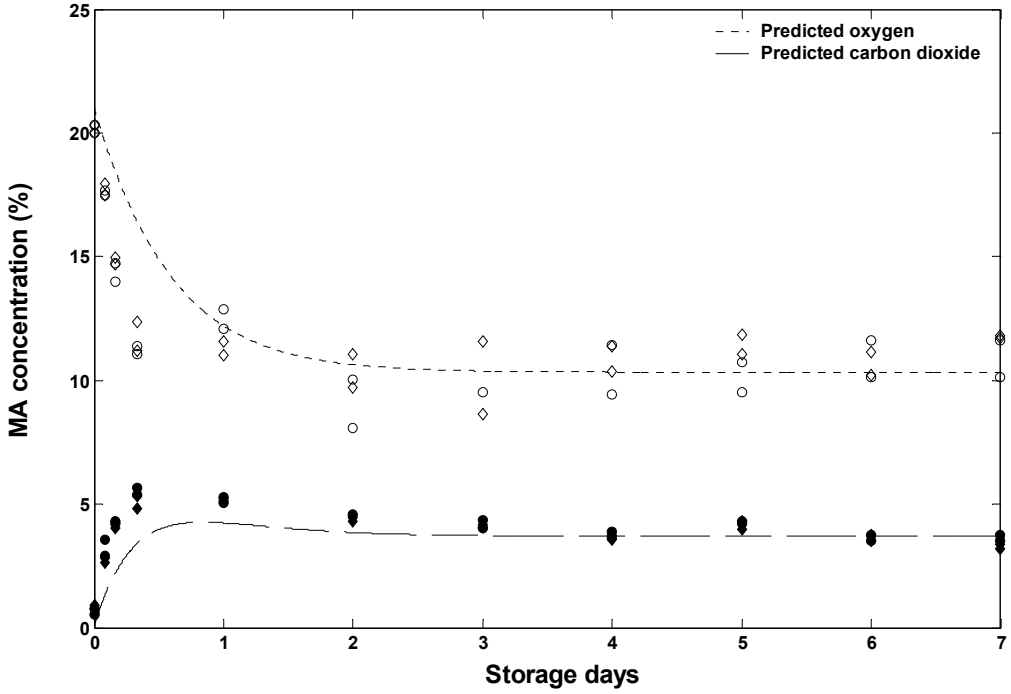

Figure 6-8 Measured and predicted headspace gas at 20ºC (2 replicates shown for each sampling time) measured in active (o and •, for O_2 and CO_2, respectively) and passive (◊ and ♦, for O_2 and CO_2, respectively) MA packages. The dotted and dashed lines are the MA model predictions.

In Chapter 3 it was shown that respiration rates were minimally affected by hexanal vapour at the MIC concentration under MA conditions. This finding is supported by the results in Figure 6-8 where there is little difference between experiments with and without the hexanal release sachet. The literature also supports a minimal effect of the presence of volatile active agents on the development of MA conditions for other horticultural products. For example Serrano et al. (2005) reported that the presence of the essential oils eugenol, thymol, eucalyptol and menthol in the package resulting from their release from active systems (gauze samples individually saturated with each compound) did not influence the equilibrium MA levels of O_2 and CO_2 (developed at both 1 and 20ºC) in OPP

bags containing sweet cherries (*Prunus avium* L. cv. 'StarKing'). Pongjaruwat (2007) similarly reported no significant effects of eugenol vapour on the development of the MA conditions inside active packages for tamarillo (*Cyphomandra betacea* cv. 'Mulligan Red').

The comparable gas compositions achieved in both passive and active MAP systems also suggest that hexanal vapour had no significant effect on LDPE film permeability of O_2 and CO_2. There is much evidence in the literature that the presence of organic compounds, including d-limonene, decanal, 2-nonanone, and hexylacetate, can change (and most likely increase) permeability to these gases in several films including LDPE, OPP, PP and HDPE. The effects are principally assumed to result from structural changes due to VOC sorption by the films causing plasticisation (as discussed in Chapter 4) which can facilitate permeation of O_2 and CO_2 through the film medium. Data and discussion on this aspect was well documented by Dury-Brun et al. (2007).

There was some lack of fit of the model predictions during the unsteady-state period with regard to CO_2 and O_2 concentration in the package headspace. The results of a sensitivity analysis with the regard to influences of key factors (namely maximum O_2 consumption rate ($r_{O_2}^{max}$), the Michaelis-Menten constant ($k_{m_{O_2}}$), film permeability and package volume) on the model predictions of CO_2 and O_2 concentrations (Appendix H.2; Table H-2) indicated that the model predictions in the both dynamic and steady-state period are highly sensitive to both $r_{O_2}^{max}$ and $k_{m_{O_2}}$. The latter is particular is subject to uncertainties arising due to estimations using nonlinear regression models (see the discussion in Ratkowsky 1990, page 88 and Ratkowsky 1986). Significant influences of film permeabilities to O_2 and CO_2 ($P_{pkfl}^{O_2}$ and $P_{pkfl}^{CO_2}$, respectively) on model predictions of the quasi steady-state concentrations were observed, as could be expected.

This discussion reinforces the need to consider all elements of the active packaging system to achieve appropriate MA conditions in the package. The outer packaging properties can not be independently adjusted to achieve desired outcomes with respect to the active agent (such as MIC) without also considering the affect of the design on (i) the levels of O_2 and CO_2 in the system, which may affect the physiology of the packaged product (mainly the

respiration rate), and/or (ii) on physico-chemical properties of the packaging films (such as packaging film permeabilities to O_2 and CO_2) that determine the final MA condition.

6.4.2 Effects of the ratio of sachet to package surface area (ω_A) on the package headspace hexanal concentrations

All tested active MA packages used in the previous validation experiments had the same ratio of sachet to bag area ($\omega_A \approx 0.024$, Table 6-1). In this section, how varying this ratio affected the hexanal concentration in the package headspace is reported. To achieve various relative area ratios the surface area of the sachets was varied whilst that of the outer bags was kept constant. The tested packages utilised for this purpose were referred to as LD5 and LD6 (Table 6-1) with ω_A values of 0.012 and 0.048, respectively. Experimental results and model predictions for these were compared to those of LD1 ($\omega_A \approx 0.024$), as this ratio was extensively used in the present study. It should be noted that LD1 and LD5 have a same sachet gel loading (1.5g), while the loading of LD6 was higher at 3.0g.

Figure 6-9A shows the experimental results and model predictions for LD1, LD5, and LD6 for 7 days storage at 20ºC. Initial unsteady-state concentrations measured in the LD6 system were approximately 2-fold higher than those measured in the other systems. However differences between LD1 and LD5 were not clear, even though a few data points of higher concentrations (at ~1-2 h) were measured in LD5 (Figure 6-9B). Model predictions followed the usual release trend, however a lack of fit between model predictions and experimental data was apparent and similar to that discussed in the previous sections.

More apparent effects of surface area ratio on headspace concentration can be observed in the quasi steady-state period (Figure 6-9A). For example by reducing the sachet area by 50%, the experimental quasi steady-steady concentrations of LD5 (i.e. 17-24 ppm) were proportionally lower than those of LD1 (i.e. 32-40 ppm). As LD6 had a higher sachet loading (double that of both LD1 and LD5) and sachet area (double and four times that of LD1 and LD5, respectively), its quasi steady-state concentration level is thus the highest. The mathematical model reasonably well predicted such observations (Figure 6-9A).

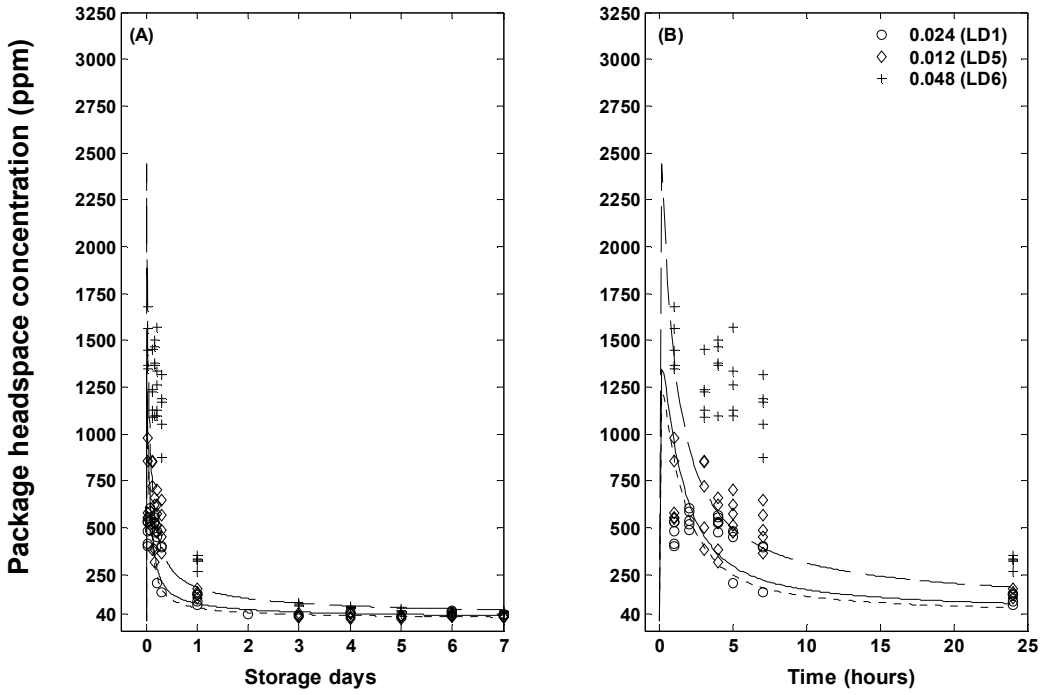

Figure 6-9 Measured and predicted hexanal concentration in the active package (at least 3 replicates shown for each sampling time), for different ratios of sachet to bag area (ω_A): 0.024 (o; LD1), 0.012 (◊; LD5), and 0.048 (+; LD6), for storage period of 7 days at 20°C (A) and the same data expanded to look at the first 24 h (B). Model predictions are shown through solid, dotted and dashed lines, respectively.

Because of the lack of fit noted during the unsteady-state period, a sensitivity analysis was performed using the LD6 system as an example. The results are graphically presented in Appendix H.2 (Table H-3). Model predictions were sensitive to variations in all chosen model inputs. The results of the sensitivity analysis are consistent with those reported in previous sections and again confirm the need to improve estimations of P_{LDPE}^{Hxl} and b_{Lgm}^{Hxl} in particular.

6.4.3 Effects of the type of sachet film on the package headspace hexanal concentration

From previous sections it was evident that the model reasonably well predicted trends in the dynamic phase and quasi steady-state headspace hexanal concentrations for a range of design variables, including the presence or absence of tomatoes in the package and the

ratio of sachet to bag area. To further validate the model the effect of packaging film on headspace hexanal concentrations was investigated. OPP and Tyvek® polymer films were used as alternatives to LDPE in example active packages referred to as OP1 and TY1 (Table 6-1). It should be noted that the concentration scales employed in the graphs of following subsections are different to those presented earlier in order to better present the data.

6.4.3.1 OPP sachet film

Headspace hexanal concentrations for the OPP sachet film are shown in Figure 6-10. The trend of hexanal release was similar to that for LDPE (Figure 6-2 and Figure 6-4), where a low quasi steady-state concentration was eventually attained after the initial release, but the initial peak concentration was ~2 to 3-fold lower than that generally observed in the LDPE system. This difference could be attributed to the higher hexanal barrier properties of OPP film compared to that of LDPE (as reported in section 4.2.2). The similar release pattern demonstrates the influence of the common Type I sorption isotherm.

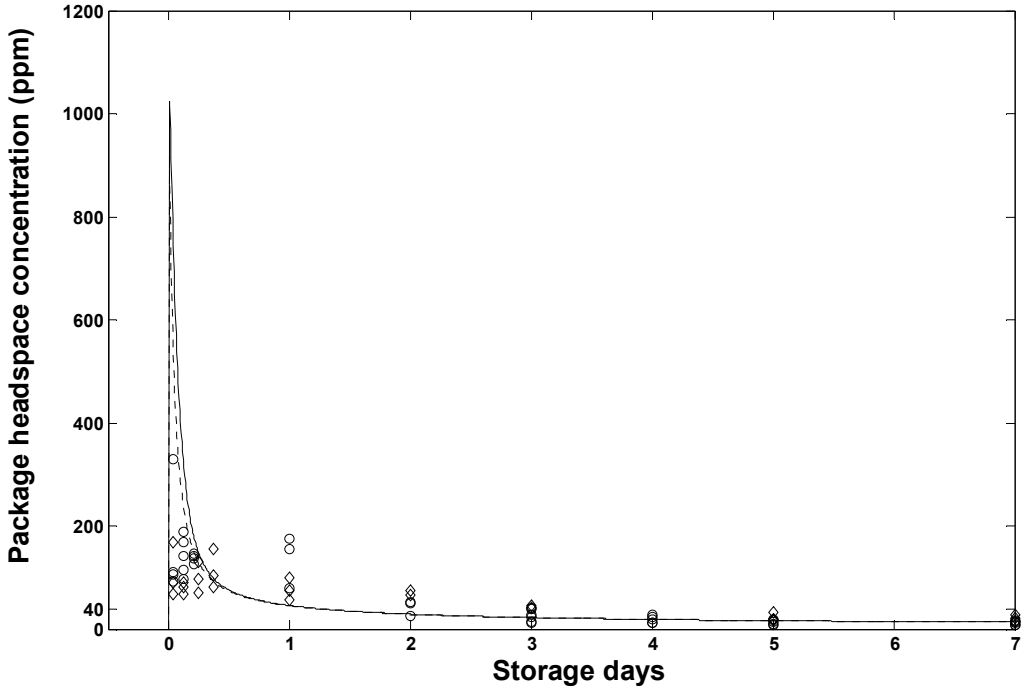

Figure 6-10 Effects of OPP sachet film on package headspace hexanal concentration (at least 3 replicates shown for each sampling time) in a LDPE package containing either a sealed glass jar (o) or tomatoes (◊) of which prediction results are represented by solid and dotted lines, respectively.

Model predictions of the quasi steady-state concentrations for the sachet with an OPP film generally agreed with the experimental data after day 3-4 (Figure 6-10). The empirical quasi steady-state concentrations were similar regardless of the package contents. This can be explained through the dominance of mass transfer across the film over hexanal uptake by tomatoes, as discussed in section 6.4.1.2. It can be noticed that the quasi steady-state concentrations were slightly lower than the MIC level, suggesting that a higher ratio of sachet to package surface area (e.g. by increasing sachet size or minimising the outer film surface area) will be required to achieve the desired antifungal concentration levels.

Similar to previous scenarios, a lack of fit between experimental data and the model predictions was noticeable during the unsteady-state conditions. Differences in the experimental initial release peaks between the package containing the inert jar and the tomatoes were apparent and these were attributed to hexanal uptake by tomatoes (although it may be unduly influenced by the data point at 1-hour; Figure 6-10). The differences in the initial peaks for these systems were also reasonably predicted by the model. A sensitivity analysis of the model predictions for headspace hexanal concentrations was conducted on the model package containing tomatoes and the all results are presented in Appendix H.2 (Table H-4).

Overall, the sensitivity analysis again yielded similar results to those obtained for other scenarios. Predictions of headspace hexanal concentration appeared sensitive to variations in L_{pkfl}, P_{LDPE}^{Hxl} (of outer film), and b_{Lgm}^{Hxl}, and less sensitive to variations in P_{OPP}^{Hxl} (sachet film) and r_{tom}^{Hxl}. The limited effect of uncertainty in the sachet film (OPP) permeability supports the discussion in Chapter 5 that changes of concentration at the sachet film are likely to occur rapidly compared to those in the carrier bed or in the package headspace. The results of the sensitivity analysis also suggest that the accuracy of the data on packaging film (LDPE) permeability and the sorption isotherm are more important to model predictions than that of the sachet, for situations where different materials are used for the sachet and outer package.

6.4.3.2 Tyvek® sachet film

Experimental results for headspace hexanal concentrations from the Tyvek® sachet systems are illustrated in Figure 6-11. In this case the initial concentration peak of the Tyvek® system was higher than for the other films, as expected given the high hexanal permeability of Tyvek® material due to its highly porous nature (refer to Chapter 4). No significant differences in the quasi steady-state concentration were observed between the sealed glass jar or tomatoes and the quasi steady-state concentration was in the MIC range. Thus a Tyvek®-based sachet active packaging system should also be suitable for extending the shelf life of tomatoes.

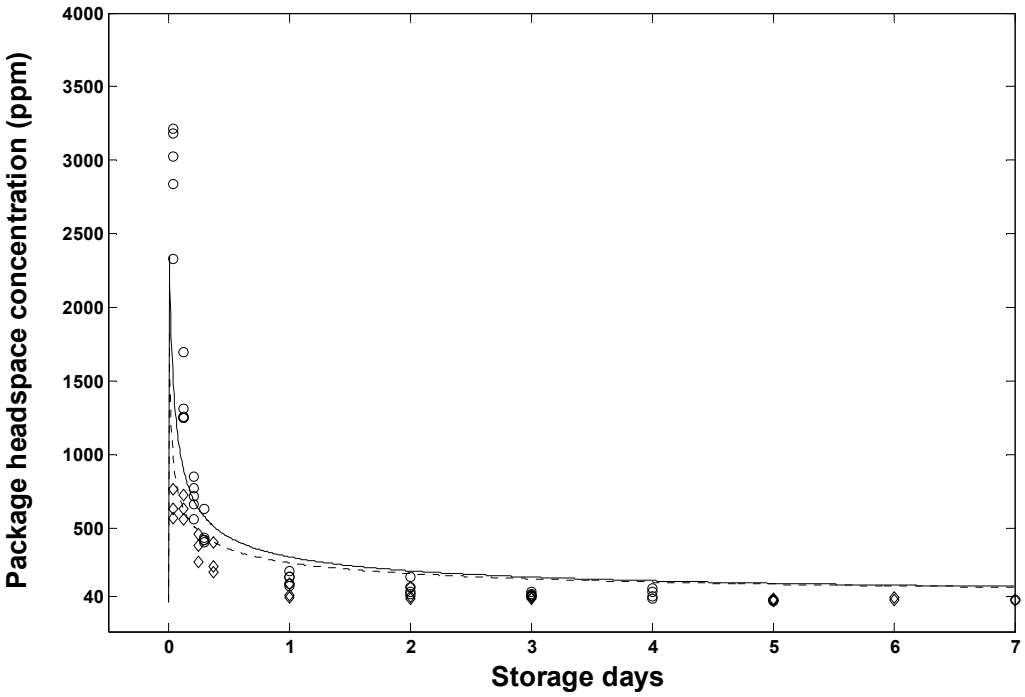

Figure 6-11 Effects of Tyvek® sachet film on hexanal accumulation in the headspace of an LDPE package (at least 3 replicates shown for each sampling time) containing either a sealed glass jar (o) or tomatoes (◊) of which model prediction results are represented by solid and dotted lines, respectively.

For the initial unsteady-state period, the experimental data show that the headspace concentration was again attenuated in the packages containing tomatoes compared to those of the packages with only a sealed glass jar. This indicates significant effects of r_{tom}^{Hxl} on

accumulation of hexanal vapour in the package headspace, which can be expected given the high hexanal concentration that developed.

It is worth noting that quasi steady-state concentrations are broadly comparable for all films, although the initial release peaks were quite different at comparable sachet loadings. These data suggest the release patterns are likely to be governed by mass transfer across the outer packaging film (LDPE for all trials outlined in this section) and its surface area, regardless of the sachet system employed.

Based on studies conducted comparing sachet systems, it then can be inferred that provided LDPE film is the outer packaging material, a LDPE film sachet with 1.5g loading can be utilised as an alternative to Tyvek® and OPP for delivering and sustaining hexanal vapour in the package headspace within the MIC level for 7 days at 20ºC.

In Figure 6-11, the model predictions of Tyvek® both underestimate the unsteady-state experimental data and overestimate quasi steady-state concentrations for each of the inert volume and tomato systems; a pattern opposite to those for OPP and LDPE sachet systems as reported previously. The sensitivity analysis was conducted to investigate effects of uncertainties in permeability to hexanal vapour of Tyvek® (P_{Tyvek}^{Hxl}) and other inputs on model predictions, and the results are summarised in Appendix H.2 (Table H-5).

The model predictions appeared less sensitive to variation in P_{Tyvek}^{Hxl} compared to those in L_{pkfl}, P_{LDPE}^{Hxl} (of outer film), and b_{Lgm}^{Hxl}. The highest sensitivity of the model predictions was obtained in respect to error in the permeability value and the predictions of the unsteady-state concentrations appeared to be improved when P_{LDPE}^{Hxl} was lowered (Table H-5). This may imply that the uncertainty in permeability of the outer film may be chiefly responsible for the underestimation of model prediction illustrated in Figure 6-11.

Influences of humidity in package headspace on the initial release of experimental data (Figure 6-11) also can not be precluded because of the high porosity property of Tyvek® film. In particular this might be responsible for the opposite in experimental and model prediction trend as mentioned above. In section 4.3.5, the influence of pre-adsorption of water vapour on silica gel on hexanal uptake could not be discounted, even though the

trends were not apparent or uniform. If adsorption of water vapour (through permeation into the sachet headspace, given ~0 (or at least low) and ~60-70% (typical ambient) RH levels at $t = 0$ in the sachet and package headspaces, respectively) did cause displacement of adsorbed hexanal molecules, this could increase the hexanal vapour concentration in the sachet headspace and in turn the concentration gradient between sachet and package headspace. The observed high initial release concentration could then result. However there was no particular evidence of a significant influence of RH on hexanal release during the quasi steady-state period where the effect of additional release of hexanal could be expected to be greater (Figure 6-11). If RH had a significant effect, lower values of b_{Lgm}^{Hxl}, greater desorption of hexanal from the carrier, and higher levels of the quasi steady-state concentration than measured should be expected.

For the OPP and LDPE sachet systems water vapour movement into the sachet is unlikely to play a role because the permeabilities of these films to water vapour are very low (Liu et al. 1991; Robertson 1993c; Selke et al. 2004). During long term storage however the eventual increase in moisture content in the sachet may lead to the effects noted above. However there was no evidence of this after the 7-day storage period, over the 14 days of the variable temperature experiments (section 6.4.4). As noted elsewhere, this type of behaviour could possibly be exploited to promote VOC release once high RH has achieved, when the risk of fungal growth is increased. The high RH in package headspace may be also utilised to promote release from the hydrophilic film sachet for which film permeabilities tend to be increased under elevated humidity.

It is evident in the sensitivity analysis (Table H-5) that individually varying the values of the key inputs did not yield better predictions. However promising improvements were achieved when values for the three identified inputs were changed simultaneously in order to change sorption equilibrium characteristics and film permeance (a combination of L_{pkfl} and P_{LDPE}^{Hxl}), as illustrated in Figure 6-12. To achieve a better prediction of the quasi steady-state concentration (dotted line; Figure 6-12), accumulation of hexanal vapour in the package headspace should be minimised and this could be manipulated by (i) increasing b_{Lgm}^{Hxl}, corresponding to increasing the affinity between hexanal (adsorbate) and the carrier (adsorbents) (Gregg & Sing 1982; Adamson 1990), and (ii) elevating permeance of the outer film (by increasing P_{LDPE}^{Hxl} and decreasing L_{pkfl}) which increases the rate of hexanal

vapour permeation across the film. A reverse of such adjustments to increase accumulation of hexanal in the headspace gives better predictions of the unsteady-state concentration profile (dashed line; Figure 6-12), even though the model then overestimates the quasi steady-state concentration. These simulations demonstrate that the difference between model predictions and experimental data might be minimised when accurate estimates of the inputs are provided. This also suggests that the model can be used as a tool to gain insights into key mass transfer processes for active packaging systems and how packaging components must be optimised to achieve the required concentration patterns and quasi steady-state level. Most importantly, it can also be used to identify needs with respect to improvement of experimental methods to collect more data.

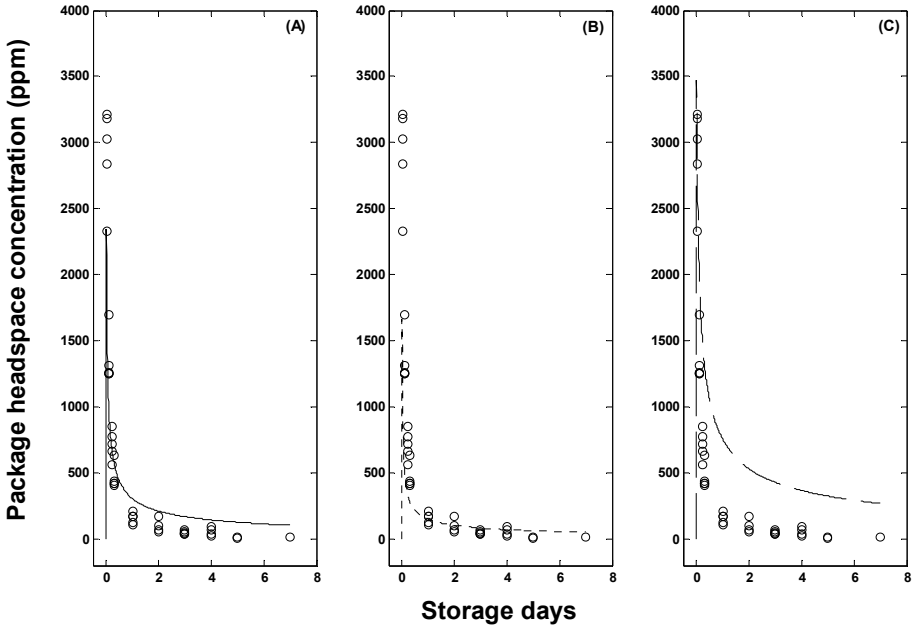

Figure 6-12 Results of sensitivity analyses of Tyvek®-sachet model package containing a sealed glass jar, by simultaneously varying values of b_{Lgm}^{Hxl} and a combination of L_{pkfl} and P_{LDPE}^{Hxl} to change equilibrium sorption characteristics and film permeance, respectively. Experimental results are represented by black symbols (at least 3 replicates shown for each sampling time). The solid line represents model predictions using the original model inputs (A). Model inputs were varied to either minimise (by increasing sorption affinity and outer film permeance) (B) or maximise (by lowering sorption affinity and outer film permeance) (C) accumulation of hexanal vapour and these model predictions are represented by the dotted and dashed lines, respectively.

6.4.4 Effects of storage temperature on the package headspace hexanal concentrations

In this section, the mathematical model was used to predict hexanal concentrations in packages subject to variable storage temperatures. This is not an uncommon situation in the horticultural industry, occurring e.g. when product is removed from cool stores for repacking or for transhipping. The model packages utilised in this section are referred to as LD4, OP2 and TY2 (Table 6-1) reflecting the different sachet films used. The effects of storage temperature on headspace hexanal concentrations in all model packages can be seen in Figure 6-13 together with the model predictions. It should be noted that different vertical scales are used for column (A) graphs to better illustrate the hexanal release patterns.

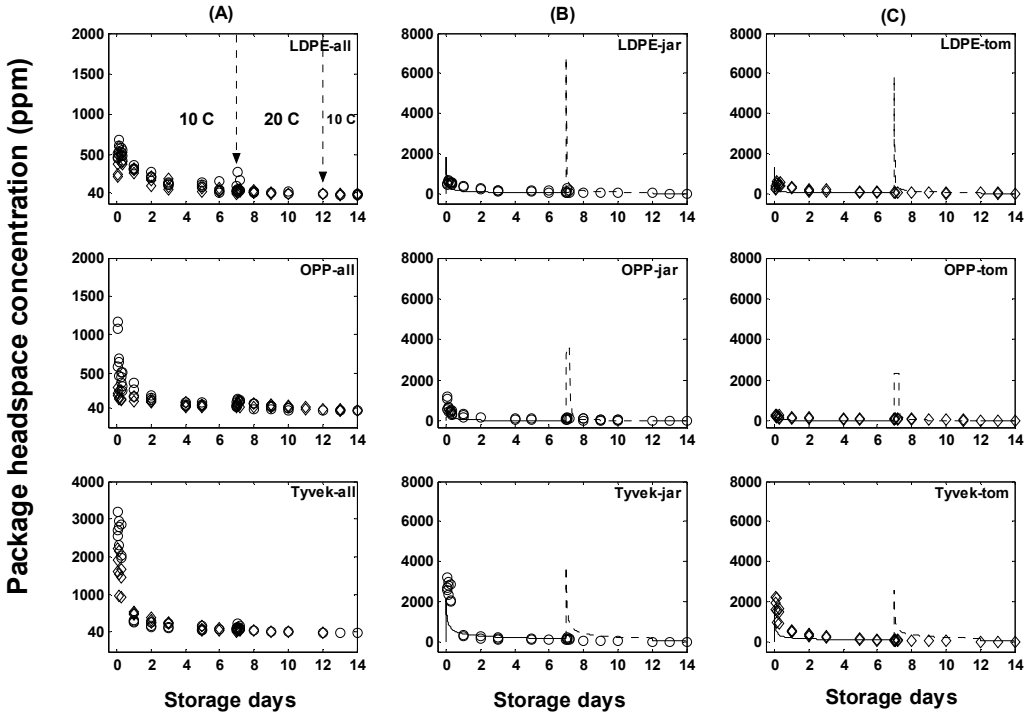

Figure 6-13 Hexanal concentrations in model packages (at least 3 replicates of individual treatments shown for each sampling time) with LDPE, OPP and Tyvek® as the sachet film material, at variable 10°C and 20°C storage conditions. Experimentally collected data for packages containing either a sealed jar (o), or tomatoes (◊) is presented in the first column (A; suffix 'all'). Individual sets (B, and C; suffix 'jar' and 'tom' representing sealed jars and tomatoes, respectively) are presented with model predictions, where solid and dotted lines describe the predicted results at 10°C and 20°C, respectively. The transitions between 10 and 20ºC occurred at day 7 (10 to 20ºC) and day 12 (20 to 10ºC) as shown in A (top).

At 10ºC, the release pattern of hexanal from the sachet and hexanal accumulation in the package during the first 7-day storage period was similar to that observed in the experiments conducted solely at 20ºC, where there was an initial high concentration peak which declined to a relatively low quasi steady-state concentration. No effect of tomatoes on the attenuation of the initial release peaks at 10ºC was apparent. This could be explained by the low apparent rate of hexanal uptake by tomatoes as a result of the low hexanal concentrations in the package headspace. While there were no clear differences in the dynamic concentrations between the OPP and LDPE systems, there were a few unexpectedly high headspace concentrations measured in the OPP sachet active MA package (without tomatoes; B middle). The results appear to be opposite to the known (and measured) lower permeability of OPP compared to that of LDPE. Furthermore the attainment of quasi steady-state concentrations after the initial release peak in the LDPE sachet systems (Figure 6-13A, top) appeared to take longer than those observed for OPP and Tyvek® systems at 10ºC and all systems at 20ºC (as reported previously). Those systems with Tyvek® as the sachet material had the highest initial release concentration as expected (given the high porosity of Tyvek® material) and the quasi steady-state concentrations were rapidly attained after the initial release peak (Figure 6-13A). The mathematical model predicted the quasi steady-state concentrations well, although some lack of fit was noticeable for the unsteady-state concentration regions (Figure 6-13B and C).

It was evident that the quasi steady-state concentrations observed in all model packages were maintained at the MIC or above. Although the MIC was quantified at 20ºC, this concentration should also be effective at the lower storage temperatures because proliferation of *B. cinerea* (and other spoilage microorganisms) is less likely at lower temperatures (Adaskaveg et al. 2002). Cool storage conditions (e.g. 10ºC) have long been utilised in transport and packaging practices for horticultural products, including tomatoes, to minimise microbial growth and biological activities (Robinson et al. 1975; Kader & Saltveit 2003a).

After some packages were transferred from 10ºC to 20ºC, there was a secondary release of hexanal into the package atmosphere. Of the active MA packages investigated, the most obvious secondary peak occurred when LDPE was the sachet material and a sealed glass

jar was the enclosed product (Figure 6-13A, top). No secondary peak was observed in the package containing tomatoes, possibly because hexanal uptake by tomatoes attenuated this additional hexanal release. The apparent rate of hexanal uptake by tomatoes (r_{tom}^{Hxl}) was observed to be dependent on both concentration and storage temperature (section 3.4.2). After the secondary release, quasi steady-state concentrations within the MIC range were quickly regained. This release pattern could be beneficial when breaks occur in the cool chain, as an increase in the ambient (and hence product) temperature could stimulate growth of *B. cinerea*. The release of a 'secondary fumigation' peak (~100-300 ppm) during the transient from 10 to 20ºC could possibly assist in controlling *B. cinerea* outgrowth, although it may be effective only for a short period (i.e. ~24-48 h as discussed in section 3.2.2). When the model packages were transferred from 20ºC to 10ºC (Figure 6-13), there were no consequential changes to headspace hexanal concentrations.

Patterns of release observed during the transient storage temperature regime could be explained by the equilibrium sorption properties of silica gel. A secondary release peak during the transition from 10 to 20°C could occur due to a change in hexanal uptake ($C_{s,bed}^{Hxl}$) as illustrated in Figure 6-14.

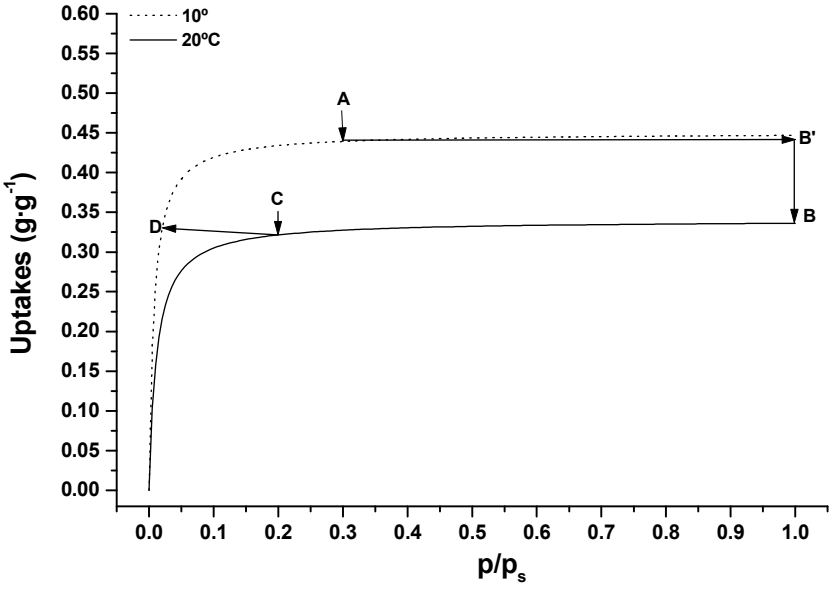

Figure 6-14 Sorption isotherm at 10 and 20ºC (calculated using the Langmuir Equation; (Eq. 2-3) and coefficients reported in Table 4-9). The letters A, B (and B′), C, and D represent those points discussed in the text regarding changes to the sorption equilibrium during temperature transitions.

Based on model simulations of accumulation of hexanal vapour in the package headspace, the calculated $C_{s,bed}^{Hxl}$ at the end of initial 10ºC storage regime (day 7) was about 0.43 g·g^{-1} (point A; Figure 6-14). As this was higher than the $C_{s,max}^{Hxl}$ value at 20ºC (~0.34 g·g^{-1}; point B), following the transfer to 20°C, the gel would be expected to release this excess adsorbed hexanal in order to achieve its equilibrium $C_{s,max}^{Hxl}$ value at the higher temperature (line A-B; Figure 6-14). Until the maximum uptake ($C_{s,max}^{Hxl}$) value at 20ºC was reached, the equilibrium vapour concentration ($C_{g,bed}^{Hxl}$) value within the sachet should be equal to the saturated concentration (vapour pressure) at 20ºC (line B′-B; Figure 6-14), provided there was local equilibrium of temperature for all packaging components. Because $C_{g,bed}^{Hxl}$ increased from its value at 10ºC, the concentration gradient between sachet and package headspace would have also increased so generating the secondary outer headspace peak. For the release during the transition from 20 to 10°C, there was no secondary peak and this could be explained by the result of the relatively low value of $C_{g,bed}^{Hxl}$ of ~0.05 mol·m^{-3} at the end of 20ºC storage (or $p/p_s \leq 0.2$, point C; Figure 6-14). As the temperature was decreased to 10°C, the $C_{s,bed}^{Hxl}$ value may have increased above ~0.32 (point D; Figure 6-14) by re-adsorption of free hexanal released previously. However such re-adsorption is unlikely to be significant as there is a very low mass capacity in the gas phase. Thus a decrease of $C_{s,bed}^{Hxl}$ on transfer to the 10°C isotherm seems likely and would yield a p/p_s (or $C_{g,bed}^{Hxl}$) of less than 0.2. Therefore, the concentration gradient between the sachet and headspace could be decreased and the outer package headspace may decrease.

Although the mathematical model could generally predict release pattern during the transient temperature change (Figure 6-13) for the case of inert volume and LDPE sachet, the model markedly overestimated the ‘breakthrough’ concentrations (secondary peak) at 20ºC. For LDPE, these predicted ‘breakthrough’ concentrations were very much higher (~2500 - ~6500 ppm) than those observed in the experiments (≤ 500 ppm). Similar patterns were also observed among OPP and Tyvek® sachet systems. Such large differences between the model and experimental values raise important questions regarding the true temperature dependence of the sorption isotherm coefficients.

From the literature (e.g. Adamson 1990; Chen et al. 2007), a strong temperature dependence of the Langmuir sorption coefficient (b_{Lgm}) is expected. This coefficient can be utilised for calculating thermodynamic parameters, including free energy (ΔG°) and apparent enthalpy change (ΔH°) as discussed in Chapter 4. In contrast to b_{Lgm}, the temperature dependence of the maximum uptake ($C_{s,max}$) is unclear. Whilst Do (1998b) (page 18) noted that $C_{s,max}$ is theoretically temperature independent, there is evidence of a temperature dependency of $C_{s,max}$, although the effect is less marked than for b_{Lgm}. For example b_{Lgm} values for butyraldehyde adsorption for silica gel grade 40 (reportedly an exothermic process) decreased by ~39% as temperature increased from 15ºC to 26ºC, whereas the $C_{s,max}$ values only decreased by ~5% (Table 4-9). Chen et al. (2007) reported that the b_{Lgm} for cationic starch adsorption on kaolin (reportedly an endothermic process) increased by 8.5-fold as the temperature increased from 15ºC to 60ºC, however, the $C_{s,max}$ values increased only ~1.2-fold.

To illustrate the case of low dependency of the isotherm on temperature, model simulations are shown in Figure 6-15A (legends refer to Figure 6-13) assuming $C_{s,max}^{Hxl}$ was constant at the value estimated at 10ºC and the b_{Lgm}^{Hxl} value was that measured at 20°C. For these values, the secondary release peak on transfer from 10 to 20ºC was virtually absent as expected (Figure 6-15A). Changes of $C_{g,bed}^{Hxl}$ values and hexanal mass on silica gel would be less obvious when the package was transferred to 20ºC (Figure 6-15B). Considering Figure 6-15A, there is however a clear secondary hexanal peak in the experimental data even though overall predicted results (except the 2nd release peak) are similar to those illustrated in Figure 6-13B (top). This implies there is some greater difference between the isotherms at 10 and 20°C than that demonstrated for the selected values in Figure 6-15B. The experimental data also show that the package headspace concentration was possibly lower after the transfer to 20°C, as discussed above.

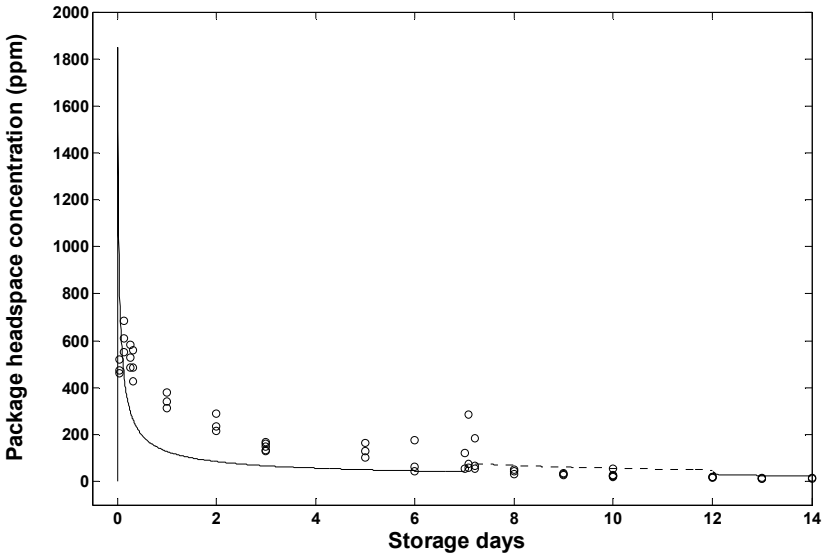

(A)

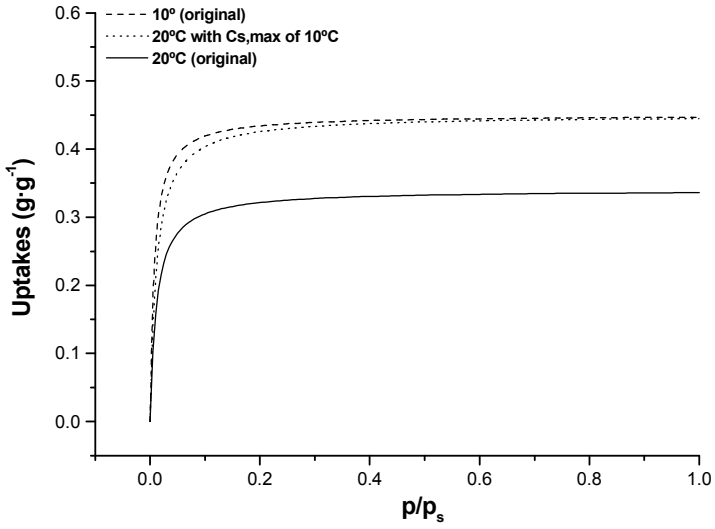

(B)

Figure 6-15 Experimental and predicted values of hexanal concentration in an LDPE-sachet package containing a sealed glass jar (at least 3 replicates shown for each sampling time) during varied storage temperature regimes. Solid and dotted lines represent model predictions on 10 and 20 ºC (A). Hexanal sorption isotherms at 10 and 20°C were calculated using the Langmuir equation (Eq. 2-3 and coefficients reported in Table 4-9) (labelled as 'original'), and the isotherm at 20°C when $C_{s,max}^{Hxl}$ value was arbitrarily assumed to be the value at 10ºC, with the b_{Lgm}^{Hxl} value as at 20°C (B).

Sensitivity analyses were conducted for headspace hexanal concentrations of model packages containing tomatoes kept at 10ºC during the first 7 days of storage. The results of sensitivity analyses are graphically illustrated in Appendix H.2 (Table H-6).

Model predictions of headspace hexanal concentrations were only sensitive to variations in b_{Lgm}^{Hxl} and r_{tom}^{Hxl}. As reported in Chapter 4, the uncertainty associated with b_{Lgm}^{Hxl} at 10°C is high and the results of all sensitivity analyses confirm its influence on model predictions. The moderate sensitivity of r_{tom}^{Hxl} at 10ºC supports the high apparent rate of hexanal uptake at 10ºC reported in Chapter 3. Mass transfer across the cuticles was assumed to be significant and governed by hexanal sorption; this rate of sorption was likely to be higher as temperature decreased at a given hexanal vapour concentration. The minimal sensitivity to packaging film permeability and thickness of the model predictions is in contrast to the sensitivity analyses conducted in previous sections. These suggest uncertainties of model inputs will have to be differentially taken into account in active packaging systems subject to variable storage temperature regimes.

In the sensitivity analysis the model predicts a faster decrease of headspace concentration after the initial release peak than the experimental data. As discussed in section 6.4.3.2 (and shown in Figure 6-12), by lowering outer film permeance (by decreasing P_{LDPE}^{Hxl} and increasing L_{pkfl}) and sorption affinity (by decreasing b_{Lgm}^{Hxl}) simultaneously, the model predictions were significantly improved for the LDPE and OPP sachet systems (Figure 6-16) as this adjustment lead to a slower decrease of hexanal vapour in the headspace. For the Tyvek® system, even though the model gave reasonably good predictions of unsteady-state concentrations, it still tended to overestimate quasi steady-state concentrations (Figure 6-16).

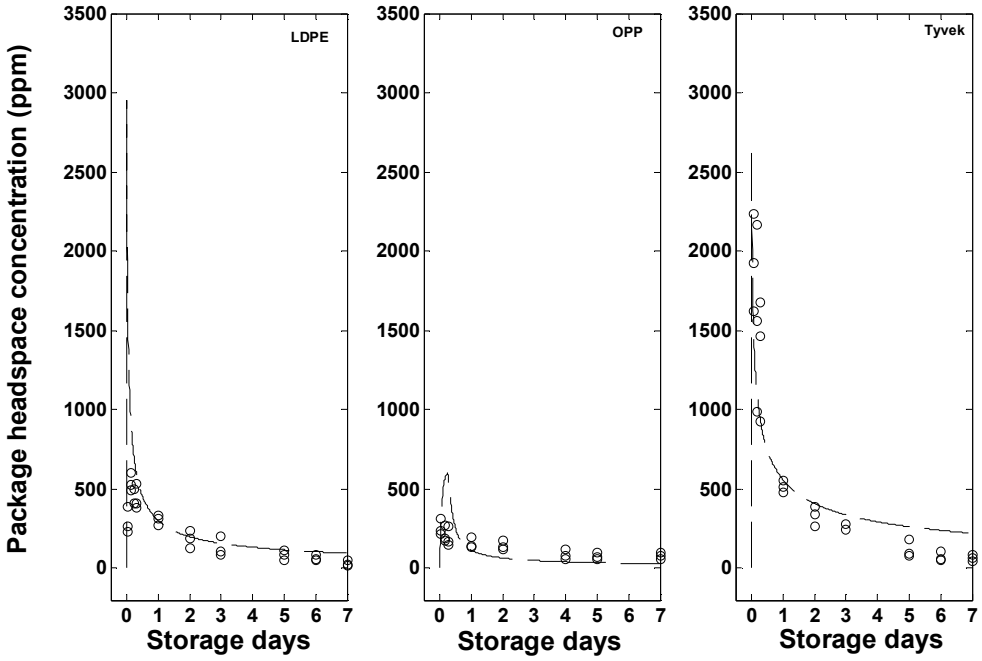

Figure 6-16 Results of sensitivity analyses of model package at 10°C containing a sealed glass jar (at least 3 replicates shown for each sampling time), by simultaneously lowering outer film permeance (by decreasing P_{LDPE}^{Hxl} and increasing L_{pkfl}) and sorption affinity (by lowering b_{Lgm}^{Hxl}).

6.4.5 Changes of hexanal adsorbed amount on silica gel

The mathematical model was also used to evaluate changes in the mass of hexanal adsorbed onto the silica gel ($C_{s,bed}^{Hxl}$). It is interesting to gain further insights into the role of $C_{s,bed}^{Hxl}$ on the system performance because this may be critical for the implementation of these active packages. In particular it will be necessary to address economic and environmental issues associated with the amount of silica gel and hexanal utilised and the fate of hexanal (or any other volatiles) remaining in the sachet at the end of the storage period (e.g. with respect to disposal, possible toxicity, and economic loss).

6.4.5.1 Materials and methods

To investigate changes in $C_{s,bed}^{Hxl}$ during hexanal release, experiments were conducted with the package referred to as LD7 (Table 6-1). This comprised only the LDPE sachet. The sachet (LDPE) film with foil base was placed foil-side down on a Mettler (0.001 g Mettler

Toledo PR5003, Switzerland) analytical balance equipped with an RS232 interface connected to a compatible computer and the change in mass of the sachet, which contained hexanal saturated silica gel (of dry weight ~1 g), was followed. The sachet was surrounded by the glass weighing chamber which comprises 3 sliding windows (2 on the sides and 1 on the top). All windows were fully opened in order to minimise accumulation of released hexanal vapour in the chamber. The bulk hexanal concentration surrounding the sachet was therefore assumed equal to zero ($C_{env}^{Hxl} = 0$), as for all other scenarios modelled. Two replicate experiments were performed in a controlled temperature cabinet at 20±1°C. As the results of the two experiments were similar, one set of the results was used for model validation. The balance reading was logged at intervals of 5 minutes for ~48 hours. The net hexanal adsorbed on the silica gel was obtained by subtracting the known combined mass of the sachet and dried silica gel from the gross mass logged from the balance.

The mathematical model for predicting $C_{s,bed}^{Hxl}$ values was similar to that used in all previous sections. In this case, the package area and free volume were assumed 20 times larger than the actual values, to model a very slow rate of hexanal accumulation in the headspace and effectively providing a zero headspace concentration during the release period.

6.4.5.2 Results and discussion

From Figure 6-17, it was evident that the initial adsorbed amount predicted by the mathematical model ($C_{s,max}^{Hxl}$ at 20ºC, or ~0.34g·g^{-1} at t = 0) was about 1.2-fold lower than that measured in the experiment (~0.43g·g^{-1}). The difference was assumed to be the result of small amounts of hexanal liquid remaining after vacuum filtering. Evidence of such remaining liquid was also observed in preparations of sachets for experiments in previous sections (see Appendix H.1), however then the focus was on the quasi steady-state hexanal headspace concentrations which were reasonably well predicted by the global model. The findings in this section will therefore be discussed along with the results reported previously, where appropriate.

The model prediction is plotted with the experimental data in Figure 6-17. There was a small but noticeable increase in the measured hexanal mass near the end of the testing period. This was possibly due to a drift in the balance baseline due to the necessary but

undesirable requirement that all windows of the balance were fully opened to minimise accumulation of hexanal vapour. The model used the measured initial adsorbed amount as the initial mass in the simulation, and assumed saturated (equilibrium) vapour concentration corresponding to the adsorbed amount ≥ $C_{s,max}^{Hxl}$ (see MATLAB® code in Appendix G.1). The adsorbed hexanal mass was predicted to rapidly decrease, which differed from the pattern obtained from the experimental data (Figure 6-17). The model predicted the quasi steady-state mass would be reached in less than 2 h and at a significantly higher mass than the experimental data (~1.2-fold).

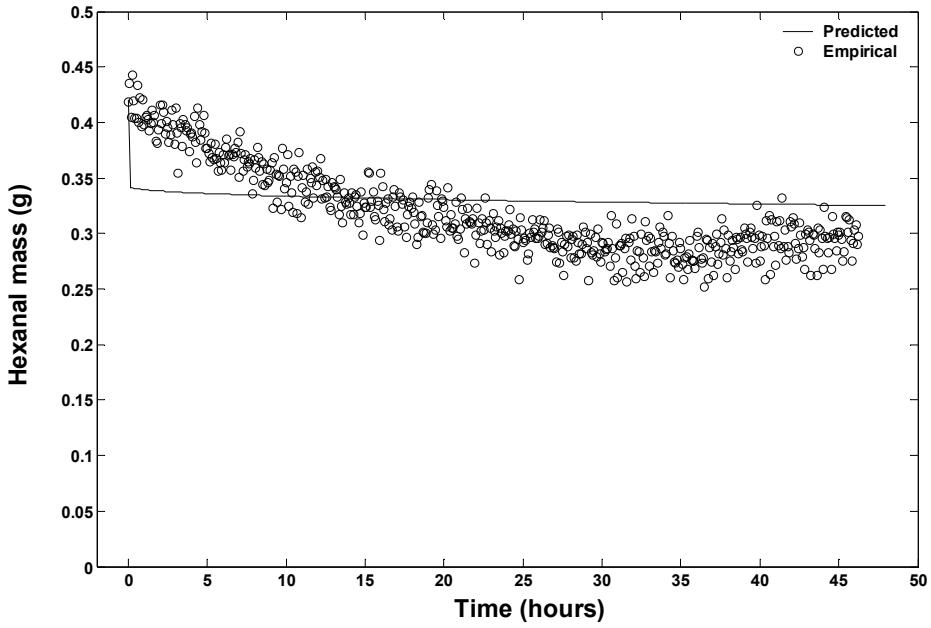

Figure 6-17 Experimental data on changes of adsorbed hexanal mass on silica gel (o) and model prediction (solid line) with an adjusted model prediction to correct for initial free liquid mass.

The poor prediction of hexanal mass suggests that the model is not appropriate to describe this important but rather artificial situation. The most likely explanation for this appears to be the extrapolation of the LDPE permeability data (quantified using only low and intermediate bulk hexanal vapour concentrations, and at low concentration gradients between the film surfaces) to calculate flux across the sachet film in this situation where the maximum possible concentration gradient (i.e. a saturated condition upstream and 0 concentration downstream of the film) (refer to Eq. 4-5 in section 4.2.2). Although mass transfer conditions where high "feed" side concentrations and large concentration gradients (as was the case for the OPP film) were taken into account in the development of Eq. 4-5,

the model predictions clearly do not predict the experimental data of the system (Figure 6-17). Because of this, the data for LDPE permeability to hexanal vapour shown in section 4.2.2 may not be suitable for this current situation.

During the first ~24 hours, the experimental data (Figure 6-17) showed a reasonably linear mass loss with time and this may be assumed to define the steady-state release flux under these (extreme) conditions. The calculated flux value was ~5.37×10^{-6} mol·s^{-1}·m^{-2} (or ~5.37×10^{-4} g·s^{-1}·m^{-2}), assuming saturated internal conditions. By using Eq. 4-5 with the inputs for LDPE film at 20ºC reported in section 4.2.2, and with $C_{h,conc}^{Hxl}$ and $C_{l,conc}^{Hxl}$ as 0.46 (saturated concentration) and 0 mol·m^{-3}, respectively, the predicted flux is ~6.82×10^{-4} mol·s^{-1}·m^{-2} (or ~6.82×10^{-2} g·s^{-1}·m^{-2}), which is over 2-orders of magnitude higher than the experimental value calculated above. The difference between the two values suggests that the film has a much lower permeability to hexanal vapour in the sachet situation in the initial stage of release. From this analysis it was clear that an alternative expression for prediction of the flux from a sachet was required.

Permeability is a product of solubility and diffusivity (Robertson 1993c). The solubility was assumed to follow Henry's law and be concentration independent for the development of the hexanal transfer model through the film (see Appendix D.1). As discussed in section 4.2.2, hexanal permeation through all tested films (LDPE, OPP and Tyvek®) appeared to be dominated by the sorption process. Therefore the relationship between hexanal vapour and film sorption was considered further.

According to Robertson (1993c), interactions between VOCs and polymeric film under situations such as those represented here may become large and relationship between solubility and vapour pressure (concentration) may require to be described by alternative models such as the Langmuir model or the dual mode (Henry's law and Langmuir) model. The Langmuir model (as expressed by Eq. 2-3) predicts linear sorption behaviour of the permeant at low concentration but the sorbed amount reaches an asymptote as the concentration increases (as for hexanal on silica gel). This behaviour could be caused for example, by saturation of specific adsorption sites or immobilisation of permanent molecules in microvoids in the polymer due to interactions between the permeant and polymer (Robertson 1993c). Matsuguchi et al (2002) reported single component sorption

of water vapour or CO_2 by highly photocrosslinked poly(vinyl cinnamate) (PVCA; a hydrophilic film) at 30ºC were well described by the Langmuir sorption relationship. Similarly Marin et al.(1992) reported that sorption of 2,6-di-tert-butyl-4-methylphenol (DTP) vapour by HDPE film (both with or without the additive heptadecane (or steric acid)) at 100-200ºC were well represented by the Langmuir sorption isotherm. The dual mode is commonly used for sorption on glassy polymers, for which sorption of gaseous molecules are governed by both Henry's law and the Langmuir model (Robertson 1993c; Mercea 2000; Selke et al. 2004). Examples of such systems are acetone vapour-PET and acetone vapour-PET/PEN copolymer (at 35ºC; McDowell et al. 1999), and acetronitrile vapour-cellulose acetate (at 25ºC; Guo & Barbari 2008).

Because the experimental temperature (20ºC) is well above the glass transition temperature of LDPE (-110ºC, see Dury-Brun et al. 2007), the LDPE sachet film can reasonably be considered as a rubbery polymer. The Langmuir model may therefore be the most appropriate for the LDPE-hexanal vapour sorption system. If so, this implies that the saturated sorption capacity of hexanal on LDPE (and on also OPP and Tyvek®) could be at or near the saturated concentration (~0.46 mol·m^{-3} at 20ºC estimated following Covarrubias-Cervantes et al. 2004), while the highest concentration levels investigated in section 4.2.2 were about 50% lower. Future work therefore is required to confirm and characterise the sorption characteristics of these polymer-VOC combinations.

Taking this assumption, if the flux model (Eq. 4-5) is replaced with one where the diffusivity is assumed constant (i.e. concentration independent to simplify mathematical complexity, although permeation of organic vapours through polymeric film typically shows a positive dependence on concentration as documented in Rogers et al. 1962; Zobel 1982; Rogers 1985) and the solubility is described by the Langmuir model (see Appendix D.3 for the mathematical model derivation), the steady-state flux across the sachet film can be described by Eq. 6-3.

$$J_{film} = Z_{Lgmfl}^{Hxl}\left(\left(\frac{1}{1+\left(k_{Lgmfl,1}^{Hxl}\cdot C_{h,conc}^{Hxl}\right)}\right)-\left(\frac{1}{1+\left(k_{Lgmfl,1}^{Hxl}\cdot C_{l,conc}^{Hxl}\right)}\right)\right) \qquad \textbf{(Eq. 6-3)}$$

where

Z_{Lgmfl}^{Hxl} = Fitted coefficient of Langmuir relationship for hexanal vapour sorption on LDPE film (mol·s^{-1}·m^{-2})

$k_{Lgmfl,1}^{Hxl}$ = Fitted coefficient of Langmuir relationship for hexanal vapour sorption on LDPE film ($m^3 \cdot mol^{-1}$)

Figure 6-18 illustrates the steady-state fluxes predicted by Eq. 6-3 (using the inputs, including $C_{h,conc}^{Hxl}$, $C_{l,conc}^{Hxl}$ and film thickness as reported in section 4.2.2) and a comparison with fluxes reported for experiments on LDPE film permeability at 20ºC (using Eq. 4-5; section 4.2.2) and the hexanal mass loss experiment (this section). Fluxes predicted by Eq. 6-3 are in a good agreement with those predicted by Eq. 4-5, however the predicted fluxes are nearly 2-fold lower than those measured in the range 0.01 to 0.02 $mol \cdot s^{-1} \cdot m^{-2}$. Good agreement is again observed at the concentration observed across sachet film in the mass loss experiment. In Figure 6-18, it can be observed that there is a reasonable linear relationship between fluxes measured and those predicted by Eq. 4-5, except the unduly high predicted steady-state flux across the sachet (contributed by the extrapolation of measured LDPE permeability as discussed earlier).

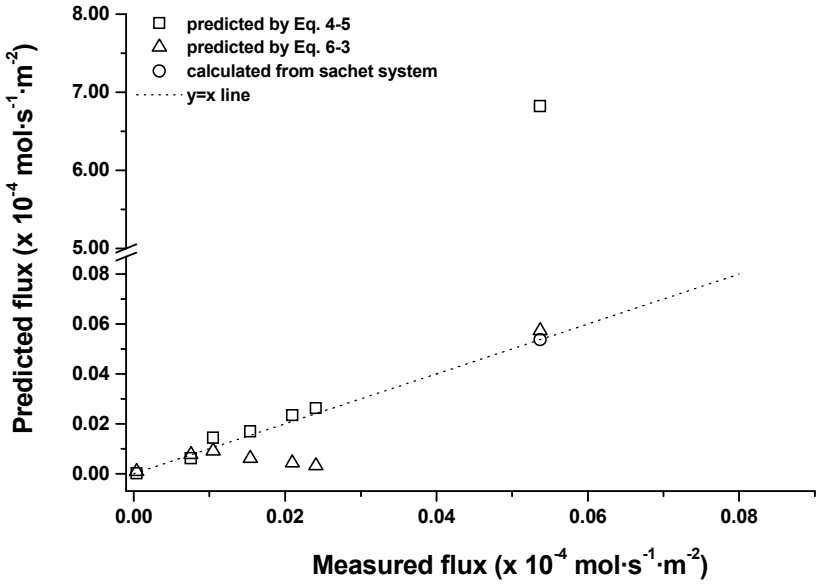

Figure 6-18 Comparisons of fluxes measured in experiments on LDPE film permeability (section 4.2.2) and hexanal mass loss (this section) to fluxes predicted by (i) Eq. 4-5 (section 4.2.2; □) or Eq. 6-3 (Δ), and flux calculated from results of hexanal mass loss (o). The dotted line represents y = x line.

However it is also clear from Figure 6-18 that neither model for flux across the sachet film (Eq. 4-5 or Eq. 6-3) appear satisfactory in all scenarios. The original exponential relationship (Eq. 4-5) fits well for low to intermediate concentrations, while the Langmuir isotherm model (Eq. 6-3) may reasonably describe the flux at very low and very high concentrations but not for intermediate scenarios. This analysis suggests more detailed hexanal transfer rate experiments will need to be carried out over the full range of conditions (e.g. of both upstream concentrations and concentration gradients) before a comprehensive model can be developed. Unfortunately this requires a very time consuming and labour intensive experimental programmes and was outside the scope of this thesis.

The current mathematical model describing steady-state flux across the sachet in the global model was replaced with Eq. 6-3 to allow prediction of hexanal mass changes (for the same conditions as those shown in Figure 6-17). The results are illustrated in Figure 6-19. The experimental hexanal mass change, particularly during the unsteady-state period, is well described by the modified mathematical model. The modified model however still overestimated the quasi steady-state mass (to the same extent as before). The sensitivity analysis (in respect to b_{Lgm}^{Hxl} and $C_{s,max}^{Hxl}$) was conducted and illustrated in Appendix H.2 (Table H-7). The model predictions, as might be expected, are highly sensitive to uncertainty in $C_{s,max}^{Hxl}$ during the quasi steady-state period. If the $C_{s,max}^{Hxl}$ value is lowered by its percentage SE, the modified model well predicted the quasi steady-state mass (Table H-7).

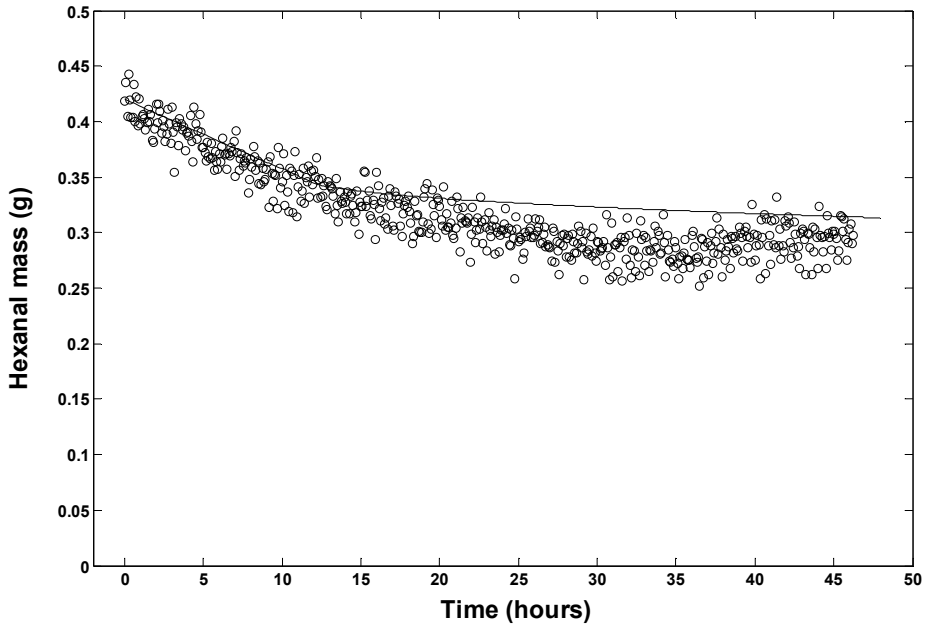

Figure 6-19 Experimental data on changes of adsorbed hexanal mass on silica gel (o) and model prediction (solid line) using Eq. 6-3.

The modified model was further utilised to predict package headspace hexanal vapour concentrations for the LD1 active packaging system (with no tomatoes; Table 6-1) as an example. As has been noted, the situation of a high sachet hexanal vapour headspace concentration and low (although only zero initially) package headspace concentration arises on first insertion of the sachet (refer to Figure 6-3). The new model prediction is compared with the experimental data and original model in Figure 6-20. The prediction of the unsteady-state headspace concentration was much improved by use of the modified model. In particular, the height of the initial release peak was attenuated and so was more similar to that measured and the predicted peak concentration was shifted later and therefore closer to the empirical data. However the modified global model now appears to overestimate the quasi steady-state concentration where previously this was well predicted by the original model. This discrepancy presumably arises from the much lower predicted flux at intermediate concentrations (shown in Figure 6-18), so that hexanal in package headspace during the quasi steady-state period is not predicted to leave the bag with a sufficiently high enough flux.

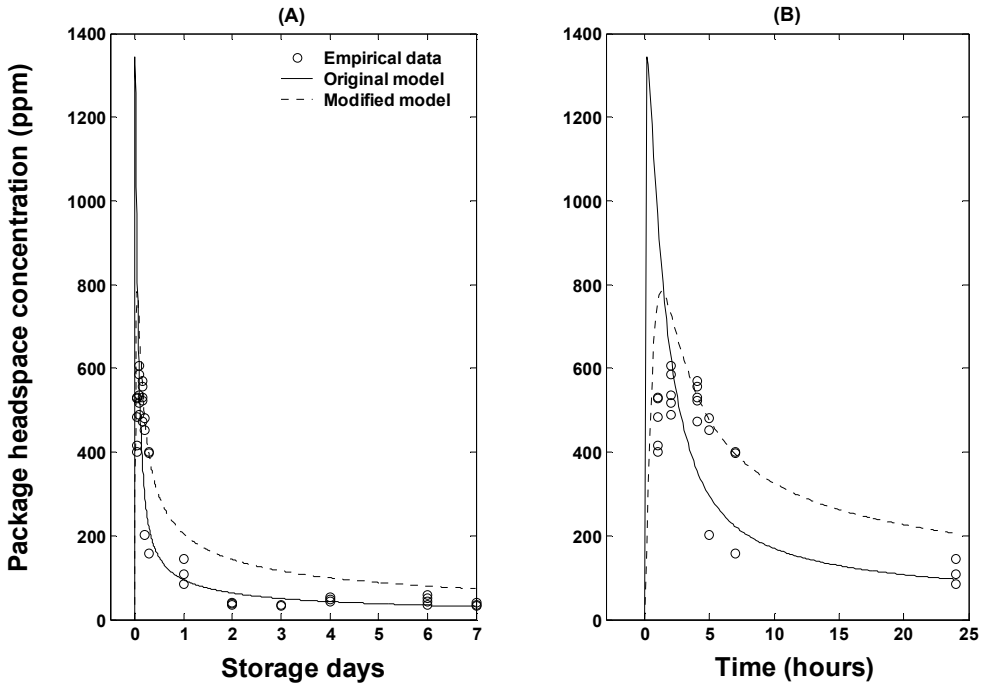

Figure 6-20 Experimental data (o; at least 3 replicates shown for each sampling time) on hexanal vapour concentrations in package headspace of LD1 active packaging system (with no tomatoes; Table 6-1) and model prediction results of original (solid line) and modified (dotted line) global mathematical model, during 7-day (A) and 24-hour storage period (B; the same data expanded to better present).

Based on results shown in Figure 6-20, it appears that development of an improved model to describe hexanal mass transfer through the sachet film is critical to effectively modelling unsteady-state concentrations.

In spite of these findings regarding these extreme conditions, the original model still predicts the overall headspace concentration trends and quasi steady-state values reasonably well. There is much evidence from the sensitivity analyses to show that improved agreement between experimental and predicted data on unsteady-state concentration, especially after the initial release peak, can be expected by improving the estimates of b_{Lgm}^{Hxl} and P_{LDPE}^{Hxl}. Therefore the discussion and conclusions offered in previous sections appear to be valid and the original model can be further used to explore the effects of different packaging designs on the likely performances (e.g. with respect to the obtaining MIC level). However caution should be exercised in implementing any model system without further experimental checks of their appropriateness and accuracy.

Based on experimental (Figure 6-17) and other modelled data, the final hexanal mass (after 7-14 days) does not differ greatly from that initially loaded on the silica gel. This implies that smaller amounts of silica gel adsorbent (i.e. less than 1 g) could be successfully deployed to still achieve the required MIC concentration, with consequently lesser amounts of hexanal left on the carrier. A preliminary analysis can be conducted using the model developed in the present study. However, the selection of appropriate loadings may have to be carefully checked given that the outcome is affected by mass transport processes occurring in the sachet, outer packaging film, and tomatoes as mentioned previously.

6.5 Summary

The mathematical model developed in this study can be used to predict hexanal vapour concentrations in the headspace of a range of model active MA packaging systems. The results of the model, in most cases, agreed reasonably well with experimental quasi steady-state concentration data, which are the key to maintaining product quality through long-term storage. A lack of fit was, however, noticeable in the unsteady-state period of the first 12-24 h and this cautions against the use of the model for quantifying “fumigation” scenarios.

When the model was implemented to predict changes of hexanal adsorbed on the carrier for the sachet only, a discrepancy between the model prediction and experimental data, especially during the unsteady-state period, led to a review of the assumption made of constant and concentration independent LDPE solubility of hexanal vapour (i.e. following Henry’s law). This assumption may be valid for low and intermediate hexanal vapour concentrations. However under extreme concentration gradients, the assumption of a Langmuir relationship between hexanal vapour and LDPE film sorption may be more appropriate. The mathematical model for describing steady-state flux across the sachet was modified accordingly and when incorporated into the global model, predictions of hexanal mass changes were improved for the initial dynamic phase of this extreme case.

Overall these validation experiments and their analysis have demonstrated that better estimates of coefficients of the sorption isotherm for silica gel, and of film solubility and permeability are required to achieve better model predictions. The gravimetric sorption

method utilised in the present work provided reasonable data but better technologies are needed for temperature control and equilibrium vapour concentration measurement, and to increase the sensitivity of the weighing scale. The latter may be achieved by using quartz-spring type microbalances (noted in Chapter 4) or thermogravimetic equipment, which includes a highly sensitive weighing scale and technically advanced controls of temperature and pressure (vapour concentration). However the risk that the weighing and pressure sensors may be damaged by hexanal vapour (or other VOCs) must be taken into account. There are alternative methods for measuring film permeability to the isostatic method employed in this study and these are summarised elsewhere (for example see Robertson 1993c). Further studies of hexanal permeability, which should also consider solubility, film swelling, and other types of VOCs-polymer interactions, should be conducted. Experiments on film permeability must be conducted over a wide range of feed side concentrations and concentration gradients to better characterise mass transfer of hexanal for a range of scenarios.

Because the mathematical model developed can reasonably predict the quasi steady-state active package performance and the MIC level during long term storage, the model can be adapted for other volatile substances, such as eugenol, ethanol and 1-MCP, provided appropriate isotherm and permeability data (and other required inputs) are available. The mathematical model can therefore be utilised as a tool to gain insights into the effects of packaging design variables on concentration levels of hexanal and other active agents for different scenarios. This is further examined in the following chapter.

Chapter 7

MATHEMATICAL MODEL APPLICATIONS

7.1 Introduction

Although a range of designs of active packaging systems were tested to validate the mathematical model (as reported in Chapter 6), a common pattern of hexanal release was observed in all scenarios. A high initial concentration in the package headspace was rapidly established, followed by a rapid drop to a relatively low level that was sustained for the remainder of the storage period. This pattern was chiefly governed by the shape of the Langmuir sorption isotherm. It is therefore of interest to explore through the model further '*what-if*' scenarios with regard to the effects of different types of sorption isotherms on release patterns. Also, it is of interest to gain insights to the mass transfer processes (with an emphasis on the steady-state fluxes) across the sachet boundary as a function of isotherm model and storage time to better understand their effects on the hexanal release patterns. Although validation of model predictions for these scenarios was not conducted, the results and their interpretation provide a theoretical basis for further development of active packaging systems to achieve a range of release patterns of other active agent from sachets.

7.2 Effects of isotherm types on hexanal release patterns

Possible release patterns that might be sought can be conceptualised as illustrated in Figure 7-1. Fumigation with a high concentration of active substance for a short period followed by the attainment of a lower (but still inhibitory) concentration has been demonstrated.

One alternative release pattern of interest is where the active agent concentration is maintained and sustained at the highest level after the initial release, for either a long (line I; Figure 7-1) or short (line II; Figure 7-1) period prior to the concentration decreasing. After the sustained period, it may be preferable for the concentration to decrease either slowly or rapidly to zero to remove the volatile from the package headspace at the opening or expiry date. Such a decrease of hexanal concentration after the sustained period could provide the benefit of, for example, minimising the odour of the active agent in the packaged product near its point of sale if this was considered sensorially undesirable by end-users/consumers. Similarly, as reported in section 3.2.2, continuous exposure of light

red tomatoes to hexanal at the MIC level can slow reddening of tomato skins. By allowing the hexanal concentration to approach zero during the retailing period (e.g. after transhipping), the tomato skin would redden normally and become visually more attractive to consumers. This release pattern might also be beneficial to the 1-MCP controlled release system (such as that developed by Lee 2003). By having a very low 1-MCP concentration prior the retailing period, then the de-greening of the skin or softening of the product when being exhibited on the supermarket shelves may not be delayed.

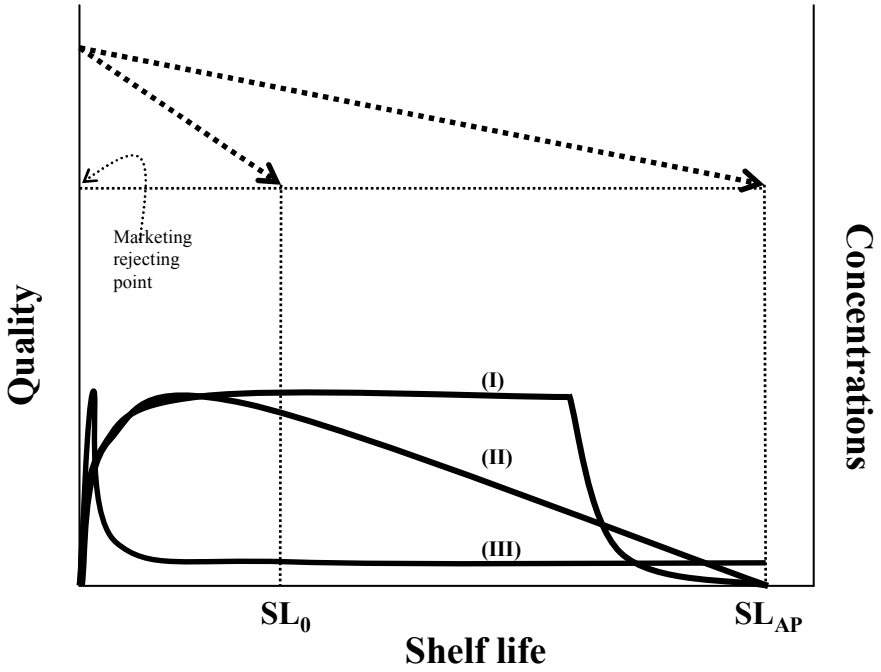

Figure 7-1 Conceptualised release patterns to extend shelf life (SL_0 and SL_{AP} represent the shelf life without and with active controlled release, respectively) and delay changes of postharvest qualities (dotted lines). Solid lines represent long (I) and short (II) sustained release period prior to concentration decreasing, while the solid line III represents the fumigation with a high concentration following by an attainment of a low concentration.

Because the fumigation release pattern (line III; Figure 7-1) was extensively discussed in Chapter 6, the long and short sustained release patterns (lines I and II, respectively; Figure 7-1) are the focus of this chapter. To achieve these patterns, changes of the equilibrium vapour concentration in the sachet bed ($C_{g,bed}^{Hxl}$) after the initial release should be minimal even though the equilibrium adsorbed amount ($C_{s,bed}^{Hxl}$) will be dynamically decreasing. Because of this, the magnitude of the concentration gradient between the sachet and package headspace could essentially remain constant to stabilise the headspace

concentrations. After a certain release period, $C_{s,bed}^{Hxl}$ should then continuously decrease to bring about a reduction of the $C_{g,bed}^{Hxl}$ value. For the pattern with a long sustained period (line I; Figure 7-1), the headspace concentration should eventually dramatically decrease (to rapidly approach zero). In such a case, the change in $C_{s,bed}^{Hxl}$ value should cause an exponential and rapid reduction of $C_{g,bed}^{Hxl}$. In contrast, comparable relative reductions of both $C_{s,bed}^{Hxl}$ and $C_{g,bed}^{Hxl}$ values are required to achieve the short sustained release period (line II). The isotherm shapes required to achieve the long and short sustained period are therefore exponential and linear, respectively.

An exponential isotherm is the Brunauer's Type III isotherm (Adamson 1990) (Figure 2-1) and conceptually this is like a reflection of the Langmuir curve (or Type I isotherm). Examples of an exponential isotherm system are the adsorption of (i) water vapour by lactose (Bronlund 1997) and (ii) ethanol vapour by amorphous Teflon AF2400 (Tokarev et al. 2006). A linear isotherm equation is illustrated in Eq. 2-2 and an example of this adsorption system is 1-MCP on silica gel (Lee 2003; Lee et al. 2006). To illustrate the effects of the isotherm form on release patterns, variable shapes of isotherms including exponential (Eq. 7-1), linear (Eq. 2-2) and Langmuir (Eq. 2-3) were examined.

$$C_{s,bed}^{Hxl} = \left(a_{exp}^{Hxl} \cdot exp\left(\frac{C_{g,bed}^{Hxl}}{b_{exp}^{Hxl}} \right) \right) - a_{exp}^{Hxl} \qquad \textbf{(Eq. 7-1)}$$

where

$C_{s,bed}^{Hxl}$ = Equilibrium adsorbed amount of hexanal on the carrier bed ($g \cdot g^{-1}$)

$C_{g,bed}^{Hxl}$ = Equilibrium hexanal vapour concentration above the carrier bed (presented as relative pressure; dimensionless see Figure 7-2)

a_{exp}^{Hxl} = Coefficient of the hexanal exponential isotherm equation ($g \cdot g^{-1}$)

b_{exp}^{Hxl} = Coefficient of the hexanal exponential isotherm equation (dimensionless)

For the Langmuir and exponential isotherms, the degree of curvature can also be varied in order to investigate its effects on changes of equilibrium conditions in the sachet and package headspace. The coefficients associated with the isotherm equations and isotherm shapes are shown in Table 7-1 and Figure 7-2, respectively. It should be noted that

desorption isotherms were assumed to be identical to the adsorption isotherm, i.e. hysteresis was negligible.

Table 7-1 Coefficients associated with alternative isotherm equations

Exponential			Linear		Langmuir		
ID.	a_{exp}^{Hxl}	b_{exp}^{Hxl}	ID.	K_{Lin}^{Hxl} ($g \cdot g^{-1}$)	ID.	$C_{s,max}^{Hxl}$ ($g \cdot g^{-1}$)	b_{Lgm}^{Hxl} (dimen-sionless)
Exp.1 [a]	3.49×10^{-8}	0.06	Lin. [b]	0.33	Lgm.1 [c]	0.34	87.07
Exp.2 [a]	1.50×10^{-4}	0.13			Lgm.2 [a]	0.34	36.80
Exp.3 [a]	7.31×10^{-3}	0.26			Lgm.3 [a]	0.37	9.20

[a] Data were obtained from the best estimates of nonlinear regressions. It should be noted that the slightly higher value of $C_{s,max}^{Hxl}$ ($g \cdot g^{-1}$; unit) of the Lgm. 3 was chosen for making the curve ending at the same point as that described by Lgm.1 and Lgm.2.

[b] Data were obtained from the best estimate of a linear regression.

[c] Original data quantified in the present work as reported in Chapter 4 (Table 4-9).

where

K_{Lin}^{Hxl} = Coefficient of the hexanal linear isotherm equation ($g \cdot g^{-1}$)

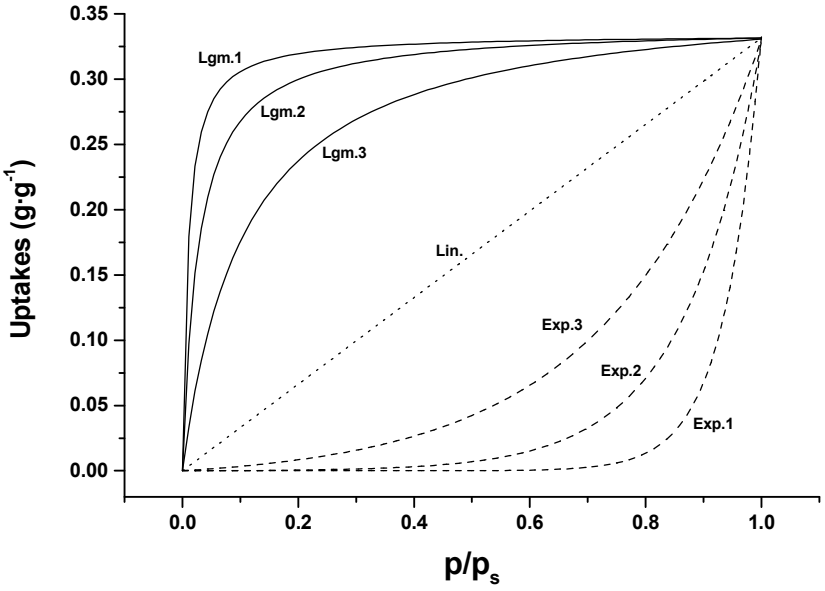

Figure 7-2 Alternative sorption isotherm shapes for simulating hexanal release patterns. Coefficients associated with the isotherm equations are those shown in Table 7-1.

The active packaging system utilised for simulating hexanal release patterns was that described previously as systems LD1 with no tomatoes (as identified in Table 6-1). The

package and sachet headspace concentrations were predicted using the global model as provided in Appendix G.1, in which the Langmuir equation was appropriately modified or replaced by either the linear or exponential isotherm. The mathematical expressions for describing $C_{g,bed}^{Hxl}$ as a function of $C_{s,bed}^{Hxl}$ for the exponential and linear isotherms are Eq. 7-2 and Eq. 7-3, respectively, and the expression for the Langmuir isotherm is Eq. 5-16.

Exponential $$C_{g,bed}^{Hxl} = ln\left(\frac{\left(C_{s,bed}^{Hxl} + a_{exp}^{Hxl}\right)}{a_{exp}^{Hxl}}\right)\cdot b_{exp}^{Hxl} \quad \textbf{(Eq. 7-2)}$$

Linear $$C_{g,bed}^{Hxl} = \frac{C_{s,bed}^{Hxl}}{K_{Lin}^{Hxl}} \quad \textbf{(Eq. 7-3)}$$

Simulations of hexanal release patterns at 20ºC arising from different sorption isotherm systems in the LD1 system (Table 6-1) are illustrated in Figure 7-3. However the predicted release patterns were indistinguishable and all profiles were similar to those observed in simulations of the Langmuir isotherm system (Figure 7-3E). On reflection, these results were not unsurprising because of the high permeability to hexanal vapour of LDPE film which was assigned as the outer packaging film. However when the system was modelled with an OPP outer bag film (with values of $P_{OPP,0}^{Hxl}$ and b_{OPP}^{Hxl} as reported for 20ºC in Table 4-2; recall OPP has a lower permeability to hexanal vapour), the predicted release patterns of all isotherm systems were still similar to those previously presented (Figure 7-3B, D and F). The similarity of both simulations may be explained by the comparable values of b_{LDPE}^{Hxl} and b_{OPP}^{Hxl} (~19.6-19.7 $m^3 \cdot mol^{-1}$; Table 4-2), even though $P_{LDPE,0}^{Hxl}$ is ~20-fold higher than $P_{OPP,0}^{Hxl}$ (Table 4-2). Based on the simulation results, it can be assumed that similar release pattern can be achieved by all isotherm forms (Table 7-1 and Figure 7-2), when LDPE is the outer film of the LD1 active MAP system (Figure 7-3A, C and E).

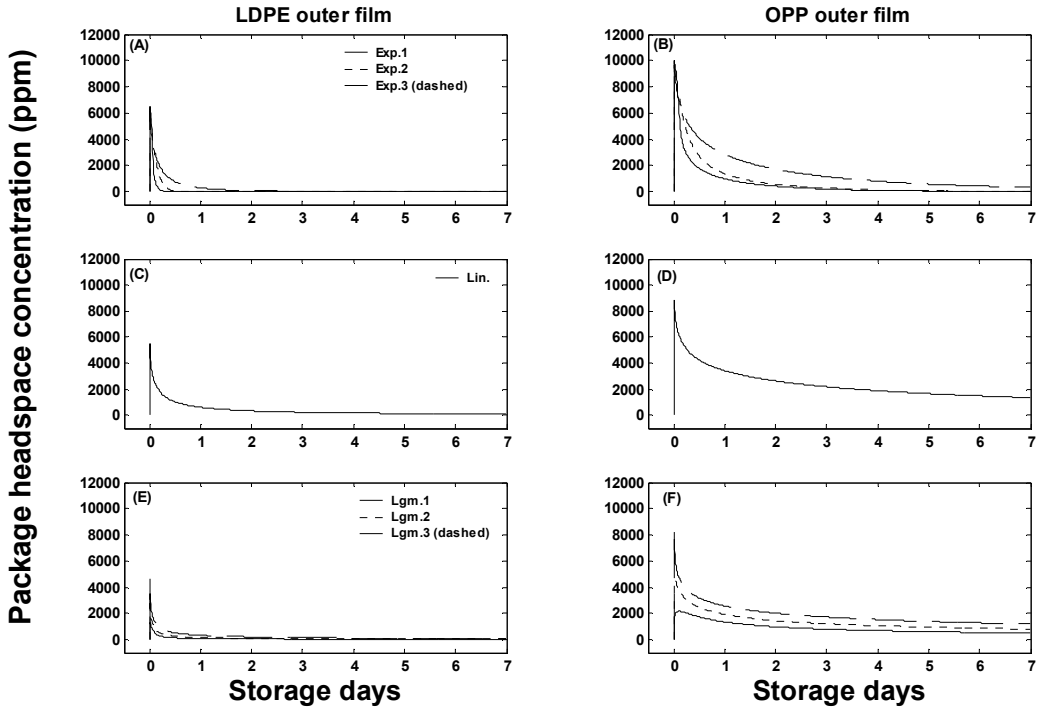

Figure 7-3 Simulated hexanal release patterns for alternative hexanal sorption isotherms: Exponential (Exp.1-3, represented by solid, dotted and dashed lines, respectively), Linear (Lin.), and Langmuir (Lgm.1-3, represented by solid, dotted and dashed lines, respectively). Graphs on the left- and right-hand-side columns refer to active MA packages having LDPE and OPP respectively as outer film materials, with the same sorption isotherm systems shown on the same row. Legends shown in these graphs (on the left-hand-side (LHS) column) refer to the parameter sets as provided in Table 7-1.

The simulations illustrated in Figure 7-3 suggest that the influence of the sorption isotherms on the release pattern should become obvious when permeability to hexanal vapour of the outer packaging film is appropriately designed. Also the results demonstrate that design of these active packaging systems requires consideration on the interactions between packaging components. The mathematical model obviously provides benefits over experimentation to meet such requirements.

To differentiate the release patterns of different sorption isotherms, it can be inferred that the value of permeability (both $P_{LDPE,0}^{Hxl}$ and b_{LDPE}^{Hxl} of the LD1 system) of the outer packaging film should be further decreased below that of OPP film (or an active agent with lower permeability should be employed). In practice, improving a film's barrier or other

properties, such as improving tensile strength, sealability or printability, may be achieved through the use of multilayer films manufactured by film lamination and co-extrusion (see Robertson 1993d). Alternatively, the metallocene catalyst processes of polymeric film manufacturing can yield improved film properties as in the case of the Exact™ 4151 which is an excellent barrier to hexanal vapour (as reported by Wolford 1998; Table 4-7). By lowering the permeability of the outer packaging film, this may also provide benefits including (i) retaining headspace concentrations at or higher than the MIC level, and (ii) minimising the release of the active agent into the storage environment. Most active agents have a distinctive odour, e.g. the grassy 'green' note of hexanal vapour or 'fermented' aroma of ethanol vapour, and these may be considered foreign by consumers as noted earlier. In addition, the effects of film alterations to film properties to achieve required release patterns on the establishment of MA conditions and consequent postharvest quality changes in the product have to be taken into account in the design of active MAP systems. These are discussed later in this section.

For simulation purposes, the values of $P_{LDPE,0}^{Hxl}$ and b_{LDPE}^{Hxl} of the outer packaging film were set arbitrarily lower by a factor of 10, while those of the sachet film were not altered. Simulations of the hexanal release pattern for the different sorption isotherms in the LD1 active MAP system are shown in Figure 7-4.

As Figure 7-4 makes clear, the different release patterns are now quite distinguishable and are consistent with the earlier discussion on the release patterns (Figure 7-1). The slowest changes of headspace hexanal concentration after the initial release were observed with the exponential isotherm systems (Figure 7-4A), while the most rapid changes occurred with the Langmuir systems (Figure 7-4E), as expected from the findings reported in Chapters 6. The linear equilibrium gave a release pattern intermediate between these two extremes (Figure 7-4C). All simulated release patterns exhibited in Figure 7-4 are sensible from a mechanistic viewpoint and are discussed below.

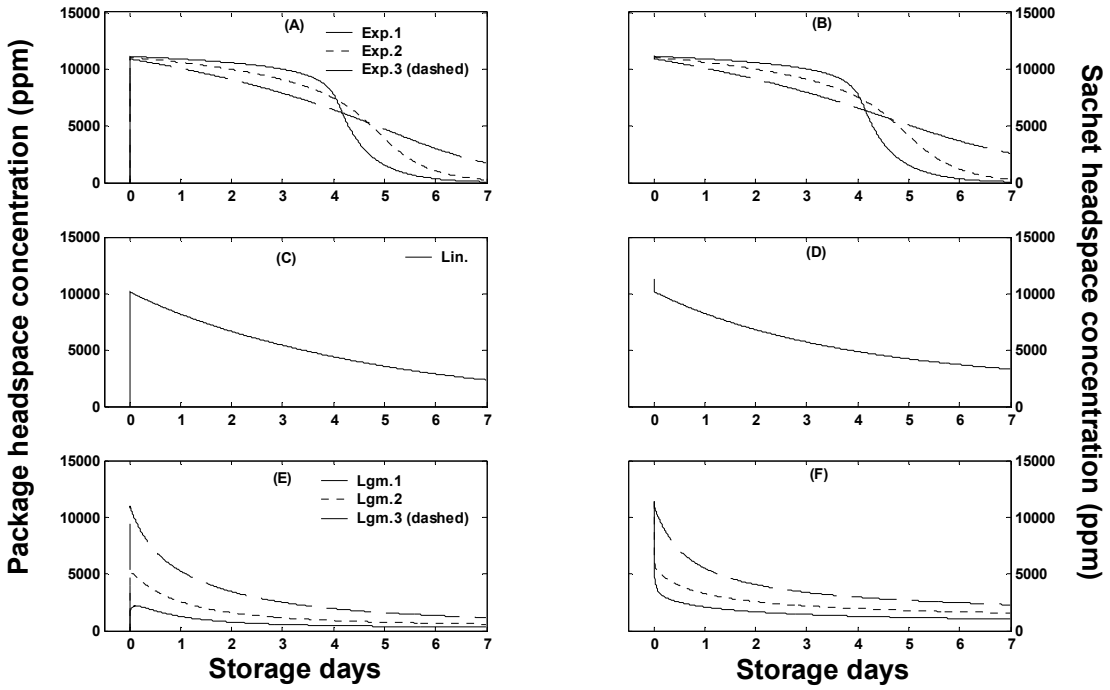

Figure 7-4 Simulated hexanal release patterns for alternative hexanal sorption isotherms with 10-fold lower outer bag permeability: Exponential (Exp.1-3 represented by solid, dotted and dashed lines, respectively), Linear (Lin.), and Langmuir (Lgm.1-3 represented by solid, dotted and dashed lines, respectively) and legends shown in these graphs (on LHS column) refer to variations as provided in Table 7-1. Graphs on the right-hand-side (RHS) column show sachet headspace concentrations and lines refer to sorption isotherm systems as provided in the same row of the LHS column.

The slow initial change in headspace concentration in the exponential system (Figure 7-4A) can be explained by the only small change in $C_{g,bed}^{Hxl}$ (Figure 7-4B) and hence in the concentration gradient between sachet and the headspace, even though $C_{s,bed}^{Hxl}$ continuously decreases. These effects manifest as reasonably stable headspace concentrations after the initial release. The changes to $C_{g,bed}^{Hxl}$ become apparent and rapid as $C_{s,bed}^{Hxl}$ approaches zero and the headspace concentration only decreases significantly at this point. For the exponential isotherms, the system having the lowest value of the exponential coefficient (a_{exp}^{Hxl}) (Exp.1; Figure 7-4A) exhibits the longest sustained period of elevated hexanal concentration because its long horizontal asymptotic yields the slowest changes in $C_{g,bed}^{Hxl}$ and the concentration gradients after the initial release (Figure 7-4B). As the a_{exp}^{Hxl} value

increases (as the cases of Exp.2 and Exp.3; Figure 7-4A), the release pattern exhibits lower curvature and becomes more similar to the linear isotherm system (Figure 7-4C). The release patterns of the Exp.3 and Lin. systems (Figure 7-4A and C) appear similar, but the headspace concentration of the Exp.3 system decreases more rapidly and this is more obvious after day 5.

For the Langmuir isotherm system, the height of the initial concentration peak exhibits a strong dependence on the b_{Lgm}^{Hxl} value. Among the Langmuir systems, a low b_{Lgm}^{Hxl} value gives a high peak (Lgm.3; Figure 7-4E) due to (i) the low affinity of hexanal and silica gel adsorbents (enhancing desorption), and (ii) the slow change of the partial pressure in the sachet headspace (from its saturated state, at $t = 0$) after the initial release (Figure 7-4F), as implied from the slight distortion of the isotherm curve in the low concentration range (Figure 7-2).

In Figure 7-4 (LHS column), the quasi steady-state concentrations of different isotherm systems were attained from day 7 of the simulation period. At the (qausi) steady-state period, the rate of release from the sachet equals the permeation through the outer film to the environment, as discussed in Chapter 6. Therefore the ratio of the product of film permeance and area with respect to both sachet and packaging films can be considered a 'design factor' to achieve a required quasi steady-state concentration for a given isotherm system. The generalised form of this ratio is illustrated in Eq. 7-4 and is designated as the permeant-area ratio (PAR) for future reference.

$$PAR = \left(\frac{P_{scfl}^{i} A_{scfl}}{L_{scfl}} \right) \Bigg/ \left(\frac{P_{pkfl}^{i} A_{pkfl}}{L_{pkfl}} \right) \qquad \textbf{(Eq. 7-4)}$$

where

P_{scfl}^{i} = Permeability to active agent *i* of sachet film material (mol·m·m^{-2}·s^{-1}·Pa^{-1})

P_{pkfl}^{i} = Permeability to active agent *i* of packaging film material (mol·m·m^{-2}·s^{-1}·Pa^{-1})

As reported in Chapter 4, permeabilities to hexanal vapour of the tested films are concentration dependent. It can be assumed that values of the permeabilities should be reasonably constant during the quasi steady-state period and hence for this period P_{scfl}^{i} and

P^i_{pkfl} in Eq. 7-4 can be assumed to be concentration independent. Figure 7-5A illustrates the plot of values of quasi steady-state concentrations (i.e. on day 7) against the PAR ratio (Eq. 7-4) predicted in the LD1 active MAP system (without tomatoes), for the different isotherms. Note that the release profile at PAR = 0.8 represent an extreme situation of very low permeability to hexanal vapour is shown in Figure 7-5B. Simulation inputs are those provided in Table 7-2. It should be noted that the same concentration (within acceptable rounding error) was predicted by the global mathematical model corresponding to the same ratio, regardless of which parameter in Eq. 7-4 was varied (data not shown). Because of this, only the value of P^i_{pkfl} was varied for consecutive simulations (Table 7-2), for constant values of the other parameters.

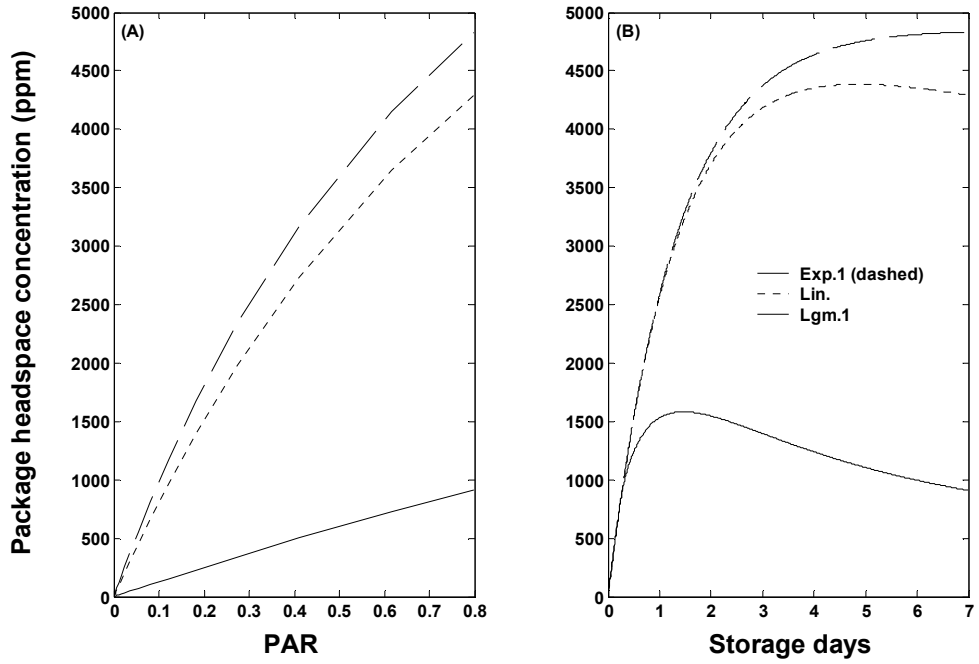

Figure 7-5 Simulation results demonstrating the influences of PAR values on package headspace quasi steady-state concentrations of hexanal vapour (on day 7; at 20ºC) in LD1 active MAP systems (without tomatoes) for Exponential (Exp.1) Linear (Lin.), and Langmuir (Lgm.1) isotherms (represented by dashed dotted and solid lines, respectively; refer to Table 7-1) (A) and release profiles considered at PAR = 0.8 (B).

Table 7-2 Model inputs for simulating the effects of PAR on quasi steady-state concentrations of LD1 active MAP systems (without tomatoes) for Exponential (Exp.1) Linear (Lin.), and Langmuir (Lgm.1) isotherms (Table 7-1)

Parameters of PAR	Values (units)
L_{scfl} and L_{pkfl}	30×10^{-6} m
A_{scfl} and A_{pkfl}	0.003 and 0.125 m^2, respectively
P^{i}_{scfl} [a]	1.90×10^{-14} mol·m·m^{-2}·s^{-1}·Pa^{-1}
P^{i}_{pkfl} [b]	Varying between 5.70×10^{-16} to 7.30×10^{-13} mol·m·m^{-2}·s^{-1}·Pa^{-1}

[a] this is the value of permeability to hexanal vapour of LDPE at 20ºC (quantified in the present work); no concentration dependence of the permeability was assumed.

[b] these values were generated from increasing and decreasing value of its original value (as equal to P^{i}_{scfl}) by a factor of 1.5 for different simulations.

Simulation results shown in Figure 7-5 confirm the important influences of active agent permeability across the outer packaging film on quasi steady-state concentration of vapour in the package headspace. As values of PAR increase (indicating a higher barrier to hexanal vapour of the outer packaging film or lower package to sachet surface area ratio), concentrations in the linear (Lin.) and exponential (Exp.1) isotherm systems are much higher than those predicted in the Langmuir (Lgm.1) system. Also note the exponential isotherm always yields slightly higher concentrations than the linear system at a given PAR.

Application of OPP films have been reported for bags or tray wrapping for a range of horticultural products such as endives (Charles et al. 2008), melon (Aguayo et al. 2003), table grapes (Artés-Hernández et al. 2006), and tomatoes (Gil et al. 2001; Maneerat & Hayata 2008). The average permeability of OPP to hexanal vapour at 20ºC is approximately 10^{-16} mol·m·m^{-2}·s^{-1}·Pa^{-1} which corresponds to a PAR value (estimated using data given in Table 7-2) of ~0.5-0.6. With an adsorption system exhibiting a Langmuir isotherm (solid line; Figure 7-5A), the quasi steady-state concentration should be approximately ~500-600 ppm and this is considerably higher than the predicted value with the LDPE outer film (~250 ppm at $PAR \approx 0.24$). When incorporating the apparent rate of hexanal uptake by tomatoes in the calculations, predicted concentrations in OPP in the bag are reduced markedly to ~220 ppm due to the high apparent rate of hexanal uptake by tomatoes under high hexanal concentrations (calculations not shown). Despite this, the concentration predicted on day 7 in the OPP bag is nearly 6-fold higher than the MIC level.

Based on the simulation results, it may be inferred that the required MIC level in the OPP bag could be achieved by using a lower sachet loading (1.5g was the loading used in scenario LD1; Table 6-1). The predicted headspace concentration for a reduced sachet loading of 0.5g (for the Langmuir isotherm system) is ~160 ppm (calculations not shown) and this is still sufficiently higher than the MIC level. Lowering the sachet loading can provide economical and environmental benefits because less hexanal mass would be utilised for saturating the silica gel and subsequently left on the adsorbent after the quasi steady-state condition was attained.

As mentioned earlier, when altering of components of the active MAP system one must also consider the impact of such changes on the MA conditions in the bag. Simulations of MA conditions for both LDPE and OPP bags are shown in Figure 7-6. It should be noted that the permeabilities to O_2 and CO_2 of OPP film used as model inputs are those for 35μm film measured at 15ºC, as reported by Rai & Paul (2007). Also, these simulations were performed based on the assumption that there are negligible adverse effects of hexanal on respiration rates or other physiological properties. Further studies may be required to investigate the influence of the hexanal concentration developed in an OPP bag on postharvest quality of tomatoes (if this was significantly higher than the MIC).

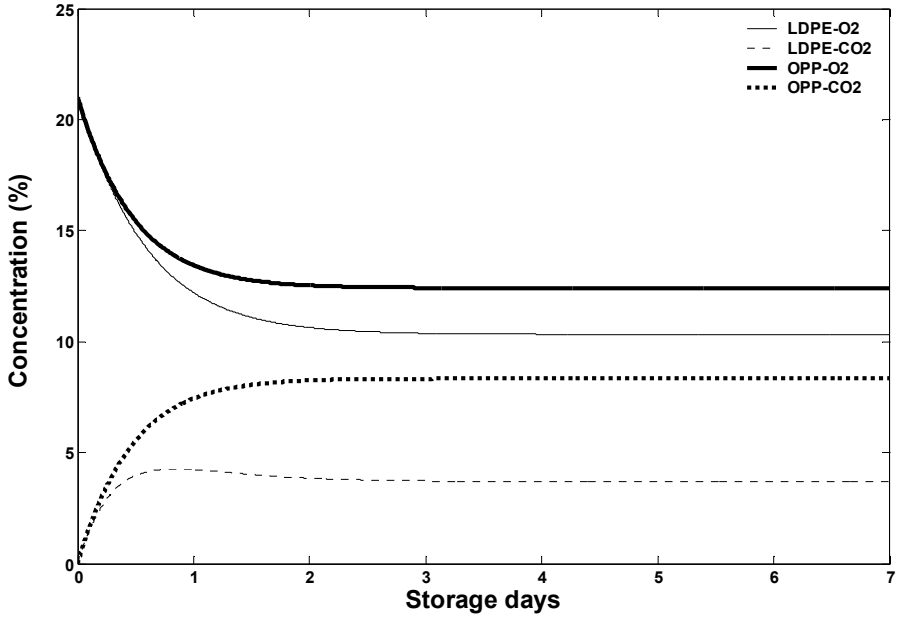

Figure 7-6 Mathematical model simulations of MA conditions at 20ºC in hexanal active MA package containing 6 medium tomatoes (~600g) having either LDPE or OPP films as outer packaging films. See text for conditions.

The simulated quasi steady-state concentration of O_2 in the OPP bag (~12.4%) is reasonably close to that predicted for LDPE (~10.3%). These results are sensible because of the similar O_2 permeability values of OPP and LDPE which are ~ 1.38×10^{-15} and 1.46×10^{-15} mol·m·m^{-2}·s^{-1}·Pa^{-1} respectively. In contrast, the predicted CO_2 concentration in the OPP bag is nearly 2-fold higher than that in LDPE bag and this is attributed to the ~3-fold lower permeability to CO_2 of OPP than that of LDPE. For some products these different gas compositions may be acceptable or beneficial, but for others a much high O_2 may not adequately reduce respiration while the higher CO_2 concentration can be detrimental so shelf life may not be prolonged as required.

Overall, those model predictions confirm the potentially significant influence of isotherm type on the pattern of release and accumulation of hexanal in the package headspace, depending on film permeability. The conceptualised release patterns illustrated in Figure 7-1 providing longer or shorter exposure periods to the active package and different peak concentrations can be achieved by utilising carriers yielding different isotherm forms, providing an outer packaging film with an appropriate permeability to the active vapour is selected. A long period of sustained release may satisfy the packaging requirements of

certain products, in which a high effective level of the active volatile is required to ensure maintenance of the targeted qualities. For this, the exponential isotherm is useful. In contrast the Langmuir isotherm is more suitable when an initial fumigation at high concentration is required for a short period, after which the concentration should decrease to a low effective level and be sustained at this level throughout the subsequent storage period. The generalised link between quasi steady-state concentration and PAR values developed in the headspace for active MAP systems having different isotherms (as shown Figure 7-5) could be used for preliminary design to achieve a desired active vapour MIC level.

7.3 Effects of isotherm shape on flux of hexanal across the sachet boundary

In this section, the objective was to further investigate the effects of isotherm shape on the flux of hexanal across the sachet boundary. As discussed in the previous section, isotherm shape significantly influences changes in the equilibrium vapour concentration in the sachet ($C_{g,bed}^{Hxl}$) which can consequently affect the concentration gradient between the sachet and the package headspace, and hence the flux across the sachet film.

7.3.1 Changes of flux as a function of isotherm shape

The steady-state flux across the sachet film boundary is simplified as shown in Eq. 7-5 if a constant permeability is assumed.

$$J_{scfl} = \frac{P_{scfl}^{Hxl} RT_{pkg}}{L_{scfl}} \left(C_{g,bed}^{Hxl} - C_{pkhs}^{Hxl} \right) \qquad \textbf{(Eq. 7-5)}$$

where

J_{scfl} = Steady-state flux at sachet boundary (mol·s^{-1}·m^{-2})

$C_{g,bed}^{Hxl}$ = Equilibrium hexanal vapour concentration above the carrier bed (mol·m^{-3})

C_{pkhs}^{Hxl} = Hexanal vapour concentration in package headspace (mol·m^{-3})

Assuming $C_{g,bed}^{Hxl} >> C_{pkhs}^{Hxl}$ (as is generally true in the concentration range of interest), Eq. 7-5 can be simplified to Eq. 7-6.

$$J_{scfl} = \frac{P_{scfl}^{Hxl} RT_{pkg}}{L_{scfl}} C_{g,bed}^{Hxl} \qquad \textbf{(Eq. 7-6)}$$

Because the $C_{g,bed}^{Hxl}$ value directly changes with the hexanal adsorbed amount ($C_{s,bed}^{Hxl}$) which dynamically decreases after the initial release, the $C_{g,bed}^{Hxl}$ term in Eq. 7-6 can thus be described as a function of $C_{s,bed}^{Hxl}$. The mathematical expression for this function for the exponential, linear and Langmuir isotherms are Eq. 7-2, Eq. 7-3 and Eq. 5-16, respectively. By substituting these into Eq. 7-6, the flux across the sachet boundary as a function of $C_{s,bed}^{Hxl}$ for individual isotherms can be expressed as Eq. 7-7 to Eq. 7-9 (note units of isotherm coefficients utilised in these equations are different from the same coefficients presented in section 7.2, for overall dimensional/unit consistency).

Exponential $$J_{scfl} = \frac{P_{scfl}^{Hxl} RT_{pkg}}{L_{scfl}} \cdot ln\left(\frac{\left(C_{s,bed}^{Hxl} + a_{exp}^{Hxl} \right)}{a_{exp}^{Hxl}} \right) \cdot b_{exp}^{Hxl} \quad \textbf{(Eq. 7-7)}$$

Linear $$J_{scfl} = \frac{P_{scfl}^{Hxl} RT_{pkg}}{L_{scfl}} \cdot \frac{C_{s,bed}^{Hxl}}{K_{Lin}^{Hxl}} \quad \textbf{(Eq. 7-8)}$$

Langmuir $$J_{scfl} = \frac{P_{scfl}^{Hxl} RT_{pkg}}{L_{scfl}} \cdot \frac{C_{s,bed}^{Hxl}}{b_{Lgm}^{Hxl} \cdot \left(C_{s,max}^{Hxl} - C_{s,bed}^{Hxl} \right)} \quad \textbf{(Eq. 7-9)}$$

where

$C_{s,bed}^{Hxl}$ = Equilibrium adsorbed amount of hexanal on the carrier bed (mol·g^{-1})

a_{exp}^{Hxl} = Coefficient of hexanal exponential isotherm equation (mol·g^{-1})

b_{exp}^{Hxl} = Coefficient of hexanal exponential isotherm equation (mol·m^{-3})

K_{Lin}^{Hxl} = Coefficient of hexanal linear isotherm equation (m^3·g^{-1})

$C_{s,max}^{Hxl}$ = Maximum amount of hexanal adsorbed on the carrier estimated by the Langmuir sorption isotherm (mol·g^{-1})

Figure 7-7 illustrates the effects of the isotherm models on the fluxes across the sachet boundary, for the simulation inputs given in Table 7-1 and Table 7-2. For the Langmuir isotherm (Lgm.1), the flux rapidly decreases even though the amount of hexanal on the carrier phase ($C_{s,bed}^{Hxl}$) only slightly decreases from its maximum, due to the exponential portion of the isotherm (Figure 7-2). Such a pattern of sachet flux underlies the dramatic decrease of the sachet and package headspace concentrations after the initial release (e.g. Figure 7-4E and most of the results reported in Chapter 6).

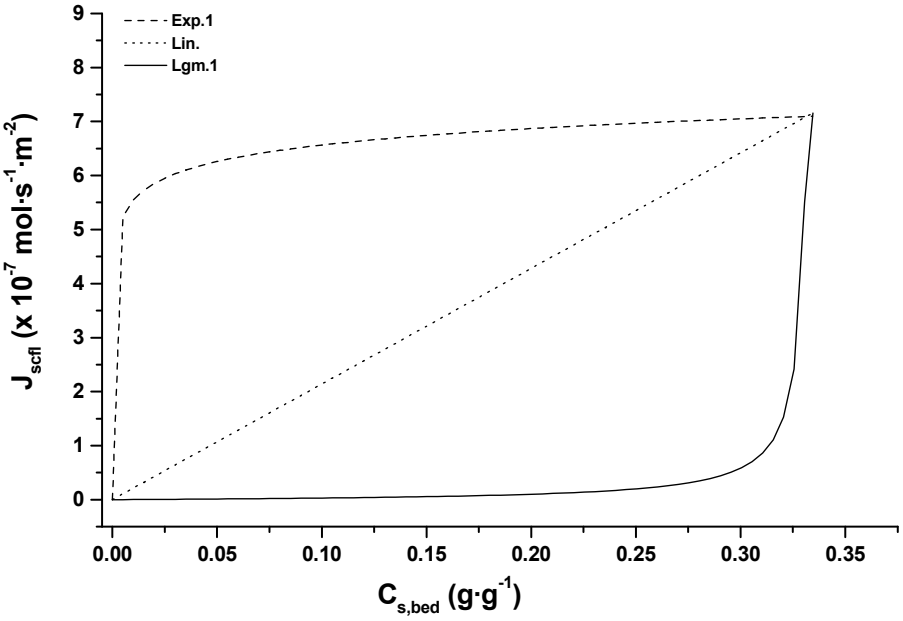

Figure 7-7 Simulated fluxes across the sachet boundary as a function of $C_{s,bed}^{Hxl}$, according to selected Exponential (Exp.1), Linear (Lin.) and Langmuir (Lgm.1) isotherm models (represented by dashed dotted and solid lines, respectively; refer to Table 7-1).

The flux pattern for the exponential isotherm system can be considered a reverse of that observed for the Langmuir isotherm system. The flux is insensitive to $C_{s,bed}^{Hxl}$ over a large $C_{s,bed}^{Hxl}$ range and this provides the sustained period of high gas phase concentrations after the initial release. Only when the $C_{s,bed}^{Hxl}$ value decreases by more than 97% (i.e. reaching ~0.01×10^{-2} mol·g^{-1}) of its initial value (0.34×10^{-2} mol·g^{-1}), does the flux drop rapidly toward zero, and the concentration in the package headspace then follows (as shown in Figure 7-4A). For the linear sorption isotherm, the flux has a linear relationship with the $C_{s,bed}^{Hxl}$ value. This pattern in turn yields a gradual decrease of headspace concentration after the initial release (Figure 7-4C).

7.3.2 Changes of flux as a function of time with regard to sorption isotherm shapes

In this section, the changes of flux as a function of time are demonstrated for different isotherm shapes. The ordinary differential equations (ODEs) describing the rate of changes

of $C_{s,bed}^{Hxl}$ as a function of time are found in Chapter 5 Eq. 5-17. By utilising the simplifications as stated in the previous section, Eq. 5-17 leads to Eq. 7-10.

$$M_{bed}\frac{\partial C_{s,bed}^{Hxl}}{\partial t} = -\frac{P_{scfl}^{Hxl} A_{scfl} RT_{pkg}}{L_{scfl}} C_{g,bed}^{Hxl} \qquad \textbf{(Eq. 7-10)}$$

Also, by describing $C_{g,bed}^{Hxl}$ as a function of $C_{s,bed}^{Hxl}$ according to the exponential, linear and Langmuir isotherms, Eq. 7-10 gives Eq. 7-11 to Eq. 7-13 (note units of isotherm coefficients utilised in these equations are same as those presented in section 7.3.1).

Exponential
$$M_{bed}\frac{\partial C_{s,bed}^{Hxl}}{\partial t} = -\frac{P_{scfl}^{Hxl} A_{scfl} RT_{pkg}}{L_{scfl}} \cdot ln\left(\frac{\left(C_{s,bed}^{Hxl} + a_{exp}^{Hxl}\right)}{a_{exp}^{Hxl}}\right) \cdot b_{exp}^{Hxl} \qquad \textbf{(Eq. 7-11)}$$

Linear
$$M_{bed}\frac{\partial C_{s,bed}^{Hxl}}{\partial t} = -\frac{P_{scfl}^{Hxl} A_{scfl} RT_{pkg}}{L_{scfl}} \cdot \frac{C_{s,bed}^{Hxl}}{K_{Lin}^{Hxl}} \qquad \textbf{(Eq. 7-12)}$$

Langmuir
$$M_{bed}\frac{\partial C_{s,bed}^{Hxl}}{\partial t} = -\frac{P_{scfl}^{Hxl} A_{scfl} RT_{pkg}}{L_{scfl}} \cdot \frac{C_{s,bed}^{Hxl}}{b_{Lgm}^{Hxl} \cdot \left(C_{s,max}^{Hxl} - C_{s,bed}^{Hxl}\right)} \qquad \textbf{(Eq. 7-13)}$$

By separating variables and integrating, the ODEs can be solved analytically and $C_{s,bed}^{Hxl}$ as a function of time (for each isotherm) is predicted by Eq. 7-14 to Eq. 7-16, respectively.

Exponential
$$li\left(\frac{a_{exp}^{Hxl} + C_{s,bed}^{Hxl}}{a_{exp}^{Hxl}}\right) = li\left(\frac{a_{exp}^{Hxl} + C_{s,bed,i}^{Hxl}}{a_{exp}^{Hxl}}\right) - \frac{P_{scfl}^{Hxl} A_{scfl} RT_{pkg} b_{exp}^{Hxl} t}{L_{scfl} M_{bed} a_{exp}^{Hxl}} \qquad \textbf{(Eq. 7-14)}$$

Linear
$$C_{s,bed}^{Hxl} = C_{s,bed,i}^{Hxl} \, exp\left(\frac{-P_{scfl}^{Hxl} A_{scfl} RT_{pkg} t}{L_{scfl} K_{Lin}^{Hxl} M_{bed}}\right) \qquad \textbf{(Eq. 7-15)}$$

Langmuir
$$C_{s,bed}^{Hxl} = C_{s,max}^{Hxl} \, ln\left(\frac{C_{s,bed}^{Hxl}}{C_{s,bed,i}^{Hxl}}\right) + \frac{P_{scfl}^{Hxl} A_{scfl} RT_{pkg} t}{L_{scfl} M_{bed} b_{Lgm}^{Hxl}} + C_{s,bed,i}^{Hxl} \qquad \textbf{(Eq. 7-16)}$$

where

$C_{s,bed,i}^{Hxl}$ = Initial hexanal adsorbed amount of the carrier bed (mol·g^{-1})

t = Time (s)

li = Log integral function

Only Eq. 7-15 has an explicit solution however solutions of both Eq. 7-14 and Eq. 7-16 can be found iteratively using the solvers in MATLAB® or Microsoft Excel. To solve Eq. 7-14, the '*Log integral function* (li)' is also required. The solved $C_{s,bed}^{Hxl}$ values of all isotherms can be substituted into Eq. 7-7 to Eq. 7-9 for calculating the steady-state fluxes across the sachet boundary (for the simulation inputs provided in Table 7-2) and these are plotted against time in Figure 7-8.

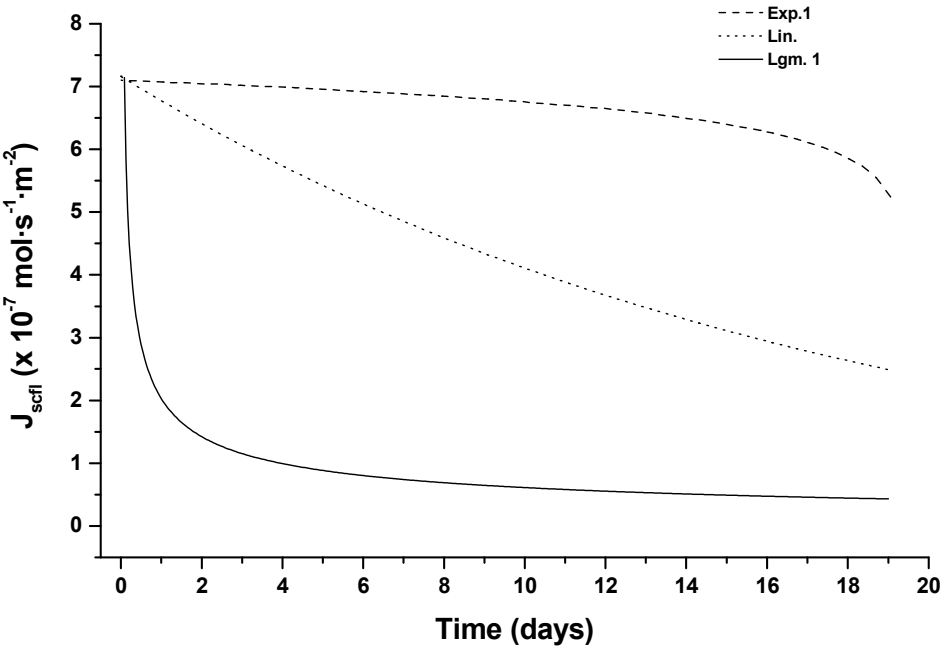

Figure 7-8 Simulated fluxes across the sachet boundary for the exponential (Exp.1), linear (Lin.) and Langmuir (Lgm.1) sorption isotherms, respectively. The coefficients of the isotherm models are those shown in Table 7-1.

The patterns of change in the sachet fluxes are similar to those observed when the fluxes were described quantitatively as a function of the isotherms (Figure 7-7). As then, the slowest change of flux occurs in the exponential isotherm system and the obvious decrease of flux near the end of storage corresponds to very low values of both $C_{s,bed}^{Hxl}$ and $C_{g,bed}^{Hxl}$. Given the saturated concentration in the sachet headspace and the MIC level in the package headspace, the estimated flux across the sachet film is ~ 7.07×10^{-7} mol·s^{-1}·m^{-2} (refer to inputs provided in Table 7-2) and this is similar to that illustrated in Figure 7-8, at $t = 0$. The exponential isotherm system thus can be considered suitable for active MA package in which the headspace concentration is required to be maintained at the MIC after the initial

release (i.e. without fumigation) providing the permeability of the outer bag film is appropriately chosen. Because a significant change in $C_{g,bed}^{Hxl}$ values requires a large extent of change in $C_{s,bed}^{Hxl}$ for the exponential isotherm (Figure 7-2), the length of time at the sustained flux (and concentration in the headspace) will depend on mass of silica gel employed.

For other sorption isotherm systems, the highest initial change in flux is observed for the Langmuir isotherm system but after the flux rapidly drops it then stabilises through the remainder of the simulated storage period (Figure 7-8). A gradual and (near) linear change is evident in the system having the linear isotherm (Figure 7-8). It can be inferred from further model simulations that the flux of linear system would reach the sustained level of the Langmuir isotherm system (i.e. ~0.5×10^{-7} mol·s^{-1}·m^{-2}) by day 47.

7.4 Conceptual designs of ethanol vapour active MAP systems

As mentioned in Chapter 2, ethanol vapour controlled release systems (such as Ethicap® and Antimold Mild®; Freundlich Co. Ltd., Japan) have been extensively used to control outgrowth of microorganisms in bakery products and table grapes. Ethanol has the benefit of minimising undesirable skin bleaching which can be caused by exposing grapes to SO_2, the traditional antimicrobial vapour used with grapes. Furthermore, studies report ethanol vapour can delay senescence of horticultural products such as tomatoes (Saltveit & Sharaf 1992; Beaulieu & Saltveit 1997), broccoli (Suzuki et al. 2004), and fresh sliced apples (Bai et al. 2004). Other than the commercial system, controlled release of ethanol vapour is most commonly done using saturated filter papers (see Chapter 2). To further illustrate the utility of the models developed in this thesis, it is interesting to examine the ethanol release patterns based on sorption isotherms selected from literature.

The selected ethanol adsorption isotherms (again assuming negligible hysteresis) for different adsorbents in a range of 25 to 30ºC are shown in Figure 7-9. For a physical system based on the LD1 scenario previously discussed (Table 6-1) (with an appropriated ethanol permeability of outer packaging film) and given minimal ethanol uptake by grapes, moderately sustained releases of ethanol vapour prior the concentration approaching zero would be expected from both activated carbon and silica gel systems (i.e.; Figure 7-9A and

B). For achieving relatively long-term high concentration prior to a rapid drop, amorphous Teflon (or similar) (Figure 7-9C) would be chosen as the carrier for ethanol vapour.

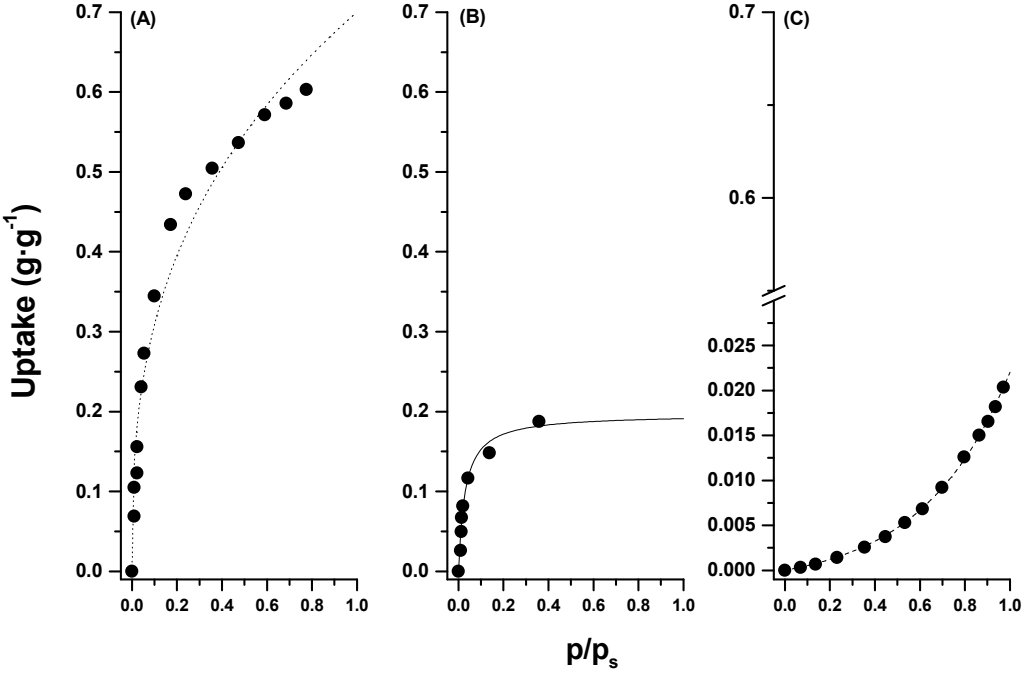

Figure 7-9 Ethanol sorption isotherms for Ajax activated carbon at 25ºC (Prasetyo et al. 2002) (A), silica gel at 25ºC (Madeley & Sing 1959) (B), and Amorphous Teflon AF2400 at 30ºC (Tokarev et al. 2006) (C). All isotherm data were digitally redrawn using the TechDig software. Dotted, solid and dashed lines represent ethanol equilibrium sorptions predicted by the Freundlich (Eq. 2-4), Langmuir (Eq. 2-3) and exponential (Eq. 7-3) models, respectively.

Isotherm models utilised to describe ethanol equilibrium sorption for activated carbon, silica gel and Teflon were the Freundlich (Eq. 2-4; a common isotherm for describing sorption on activated carbon as discussed in section 2.4), Langmuir (Eq. 2-3; also see discussion made in section 4.3.4) and, exponential (Eq. 7-3), respectively. The models were fitted to the literature data sets by nonlinear regression (Origin 5.0, Microcal Software Inc., US) as illustrated in Figure 7-9. Estimated isotherm coefficients are provided in Table 7-3 and these were later used as model inputs for simulations of release dynamics and PAR estimations (similar to those demonstrated in section 7.2).

Table 7-3 Parameters of the Freundlich, and exponential model equations estimated using nonlinear regression for literature data on ethanol sorption for activated carbon and Teflon.

Isotherms	Coefficients		
Freundlich [a]	K_{Frd}	=	0.70 (3.74) [b]
	n_{Frd}	=	0.36 (7.36)
Langmuir [c]	$C_{s\,max}$	=	0.19 (7.7)
	b_{Lgm}	=	34.41 (25.1)
Exponential [d]	a_{exp}	=	0.002 (3.89)
	b_{exp}	=	0.37 (1.56)

[a] Units of K_{Frd} and n_{Frd} are $g \cdot g^{-1}((p_s/p)^{nFrd})$ and dimensionless, respectively.

[b] Values in parentheses are standard errors (SE) expressed as a percentage of the estimated values.

[c] Units of the Langmuir model are as those shown in Table 4-9.

[d] Units of the exponential model are as those shown in Eq. 7-1.

Figure 7-10 illustrates ethanol vapour release patterns in the headspace of active MA packages containing grapes as reported by Lurie et al. (2006) and a summary of the package is provided as follow:

- Ethanol vapour was released from liquid ethanol saturated papers (two loadings 4 ml_{EtOH}/kg_{fruit} and 8 ml_{EtOH}/kg_{fruit}, respectively), were examined into the package headspace above 5 kg 'Thompson Seedless' grapes contained in a plastic box (30 cm wide × 40 cm long × 20 cm height).
- The box was additionally covered by the plastic liner (GR-4, Xtend®, Stepac Ltd. Tefen, Israel; a secondary package) and sealed by the rubber band (24 h after the beginning of cold storage) for generating a modified atmosphere condition.
- The active packaging system was kept at 0°C for ~58 days.

Lurie et al. (2006) reported high ethanol concentrations after the initial release (~1200-1300 ppm reported on day 4 for both ethanol loadings; no data was reported on day 1 to 3), however these continuously declined to attain their quasi steady-state concentrations within ~20 days (Figure 7-10). The active paper with 8 ml_{EtOH}/kg_{fruit} loading ratio could apparently generate higher quasi steady-state concentration (~100-110 ppm) than the lower loading treatment could (~50-70 ppm) (Figure 7-9). The release pattern reported by Lurie et al. (2006) is similar to that observed for hexanal release from silica gel (refer to Chapter

6) suggesting Type I equilibrium desorption of ethanol from the paper. This pattern has also been found for other VOCs including acetophenone, naphthalene, benzophenone, dibutyl phthalate (DBP) and methyl stearate, for corrugated liners and paperboards (containing either virgin or recycled paper pulps) at 70 and 100ºC (Triantafyllou et al. 2005). To date, there is no report on the ethanol sorption isotherm for paper, nor on the ethanol permeability of Xtend® plastic liner.

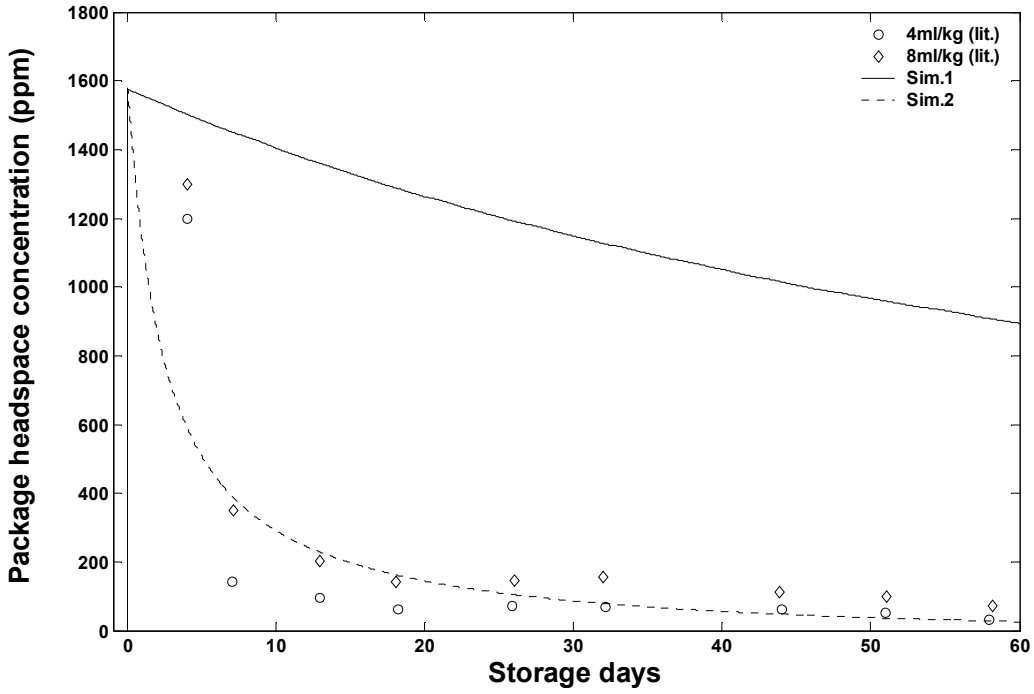

Figure 7-10 Ethanol vapour concentrations released from 4 ml_{EtOH}/kg_{fruit} (o) and 8 ml_{EtOH}/kg_{fruit} (◊) loading ratios of liquid ethanol saturated paper as reported by Lurie et al. (2006) and data were digitally redrawn using the TechDig software. Solid and dotted lines represent model predictions of the Langmuir ethanol sorption isotherm for silica gel, provided model in puts in Table 7-4. See text for simulation conditions (for Sim.1 and Sim.2).

It is interesting to try to predict the ethanol vapour release pattern in the headspace of package using the mathematical model developed in Chapter 6 based on the Langmuir ethanol vapour sorption isotherm for silica gel (Table 7-3) and a package having a physical dimension as reported by Lurie et al. (2006). The model inputs for these simulations were selected appropriately and shown in Table 7-4; interactions between grapes and ethanol vapour were assumed negligible. These simulated results are also illustrated in Figure 7-10.

Table 7-4 Key model inputs used for simulations of ethanol vapour releases

Model inputs	Units	Values
P^i_{scfl} and P^i_{pkfl} [a]	$mol \cdot m \cdot m^{-2} \cdot s^{-1} \cdot Pa^{-1}$	1.14×10^{-4} and 1.14×10^{-16}, respectively
L_{scfl} and L_{pkfl}	m	30×10^{-6}
A_{scfl}	m^2	0.003
A_{pkfl}	m^2	0.52 [b]
V_{pkg}	m^3	0.02 [c]
T_{pkg}	ºC	25
M_{bed}	g	1.5
Langmuir isotherm coefficients [d]	-	-

[a] Ethanol permeability of sachet film (P^i_{scfl}) was arbitrarily assumed to be relatively high to represent the ethanol vapour release from the paper (i.e. no barrier) while the permeability of the packaging film (P^i_{pkfl}) is that of LDPE film at 25ºC reported by Pauly (1999). Also permeability was assumed to be concentration independent.

[b] Plastic liner (Xtend® film reported by Lurie et al. 2006) was assumed tightly covering a plastic box (like shrink wrap configuration) containing a release sachet and grapes, thus an outer film surface area was presumably equal to that of a box.

[c] Package headspace or free volume was calculated as the difference between the volume of the box and that of the grape cluster. The grape volume was estimated from the 5 kg mass reported Lurie (2006) using an average density of 'Kyoho' grape cluster (~1100 $kg \cdot m^{-3}$) reported by Sugiura et al. (2001).

[d] Referred to those reported in Table 7-3.

The predicted ethanol vapour concentrations exhibit the release pattern governed by the Langmuir isotherm (Figure 7-10) but the headspace concentration after the initial release appear to be much higher than those reported by Lurie et al. (2006) (solid line or Sim.1; Figure 7-10) suggesting important differences of permeability to ethanol vapour (P^i_{pkfl}) of Xtend® liner (Lurie et al. 2006) and LDPE film (Pauly 1999). The latter appears to provide a higher barrier to ethanol vapour. It can be inferred from the simulation results that the lower headspace concentrations obtained could be experimentally achieved by increasing the P^i_{pkfl} value to reduce accumulation of ethanol vapour in the package headspace. To examine this, the original value as provided in Table 7-4 was arbitrarily increased by ~30-fold (i.e. becoming 3.42×10^{-15} $mol \cdot m \cdot m^{-2} \cdot s^{-1} \cdot Pa^{-1}$) and the resulting model prediction is represented by the dotted line (Sim.2; Figure 7-10). The simulated release pattern and quasi steady-state concentrations were greatly improved and comparable to those reported by Lurie et al. (2006) (Figure 7-10). Such simulation results confirm the importance of appropriated selections of outer film permeability, in addition to the isotherm forms, for

achieving the required release pattern. Further information on film permeabilities to ethanol vapour (under a range of vapour concentrations and concentration gradients) and sorption isotherms (e.g. of paper material and other adsorbents) is required, to further validate the model to permit accurate design of ethanol release active MA package.

By using a similar approach as demonstrated in section 7.2, the generalised influences of PAR values on quasi steady-state concentrations of ethanol vapour can be developed and these are illustrated in Figure 7-11. Note, for estimating PAR, the permeability of sachet film (P^i_{scfl}) was fixed at 1.14×10^{-16} mol·m·m^{-2}·s^{-1}·Pa^{-1} (Table 7-4) while that of outer bag film(P^i_{pkfl}) was varied by a factor of 2 from its original value (as shown in Table 7-4) between 3.58×10^{-18} to 3.66×10^{-15} mol·m·m^{-2}·s^{-1}·Pa^{-1} for different simulations. The thickness and areas of both sachet and packaging films were the same as those provided in Table 7-2.

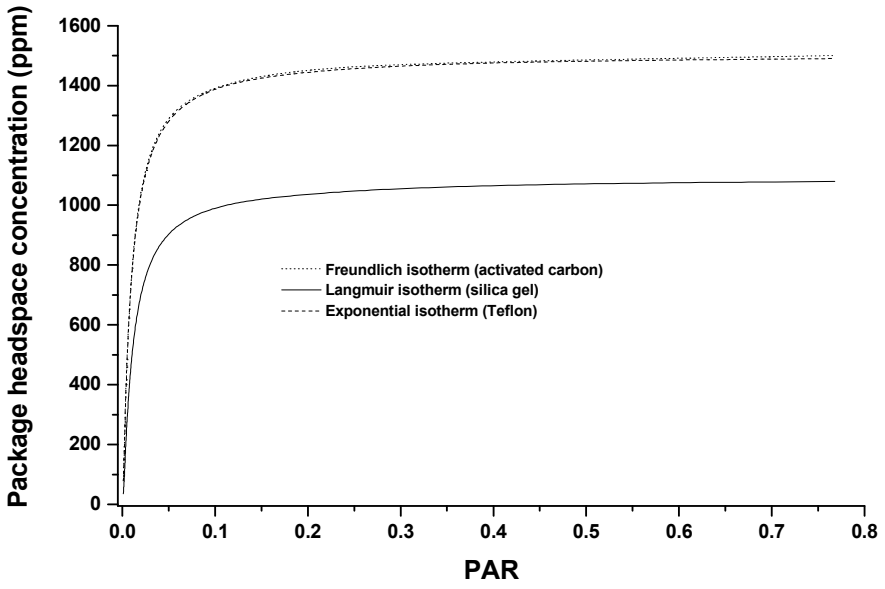

Figure 7-11 Simulated results of influences of PAR values on package headspace quasi steady-state concentrations of ethanol vapour (on day 7) in LD1 active MAP systems having different sorption isotherms which are Freundlich, Langmuir and exponential isotherms for activated carbon (A), silica gel (B) and Teflon (C) systems, respectively.

For a given PAR value, the model predicts high and similar ethanol vapour concentrations for activated carbon and Teflon, while low concentrations are predicted in the silica gel

systems (Figure 7-11). These results appear to be sensible and can be explained by the extents of change of sachet headspace concentration after initial release in respect to isotherm forms, as discussed above. It should be noted that the controlled release of ethanol vapour from the activated carbon however may have to be carefully designed because ethanol vapour (and other organic vapours such as 1-MCP as reported by Lee 2003) has a strong affinity with activated carbon adsorbents (Thomas & Crittenden 1998a). Furthermore the patterns observed in Figure 7-11 were different from those illustrated in Figure 7-5. In this case, the ethanol vapour quasi steady-state concentration reaches its maximum value and levels off when PAR value $\geq \sim 0.1$. This pattern is attributed to the low permeability to ethanol vapour in both the sachet and outer packaging film (noted above). These film properties can contribute to low rates of both ethanol vapour release from the sachet and permeation through the packaging film.

7.5 Summary

The global mathematical model developed in the present work can be implemented to predict sensible hexanal release patterns for different active packaging systems where the sorption isotherm is the key variable. The mathematical equations formulated in the model can be adjusted to suit particular scenarios for gaining insights into the steady-state fluxes across the sachet boundary, which significantly influence the vapour release into the package headspace. Overall, this chapter illustrates the applications of the mathematical model and confirms its generality and potential to be utilised as a tool to mechanistically understand key mass transfer processes and design active packaging systems with an emphasis on the controlled release of volatile active agents for assuring the quality of horticultural and other food products.

Chapter 8

GENERAL DISCUSSION AND CONCLUSIONS

8.1 General discussion

The first step in the development of mathematical models for the design and analysis of simple active packaging systems have recently appeared in the literature. Unsteady-state mass balances for describing oxygen concentrations in oxygen scavenging active MA packages for tomatoes and endives was reported by Charles et al. (2003) and Charles et al. (2008), respectively. Models are important tools that can be used to identify key aspects for the design of active packaging systems for horticultural products, such as identifying ideal properties of active agents with respect to interactive control of postharvest qualities, and the requirements of sorption isotherms of porous adsorbents and film permeability. However the development of generalised models for the controlled release of volatiles into a packaging headspace to inhibit spoilage or modify the physiological response of the product have not so far been reported. This work set out to develop such models, to provide clear guidelines on how such models of active MAP systems should be constructed, and demonstrate their potential uses.

The work was based on a model active packaging system of hexanal vapour released from a sachet (with silica gel adsorbent as the carrier) to inhibit growth of *Botrytis cinerea* (the postharvest pathogen) on tomatoes, during storage under a MA generated using a LDPE bag.

The antifungal activity of hexanal vapour to suppress *in vivo* growth of *B. cinerea* on tomatoes under ambient atmosphere and extreme storage condition (20ºC; ~99% RH) was demonstrated. Good results were achieved by continuous exposure of tomatoes to ~40-270 ppm hexanal vapour concentration. These findings are consistent with previous reports on the antimicrobial properties of hexanal vapour on postharvest pathogens (e.g. Song et al. 1996; Archbold et al. 1997; Fan et al. 2006; Song et al. 2007). The minimum inhibition concentration (MIC) was chosen from the effective concentration range as ~40-70 ppm and this was assigned as the target for the sustained concentration to be achieved in active MAP designs.

Although there is much evidence of the antifungal role of hexanal vapour, there was no information on its influence on postharvest quality. This work has shown that continuous exposure of intact light red tomatoes to MIC hexanal vapour for 7 days under ambient conditions significantly stimulated the respiration rate and delayed skin reddening, while changes in other quality parameters (i.e. firmness, mass loss and ethylene generation rate) were not apparent. Under MA conditions (i.e.~10% O_2 and ~5% CO_2) such effects of hexanal were minimal. However for both cases, there was apparent uptake of hexanal by the tomatoes as evidenced by changes to the headspace hexanal concentration.

The presence of hexanal vapour was found not to significantly influence the steady-state MA condition in LDPE bag as similar levels of O_2 and CO_2 in packages were found, with or without hexanal vapour present. This finding is consistent with literature reports on other active MAP systems utilising volatile active agents, such as the essential oils eugenol, thymol, and menthol. These results further suggested that there was minimal influence of hexanal vapour on the film permeability to O_2 and CO_2. As such, existing models for passive MAP systems could be used to predict changes to O_2 and CO_2 in the active MA package. This confirmed that it is possible to combine the benefits of applying passive MAP systems (e.g. minimising respiration rates) with active controls of postharvest quality to extend shelf life.

The apparent rate of hexanal uptake by tomatoes emphasised the influence of horticultural products on the rate and extent of build up of the active agent in the package headspace. It also provided insights to key mechanisms limiting hexanal uptake by tomatoes. It is likely that the apparent rate of uptake is limited by mass transport (i.e. sorption and diffusion processes) across the tomato cuticle, rather than reaction rate, because the apparent uptake rate was higher at lower temperature (10°C). This observation mimics the so-called sorption-dominated permeation of VOCs across polymer films, which is well documented in the literature and experimentally quantified in the hexanal permeability data for LDPE, Tyvek®, and OPP films quantified in this work. Further studies on mass transport across the cuticle should provide insights on how the cuticle limits the penetration of active agents, (e.g. the extent of plasticisation that may occur due to sorption of hexanal and other volatile active agents to the cuticle).

There were no previous data reported in the literature on the hexanal permeability of Tyvek® and OPP films. These were therefore measured in the present research along with that of LDPE. The Tyvek® material provided the fastest rate of hexanal release from the sachet due to its high porosity; while the OPP film could be selected for sachet materials to achieve very slow release rates, principally because of the high crystallinity of the polymer structure providing a good barrier to hexanal permeation. From literature, metallocene catalyst-based polyethylene film (commercially traded under Exact™ 4151; reported by Wolford 1998) and EVOH film (Johansson & Leufven 1994) were reported to have excellent barrier properties to hexanal vapour and these could be utilised as possible alternative sachet materials to OPP for achieving slow release. In particular EVOH, which is a hydrophilic film and its permeability to hexanal vapour reportedly increased with RH level (see Johansson & Leufven 1994), could also be useful for a sachet to be utilised in high RH environments (as in MA package of horticultural products) because the high RH could promote hexanal permeation through the EVOH film. This may assist control of microbial proliferations when the RH conditions favour mould growth. In contrast to Tyvek® and OPP films, LDPE film permeability to the hexanal vapour was reported in the literature. The magnitude of LDPE permeability quantified in the present research was reasonably consistent with this data, given comparable hexanal concentrations and ambient conditions. This finding indicated that the experimental methodology used yielded reliable data.

Significant dependence on temperature and concentration of hexanal permeability of Tyvek®, OPP and LDPE was observed, as expected for volatile permeation through polymer films. Relationships between hexanal vapour concentration and permeability were well described by the exponential growth model and this information, which has not previously been reported in the literature, was critical for modelling these active packaging systems. This is because the films are subjected to a wide range of hexanal concentrations, from the very high initial concentration at the sachet boundary observed immediately after placing the sachet in the MA bag, through varying concentrations in the package headspace to the relatively low and sustained quasi steady-state concentration levels. High variation was however observed in the estimated coefficients of the model obtained from nonlinear regression, especially in the LDPE film systems. This finding is in agreement with the principles of VOC permeation through polymer films, where complex mass transport mechanisms and polymer structure arrangement are likely due to the concentration

dependence of solubility and diffusivity, and in turn contribute to high variation in measured permeability.

Hexanal sorption isotherms for silica gel adsorbents showed the Type I isotherm pattern as expected for the adsorption of volatiles on a microporous adsorbent where pore diameters are about or no more than a few molecular diameters of the adsorbate. Hexanal sorption isotherms were also reasonably well described by the Langmuir sorption equation and this could indicate that adsorbed hexanal molecules on silica gel surfaces principally arrange in a monolayer due to the limits of pore size. The estimated values of b_{Lgm}^{Hxl} obtained from the nonlinear regression were highly dependent on temperature (b_{Lgm}^{Hxl} at 10ºC was significantly higher than that at 20ºC) and contained significant levels of uncertainty. These were in contrast to estimated results for $C_{s,max}^{Hxl}$. Evidence from experiments using both gravimetric and volumetric methods suggested that the highest changes in sorption extent occurred at low vapour phase concentrations. Small errors in measurements in this region could yield high errors in b_{Lgm}^{Hxl} which represented the affinity between the adsorbate and the adsorbent. In contrast, variation in estimates for $C_{s,max}^{Hxl}$ was small because the assumed monolayer formation resulted in the maximum adsorption value minimally sensitive to hexanal vapour concentrations. The calculated thermodynamic parameters, including free energy, apparent enthalpy and entropy using b_{Lgm}^{Hxl} values, confirmed the exothermic nature of hexanal sorption on silica gels at 10ºC and 20ºC. The calculated apparent enthalpy in particular indicated that hexanal sorption on silica gels was a physical adsorption, where desorption of physically adsorbed molecules became more likely under stimulated conditions such as high concentration gradients or heat. Hexanal molecules are released as the temperature increases (due to the lower adsorption capacity) and this should provide a quick response of the controlled release system when the higher temperature storage regime may enhance proliferation of postharvest pathogens.

The sorption of hexanal on silica gel in the presence of water vapour gave variable results suggesting that multicomponent sorption is complex. Other literature have also reported complex trends arising from pre-adsorption of water vapour in the case of methane sorptions on activated carbon (Zhou et al. 2002) and silica gel (Zhou et al. 2006). The utilisation of sachets with polymeric film of relatively low water vapour permeability such as LDPE and OPP should result in only minimal influence of water vapour on the hexanal

desorption from the silica gel in these active MAP systems. In the case of sachets constructed of Tyvek®, there could potentially be high rates of water vapour transport into the sachet. The experimentally observed initial release peak from the Tyvek® system was higher than the model prediction, a trend opposite to those observed for both the OPP and LDPE systems. These results might be due to uptake of water vapour by silica gel if this caused displacement of adsorbed hexanal molecules, so leading to increasing hexanal concentration in sachet headspace and in turn greater concentration gradients across the sachet film. In contrast, the influence of RH on hexanal release appeared to be insignificant during the quasi steady-state period (even though the RH in the package headspace with tomatoes was >95%).

Two alternative methods of sorption isotherm measurement, inverse gas chromatography (IGC) and the volumetric technique, were attempted to compare with the gravimetric method results. The gravimetric method provided results in good agreement with the literature when it was used to quantify sorption of ethanol and acetaldehyde on silica gel. For both the IGC and volumetric techniques it appeared that the exposure time of the hexanal vapour to silica gel was not sufficiently long to allow full penetration of the hexanal molecules to reach all available sites of the microporous adsorbent. This contributed to incompletely developed equilibrium conditions. Given such limits, the gravimetric method was considered a more practical method for quantifying sorption isotherms for the silica gel and potentially for other microporous adsorbents. The IGC and volumetric techniques may be more suitable for systems having fast development of equilibrium conditions, (e.g. adsorption on wide pore adsorbents or nonporous solids). These studies of isotherm measurements highlighted the importance of method selection on the validity of sorption isotherm data. Isotherm data obtained from one measurement must be verified by correlations with literature data or by comparison with data obtained from alternative methods.

The proposed generalised modelling methodology and the decision tree developed in this work allow further exploration of key mass transfer processes for active MA packages incorporating a volatile controlled release sachet. A model was developed to demonstrate this process for the example system of an active MA package of tomatoes with hexanal release from silica gel in order to sustain the concentration at effective levels in the package headspace during the storage period. The criteria provided with the decision tree

can be employed for appropriate simplification of the processes, thereby minimising complexity in the formulation of mathematical models. The models were numerically solved using MATLAB® and the solution checked to ensure no coding or numerical errors.

Hexanal mass transfer phenomena were successfully simulated using the global mathematical model for a range of example active MA packages for tomatoes and storage temperature regimes. These simulations were carried out using the hexanal mass transport properties collected in the early parts of the research work. Both experimental and model predictions showed rapid decreases of the hexanal concentration after the initial release in all model packaging systems, owing to a small decrease of the adsorbed amount causing a significant reduction in the equilibrium vapour concentration above the carrier. This finding confirmed the significant influence of the isotherm shape on the release profile.

The model predictions and experimental measurements for the package headspace concentrations showed reasonably good agreement, particularly during the quasi steady-state region after the initial release peak. The quasi steady-state concentrations were generally in the MIC level and found to be sustained at this level during the storage period evaluated (7 days) but would also be expected to be maintained for longer storage. These results suggested the potential of further developing the example active packages for practical applications in the horticultural industry. The mathematical models developed for active substance release could be combined with further models relating antimicrobial efficacy as a function of vapour concentration (or partial pressure). An example of such models is the Gompertz equation, which is reportedly able to reasonably predict experimental results for a range of active agent-pathogen systems including hexanal and *Aspergillus niger* (Gardini et al. 1997), trans-2-hexenal and *Aspergillus flavus* (Gardini et al. 2001), and thymol and *Bacillus cereus*, *Candida lusitaniae*, *Streptococcus thermophilus* and *Pseudomonas spp.* (Del Nobile et al. 2008).

The model predictions provide insights to the key factors governing accumulation of hexanal in the package. The sorption isotherm and volatile compound permeability were shown to have great influence throughout the course of the release profile. Hexanal uptake by tomatoes influenced the overall hexanal accumulation only during the unsteady-state release period (the first few days of storage). The rate of hexanal uptake by tomatoes became negligibly small after the MIC level was attained due to its exponential

dependency on hexanal concentration. The similar quasi steady-state headspace concentrations in packages having tomatoes or inert sealed glass jars, (observed in both experiments and model predictions), support the finding that the apparent rate of hexanal uptake by tomatoes was minimal at low hexanal concentrations.

In this work, a paper packaging material e.g. used in forms of moulded pulp tray (Eagleton & Marcondes 1994), and corrugated box (Parker et al. 2006) was not taken into account in the conceptual and mathematical model development. However the paper-based packages may become significant as (i) a 'source' of hexanal vapour, because hexanal is a common volatile compound that can be released from paper-based packaging materials, and/or (ii) a 'sink' due to the partitioning of the volatile into paper materials, as evidenced in other VOCs-paper material systems (see Nerín & Asensio 2004; Triantafyllou et al. 2005). In such systems, mathematical models describing such hexanal vapour transfer processes would have to be appropriately incorporated into the current global model because additional transport processes could affect dynamic accumulation of hexanal vapour within the bag headspace.

The model also showed the possibility to predict the release trend during transient storage temperature regimes. It was also found that the MIC was attained even though the model packages were stored in varying temperatures. The interactions between temperature and sorption isotherm properties offer potential benefits with regard to the active packaging system assisting in maintaining quality during storing and handling of products in fluctuating temperature conditions. Experiments were carried out for a transition from storage at 10 to 20ºC and compared to model predictions. Although disagreement was noted between the model predictions and experimental results during the transition between temperatures, the model well predicted the quasi steady-state concentrations in both storage temperatures. Whilst very high secondary release peaks were predicted by the model, the measured peaks at the change in temperature were small. These results raise important question concerning the temperature dependence of the sorption isotherm coefficients. In the present work, $C_{s,max}^{Hxl}$ values were less sensitive to temperature than b_{Lgm}^{Hxl}. Trends of the temperature dependent properties of both $C_{s,max}^{Hxl}$ and b_{Lgm}^{Hxl} of the hexanal-silica gel system are in line with literature for other sorption systems, for example sorption of acetaldehyde, propionaldehyde and butyraldehyde for silica gel (Ghosh & Hines 1990).

A lack of fit between the experimental data and model predictions were mainly observed in the unsteady-state period and were evident in both headspace concentration and the adsorbed hexanal mass on the carrier bed. Trends of unsteady-state hexanal release into headspaces of a range of active MA packages were generally described by the model and in most cases predictions were improved by considering the uncertainties of input data, especially the estimated coefficients of permeability and the Langmuir sorption isotherm.

Measured data on the steady and slow change of adsorbed hexanal weight on the silica gel bed (LD7; Table 6-1) during the dynamic period (~10 h) differed from the model prediction results (which showed a rapid decline and apparent stability within 2 h). This posed questions on the validity of the model used to describe the flux across the sachet film. The model used for mass transport through the film was capable of describing fluxes through films (in particular OPP films), in which the nonlinear concentration gradient was significant due to the low permeability and dependency of permeability on concentration. The model may not be suitable however for the extreme situation initially occurring in the sachet (i.e. with one film surface exposed to a very high, saturated concentration (inside the sachet) and the other effectively zero in the package headspace). In this case the film transport model used effectively extrapolates the measured concentration dependency of permeability, so that very rapid release is predicted.

An alternative approach examined was to assume that solubility of the vapour in the film follows the Langmuir type relationship rather than the linear Henry's law model used initially. This resulted in the localised permeability effectively reaching a maximum when the film became saturated with vapour and this phenomenon may be responsible for the slower measured flux of hexanal vapour loss through the sachet and subsequently would cause the slower changes of adsorbed amount on the carrier bed. While this model could better predict flux through the film with high concentration differences, some of the experimental data collected during permeability measurements with lower concentration differences, but medium adsorbed concentrations, were underestimated.

The global model was modified accordingly, providing improved predictions for the unsteady-state hexanal mass changes and hexanal vapour release pattern (especially the significant attenuation of the initial release peak). However there was poorer agreement between predictions and experimental results in the quasi steady-state region, which were

better predicted by the original model. Clearly a more thorough investigation into volatile mass transfer rates through packaging films is required to enable fitting of a transport model appropriate for all conditions.

Although the modified global model provides insights to the changes occurring during the unsteady-state period, the overall utility of the original model to predict vapour release trends and (particularly) the quasi steady-state headspace concentration are reasonable and valid. The original model was therefore used for exploring the outcomes of '*what-if*' scenarios for a range of active packaging systems (such as changing sorption isotherm forms). The simulation results suggest the importance of appropriated selections of outer bag film permeability, in addition to the sorption isotherm form, for achieving the required release patterns. With an appropriately selected outer film permeability, VOC release with either a short and long term sustained period prior to decreasing to or near zero concentration could be achieved by the linear and exponential isotherms, respectively. These patterns could be useful to achieve a required concentration after initial release (i.e. minimal or without fumigation) and to later 'evacuate' the active agents at or near the opening or expiry date. Thus, with appropriate data selection, the model can be used to design active packaging system to meet a range of product and/or market needs.

8.2 Conclusions

Hexanal vapour is a potential volatile active agent that can control key postharvest pathogens without causing significant detrimental effects on other postharvest qualities. Because of its degree of volatility and physical adsorption on silica gel adsorbents, incorporation of hexanal to silica gel can be used to achieve slow release of the vapour into the package headspace. This system was used as a practical example to maintain tomato quality from which it was possible to demonstrate a model for active MA packaging systems.

The generalised modelling methodology and the mathematical model developed is a promising mechanistic tool with the advantage of reasonable simplicity and practical accuracy for active packaging design. Because of the generality and confidence in model performance demonstrated through validation trials of the hexanal/silica gel/tomato active MA packages, the global mathematical model can potentially be applied for other active

packaging systems for other horticultural and food products, in which volatile active agents are delivered from carriers encased in a sachet. The model could be further applied to other configurations such as surface coatings or film impregnations (with the carrier or active agent(s) *per se*) of which mass transfer processes (e.g. desorption from carrier into and diffusion through accommodated film or coating material) would be generally considered analogous to those identified for the sachet-based active MA packages.

8.3 Suggestions for future research

This work has significantly advanced the knowledge of and design capability for, active packaging systems for horticultural products. In order to refine and extend this knowledge, the following areas are recommended for further research:

- To study the effects of active agents on the products physiology such as the mechanisms by which respiration is stimulated when tomatoes were continuously exposed to hexanal vapour, or the antifungal mechanisms of hexanal on *B. cinerea*.
- To improve the experimental procedures for measuring film permeability to active compounds and of sorption isotherms to minimise uncertainties associated with these estimated data.
- To develop and model different configurations of controlled release systems, for example film materials impregnated with active agents and activated systems which can release active agents under pre-determined conditions such as high RH (as in the case of 1-MCP release stimulated by high RH conditions) or high O_2 levels (as could arise from leaks in the MA package).
- To model multi-component sorption isotherms for different active agents on carriers, where knowledge of this would support the modelling of controlled release systems as mentioned above.
- To extend the capability of the global mathematical model to predict heat and mass transfer processes of active agents in bulk storage systems, e.g. palletisation of boxes containing individual active packages.
- To address the impact of active agents on sensory and overall acceptability of the product and packaging systems within the context of commercial supply chains.

REFERENCES

Abe K, & Watada A E (1991). Ethylene absorbent to maintain quality of lightly processed fruits and vegetables. *Journal of Food Science* **56** 1589-1592.

Adamson A W (1990). Adsorption of gases and vapors on solids. In *Physical Chemistry of Surfaces*, pp. 591-681. New York: Wiley.

Adaskaveg J E, Förster H, & Sommer N F (2002). Principles of postharvest pathology and management of decays of edible horticultural crops. In *Postharvest Technology of Horticultural Crops*, 3rd, A A Kader (Ed.), pp. 163-195. Oakland: University of California Agriculture and Natural Resources.

Adedeji O, Taiwo K A, Akanbi C T, & Ajani R (2006). Physicochemical properties of four tomato cultivars grown in Nigeria. *Journal of Food Processing and Preservation* **30** 79-86.

Aguayo E, Allende A, & Artes F (2003). Keeping quality and safety of minimally fresh processed melon. *European Food Research and Technology* **216** 494-499.

Aguayo E, Jansasithorn R, & Kader A A (2006). Combined effects of 1-methylcyclopropene, calcium chloride dip, and/or atmospheric modification on quality changes in fresh-cut strawberries. *Postharvest Biology and Technology* **40** 269-278.

Ahvenainen R (2003). Active and intelligent packaging: an introduction. In *Novel Food Packaging Techniques*, R Ahvenainen (Ed.), pp. 5-21. Cambridge: Woodhead Publishing Limited.

Almenar E, Auras R, Rubino M, & Harte B R (2006). Design of biodegradable antimicrobial packaging film for prevention of postharvest fungal diseases. In *Proceedings of 15th IAPRI World Conference on Packaging*. *Conference Proceedings*. pp. 159-163. Tokyo, Japan.

Anonymous. (2004. July 2007). *DuPont™, Tyvek® Users Manual* Retrieved 14 November, 2007, from http://www.graphics.dupont.com/en/productServices/HANDBOOK.pdf

Ansón A, Callejas M A, Benito A M, Maser W K, Izquierdo M T, Rubio B, Jagiello J, Thommes M, Parra J B, & Martínez M T (2004). Hydrogen adsorption studies on single wall carbon nanotubes. *Carbon* **42** 1243-1248.

Apostolopoulos D, & Gilbert S G (1983). Water sorption of coffee solubles by inverse gas chromatography. In *The 3rd International Flavor Conference*. *Conference Proceedings*. G Charalambous & G Inglett (Eds.) pp. 51-92. Corfu, Greece.

Apostolopoulos D V (1985). *Inverse Gas Chromatography as Used in Studying Water Sorption of Coffee Solubles.* The State University of New Jersey, New Brunswick Rutgers, US.

Archbold D D, Hamilton-Kemp T R, Barth M M, & Langlois B E (1997). Identifying natural volatile compounds that control gray mold (*Botrytis cinerea*) during postharvest storage of strawberry, blackberry, and grape. *Journal of Agricultural and Food Chemistry* **45** 4032-4037.

Archbold D D, Hamilton-Kemp T R, Clements A M, & Collins R W (1999). Fumigating 'Crimson Seedless' table grapes with (E)-2-hexenal reduces mold during long-term postharvest storage. *HortScience* **34** 705-707.

Artés-Hernández F, Tomás-Barberán F A, & Artés F (2006). Modified atmosphere packaging preserves quality of SO_2-free 'Superior seedless' table grapes. *Postharvest Biology and Technology* **39** 146-154.

Artés F, Conesa M A, Hernández S, & Gil M I (1999). Keeping quality of fresh-cut tomato. *Postharvest Biology and Technology* **17** 153-162.

Artes F, Garcia F, Marquina J, Cano A, & Fernandez-Trujillo J P (1998). Physiological responses of tomato fruit to cyclic intermittent temperature regimes. *Postharvest Biology and Technology* **14** 283-296.

Ayala-Zavala J F, del-Toro-Sanchez L, Alvarez-Parrilla E, & Gonzalez-Aguilar G A (2008). High relative humidity in-package of fresh-cut fruits and vegetables: advantage or disadvantage considering microbiological problems and antimicrobial delivering systems? *Journal of Food Science* **73** R41-R47.

Bai J H, Baldwin E A, Fortuny R C S, Mattheis J P, Stanley R, Perera C, & Brecht J K (2004). Effect of pretreatment of intact 'Gala' apple with ethanol vapor, heat, or 1-methylcyclopropene on quality and shelf life of fresh-cut slices. *Journal of the American Society for Horticultural Science* **129** 583-593.

Bailén G, Guillén F, Castillo S, Serrano M, Valero D, & Martínez-Romero D (2006). Use of activated carbon inside modified atmosphere packages to maintain tomato fruit quality during cold storage. *Journal of Agricultural and Food Chemistry* **54** 2229-2235.

Banerjee T l, Singh M K, Sahoo R K, & Khanna A (2005). Volume, surface and UNIQUAC interaction parameters for imidazolium based ionic liquids via Polarizable Continuum Model. *Fluid Phase Equilibria* **234** 64-76.

Banks N H, Cleland D J, Cameron A C, Beaudry R M, & Kader A A (1995). Proposal for a rationalized system of units for postharvest research in gas-exchange. *HortScience* **30** 1129-1131.

Barbara L L, Henryk D, & G. S G (1991). Water sorption of gliadin. *Journal of Food Science* **56** 510-512.

Beaulieu J C, & Saltveit M E (1997). Inhibition or promotion of tomato fruit ripening by acetaldehyde and ethanol is concentration dependent and varies with initial fruit maturity. *Journal of the American Society for Horticultural Science* **122** 392-398.

Begley T H, Biles J E, Cunningham C, & Piringer O (2004). Migration of a UV stabilizer from polyethylene terephthalate (PET) into food simulants. *Food Additives and Contaminants* **21** 1007-1014.

Belmabkhout Y, Frere M, & De Weireld G (2004). High-pressure adsorption measurements. A comparative study of the volumetric and gravimetric methods. *Measurement Science & Technology* **15** 848-858.

Ben-Yehoshua S, & Cameron A C (1989). Exchange determination of water vapour, carbon dioxide, oxygen, ethylene and other gases of fruits and vegetables. In *Modern Methods of Plant Analysis: Volume 9-Gases in Plant and Microbial Cells*, H F Linskens & J F Jackson (Eds.), pp. 177-193. Berlin: Spinger-Verlag.

Beu T A (2000). Numerical solutions of the diffusion equation. In *Plastic Packaging Materials for Food : Barrier Function, Mass Transport, Quality Assurance and Legislation*, O-G Piringer & A L Baner (Eds.), pp. 221-238. Weinheim ; Cambridge: Wiley-VCH.

Blahovec J (2004). Sorption isotherms in materials of biological origin mathematical and physical approach. *Journal of Food Engineering* **65** 489-495.

Blankenship S M, & Dole J M (2003). 1-Methylcyclopropene: a review. *Postharvest Biology and Technology* **28** 1-25.

Bodenhofer K, Hierlemann A, Schlunk R, & Gopel W (1997). New method of vaporising volatile organics for gas tests. *Sensors and Actuators B: Chemical* **45** 259-264.

Boukobza F, & Taylor A J (2002). Effect of postharvest treatment on flavour volatiles of tomatoes. *Postharvest Biology and Technology* **25** 321-331.

Brandsch J, & Piringer O-G (2000). Characteristics of plastic materials. In *Plastic Packaging Materials for Food : Barrier Function, Mass Transport, Quality Assurance and Legislation*, O-G Piringer & A L Baner (Eds.), pp. 9-45. Weinheim ; Cambridge: Wiley-VCH.

Brecht J K (2003). Harvesting and handling techniques. In *Postharvest Physiology and Pathology of Vegetables*, 2nd, J A Bartz & J K Brecht (Eds.), pp. 383-412. New York: Marcel Dekker.

Brody A L (2002). Active and intelligent packaging: the saga continues. *Food Technology* **56** 65-66.

Brody A L, Strupinsky E R, & Kline L R (2001a). Ethylene control. In *Active Packaging for Food Applications*, pp. 99-106. Lancaster: Technomic Publishing.

Brody A L, Strupinsky E R, & Kline L R (2001b). Moisture control. In *Active Packaging for Food Applications*, pp. 87-94. Lancaster: Technomic Publishing.

Bronlund J E (1997). *The Modelling of Caking in Bulk Lactose.* Massey University, Palmerston North, New Zealand.

Buonocore G G, Sinigaglia M, Corbo M R, Bevilacqua A, La Notte E, & Del Nobile M A (2004). Controlled release of antimicrobial compounds from highly swellable polymers. *Journal of Food Protection* **67** 1190-1194.

Burt S (2004). Essential oils: their antibacterial properties and potential applications in foods-a review. *International Journal of Food Microbiology* **94** 223-253.

Buttery R G, Teranishi R, & Ling L C (1987). Fresh tomato aroma volatiles: a quantitative study. *Journal of Agricultural & Food Chemistry* **35** 540-544.

Cameron A C, Boylanpett W, & Lee J (1989). Design of modified atmosphere packaging systems - modeling oxygen concentrations within sealed packages of tomato fruits. *Journal of Food Science* **54** 1413-1416.

Cameron A C, Talasila P C, & Joles D W (1995). Predicting film permeability needs for modified atmosphere packaging of lightly processed fruits and vegetables. *HortScience* **30** 25-34.

Carslaw H S, & Jaeger J C (1959). Linear flow of heat in the solid bounded by two parallel planes. In *Conduction of Heat in Solids*, 2nd, pp. 92-132. Oxford: Oxford University Press.

Charara Z N, Williams J W, Schmidt R H, & Marshall M R (1992). Orange flavor absorption into various polymeric packaging materials. *Journal of Food Science* **57** 963-966 & 972.

Charles F, Guillaume C, & Gontard N (2008). Effect of passive and active modified atmosphere packaging on quality changes of fresh endives. *Postharvest Biology and Technology* **48** 22-29.

Charles F, Sanchez J, & Gontard N (2003). Active modified atmosphere packaging of fresh fruits and vegetables: modeling with tomatoes and oxygen absorber. *Journal of Food Science* **68** 1736-1742.

Charles F, Sanchez J, & Gontard N (2005). Modeling of active modified atmosphere packaging of endives exposed to several postharvest temperatures. *Journal of Food Science* **70** E443-E449.

Chen X Y, Hertog M L A T M, & Banks N H (2000). The effect of temperature on gas relations in MA packages for capsicums (*Capsicum annuum* L., cv. Tasty): an integrated approach. *Postharvest Biology and Technology* **20** 71-80.

Chen Y, Liu S, & Wang G (2007). A kinetic investigation of cationic starch adsorption and flocculation in kaolin suspension. *Chemical Engineering Journal* **133** 325-333.

Chervin C, Westercamp P, & Monteils G (2005). Ethanol vapours limit *Botrytis* development over the postharvest life of table grapes. *Postharvest Biology and Technology* **36** 319-322.

Choehom R, Ketsa S, & van Doorn W G (2004). Senescent spotting of banana peel is inhibited by modified atmosphere packaging. *Postharvest Biology and Technology* **31** 167-175.

Chu K H, & Hashim M A (2002). Adsorption and desorption characteristics of zinc on ash particles derived from oil palm waste. *Journal of Chemical Technology and Biotechnology* **77** 685-693.

Clarke R (2001). Temperature switchable membranes for creating and maintaining beneficial package atmospheres for fresh produce. *Journal of Plastic Film and Sheeting* **17** 22-34.

Cleland D J, Cleland A C, & Jones R S (1994). Collection of accurate experimental data for testing the performance of simple methods for food freezing time prediction. *Journal of Food Process Engineering* **17** 93-117.

Conway W S, Janisiewicz W J, Klein J D, & Sams C E (1999). Strategy for combining heat treatment, calcium infiltration, and biological control to reduce postharvest decay of 'Gala' apples. *HortScience* **34** 700-704.

Conway W S, Leverentz B, Janisiewicz W J, Saftner R A, & Camp M J (2005). Improving biocontrol using antagonist mixtures with heat and/or sodium bicarbonate to control postharvest decay of apple fruit. *Postharvest Biology and Technology* **36** 235-244.

Conway W S, & Sams C E (1983). Calcium infiltration of Golden Delicious apples and its effect on decay. *Phytopathology* **73** 1068-1071.

Corbo M R, Lanciotti R, Gardini F, Sinigaglia M, & Guerzoni M E (2000). Effects of hexanal, trans-2-hexenal, and storage temperature on shelf life of fresh sliced apples. *Journal of Agricultural and Food Chemistry* **48** 2401-2408.

Crank J (1975). *The Mathematics of Diffusion*. London: Oxford University Press.

Crisosto C H, Garner D, & Crisosto G (2002). Carbon dioxide-enriched atmospheres during cold storage limit losses from *Botrytis* but accelerate rachis browning of 'Redglobe' table grapes. *Postharvest Biology and Technology* **26** 181-189.

D'Aniello C, Guadagno L, Gorrasi G, & Vittoria V (2000). Influence of the crystallinity on the transport properties of isotactic polypropylene. *Polymer* **41** 2515-2519.

Daifas D P, Smith J P, Blanchfield B, Cadieux B, Sanders G, & Austin J W (2003). Challenge studies with proteolytic *Clostridium Botulinum* in yeast and chemically leavened crumpets packaged under modified atmospheres. *Journal of Food Safety* **23** 107-125.

Daifas D P, Smith J P, Tarte I, Blanchfield B, & Austin J W (2000). Effect of ethanol vapor on growth and toxin production by *Clostridium botulinum* in a high moisture bakery product. *Journal of Food Safety* **20** 111-125.

Daly J, & Kourelis B (2001). Synthesis methods, complexes and delivery methods for the safe and convenient storage, transport and application of compounds for inhibiting the ethylene response in plants. US Patent 6,313,068.

Davidson P M (2001). Chemical preservatives and natural antimicrobial compounds. In *Food Microbiology: Fundamentals and Frontiers*, 2nd, M P Doyle, L R Beuchat & T J Montville (Eds.), pp. 593-627. Washington, D.C.: ASM Press.

Day B P F (1989). Extension of shelf-life of chilled foods. *European Food and Drink Review* **4** 47-56.

Day B P F (2003). Active packaging. In *Food Packaging Technology*, R Coles, D McDowell & M J Kirwan (Eds.), pp. 282-302. Boca Raton: CRC Press.

De Jong A R, Boumans H, Slaghek T, Van Veen J, Rijk R, & Van Zandvoort M (2005). Active and intelligent packaging for food: Is it the future? *Food Additives and Contaminants* **22** 975-979.

De Pooter H L, Montens J P, Willaert G A, Dirinck P J, & Schamp N M (1983). Treatment of Golden Delicious apples with aldehydes and carboxylic acids: effect on the headspace composition. *Journal of Agricultural and Food Chemistry* **31** 813-818.

de Wild H P J, Balk P A, Fernandes E C A, & Peppelenbos H W (2005). The action site of carbon dioxide in relation to inhibition of ethylene production in tomato fruit. *Postharvest Biology and Technology* **36** 273-280.

Del-Valle V, Almenar E, Hernandez-Munoz P, Lagaron J M, Catala R, & Gavara R (2004). Volatile organic compound permeation through porous polymeric films for modified atmosphere packaging of foods. *Journal of the Science of Food and Agriculture* **84** 937-942.

Del-Valle V, Almenar E, Lagaron J M, Catala R, & Gavara R (2003). Modelling permeation through porous polymeric films for modified atmosphere packaging. *Food Additives and Contaminants* **20** 170-179.

Del Nobile M A, Buonocore G G, Fava P, & Piergiovanni L (2002). Modeling of hexanal sorption kinetic in an aldehydes scavenger film intended for food packaging. *Journal of Food Science* **67** 2687-2691.

Del Nobile M A, Conte A, Incoronato A L, & Panza O (2008). Antimicrobial efficacy and release kinetics of thymol from zein films. *Journal of Food Engineering* **89** 57-63.

DeLassus P T (1997). Barrier polymers. In *The Wiley Encyclopaedia of Packaging Technology*, 2nd, A L Brody & K S Marsh (Eds.), pp. 71-77. New York: Wiley.

DeLassus P T, & Jenkins S R (1986). Advances in flavour and aroma testing in relation to polymer barrier performance. In *The Fifth International Seminar on Packaging. Conference Proceedings*. pp. 116-130. University of Auckland, New Zealand.

DeLassus P T, Tou J C, Babinec M A, Rulf D C, Karp B K, & Howell B A (1988). Transport of apple aroma in polymer films. In *Food and Packaging Interactions*, *ACS Symposium Series 365,* J H Hotchkiss (Ed.), pp. 11-27. Washington D.C.: American Chemical Society.

Do D D (1998a). Fundamentals of diffusion and adsorption in porous media. In *Adsorption Analysis: Equilibria and Kinetics*, pp. 337-414. London: Imperial College Press.

Do D D (1998b). Fundamentals of pure component adsorption equilibria. In *Adsorption Analysis: Equilibria and Kinetics*, pp. 2-48. London: Imperial College Press.

Dury-Brun C, Chalier P, Desobry S, & Voilley A (2007). Multiple mass transfers of small volatile molecules through flexible food packaging. *Food Reviews International* **23** 199-255.

Eagleton D G, & Marcondes J A (1994). Moisture-sorption isotherms for paper-based components of transport packaging for fresh produce. *Tappi Journal* **77** 75-81.

Earle M D, & Earle R L (2003). Product changes during processing. In *Fundamentals of Food Reaction Technology*, pp. 32-72. Leatherhead: Leatherhead Food International.

Emond J P, Castaigne F, Toupin C J, & Desilets D (1991). Mathematical-modeling of gas-exchange in modified atmosphere packaging. *Transactions of the ASAE* **34** 239-245.

Fan L H, Song J, Beaudry R M, & Hildebrand P D (2006). Effect of hexanal vapor on spore viability of *Penicillium expansum*, lesion development on whole apples and fruit volatile biosynthesis. *Journal of Food Science* **71** M105-M109.

Felder R M, & Huvard G S (1980). Permeation, diffusion, and sorption of gases and vapours. In *Methods of Experimental Physics*, R A Fava (Ed.), pp. 315-377. New York: Academic Press.

Feldman D, Shapiro M M, & Banu D (1986). Organic phase change materials for thermal energy storage. *Solar Energy Materials* **13** 1-10.

Fishman S, Rodov V, & S B Y (1996). Mathematical model for perforation effect on oxygen and water vapor dynamics in modified-atmosphere packages. *Journal of Food Science* **61** 956-961.

Fonseca S C, Oliveira F A R, & Brecht J K (2002a). Modelling respiration rate of fresh fruits and vegetables for modified atmosphere packages: a review. *Journal of Food Engineering* **52** 99-119.

Fonseca S C, Oliveira F A R, Frias J M, Brecht J K, & Chau K V (2002b). Modelling respiration rate of shredded Galega kale for development of modified atmosphere packaging. *Journal of Food Engineering* **54** 299-307.

Forney C F, & Brandl D G (1992). Control of humidity in small controlled-environment chambers using glycerol-water solutions. *HortTechnology* **2** 52-54.

Franke I, Wijma E, & Bouma K (2002). Shelf life extension of pre-baked buns by an active packaging ethanol emitter. *Food Additives and Contaminants* **19** 314-322.

Friedman M, Henika P R, Levin C E, & Mandrell R E (2004). Antibacterial activities of plant essential oils and their components against *Escherichia coli* O157:H7 and *Salmonella enterica* in apple juice. *Journal of Agricultural and Food Chemistry* **52** 6042-6048.

Friess K, Sipek M, Hynek V, Sysel P, Bohata K, & Izak P (2004). Comparison of permeability coefficients of organic vapors through non-porous polymer membranes by two different experimental techniques. *Journal of Membrane Science* **240** 179-185.

Gardini F, Lanciotti R, Caccioni D R L, & Guerzoni M E (1997). Antifungal activity of hexanal as dependent on its vapor pressure. *Journal of Agricultural and Food Chemistry* **45** 4297-4302.

Gardini F, Lanciotti R, & Guerzoni M E (2001). Effect of trans-2-hexenal on the growth of *Aspergillus flavus* in relation to its concentration, temperature and water activity. *Letters in Applied Microbiology* **33** 50-55.

Gardner H W, Dornbos D L, & Desjardins A E (1990). Hexanal, trans-2-hexenal, and trans-2-nonenal inhibit soybean, glycine-max, seed-germination. *Journal of Agricultural and Food Chemistry* **38** 1316-1320.

Gaysinsky S, Taylor T M, Davidson P M, Bruce B D, & Weiss J (2007). Antimicrobial efficacy of eugenol microemulsions in milk against *Listeria monocytogenes* and *Escherichia coli* O157 : H7. *Journal of Food Protection* **70** 2631-2637.

Geankoplis C J (1993a). Liquid-liquid and fluid-solid separation processes. In *Transport Processes and Unit Operations*, pp. 697-753. New Jersey: Prentice Hall.

Geankoplis C J (1993b). Principles of unsteady-state and convection mass transfer. In *Transport Processes and Unit Operations*, pp. 426-487. New Jersey: Prentice Hall.

Geankoplis C J (1993c). Principles of unsteady-state heat transfer. In *Transport Processes and Unit Operations*, pp. 330-380. New Jersey: Prentice Hall.

Ghosh T K, & Hines A L (1990). Adsorption of acetaldehyde, propionaldehyde, and butyraldehyde on silica gel. *Separation Science and Technology* **25** 1101-1115.

Giacin J R (1987). Chemical structure and properties of polymers. In *Principles of Aseptic Processing and Packaging*, P E Nelson, J V Chambers & J H Rodriguez (Eds.), pp. 81-96. Washington, D.C.: Food Processors Institute.

Gil M I, Conesa M A, & Artes F (2001). Modified atmosphere packaging of fresh-cut tomato. *Acta Horticulturae* **2** 703-704.

Gil M I, Conesa M A, & Artes F (2002). Quality changes in fresh cut tomato as affected by modified atmosphere packaging. *Postharvest Biology and Technology* **25** 199-207.

Gilbert S G (1993). Applications of IGC for research in kinetic thermodynamic problems in food science. In *Shelf Life Studies of Foods and Beverages : Chemical, Biological, Physical, and Nutritional Aspects*, G Charalambous (Ed.), pp. 1071-1079. Amsterdam ; New York: Elsevier.

Gorna-Binkul A, Kaczmarski K, & Buszewski B (2001). Modeling of the sorption and diffusion processes of volatile organic air pollutants in grape fruits. *Journal of Agricultural & Food Chemistry* **49** 2889-2893.

Gouble B, Fath D, & Soudain P (1995). Nitrous oxide inhibition of ethylene production in ripening and senescing climacteric fruits. *Postharvest Biology and Technology* **5** 311-321.

Gregg S J, & Sing K S W (1982). The physical adsorption of gases by microporous solids: the Type-I isotherm. In *Adsorption, Surface Area and Porosity*, 2nd, pp. 195-247. London: Academic Press.

Grierson D, & Kader A A (1986). Fruit ripening and quality. In *The Tomato Crop: A Scientific Basis for Improvement*, J G Atherton & J Rudich (Eds.), pp. 241-280. London, New York: Chapman and Hall.

Groen J C, Perez-Ramirez J, & Zhu W (2002). Adsorption of nitrous oxide on silicalite-1. *Journal of Chemical and Engineering Data* **47** 587-589.

Hamilton-Kemp T R, Archbold D D, Loughrin J H, Collins R W, & Byers M E (1996). Metabolism of natural volatile compounds by strawberry fruit. *Journal of Agricultural and Food Chemistry* **44** 2802-2805.

Hamilton-Kemp T R, McCracken C T, Loughrin J H, Andersen R A, & Hildebrand D F (1992). Effects of some natural volatile compounds on the pathogenic fungi *Alternaria alternata* and *Botrytis cinerea*. *Journal of Chemical Ecology* **18** 1083-1091.

Han J H (2000). Antimicrobial food packaging. *Food Technology* **54** 56-65.

Han J H (2003). Antimicrobial food packaging. In *Novel Food Packaging Techniques*, R Ahvenainen (Ed.), pp. 50-70. Cambridge: Woodhead Publishing Limited.

Han J H, & Floros J D (1998). Simulating diffusion model and determining diffusivity of potassium sorbate through plastics to develop antimicrobial packaging films. *Journal of Food Processing and Preservation* **22** 107-122.

Han J H, Ho C H L, & Rodrigues E T (2005). Intelligent packaging. In *Innovations in Food Packaging*, J H Han (Ed.), pp. 138-156. San Diego, Calif.: Elsevier Academic.

Hardenburg R E, Watada A E, & Wang C Y (1986). Summary of respiration and ethylene production rates. In *The Commercial Storage of Fruits, Vegetables, and Florist and Nursery Stocks Agriculture Handbook, no. 66*. Washington, D.C.: U.S. Dept. of Agriculture, Agricultural Research Service.

Harima Y (1990). Free oxygen scavenging packaging. In *Food Packaging*, T Kadoya (Ed.), pp. 229-252. San Diego: Academic Press.

Haros C M, Aguerre R J, & Suarez C (2005). Modeling sulfur dioxide uptake in dent corn during steeping. *Lebensmittel-Wissenschaft und-Technologie* **38** 393-398.

Heirlings L, Siró I, Devlieghere F, Van Bavel E, Cool P, De Meulenaer B, Vansant E F, & Debevere J (2004). Influence of polymer matrix and adsorption onto silica materials on the migration of α-tocopherol into 95% ethanol from active packaging. *Food Additives and Contaminants* **21** 1125-1136.

Hernandez-Munoz P, Catala R, & Gavara R (1999). Effect of sorbed oil on food aroma loss through packaging materials. *Journal of Agricultural & Food Chemistry* **47** 4370-4374.

Hernandez-Munoz P, Catala R, Hernandez R J, & Gavara R (1998). Food aroma mass transport in metallocene ethylene-based copolymers for packaging applications. *Journal of Agricultural and Food Chemistry* **46** 5238-5243.

Hernandez R J (1997). Food packaging materials, barrier properties, and selection. In *Handbook of Food Engineering Practice*, K J Valentas, E Rotstein & R P Sing (Eds.), pp. 291-360. Boca Raton: CRC Press.

Hertog M L A T, Peppelenbos H W, Evelo R G, & Tijskens L M M (1998). A dynamic and generic model of gas exchange of respiring produce: the effects of oxygen, carbon dioxide and temperature. *Postharvest Biology and Technology* **14** 335-349.

Hertog M L A T M, Ben-Arie R, Roth E, & Nicolai B M (2004a). Humidity and temperature effects on invasive and non-invasive firmness measures. *Postharvest Biology and Technology* **33** 79-91.

Hertog M L A T M, Lammertyn J, Desmet M, Scheerlinck N, & Nicolai B M (2004b). The impact of biological variation on postharvest behaviour of tomato fruit. *Postharvest Biology and Technology* **34** 271-284.

Hotchkiss J H, Watkins C B, & Sanchez D G (2007). Release of 1-methylcyclopropene from heat-pressed polymer films. *Journal of Food Science* **72** E330-E334.

Huang S J, & Giacin J R (1998). Evaluating the effect of temperature and vapor concentration on the organic vapor barrier properties of polymer membranes by an isostatic procedure. *Journal of Plastic Film & Sheeting* **14** 308-333.

Hurme E, Sipilainen-Malm T, Ahvenainen R, & Nielsen T (2002). Active and intelligent packaging. In *Minimal Processing Technologies in the Food Industry*, T Ohlsson & N Bengtsson (Eds.), pp. 87-123. Cambridge: Woodhead Publishing Limited.

Illeperuma C K, & Jayasuriya P (2002). Prolonged storage of 'Karuthacolomban' mango by modified atmosphere packaging at low temperature. *Journal of Horticultural Science and Biotechnology* **77** 153-157.

Järvi-Kääriäinen T (2003). Integrating intelligent packaging, storage and distribution. In *Novel Food Packaging Techniques*, R Ahvenainen (Ed.), pp. 535-549. Cambridge: Woodhead Publishing Limited.

Jayathunge K G L R, & Illeperuma C K (2001). Extension of postharvest life of oyster mushroom under ambient conditions by modified atmosphere packaging. *Tropical Agricultural Research* **13** 78-89.

Jeong J, Huber D J, & Sargent S A (2002). Influence of 1-methylcyclopropene (1-MCP) on ripening and cell-wall matrix polysaccharides of avocado (*Persea americana*) fruit. *Postharvest Biology and Technology* **25** 241-256.

Johansson F, & Leufven F (1994). Food packaging polymer films as aroma vapor barriers at different relative humidities. *Journal of Food Science* **59** 1328-1331.

Johnson A T (1999). Mass transfer. In *Biological Process Engineering : An Analogical Approach to Fluid Flow, Heat Transfer, and Mass Transfer Applied to Biological Systems*, pp. 494-700. New York: Wiley.

Johnston J H, Grindrod J E, Dodds M, & Schimitschek K (2008). Composite nano-structured calcium silicate phase change materials for thermal buffering in food packaging. *Current Applied Physics* **8** 508-511.

Johnston J W, Hewett E W, Hertog M, & Harker F R (2002). Temperature and ethylene affect induction of rapid softening in 'Granny Smith' and 'Pacific Rose^{TM}' apple cultivars. *Postharvest Biology and Technology* **25** 257-264.

Kader A A (1992). Postharvest biology and technology: an overview. In *Postharvest Technology of Horticultural Crops*, 2nd, A A Kader (Ed.), pp. 15-20. Oakland, Calif.: University of California, Division of Agriculture and Natural Resources.

Kader A A (2002). Postharvest biology and technology: an overview. In *Postharvest Technology of Horticultural Crops*, 3rd, A A Kader (Ed.), pp. 39-47. Oakland: University of California Agriculture and Natural Resources.

Kader A A, & Saltveit M E (2003a). Atmosphere modification. In *Postharvest Physiology and Pathology of Vegetables*, 2nd, J A Bartz & J K Brecht (Eds.), pp. 229-246. New York: Marcel Dekker.

Kader A A, & Saltveit M E (2003b). Respiration and gas exchange. In *Postharvest Physiology and Pathology of Vegetables*, 2nd, J A Bartz & J K Brecht (Eds.), pp. 7-29. New York: Marcel Dekker.

Kader A A, Zagory D, & Kerbel E L (1989). Modified atmosphere packaging of fruits and vegetables. *Critical Reviews in Food Science and Nutrition* **28** 1-30.

Karel M (1975). Protective packaging of foods. In *Principles of Food Science. Part II. Physical Principles of Food Preservation*, O R Fennema (Ed.), pp. 399-465. New York: Marcel Dekker.

Kays S J (1991). Movement of gases, solvents, and solutes, within harvested products and their exchange between the product and its external environment. In *Postharvest Physiology of Perishable Plant Products*, pp. 409-455. New York: Van Nostrand Reinhold.

Kim H O, Hewett E W, & Lallu N (2001). Softening and ethylene production of kiwifruit reduced with 1- Methylcyclopropene. *Acta Horticulturae* **1** 167-170.

Knoche M, Petracek P D, & Bukovac M J (1994). Urea penetration of isolate tomato fruit cuticles. *Journal of the American Society for Horticultural Science* **119** 761-764.

Kontominas M G, Gavara R, & Giacin J R (1994). The adsorption of hydrocarbons on Polystyrene by inverse gas chromatography - infinite dilution concentration region. *European Polymer Journal* **30** 265-269.

Kopac T, & Kocabas S (2002). Adsorption equilibrium and breakthrough analysis for sulfur dioxide adsorption on silica gel. *Chemical Engineering and Processing* **41** 223-230.

Kostansek E C (2003). Delivery systems for cyclopropenes. US Patent 6,548,448

Kou L, Luo Y, Wu D, & Liu X (2007). Effects of mild heat treatment on microbial growth and product quality of packaged fresh-cut table grapes. *Journal of Food Science* **72** S567-S573.

Krantz W B (2007). Applications in heat transfer. In *Scaling Analysis in Modeling Transport and Reaction Processes: A Systematic Approach to Model Building and the Art of Approximation*, pp. 145-251. Hoboken, New Jersey: Wiley-Interscience.

Krumbein A, Peters P, & Bruckner B (2004). Flavour compounds and a quantitative descriptive analysis of tomatoes (*Lycopersicon Esculentum* Mill.) of different cultivars in short-term storage. *Postharvest Biology and Technology* **32** 15-28.

Labuza T P (1982). Scientific evaluation of shelf-life. In *Shelf-Life Dating of Foods*, pp. 41-87. Westport, Conn., USA Food & Nutrition Press.

Labuza T P, & Breene W M (1989). Applications of active packaging for improvement of shelf-life and nutritional quality of fresh and extended shelf-life foods. *Journal of Food Processing and Preservation* **13** 1-69.

Lanciotti R, Corbo M R, Gardini F, Sinigaglia M, & Guerzoni M E (1999). Effect of hexanal on the shelf life of fresh apple slices. *Journal of Agricultural and Food Chemistry* **47** 4769-4776.

Lanciotti R, Gianotti A, Patrignani F, Belletti N, Guerzoni M E, & Gardini F (2004). Use of natural aroma compounds to improve shelf-life and safety of minimally processed fruits. *Trends in Food Science & Technology* **15** 201-208.

Lee C H, An D S, Lee S C, Park H J, & Lee D S (2004). A coating for use as an antimicrobial and antioxidative packaging material incorporating nisin and α–tocopherol. *Journal of Food Engineering* **62** 323-329.

Lee D S, Haggar P E, Lee J, & Yam K L (1991). Model for fresh produce respiration in modified atmospheres based on principles of enzyme kinetics. *Journal of Food Science* **56** 1580-1585.

Lee D S, Hwang Y L, & Cho S H (1998). Developing antimicrobial packaging film for curled lettuce and soybean sprouts. *Food Science and Biotechnology* **7** 117-121.

Lee Y S (2003). *Development of a 1-Methylcyclopropene Delivery System to Control Tomato Ripening.* Michigan State University, US.

Lee Y S, Beaudry R, Kim J N, & Harte B R (2006). Development of a 1-methylcyclopropene (1-MCP) sachet release system. *Journal of Food Science* **71** C1-C6.

Leshem Y Y, & Wills R B H (1998). Harnessing senescence delaying gases nitric oxide and nitrous oxide: a novel approach to postharvest control of fresh horticultural produce. *Biologia Plantarum* **41** 1-10.

Leufven A, & Stollman U (1992). Polymer films as aroma barriers at different temperatures. *Zeitschrift für Lebensmitteluntersuchung und -Forschung A* **194** 355-359.

Levenspiel O (1972). Introduction. In *Chemical Reaction Engineering*, 2nd, pp. 1-7. New York: Wiley.

Liu K J, Hernandez R J, & Giacin J R (1991). The effect of water activity and penetrant vapor activity on the permeation of toluene vapor through a two-side PVDC coated opaque oriented polypropylene film. *Journal of Plastic Film & Sheeting* **7** 56-67.

Longhurst T J, Tung H F, & Brady C J (1990). Development regulation of the expression of alcohol dehydrogenase in ripening tomato fruits. *Journal of Food Biochemistry* **14** 421-433.

Lurie S, Pesis E, Gadiyeva O, Feygenberg O, Ben-Arie R, Kaplunov T, Zutahy Y, & Lichter A (2006). Modified ethanol atmosphere to control decay of table grapes during storage. *Postharvest Biology and Technology* **42** 222-227.

Lutzow N, Tihminlioglu A, Danner R P, Duda J L, De Haan A, Warnier G, & Zielinski J M (1999). Diffusion of toluene and n-heptane in polyethylenes of different crystallinity. *Polymer* **40** 2797-2803.

Macnish A J, Joyce D C, Irving D E, & Wearing A H (2004). A simple sustained release device for the ethylene binding inhibitor 1-Methylcyclopropene. *Postharvest Biology and Technology* **32** 321-338.

Madeley J D, & Sing K S W (1959). Adsorption of ethyl alcohol vapour by silica gel. *Chemistry & Industry* **9** 289-290.

MAF. (2007. August 2007). *Situation and Outlook for New Zealand Agriculture and Forestry 2007* Retrieved 05/05, 2008, from http://www.maf.govt.nz/mafnet/rural-nz/statistics-and-forecasts/sonzaf/2007/index.htm

Mahovic M J, Tenney J D, & Bartz J A (2007). Applications of chlorine dioxide gas for control of bacterial soft rot in tomatoes. *Plant Disease* **91** 1316-1320.

Maneerat C, & Hayata Y (2008). Gas-phase photocatalytic oxidation of ethylene with TiO_2-coated packaging film for horticultural products. *Transactions of the ASABE* **51** 163-168.

Mannapperuma J D, & Singh R P (1994). Modeling of gas exchange in polymeric packages of fresh fruits and vegetable. In *Minimal Processing of Foods and Process Optimization : An Interface*, R P Singh & F A R Oliveira (Eds.), pp. 437-458. Boca Raton, FL: CRC Press.

Mannapperuma J D, Singh R P, & Montero M E (1991). Simultaneous gas diffusion and chemical reaction in foods stored in modified atmospheres. *Journal of Food Engineering* **14** 167-183.

Mannapperuma J D, Zagory D, & Kader A A (1989). Design of polymeric packages for modified atmosphere storage of fresh produce. In *International Controlled Atmosphere Research Conference*. *Conference Proceedings*. J K Fellman (Ed.), pp. 225-233. Wenatchee, Washington, USA

Mari M, & Guizzardi M (1998). The postharvest phase: emerging technologies for the control of fungal diseases. *Phytoparasitica* **26** 59-66.

Marin A P, Shlyapnikov Y A, Makhkamov A Z, & Dzhalilov A T (1992). Effect of heptadecane on sorption of 2,6-di-tert-butyl-4-methylphenol by polyethylene. *International Journal of Polymeric Materials* **16** 37-44.

Marotta C (1997). Medical packaging. In *The Wiley Encyclopedia of Packaging Technology*, 2nd, A L Brody & K S Marsh (Eds.), pp. 610-615. New York Wiley.

Matan N (2008). Control of *Aspergillus niger* growth on the surface of tomatoes by cinnamon oil and clove oil. *Food New Zealand* **8** 44-47.

Matan N, Rimkeeree H, Mawson A J, Chompreeda P, Haruthaithanasan V, & Parker M (2006). Antimicrobial activity of cinnamon and clove oils under modified atmosphere conditions. *International Journal of Food Microbiology* **107** 180-185.

Matsuguchi M, Maeda N, & Sakai Y (2002). Competitive sorption of water vapor and CO_2 in photocrosslinked PVCA film for a capacitive-type humidity sensor. *Journal of Applied Polymer Science* **83** 401-407.

Maul F, Sargent S A, Sims C A, Baldwin E A, Balaban M O, & Huber D J (2000). Tomato flavor and aroma quality as affected by storage temperature. *Journal of Food Science* **65** 1228-1237.

McCabe W L, Smith J C, & Harriott P (2001). Fixed-bed separation. In *Unit Operations of Chemical Engineering*, pp. 812-856. Boston: McGraw Hill.

Meas P (2006). *Mathematical Modelling and Improvement of Operating Practices of Sun Drying of Rice.* Massey University, Palmerston North, New Zealand.

Menniti A M, Gregori R, & Donati I (2004). 1-Methylcyclopropene retards postharvest softening of plums. *Postharvest Biology and Technology* **31** 269-275.

Mercea P (2000). Models for diffusion in polymers. In *Plastic Packaging Materials for Food : Barrier Function, Mass Transport, Quality Assurance and Legislation*, O-G Piringer & A L Baner (Eds.), pp. 125-157. Weinheim ; Cambridge: Wiley-VCH.

Merts I (1996). *Mathematical Modelling of Modified Atmosphere Packaging Systems for Apples.* Massey University, Palmerston North, New Zealand.

Miller W R, Spalding D H, Risse L A, & Chew V (1984). The effects of an imazalil-impregnated film with chlorine and imazalil to control decay of bell peppers. *Proceedings of the Florida State Horticultural Society* **97** 108-111.

Mills A F (1995a). Mass transfer. In *Basic Heat and Mass Tranfer*, pp. 677-824. Chicago: Irwin.

Mills A F (1995b). Multidimensional and unsteady state conduction. In *Basic Heat and Mass tranfer*, pp. 113-207. Chicago: Irwin.

Miltz J, Hoojjat P, Han J, Giacin J R, Harte B R, & Gray I J (1988). Loss of antioxidants from high density polyethylene-its effect on oatmeal cereal oxidation. In *Food and Packaging Interactions*, *ACS symposium 365,* J H Hotchiss (Ed.), pp. 83-93. Washington, D.C.: American Chemical Society.

Mohsenin N N (1986). Physical characteristics. In *Physical Properties of Plant and Animal Materials: Structure, Physical Characteristics, and Mechanical Properties*, 2nd Updated and Revised Edition, pp. 79-127. New York: Gordon and Breach Science Publishers Inc.

Moler C. (2003. May 2003). *Stiff Differential Equations. Stiffness is a Subtle, Difficult, and Important Concept in the Numerical Solution of Ordinary Differential Equations*. Retrieved 21/01, 2008, from http://www.mathworks.com/company/newsletters/news_notes/clevescorner/may03_cleve.html

Moore J E, Cherie Millar B, Kenny F, Lowery C J, Xiao L, Rao J R, Nicholson V, Watabe M, Heaney N, Sunnotel O, McCorry K, Rooney P J, Snelling W J, & Dooley J S G (2007). Detection of *Cryptosporidium parvum* in lettuce. *International Journal of Food Science & Technology* **42** 385-393.

Moyls A L (2004). Whole bag method for determining oxygen transmission rate. *Transactions of the ASAE* **47** 159-164.

Mugge J, Bosch H, & Reith T (2001). Measuring and modeling gas adsorption kinetics in single porous particles. *Chemical Engineering Science* **56** 5351-5360.

Mulder M (1991). Transport in membranes. In *Basic Principles of Membrane Technology*, pp. 145-197. Dordrecht, Netherlands; Boston Kluwer Academic.

Mustonen H M (1992). The efficacy of a range of sulfur dioxide generating pads against *Botrytis cinerea* infection and on out-turn quality of Calmeria table grapes. *Australian Journal of Experimental Agriculture* **32** 389-393.

Nanthachai N, Ratanachinakorn B, Kosittrakun M, & Beaudry R M (2007). Absorption of 1-MCP by fresh produce. *Postharvest Biology and Technology* **43** 291-297.

Nerín C, & Asensio E (2004). Behaviour of organic pollutants in paper and board samples intended to be in contact with food. *Analytica Chimica Acta* **508** 185-191.

Nevins A L, Bronlund J E, Mawson A J, Chalmers I, & McKenzie A (2004) The effect of moisture on the strength of corrugated cardboard packaging, *9th International Congress on Engineering and Food (ICEF)*. Montpellier, France: Boca Raton, FL.

Ng K C, Chua H T, Chung C Y, Loke C H, Kashiwagi T, Akisawa A, & Saha B B (2001). Experimental investigation of the silica gel-water adsorption isotherm characteristics. *Applied Thermal Engineering* **21** 1631-1642.

Nielsen T J, Jagerstad I M, & Oste R E (1992). Study of factors affecting the absorption of aroma compounds into low-density polyethylene. *Journal of the Science of Food and Agriculture* **60** 377-381.

Ning B, Kubo Y, Inaba A, & Nakamura R (1997). Physiological responses of Chinese pear 'Yali' fruit to CO_2-enriched and/or O_2-reduced atmospheres. *Journal of the Japanese Society for Horticultural Science* **66** 613-620.

Nychas G J E (1995). Natural antimicrobials from plants. In *New Methods ofFood Preservation*, G W Gould (Ed.), pp. 58-89. London: Blackie Academic & Professional.

Ozdemir M, & Floros J D (2004). Active food packaging technologies. *Critical Reviews in Food Science and Nutrition* **44** 185-193.

Parker M E, Bronlund J E, & Mawson A J (2006). Moisture sorption isotherms for paper and paperboard in food chain conditions. *Packaging Technology & Science* **19** 193-209.

Patterson B D, & Joyce D C (1993). A package allowing cooling and preservation of horticultural produce without condensation of desiccants. International Patent Application PCT/AU93/00398

Paul D R, & Clarke R (2002). Modeling of modified atmosphere packaging based on designs with a membrane and perforations. *Journal of Membrane Science* **208** 269-283.

Pauly S (1999). Permeability and diffusion data. In *Polymer Handbook*, J. Brandrup, E H Immergut & E A Grulke (Eds.), pp. VI/543-VI/569. New York: Wiley.

Picón A, Martinez-Jávega J M, Cuquerella J, Delrio M A, & Navarro P (1993). Effects of precooling, packaging film, modified atmosphere and ethylene absorber on the quality of refrigerated Chandler and Douglas strawberries. *Food Chemistry* **48** 189-193.

Piringer O-G (2000). Permeation of gases, water vapor and volatile organic compounds. In *Plastic Packaging Materials for Food : Barrier Function, Mass Transport, Quality Assurance and Legislation*, O-G Piringer & A L Baner (Eds.), pp. 238-285. Weinheim ; Cambridge: Wiley-VCH.

Plotto A, Bai J, Narciso J A, Brecht J K, & Baldwin E A (2006). Ethanol vapor prior to processing extends fresh-cut mango storage by decreasing spoilage, but does not always delay ripening. *Postharvest Biology and Technology* **39** 134-145.

Ponce A G, Valle C, & Roura S I (2004). Shelf life of leafy vegetables treated with natural essential oils. *Journal of Food Science* **69** FMS50-FMS56.

Pongjaruwat W (2007). *Effect of Modified Atmosphere on Storage Life of Purple Passionfruit and Red Tamarillo.* Massey University, Palmerston North, New Zealand.

Pospisil J, Cikovic N, Dragovic-Uzelac V, Lukin V, & Brusic D (2001). The quality of sliced carrots affected by modified polyethylene foil and storage temperatures. *Acta Alimentaria* **30** 233-246.

Prasetyo I, & Do D D (1998). Adsorption rate of methane and carbon dioxide on activated carbon by the semi-batch constant molar flow rate method. *Chemical Engineering Science* **53** 3459-3467.

Prasetyo I, Do H D, & Do D D (2002). Surface diffusion of strong adsorbing vapours on porous carbon. *Chemical Engineering Science* **57** 133-141.

Rai D R, & Paul S (2007). Transient state in-pack respiration rates of mushroom under modified atmosphere packaging based on enzyme kinetics. *Biosystems Engineering* **98** 319-326.

Ratkowsky D A (1986). A suitable parameterization of the Michaelis-Menten enzyme reaction. *Biochemical Journal* **240** 357-360.

Ratkowsky D A (1990). Models with one x variable, convex/concave curves. In *Handbook of Nonlinear Regression Models*, pp. 71-121. New York: M. Dekker.

Renault P, Houal L, Jacquemin G, & Chambroy Y (1994a). Gas-exchange in modified atmosphere packaging. 2. Experimental results with strawberries. *International Journal of Food Science and Technology* **29** 379-394.

Renault P, Souty M, & Chambroy Y (1994b). Gas-exchange in modified atmosphere packaging.1. A new theoretical approach for micro-perforated packs. *International Journal of Food Science and Technology* **29** 365-378.

Riederer M (2006). Introduction: biology of the plant cuticle. In *Biology of the Plant Cuticle*, M Riederer & C Müller (Eds.), pp. 1-10. Oxford, UK; Ames, Iowa Blackwell Pub.

Robertson G L (1993a). Deterioration reactions in foods. In *Food Packaging: Principles and Practice*, pp. 252-302. New York: Marcel Dekker.

Robertson G L (1993b). Metal packaging materials. In *Food Packaging: Principles and Practice*, pp. 173-203. New York: Marcel Dekker.

Robertson G L (1993c). Permeability of thermoplastic polymers. In *Food Packaging: Principles and Practice*, pp. 73-110. New York: Marcel Dekker.

Robertson G L (1993d). Shelf life of foods. In *Food Packaging: Principles and Practice*, pp. 338-380. New York: Marcel Dekker.

Robinson J E, Browne K M, & Burton W G (1975). Storage characteristics of some vegetables and soft fruits. *Annals of Applied Biology* **81** 399-408.

Rogers C E (1985). Permeation of gases and vapours in polymers. In *Polymer Permeability*, J Comyn (Ed.), pp. 11-73. New York: Elsevier.

Rogers C E, Stannett V, & Szwarc M (1962). The permeation of organic vapors. In *Permeability of Plastic Films and Coated Paper to Gases and Vapors*, V Stannett (Ed.), pp. 78-101. New York: Technical Association of the Pulp and Paper Industry.

Romanazzi G, Karabulut O A, & Smilanick J L (2007). Combination of chitosan and ethanol to control postharvest gray mold of table grapes. *Postharvest Biology and Technology* **45** 134-140.

Rooney M L (1995a). Active packaging in polymer films. In *Active Food Packaging*, M.L.Rooney (Ed.), pp. 74-110. Glasgow: Blackie Academic & Professional.

Rooney M L (1995b). Overview of active food packaging. In *Active Food Packaging*, M L Rooney (Ed.), pp. 1-37. Glasgow: Blackie Academic & Professional.

Ruiz J J, Alonso A, García-Martínez S, Valero M, Blasco P, & Ruiz-Bevia F (2005). Quantitative analysis of flavour volatiles detects differences among closely related traditional cultivars of tomato. *Journal of the Science of Food and Agriculture* **85** 54-60.

Rychter A, Janes H W, Chin C K, & Frenkel C (1979). Effect of ethanol, acetaldehyde, acetic-acid, and ethylene on changes in respiration and respiratory metabolites in potato-tubers. *Plant Physiology* **64** 108-111.

Sajilata M G, Savitha K, Singhal R S, & Kanetkar V R (2007). Scalping of flavors in packaged foods. *Comprehensive Reviews in Food Science and Food Safety* **6** 17-35.

Saltveit M E, & Sharaf A R (1992). Ethanol inhibits ripening of tomato fruit harvested at various degrees of ripeness without affecting subsequent quality. *Journal of the American Society for Horticultural Science* **117** 793-798.

Schotte S, De Belie N, & De Baerdemaeker J (1999). Acoustic impulse-response technique for evaluation and modelling of firmness of tomato fruit. *Postharvest Biology and Technology* **17** 105-115.

Schreiber L, Kirsch T, & Riederer M (1996). Diffusion through cuticles: principles and models. In *Plant Cuticles : An Integrated Functional Approach*, *Environmental Plant Biology Series,* G Kerstiens (Ed.), pp. 109-119. Oxford, UK Bios Scientific.

Selke S E M, Culter J D, & Hernandez R J (2004). Mass transfer in polymeric packaging systems: sorption, diffusion, permeation and shelf life. In *Plastics Packaging :*

Properties, Processing, Applications, and Regulations, 2nd, pp. 333-374. Cincinnati, Ohio: Hanser Gardner Publications.

Serrano M, Martinez-Romero D, Castillo S, Guillen F, & Valero D (2005). The use of natural antifungal compounds improves the beneficial effect of MAP in sweet cherry storage. *Innovative Food Science & Emerging Technologies* **6** 115-123.

Shirazi A, & Cameron A C (1992). Controlling relative humidity in modified atmosphere packages of tomato fruit. *HortScience* **2** 14-16.

Sholberg P, Haag P, Hocking R, & Bedford K (2000). The use of vinegar vapor to reduce postharvest decay of harvested fruit. *HortScience* **35** 898-903.

Singh S P, & Rao D V S (2005). Quality assurance of papaya by shrink film wrapping during storage and ripening. *Journal of Food Science and Technology-Mysore* **42** 523-525.

Smith J P, Hoshino J, & Abe Y (1995). Interactive packaging involving sachet technology. In *Active Food Packaging*, M L Rooney (Ed.), pp. 143-173. Glasgow: Blackie Academic & Professional.

Smith J P, Ooraikul B, Koersen W J, Voort F R v d, Jackson E D, & Lawrence R A (1987). Shelf life extension of a bakery product using ethanol vapor. *Food Microbiology* **4** 329-337.

Solbakken A, & Reyerson L H (1959). Sorption and magnetic susceptibility studies on nitric oxide-silica gel systems at a number of temperature. *Journal of Physical Chemistry* **63** 1622-1625.

Solomos T (1987). Principles of gas exchange in bulky plant tissues. *HortScience* **22** 766-771.

Song J, Hildebrand P D, Fan L H, Forney C F, Renderos W E, Campbell-Palmer L, & Doucette C (2007). Effect of hexanal vapor on the growth of postharvest pathogens and fruit decay. *Journal of Food Science* **72** M108-M112.

Song J, Leepipattanawit R, Deng W M, & Beaudry R M (1996). Hexanal vapor is a natural, metabolizable fungicide: inhibition of fungal activity and enhancement of aroma biosynthesis in apple slices. *Journal of the American Society for Horticultural Science* **121** 937-942.

Song Y, Vorsa N, & Yam K L (2002). Modeling respiration-transpiration in a modified atmosphere packaging system containing blueberry. *Journal of Food Engineering* **53** 103-109.

Soroka W (1995). Paper and paperboard. In *Fundamentals of Packaging Technology*, 2nd, pp. 97-115. Virginia: Institute of Packaging Professionals.

Spotts R A, Sholberg P L, Randall P, Serdani M, & Chen P M (2007). Effects of 1-MCP and hexanal on decay of d'Anjou pear fruit in long-term cold storage. *Postharvest Biology and Technology* **44** 101-106.

Steffan D G, & Akgerman A (2001). Thermodynamic modeling of binary and ternary adsorption on silica gel. *AIChE Journal* **47** 1234-1246.

Stone E J, Hall R M, & Kazeniac S J (1975). Formation of aldehydes and alcohols in tomato fruit from U-^{14}C-labeled linolenic and linoleic acids. *Journal of Food Science* **40** 1138-1141.

Sugiura T, Kuroda H, Ito D, & Honjo H (2001). Correlations between specific gravity and soluble solids concentration in grape berries. *Journal of the Japanese Society for Horticultural Science* **70** 380-384.

Suzuki Y, Uji T, & Terai H (2004). Inhibition of senescence in broccoli florets with ethanol vapor from alcohol powder. *Postharvest Biology and Technology* **31** 177-182.

Talasila P C, & Cameron A C (1997). Free-volume changes in flexible, hermetic packages containing respiring produce. *Journal of Food Science* **62** 659-664.

Tanner D J (1998). *Mathematical Modelling for Design of Horticultural Packaging.* Massey University, Palmerston North, New Zealand.

Terry L A, Ilkenhans T, Poulston S, Rowsell L, & Smith A W J (2007). Development of new palladium-promoted ethylene scavenger. *Postharvest Biology and Technology* **45** 214-220.

Thiagu R, Chand N, Habibunnisa E A, Prasad B A, & Ramana K V R (1991). Effect of evaporative cooling storage on ripening and quality of tomato. *Journal of Food Quality* **14** 127-144.

Thielmann F (2004). Introduction into the characterisation of porous materials by inverse gas chromatography. *Journal of Chromatography A* **1037** 115-123.

Thomas W J, & Crittenden B (1998a). Adsorbents. In *Adsorption Technology and Design*, pp. 8-30. Oxford, Boston: Butterworth-Heinemann.

Thomas W J, & Crittenden B (1998b). Fundamentals of adsorption equilibrium. In *Adsorption Technology and Design*, pp. 31-65. Oxford, Boston: Butterworth-Heinemann.

Thompson J F, & Mitchell F G (2002). Packages for horticultural crops. In *Postharvest Technology of Horticultural Crops*, 3rd, A A Kader (Ed.), pp. 85-95. Oakland: University of California Agriculture and Natural Resources.

Tien C (1994). Respresentation, correlation, and prediction of single-component adsorption equilibrium. In *Adsorption Calculations and Modeling*, pp. 15-41. Boston: Butterworth-Heinemann.

Tokarev A, Friess K, Machkova J, Sipek M, & Yampolskii Y (2006). Sorption and diffusion of organic vapors in amorphous Teflon AF2400. *Journal of Polymer Science Part B-Polymer Physics* **44** 832-844.

Triantafyllou V I, Akrida-Demertzi K, & Demertzis P G (2005). Determination of partition behavior of organic surrogates between paperboard packaging materials and air. *Journal of Chromatography A* **1077** 74-79.

Tripathi P, & Dubey N K (2004). Exploitation of natural products as an alternative strategy to control postharvest fungal rotting of fruit and vegetables. *Postharvest Biology and Technology* **32** 235-245.

Utama I M S, Wills R B H, Ben-Yehoshua S, & Kuek C (2002). *In vitro* efficacy of plant volatiles for inhibiting the growth of fruit and vegetable decay microorganisms. *Journal of Agricultural and Food Chemistry* **50** 6371-6377.

Utto W (2001). *The Design of Modified Atmosphere Perforated Plastic Packaging for Fresh Chillies.* Massey University, Palmerston North, New Zealand.

Utto W, Mawson A J, Bronlund J E, & Wong K K Y (2005). Active packaging technologies for horticultural produce. *Food New Zealand* **5** 21-32.

Valenzuela D P (1989). *Adsorption Equilibrium Data Handbook*. Englewood Cliffs, N.J.: Prentice Hall.

Valverde J M, Guillen F, Martinez-Romero D, Castillo S, Serrano M, & Valero D (2005). Improvement of table grapes quality and safety by the combination of modified atmosphere packaging (MAP) and eugenol, menthol, or thymol. *Journal of Agricultural and Food Chemistry* **53** 7458-7464.

Vaughn S F, Spencer G F, & Shasha B S (1993). Volatile compounds from raspberry and strawberry inhibit postharvest decay fungi. *Journal of Food Science* **58** 793-796.

Vermeiren L, Heirlings L, F D, & Debevere J (2003). Oxygen, ethylene and other scavengers. In *Novel Food Packaging Techniques*, R.Ahvenainen (Ed.), pp. 22-49. Cambridge: Woodhead Publishing Limited.

Vick B A, & Zimmerman D C (1987). Oxidative systems for modification of fatty acids: the lipoxygenase pathway. In *The Biochemistry of Plants*, P K Stumpf (Ed.), pp. 53-90. New York: Academic Press.

Weber W J (1985). Adsorption theory, concepts and models. In *Adsorption Technology : A Step-by-Step Approach to Process Evaluation and Application*, F L Slejko (Ed.), pp. 1-35. New York: Marcel Dekker.

Wenzl T, & Lankmayr E P (2001). Effect of the water content of cardboard on the static headspace extraction of volatile aldehydes. *Journal of Separation Science* **24** 885-888.

Wijeratnam R S W, Hewajulige I G N, & Abeyratne N (2005). Postharvest hot water treatment for the control of *Thielaviopsis* black rot of pineapple. *Postharvest Biology and Technology* **36** 323-327.

Willige R v, Schoolmeester D, Ooij A v, Linssen J, & Voragen A (2002). Influence of storage time and temperature on absorption of flavor compounds from solutions by plastic packaging material. *Journal of Food Science* **67** 2023-2031.

Wills R B H, McGlasson W B, Graham D, Lee T H, & Hall E G (1989). Effects of water loss and humdity. In *Postharvest: An Introduction to the Physiology and Handling of Fruit and Vegetables*, pp. 53-60. New South Wales: New South Wales University Press.

Wilson C L, & Wisniewski M E (1989). Biological control of postharvest diseases of fruits and vegetables - an emerging technology. *Annual Review of Phytopathology* **27** 425-441.

Wisniewski M E, & Wilson C L (1992). Biological control of postharvest diseases of fruits and vegetables-recent advances. *HortScience* **27** 94-98.

Wolford J J (1998). *Hexanal Vapor to Control Decay of Sliced Apples in Modified Atmosphere Packages Using Metallocene Film.* Michigan State University, US.

Yahia E M, & Gonzalez-Aguilar G (1998). Use of passive and semi-active atmospheres to prolong the postharvest life of avocado fruit. *Food Science and Technology-Lebensmittel-Wissenschaft & Technologie* **31** 602-606.

Yam K L, & Lee D S (1995). Design of modified atmosphere packaging for fresh produce. In *Active Food Packaging*, M L Rooney (Ed.), pp. 55-73. Glasgow: Blackie Academic & Professional.

Yang M, Dang T Q, Zhang J S, Gao X F, & Li H (2005). Determination of building materials' transport properties for modeling VOC emissions. *ASHRAE Transactions* **111** 88-100.

Yearsley C W, Banks N H, Ganesh S, & Cleland D J (1996). Determination of lower oxygen limits for apple fruit. *Postharvest Biology and Technology* **8** 95-109.

Zagory D (1995). Ethylene-removing packaging. In *Active Food Packaging*, M L Rooney (Ed.), pp. 38-54. Glasgow: Blackie Academic & Professional.

Zhang W, Li X, Wang X, Wang G, Zheng J, Abeysinghe D C, Ferguson I B, & Chen K (2007). Ethanol vapour treatment alleviates postharvest decay and maintains fruit quality in Chinese bayberry. *Postharvest Biology and Technology* **46** 195-198.

Zhou L, Liu X W, Li J W, Sun Y, & Zhou Y P (2006). Sorption/desorption equilibrium of methane in silica gel with pre-adsorption of water. *Colloids and Surfaces a-Physicochemical and Engineering Aspects* **273** 117-120.

Zhou L, Sun Y, & Zhou Y P (2002). Enhancement of the methane storage on activated carbon by preadsorbed water. *AIChE Journal* **48** 2412-2416.

Zhu L, Chiu F C, Fu Q, Quirk R P, & Cheng S Z D (1999). Physical constants of poly(ethylene). In *Polymer Handbook*, J. Brandrup, E H Immergut & E A Grulke (Eds.), pp. V/9-V/18. New York: Wiley.

Zobel M G R (1982). Measurement of odour permeability of polypropylene packaging films at low odourant levels. *Polymer Testing* **3** 133-142.

Zobel M G R (1985). The odor permeability of polypropylene packaging film. *Polymer Testing* **5** 153-165.

Appendix A

ACTIVE PACKAGING TECHNOLOGIES FOR HORTICULTURAL PRODUCE

Material from this chapter was published in *Food New Zealand* as:

Utto W, Mawson A J, Bronlund J E, & Wong K K Y (2005). Active packaging technologies for horticultural produce. *Food New Zealand* **5** 21-32.

The published article is provided in the 'PDF' format in the attached CD-ROM. The filename is 'Peer Review_Active Packaging Technology_FNZMarApr2005.pdf'.

Appendix B

HEXANAL REDUCES INFECTION OF TOMATOES BY *BOTRYTIS CINEREA* WHILST MAINTAINING QUALITY

Material from this chapter was published in *Postharvest Biology and Technology* as:

Utto W, Mawson A J, & Bronlund J E (2008). Hexanal reduces infection of tomatoes by *Botrytis cinerea* whilst maintaining quality. *Postharvest Biology and Technology* **47** 434-437.

The published article is provided in the 'PDF' format in the attached CD-ROM. The filename is 'Hexanal_Bcinerea_PBT2008_.pdf'.

Appendix C

GAS CHROMATOGRAPHIC ANALYSIS PROCEDURES

Gas chromatography conditions for identifying acetaldehyde and ethanol using the FID-GC described in Chapter 3 are provided in Table C-1. Standard solutions were prepared by dissolving acetaldehyde (≥ 99%, GC grade, Fluka, supplied by Sigma Aldrich, New Zealand) or ethanol (≥99.8% GC grade, Riedel-de Haën supplied by Sigma Aldrich, New Zealand) individually in high purity deionised water (Milli-Q® water, Millipore Corporation, US). For hexanol and hexylacetate, standard curves were not developed and identification of the peaks was based on their retention times determined using solutions of these chemicals in liquid ethanol (as described above). GC procedures utilised to quantify hexanol and hexylacetate were the same as those used for identifying hexanal (described in Chapter 3).

Table C-1 Gas chromatography conditions for identifying acetaldehyde and ethanol

Operation condition	Compound	
	Acetaldehyde	**Ethanol**
Detector temperature (ºC)	250	260
Inlet temperature (ºC)	140	250
Column temperature (ºC)	35	100
Carrier gas flowrate (ml·min^{-1})	2	2
Optimal spilt flow ratio	2:400	2:400
Peak retention time (min)	1.57± 0.02	1.71± 0.02

Concentrations (mol·m^{-3}) of VOCs including hexanal, acetaldehyde, and ethanol were calculated using Eq. C-1.

$$C^i = \frac{K^i_{GC} A^i_{GC}}{Vol_{inj}} \qquad \textbf{(Eq. C-1)}$$

where

C^i = Concentration of VOC *i* (mol·m^{-3})

K^i_{GC} = Detector response or slope (mol·area^{-1}) of standard curve of VOC *i* as shown in Figure C-1

A^i_{GC} = Area of gas chromatogram peak from the injected volume of sample

(area)

Vol_{inj} = Injected volume of sample (m^3)

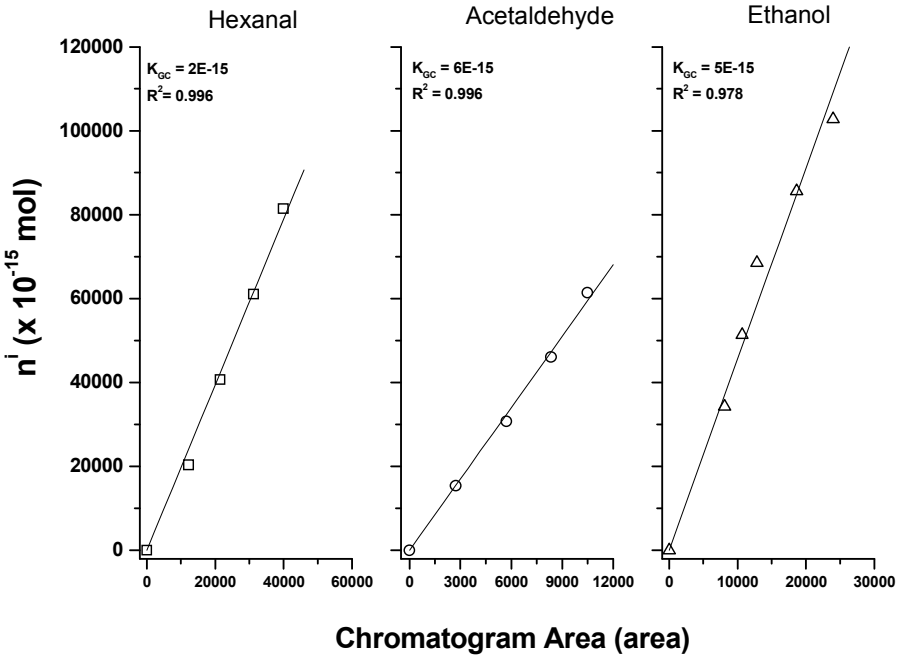

Figure C-1 Standard curves of hexanal, acetaldehyde, and ethanol (n^i = number of moles)

Appendix D

MODELLING MASS TRANSFER ACROSS FILM

D.1 Derivations of mathematical models describing rate of hexanal release from sachet to package headspace

Diffusion mass transfer of hexanal vapour across the sachet film to the package headspace can be described as shown in Eq. D-1.

$$\frac{\partial C_{scfl}^{Hxl}}{\partial t} = \frac{\partial}{\partial x_{scfl}}\left(D_{scfl}^{Hxl} \frac{\partial C_{scfl}^{Hxl}}{\partial x_{scfl}} \right) \quad \textbf{(Eq. D-1)}$$

where

D_{scfl}^{Hxl} = Hexanal mass diffusivity in the sachet film ($m^2 \cdot s^{-1}$)

C_{scfl}^{Hxl} = Hexanal concentration in sachet film ($mol \cdot m^{-3}$)

Initial and boundary conditions can be expressed as:

$$C_{scfl}^{Hxl} = 0 \qquad for\ t = 0\ and\ 0 < x_{scfl} < L_{scfl} \quad \textbf{(Eq. D-2)}$$

$$C_{scfl}^{Hxl} = S_{scfl}^{Hxl} \cdot C_{g,bed}^{Hxl} \cdot RT_{pkg} \qquad for\ all\ t\ and\ x_{scfl} = 0 \quad \textbf{(Eq. D-3)}$$

$$C_{scfl}^{Hxl} = S_{scfl}^{Hxl} \cdot C_{pkhs}^{Hxl} \cdot RT_{pkg} \qquad for\ all\ t\ and\ x_{scfl} = L_{scfl} \quad \textbf{(Eq. D-4)}$$

where

S_{scfl}^{Hxl} = Sachet film solubility to hexanal ($mol \cdot m^{-3} \cdot Pa^{-1}$)

According to Zobel (1982) and Robertson (1993c), the solubility coefficient is likely to increase with concentration due to interactions between the VOCs and the polymer film, and this can occur in hexanal permeation systems. Piringer (2000) (page 270) suggested that if solubility is constant, a linear plot should result of the equilibrium amount adsorbed (m_e; determined by the gained weight of film after the permeability experiment) against the equilibrium pressure of gas being used (p_e), following Henry's law. From experimental results in the present work, the relationship between m_e and p_e for all tested films at both 10 and 20ºC was reasonably linear and this model explained more than 75% (R^2) of the total variation in the data. The lowest R^2 value (i.e. 0.75) was observed at

20ºC for LDPE. This finding supported the information discussed in Chapter 4 where high variation of permeability values was observed amongst LDPE films. Based on the discussion above, it could be assumed that solubility stays reasonably constant and presumably concentration independent. Because of this, Eq. D-1 becomes:

$$\frac{\partial C_{scfl}^{Hxl}}{\partial t} = \frac{\partial}{\partial x_{scfl}} \left(D_{scfl}^{Hxl} S_{scfl}^{Hxl} RT_{pkg} \frac{\partial C_{g,x_{scfl}}^{Hxl}}{\partial x_{scfl}} \right) \quad \textbf{(Eq. D-5)}$$

where

$C_{g,x_{scfl}}^{Hxl}$ = Hexanal concentration in gas phase which is in equilibrium with the sachet film material at a position x (x_{scfl}) (mol·m^{-3})

The product of diffusion coefficient and solubility coefficient is commonly considered as permeability (Robertson 1993c; Selke et al. 2004). Therefore, a relationship between the effective permeability to hexanal of sachet films (referred to in Chapter 4) and D_{scfl}^{Hxl} and S_{scfl}^{Hxl} can be described by Eq. D-6.

$$P_{scfl}^{Hxl} = D_{scfl}^{Hxl} \cdot S_{scfl}^{Hxl} = P_{scfl,0}^{Hxl} \, exp\left(C_{g,x_{scfl}}^{Hxl} \cdot b_{scfl} \right) \quad \textbf{(Eq. D-6)}$$

Substituting Eq. D-6 in Eq. D-5 then yields:

$$\frac{\partial C_{scfl}^{Hxl}}{\partial t} = \frac{\partial}{\partial x_{scfl}} \left(P_{scfl,0}^{Hxl} RT_{pkg} \, exp\left(C_{g,x_{scfl}}^{Hxl} \cdot b_{scfl} \right) \frac{\partial C_{g,x_{scfl}}^{Hxl}}{\partial x_{scfl}} \right) \quad \textbf{(Eq. D-7)}$$

Initial and boundary conditions then become:

$C_{g,x_{scfl}}^{Hxl} = 0$ *for* $t = 0$ *and* $0 < x_{scfl} < L_{scfl}$ **(Eq. D-8)**

$C_{g,x_{scfl}}^{Hxl} = C_{g,bed}^{Hxl}$ *for all* t *and* $x_{scfl} = 0$ **(Eq. D-9)**

$C_{g,x_{scfl}}^{Hxl} = C_{pkhs}^{Hxl}$ *for all* t *and* $x_{scfl} = L_{scfl}$ **(Eq. D-10)**

At steady state permeation conditions, Eq. D-7 becomes:

$$0 = \frac{\partial}{\partial x_{scfl}} \left(P_{scfl,0}^{Hxl} RT_{pkg} \, exp\left(C_{g,x_{scfl}}^{Hxl} \cdot b_{scfl} \right) \right) \frac{\partial C_{g,x_{scfl}}^{Hxl}}{\partial x_{scfl}} \quad \textbf{(Eq. D-11)}$$

By integrating Eq. D-11 once, it becomes:

$$-J_{scfl} = P^{Hxl}_{scfl,0} RT_{pkg} \; exp\left(C^{Hxl}_{g,x_{scfl}} \cdot b_{scfl} \right) \frac{\partial C^{Hxl}_{g,x_{scfl}}}{\partial x_{scfl}} \qquad \textbf{(Eq. D-12)}$$

where

J_{scfl} = Integration constant or steady-state flux at sachet boundary ($mol \cdot m^{-2} \cdot s^{-1}$)

Rearranging Eq. D-12 and integrating yields Eq. D-13 and Eq. D-14.

$$-J_{scfl} \partial x_{scfl} = P^{Hxl}_{scfl,0} RT_{pkg} \; exp\left(C^{Hxl}_{g,x_{scfl}} \cdot b_{scfl} \right) \partial C^{Hxl}_{g,x_{scfl}} \qquad \textbf{(Eq. D-13)}$$

$$-J_{scfl} x_{scfl} + d = \frac{P^{Hxl}_{scfl,0} RT_{pkg}}{b_{scfl}} exp\left(C^{Hxl}_{g,x_{scfl}} \cdot b_{scfl} \right) \qquad \textbf{(Eq. D-14)}$$

where

d = Integration constant ($mol \cdot m^{-1} \cdot s^{-1}$)

From the boundary condition at $x_{scfl} = 0$ where $C^{Hxl}_{g,x_{scfl}} = C^{Hxl}_{g,bed}$, Eq. D-14 becomes:

$$d = \frac{P^{Hxl}_{scfl,0} RT_{pkg}}{b_{scfl}} exp\left(C^{Hxl}_{g,bed} \cdot b_{scfl} \right) \qquad \textbf{(Eq. D-15)}$$

Substituting Eq. D-15 in Eq. D-14 yields:

$$-J_{scfl} x_{scfl} + \frac{P^{Hxl}_{scfl,0} RT_{pkg}}{b_{scfl}} exp\left(C^{Hxl}_{g,bed} \cdot b_{scfl} \right) = \frac{P^{Hxl}_{scfl,0} RT_{pkg}}{b_{scfl}} exp\left(C^{Hxl}_{g,x_{scfl}} \cdot b_{scfl} \right) \qquad \textbf{(Eq. D-16)}$$

From the boundary condition $x_{scfl} = L_{scfl}$ where $C^{Hxl}_{g,x_{scfl}} = C^{Hxl}_{pkhs}$, Eq. D-16 becomes:

$$-J_{scfl} L_{scfl} + \frac{P^{Hxl}_{scfl,0} RT_{pkg}}{b_{scfl}} exp\left(C^{Hxl}_{g,bed} \cdot b_{scfl} \right) = \frac{P^{Hxl}_{scfl,0} RT_{pkg}}{b_{scfl}} exp\left(C^{Hxl}_{pkhs} \cdot b_{scfl} \right) \qquad \textbf{(Eq. D-17)}$$

By rearranging Eq. D-17, the steady-state permeation of hexanal vapour through the sachet film material of which film permeability is dependent on hexanal vapour concentration can be described as shown in Eq. D-18.

$$J_{scfl} = \frac{P^{Hxl}_{scfl,0} RT_{pkg}}{b_{scfl} L_{scfl}} \left(exp\left(C^{Hxl}_{g,bed} \cdot b_{scfl} \right) - exp\left(C^{Hxl}_{pkhs} \cdot b_{scfl} \right) \right), \text{ for } t > 0 \qquad \textbf{(Eq. D-18)}$$

D.2 Modelling concentration gradients and fluxes across experimentally utilised films

D.2.1 Modelling concentration gradients

From section D.1, the mathematical model for describing a relationship between equilibrium vapour concentration and film position (the concentration gradient) can be obtained by substituting Eq. D-18 in Eq. D-16 and rearranging to yield Eq. D-19.

$$\frac{x_{scfl}}{L_{scfl}} = \frac{exp\left(C^{Hxl}_{g,bed} \cdot b_{scfl} \right) - exp\left(C^{Hxl}_{g,x_{scfl}} \cdot b_{scfl} \right)}{exp\left(C^{Hxl}_{g,bed} \cdot b_{scfl} \right) - exp\left(C^{Hxl}_{pkhs} \cdot b_{scfl} \right)} \qquad \textbf{(Eq. D-19)}$$

Given similar initial and boundary conditions to those of the sachet film, concentration gradient of films (Tyvek®, OPP and LDPE) used in the determination of hexanal permeability (section 4.2.2) could be described by Eq. D-19 and this is expressed as Eq. D-20.

$$\frac{x_{film}}{L_{film}} = \frac{exp\left(C^{Hxl}_{h,conc} \cdot b_{film} \right) - exp\left(C^{Hxl}_{g,x_{film}} \cdot b_{film} \right)}{exp\left(C^{Hxl}_{h,conc} \cdot b_{film} \right) - exp\left(C^{Hxl}_{l,conc} \cdot b_{film} \right)} \qquad \textbf{(Eq. D-20)}$$

Given the initial and boundary conditions of permeation through films in the permeability cell as:

$$C^{Hxl}_{g,x_{film}} = 0 \qquad for\ t = 0\ and\ 0 < x_{film} < L_{film} \qquad \textbf{(Eq. D-21)}$$

$$C^{Hxl}_{g,x_{film}} = C^{Hxl}_{h,conc} \qquad for\ all\ t\ and\ x_{film} = 0 \qquad \textbf{(Eq. D-22)}$$

$$C^{Hxl}_{g,x_{film}} = C^{Hxl}_{l,conc} \qquad for\ all\ t\ and\ x_{film} = L_{film} \qquad \textbf{(Eq. D-23)}$$

D.2.2 Modelling fluxes

In section 4.2.2, comparisons of flux across a LDPE film calculated using Eq. 2-8 (Fick's first law) and Eq. 4-5 were demonstrated. The derivation of Eq. 4-5 was based on Eq. D-18, in which parameters were appropriately replaced and can be expressed as Eq. D-24.

$$J_{film} = \frac{P_{film,0}^{Hxl} RT_{pkg}}{b_{film} L_{scfl}} \left(exp\left(C_{h,conc}^{Hxl} \cdot b_{film} \right) - exp\left(C_{l,conc}^{Hxl} \cdot b_{film} \right) \right) \quad \textbf{(Eq. D-24)}$$

D.3 Alternative model describing the rate of hexanal release from sachet to package headspace (based on an assumption of the Langmuir relationship between hexanal vapour and LDPE film sorption)

As an alternative to assuming a Henry's law isotherm relationship between the vapour phase concentration and absorbed volatile concentrations in the film, the Langmuir type relationship can be used. In this situation the effective permeability will be a strong function of concentration at low partial pressures but less variable when the film becomes saturated with absorbed volatile. As such the equations derived in section D.2.2 would overpredict mass transfer rates through the film at high feed hexanal partial pressure.

At steady-state and provided concentration-independent mass transfer diffusivity (D_{scfl}^{Hxl}), diffusion mass transfer of hexanal vapour across the sachet film to package headspace can be described as shown in Eq. D-25.

$$0 = \frac{\partial}{\partial x_{scfl}} \left(D_{scfl}^{Hxl} \frac{\partial C_{scfl}^{Hxl}}{\partial x_{scfl}} \right) \quad \textbf{(Eq. D-25)}$$

By separating variables in Eq. D-25 and incorporating $C_{g,x_{scfl}}^{Hxl}$, Eq. D-26 is obtained:

$$0 = \frac{\partial}{\partial x_{scfl}} \left(D_{scfl}^{Hxl} \frac{\partial C_{scfl}^{Hxl}}{\partial C_{g,x_{scfl}}^{Hxl}} \frac{\partial C_{g,x_{scfl}}^{Hxl}}{\partial x_{scfl}} \right) \quad \textbf{(Eq. D-26)}$$

The Langmuir relationship between hexanal vapour and LDPE film sorption (considered at position x_{scfl}) can be described as:

$$C_{scfl}^{Hxl} = \frac{k_{Lgmfl,2}^{Hxl} \cdot C_{g,x_{scfl}}^{Hxl}}{1 + k_{Lgmfl,1}^{Hxl} \cdot C_{g,x_{scfl}}^{Hxl}} \quad \textbf{(Eq. D-27)}$$

where

$k_{Lgmfl,1}^{Hxl}$ = Coefficient of Langmuir relationship between hexanal vapour and LDPE film sorption ($m^3 \cdot mol^{-1}$)

$k^{Hxl}_{Lgmfl,2}$ = Coefficient of Langmuir relationship between hexanal vapour and LDPE film sorption (dimensionless)

The derivative of C^{Hxl}_{scfl} in respect to $C^{Hxl}_{g,x_{scfl}}$ can be expressed as:

$$\frac{\partial C^{Hxl}_{scfl}}{\partial C^{Hxl}_{g,x_{scfl}}} = \frac{k^{Hxl}_{Lgmfl,2}}{\left(1 + k^{Hxl}_{Lgmfl,1} \cdot C^{Hxl}_{g,x_{scfl}}\right)^2} \quad \textbf{(Eq. D-28)}$$

Substituting Eq. D-28 in Eq. D-26, Eq. D-29 is obtained:

$$0 = \frac{\partial}{\partial x_{scfl}}\left(D^{Hxl}_{scfl} \frac{k^{Hxl}_{Lgmfl,2}}{\left(1 + k^{Hxl}_{Lgmfl,1} \cdot C^{Hxl}_{g,x_{scfl}}\right)^2} \frac{\partial C^{Hxl}_{g,x_{scfl}}}{\partial x_{scfl}}\right) \quad \textbf{(Eq. D-29)}$$

Initial and boundary conditions can be expressed as:

$C^{Hxl}_{g,x_{scfl}} = 0$ *for* $t = 0$ *and* $0 < x_{scfl} < L_{scfl}$ **(Eq. D-30)**

$C^{Hxl}_{g,x_{scfl}} = C^{Hxl}_{g,bed}$ *for all* t *and* $x_{scfl} = 0$ **(Eq. D-31)**

$C^{Hxl}_{g,x_{scfl}} = C^{Hxl}_{pkhs}$ *for all* t *and* $x_{scfl} = L_{scfl}$ **(Eq. D-32)**

Integrating Eq. D-29 once, it becomes:

$$-J_{scfl} = \frac{D^{Hxl}_{scfl} \cdot k^{Hxl}_{Lgmfl,2}}{\left(1 + k^{Hxl}_{Lgmfl,1} \cdot C^{Hxl}_{g,x_{scfl}}\right)^2} \frac{\partial C^{Hxl}_{g,x_{scfl}}}{\partial x_{scfl}} \quad \textbf{(Eq. D-33)}$$

Rearranging Eq. D-33 and integrating yields Eq. D-34 and Eq. D-35.

$$-J_{scfl}\,\partial x_{scfl} = D^{Hxl}_{scfl} \cdot k^{Hxl}_{Lgmfl,2} \frac{\partial C^{Hxl}_{g,x_{scfl}}}{\left(1 + k^{Hxl}_{Lgmfl,1} \cdot C^{Hxl}_{g,x_{scfl}}\right)^2} \quad \textbf{(Eq. D-34)}$$

$$-J_{scfl} x_{scfl} + d = -D^{Hxl}_{scfl} \cdot k^{Hxl}_{Lgmfl,2}\left(\frac{1}{\left(k^{Hxl}_{Lgmfl,1} + \left(\left(k^{Hxl}_{Lgmfl,1}\right)^2 \cdot C^{Hxl}_{g,x_{scfl}}\right)\right)}\right) \quad \textbf{(Eq. D-35)}$$

From the boundary condition at $x_{scfl} = 0$ where $C^{Hxl}_{g,x_{scfl}} = C^{Hxl}_{g,bed}$, Eq. D-35 becomes:

$$d = -D_{scfl}^{Hxl} \cdot k_{Lgmfl,2}^{Hxl} \left(\frac{1}{\left(k_{Lgmfl,1}^{Hxl} + \left(\left(k_{Lgmfl,1}^{Hxl} \right)^2 \cdot C_{g,bed}^{Hxl} \right) \right)} \right) \quad \textbf{(Eq. D-36)}$$

Substituting Eq. D-36 in Eq. D-35 yields:

$$-J_{scfl} x_{scfl} - D_{scfl}^{Hxl} \cdot k_{Lgmfl,2}^{Hxl} \left(\frac{1}{\left(k_{Lgmfl,1}^{Hxl} + \left(\left(k_{Lgmfl,1}^{Hxl} \right)^2 \cdot C_{g,bed}^{Hxl} \right) \right)} \right) = -D_{scfl}^{Hxl} \cdot k_{Lgmfl,2}^{Hxl} \left(\frac{1}{\left(k_{Lgmfl,1}^{Hxl} + \left(\left(k_{Lgmfl,1}^{Hxl} \right)^2 \cdot C_{g,x_{scfl}}^{Hxl} \right) \right)} \right)$$

(Eq. D-37)

From the boundary condition $x_{scfl} = L_{scfl}$ where $C_{g,x_{scfl}}^{Hxl} = C_{pkhs}^{Hxl}$, Eq. D-37 becomes:

$$-J_{scfl} L_{scfl} - D_{scfl}^{Hxl} \cdot k_{Lgmfl,2}^{Hxl} \left(\frac{1}{\left(k_{Lgmfl,1}^{Hxl} + \left(\left(k_{Lgmfl,1}^{Hxl} \right)^2 \cdot C_{g,bed}^{Hxl} \right) \right)} \right) = -D_{scfl}^{Hxl} \cdot k_{Lgmfl,2}^{Hxl} \left(\frac{1}{\left(k_{Lgmfl,1}^{Hxl} + \left(\left(k_{Lgmfl,1}^{Hxl} \right)^2 \cdot C_{pkhs}^{Hxl} \right) \right)} \right)$$

(Eq. D-38)

By rearranging Eq. D-38, the steady-state permeation (i.e. positive flux) of hexanal vapour through sachet film material for which film solubility is described by Langmuir relationship can be expressed as shown in Eq. D-39.

$$J_{scfl} = \frac{D_{scfl}^{Hxl} \cdot k_{Lgmfl,2}^{Hxl}}{L_{scfl} k_{Lgmfl,1}^{Hxl}} \left(\frac{1}{\left(1 + k_{Lgmfl,1}^{Hxl} \cdot C_{g,bed}^{Hxl} \right)} - \frac{1}{\left(1 + k_{Lgmfl,1}^{Hxl} \cdot C_{pkhs}^{Hxl} \right)} \right), \text{ for } t > 0 \quad \textbf{(Eq. D-39)}$$

Given $Z_{Lgmfl}^{Hxl} = \frac{D_{scfl}^{Hxl} \cdot k_{Lgmfl,2}^{Hxl}}{L_{scfl} k_{Lgmfl,1}^{Hxl}}$ (where L_{scfl} is the LDPE film thickness; 30μm); Z_{Lgmfl}^{Hxl} and $k_{Lgmfl,1}^{Hxl}$ were identified through fitting by minimising sum of squared residuals in Microsoft Excel® using steady-state flux data of the sachet system (Figure 6-17). Values of Z_{Lgmfl}^{Hxl} and $k_{Lgmfl,1}^{Hxl}$ are -1.26×10^{-4} mol·s^{-1}·m^{-2} and 0.10 m^3·mol^{-1}, respectively.

To predict fluxes across LDPE films at 20ºC using Eq. D-39 for analysis of hexanal mass loss (refer discussion in section 6.4.5.2), $C_{g,bed}^{Hxl}$ and C_{pkhs}^{Hxl} in Eq. D-39 were appropriately substituted by $C_{h,conc}^{Hxl}$ and $C_{l,conc}^{Hxl}$, respectively.

Appendix E

COMPARISON OF HEXANAL SORPTION ISOTHERM FOR SILICA GEL ADSORBENTS ESTIMATED BY DIFFERENT METHODS

E.1 Verification using IGC techniques

Two IGC techniques were investigated to collect hexanal sorption isotherm data in order to verify those measured using the gravimetric method. The techniques included (i) pulse, and (ii) frontal inverse gas chromatography. The principles of IGC can be found in a number of reports in the literature (Apostolopoulos & Gilbert 1983; Apostolopoulos 1985; Kontominas et al. 1994; Thielmann 2004). In both systems the absorbing compound of interest is packed into a GC column as the stationary phase. In pulse IGC, a known amount of the adsorbate is injected into the carrier before it flows through the stationery phase (Thielmann 2004). The adsorbate subsequently adsorbs onto the stationaly phase and later desorbs into the carrier steam. The key assumption of pulse IGC is that equilibrium is achieved quickly between the adsorbate molecules on the surface of the stationery phase. Frontal IGC (FIGC) involves the introduction of a continuous flow of adsorbate at a constant concentration through the packed bed of adsorbent, by means of a gaseous carrier as used in gas chromatography analysis (Thielmann 2004). After the adsorbate breaks through (i.e. is detected in the outlet stream from the column), a frontal chromatogram is developed and levels off at the plateau when an equilibrium condition is established between the mobile and stationery phases. A key assumption of the FIGC technique is that equilibrium can always be established due to its continuous nature.

E.2 Isotherm determination by pulse IGC method

E.2.1 Experimental procedures of pulse IGC

The pulse IGC experiments were performed with a gas chromatograph equipped with FID (as used in Chapter 3), following the method of Lee (2003). The injector, detector, and oven temperatures of the gas chromatograph were 200, 250, and 20ºC, respectively. The GC grade stainless steel column (100 mm long and 6 mm outer diameter, Carlo Erba, Italy)

was filled with silica gel (~ 0.3 g). Nitrogen was used as the carrier gas with a flow rate of 60 ml·min^{-1}. Methane as a nonretained species to determine the residence time of the column. The silica gel adsorbents were conditioned at 100ºC in the chromatographic column under nitrogen gas flow for ~12 hours prior to the measurement. Injection volumes of hexanal liquid (presumed to be totally evaporated after injection) were 0.1 to 1.0 ml, and 3 replicate injections were carried out. The chromatographic peak heights and areas were used to calculate isotherm data following the method of Lee (2003). From preliminary work, these experimental settings resulted in reproducible peak height, peak area, and retention time.

E.2.2 Results and discussion of pulse IGC

The hexanal sorption isotherm of silica gel adsorbents quantified by pulse IGC is shown in Figure E-1. Equilibrium sorption quantities (magnitude of 10^{-6}) at corresponding pressures were very low compared to those measured using the gravimetric method as reported in Chapter 4. Lee (2003) reported low extents of 1-MCP sorption quantified by pulse IGC at 50-70ºC for silica gel (and other adsorbents including activated clay and Tenax® sorbents), where the uptake magnitude and corresponding 1-MCP pressure were 10^{-7} g·g^{-1} and 0.1-1.4 Pa, respectively. According to Thielmann (2004), the usefulness of pulse IGC is usually limited to adsorption systems for low concentration of adsorbates (known as the Henry's law region) because high concentrations tend to broaden chromatographic peaks, indicating that the column is not at optimal conditions for analyses. In the present work, the injection volumes were more than 0.5 ml (equivalent to pressure > 0.1 Pa; calculated following Lee 2003) and yielded broad peaks, and thus it was likely that local equilibrium in the column was not achieved. Pulse IGC was accordingly considered impractical for quantifying hexanal sorption at the high concentrations required for the present work.

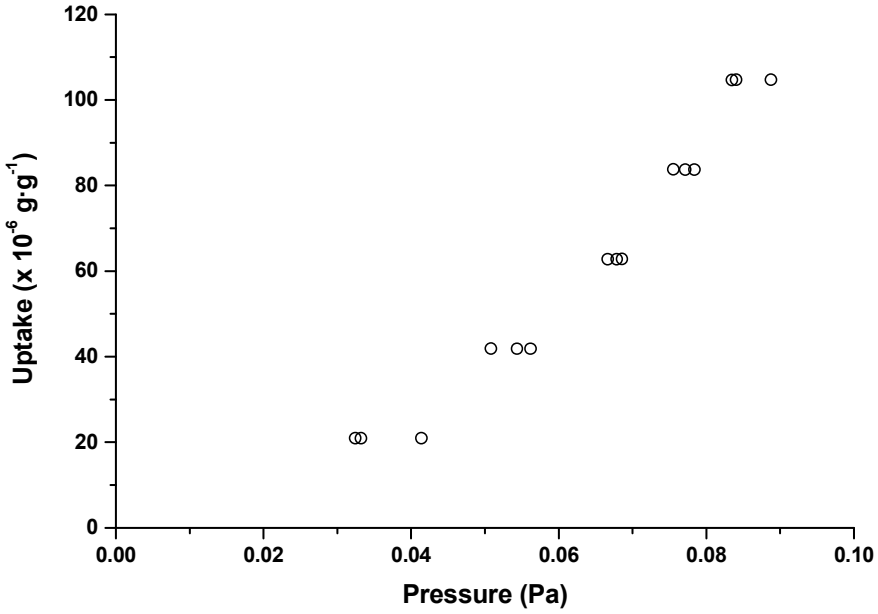

Figure E-1 Hexanal sorption isotherm for silica gel at 20ºC (3 replicates shown for each uptake) quantified by the Pulse IGC technique

E.3 Isotherm determination by frontal IGC method

E.3.1 Experimental procedures

Due to the limitations of pulse IGC, the frontal IGC method was evaluated. According to Thielmann (2004), the peak broadening caused by the uneven distribution of adsorbate within the column of the pulse technique could be minimised by using the frontal technique, because a uniform amount of adsorbate is mixed with the gaseous carrier and continuously introduced into the packed column.

The frontal IGC experimental settings and sorption isotherm calculations were performed following Apostolopoulos & Gilbert (1983) and Apostolopoulos (1985). The IGC column preparation and chromatographic operation conditions were similar to those reported for pulse IGC. The continuous flow of the saturated hexanal vapour at 21-22ºC (slightly higher than the oven temperature to minimise condensations occurring in the GC column) was generated with flow rates of 20-22 $ml \cdot min^{-1}$ (controlled by the rotameter; Aalborg VA, US) following the method of Bodenhofer et al. (1997). From preliminary work, these

experimental settings resulted in reproducible detector signal response shape, time of breakthrough and level-off (reaching plateau) at peak height.

E.3.2 Results and discussion of FIGC

The hexanal sorption isotherm determined by FIGC is shown in Figure E-2. The extent of equilibrium uptake estimated from the FIGC data were up to 3.5-fold (considered at p/p_s = 1) lower than those measured by the gravimetric method. Whilst the FIGC estimated isotherm was noticeably linear, the isotherm measured by the gravimetric method (reported in Chapter 4) showed the Type I isotherm pattern. These experimental results suggested that hexanal uptake by silica gels packed in the IGC column increased with vapour pressure but occurred with at a slow rate.

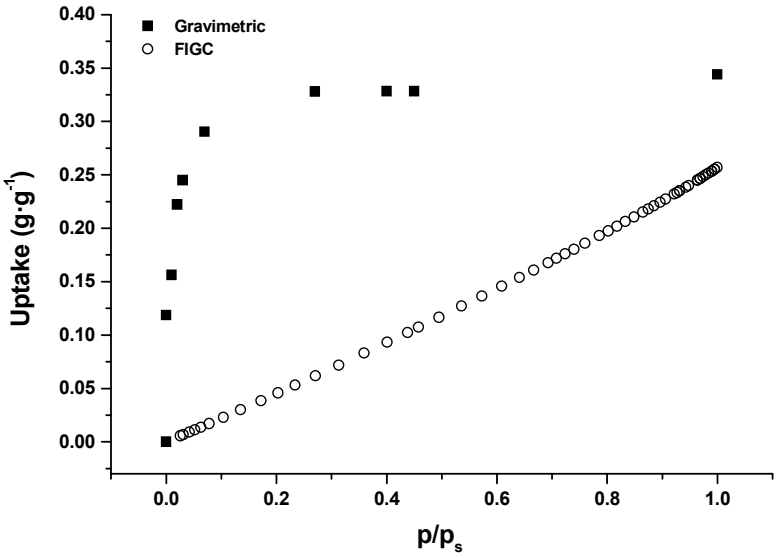

Figure E-2 Comparison of hexanal uptake by silica gel grade 40 at 20ºC, quantified by FIGC method (o) and gravimetric method (■; reported in Chapter 4)

The reason for the lower equilibrium uptake in the FIGC method (Figure E-2) may be that equilibrium conditions were not achieved within the chromatographic column. Evidence of underestimation of equilibrium uptake by the FIGC method is also available in literature, including for equilibrium sorption of water vapour sorption for dried coffee (Apostolopoulos & Gilbert 1983; Apostolopoulos 1985), and crude gliadin (a mixture of proteins of similar amino acid composition with both hydrophobic and hydrophilic properties) (Barbara et al. 1991). Apostolopoulos (1985) suggested that uptake

underestimated by the frontal method at the low pressure region was because the solid phase was not in equilibrium with the flow of adsorbate at the beginning of the sorption process. A longer contact time between mobile and solid phase would provide better equilibrium conditions because adsorbate molecules could have more opportunities to penetrate deeper inside the particles and reach more available adsorption sites (Apostolopoulos 1985). This proposition suggested that a lower flow rate of adsorbate may be required for improving the equilibrium condition in the column. By lowering hexanal flow rate from 20-22 to ~5-7 $ml \cdot min^{-1}$(the practical minimum using the apparatus used in the present work), fluctuating vapour concentrations were found, which in turn caused highly fluctuating chromatographic responses. Barbara et al. (1991) reported that even when flow rates of water vapour were sufficiently low (as < 5 $ml \cdot min^{-1}$), evidence of non-equilibrium condensation was still noticeable. Based on the findings in the present work and evidence in the literature, FIGC was not considered reliable enough to provide accurate sorption data for the hexanal/silica gel system.

Although quantifying hexanal sorption isotherm using the FIGC technique was not practical here, there is evidence in the literature showing that FIGC is a promising tool to quantify sorption isotherms (e.g. Apostolopoulos & Gilbert 1983; Apostolopoulos 1985; Steffan & Akgerman 2001). To further investigate applications of FIGC, the acetaldehyde sorption isotherm for silica gel at 14ºC as reported by Ghosh & Hines (1990) (also discussed in Chapter 4) was used as a reference. The same experimental settings as utilised for the hexanal experiments were employed for the acetaldehyde work. The saturated acetaldehyde vapour was generated following the method of Bodenhofer et al. (1997) and the flow rate was 5-7 $ml \cdot min^{-1}$. Unlike the behaviour for hexanal vapour, this flow rate range yielded uniform inlet vapour concentrations, most likely because of the very high vapour pressure of acetaldehyde (~80 kPa), compared to that of hexanal vapour (~1.1 kPa). Figure E-3 illustrates the acetaldehyde sorption isotherm determined by FIGC and compares this to the isotherm data reported by Ghosh & Hines (1990). The pattern of the acetaldehyde sorption isotherm estimated by the FIGC method was similar to that of the hexanal sorption isotherm, suggesting that equilibrium conditions between acetaldehyde and silica gel packed in the column were still not fully developed. These findings suggested that further studies are required to modify the current experimental settings to achieve better estimations of uptake, especially at the low pressure regions.

As a result of these trials, IGC is not a suitable method for obtaining sorption isotherm data for volatile compounds on carriers such as silica gel.

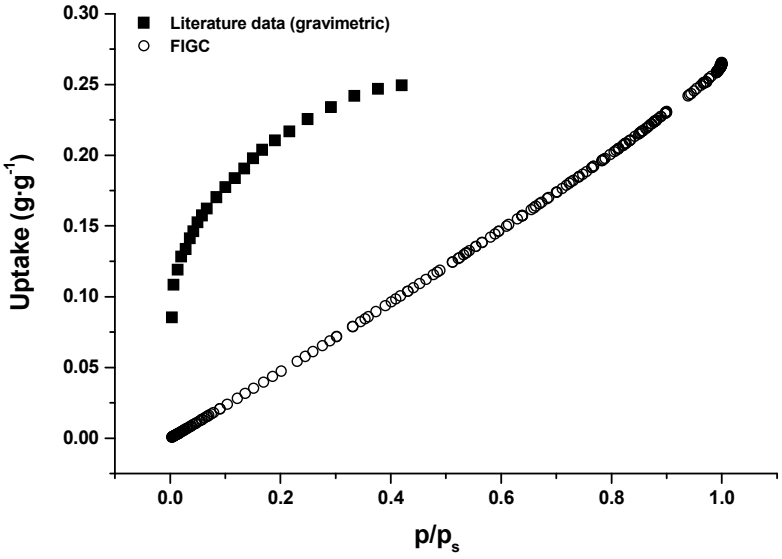

Figure E-3 Comparison of acetaldehyde uptake by silica gel grade 40 at 14ºC, quantified by the FIGC method (o) and gravimetric method (■; as reported by Ghosh & Hines 1990)

E.4 Isotherm determinations by the volumetric sorption method

E.4.1 Experimental procedures

Equilibrium data for hexanal sorption by silica gels at 10 and 20ºC were also obtained using volumetric sorption equipment (Autosorb-1; Quantachrome Inc., US). This work was conducted by Quantachrome Inc. (Florida, US) as an independent study for verifying the hexanal sorption isotherm. Sorption is determined in the Autosorb system by generating a known vapour pressure of the volatile compound in a fixed volume and then allowing this to become exposed to the sorbent. The amount of sorption or desorption is then calculated from the change in vapour pressure measured in the system. The Autosorb-1 equipment has been utilised to measured sorption isotherms of other systems for example hydrogen on single walled carbon nanotubes (SWNTs) as reported by Ansón et al. (2004).

E.4.2 Results and discussion

Hexanal sorption isotherms (adsorption and desorption) at 10 and 20ºC quantified by the volumetric method are shown in Figure E-4. Measured equilibrium data showed the Type I

isotherm and minimal hysteresis loops in the desorption branch as assumed elsewhere in this work. Although these experimental results supported the sorption isotherm shape measured by the gravimetric technique (as reported in Chapter 4), two differences were observed (i) effects of temperature on hexanal uptake were not apparent at 10 and 20ºC, and (ii) the extent of hexanal uptake measured by the volumetric method were about 3-fold lower than those observed with the gravimetric technique.

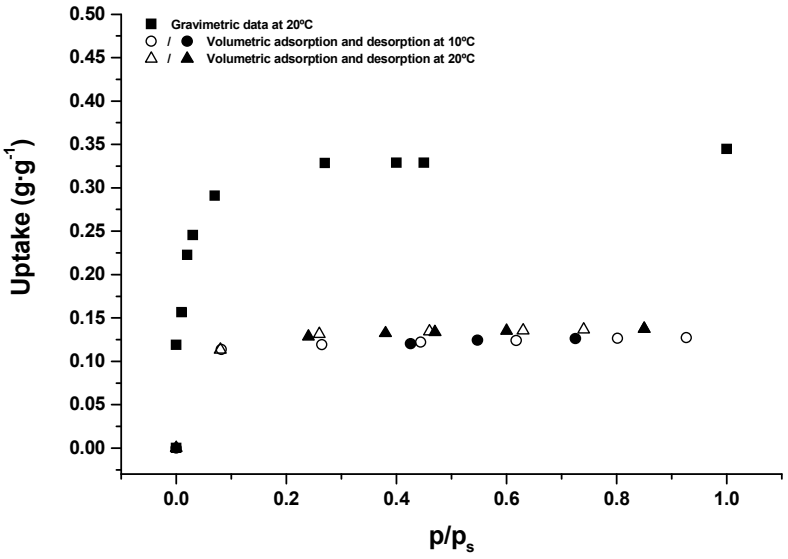

Figure E-4 Comparison of hexanal uptake by silica gel grade 40 at 20ºC quantified by the gravimetric method (as reported in Chapter 4) and by the volumetric method at 10 and 20ºC

According to Gregg & Sing (1982), minimal effects of temperature on adsorption extents may be due to non-equilibrium conditions. This could be possibly attributed to pore constrictions restricting diffusion of adsorbate into particle cavities as such effects on adsorption processes are likely among microporous adsorbents. Gregg & Sing (1982) suggested in this circumstance a sufficiently long period of time or stimulating condition (e.g. elevation of system temperature to increase diffusion kinetics of adsorbate) is required for fully-developed equilibrium of adsorption processes. The hypothesis of non-equilibrium conditions could be supported by the fact that the cumulative time of the complete sorption processe (of the Autosorb-1) was about 37 hours (at 20ºC). Such a period was considered very short compared to the timeframes utilised to obtain equilibrium condition for the gravimetric measurement, which were 4 and 2 weeks for 10 and 20ºC,

respectively. The longest cumulative time (i.e. 30 hours) was recorded at $p/p_s \approx 0.1$ and this data supported the Type I equilibrium behaviour of hexanal sorption for silica gel where most sorption processes occurred at low pressure. The hypothesis proposed in that constriction effects yielded underestimates of uptake data from the volumetric method, and improved estimates could be expected if the contact time between hexanal and silica gel was increased.

In addition to limits of mass transfer within the adsorbent, Dixon (2007)[12] suggested that the volumetric method (Autosorb-1) was limited by condensation of hexanal vapour among other key factors. Because the tubing and manifold systems of the Autosorb-1 could be heated to only 50°C, the controlled temperature was well below the normal boiling point of hexanal (~120°C), which was utilised to generate hexanal vapour. Condensation occurring inside the tubing and manifold system was therefore likely. The condensed fluid was not measured by the pressure transducers in the Autosorb-1, and was thus not correctly considered in the uptake values and may subsequently yield the differences in hexanal uptake observed. In addition to condensation, other potential factors contributing to experimental errors include leakage from the sorption chamber, sorption into rubber seals, and sample contamination. Sorption data obtained from the volumetric method were well described by the Langmuir equation. The coefficients of the Langmuir equation estimated by the nonlinear regression as discussed in Chapter 4 are summarised in Table E-1.

Table E-1 Parameter estimates and standard errors (SE) from nonlinear regression analysis of the hexanal sorption isotherm data at 20ºC as measured by the volumetric-method

Temperatures (ºC)	$C_{s,max}^{Hxl}$ (SE) [a,b]	b_{Lgm}^{Hxl} (SE)[b]	n [c]
20 [d]	0.14 (0.20)	53.06 (2.59)	6

[a] The standard errors (SE) are expressed as a percentage of the estimated values. The nonlinear regressions were conducted using the Nonlinear Regression package of the Origin 5.0 (Microcal Software Inc.)

[b] Units of $C_{s,max}^{Hxl}$ and b_{Lgm}^{Hxl} are g·g^{-1} and dimensionless, respectively

[c] n is the number of observations

[d] Because isotherm data at 10 and 20ºC are reasonably similar (refer to Figure E-4), only data at 20ºC therefore were chosen for the nonlinear regression.

[12] J. Dixon, a scientist, Quantachrome Instruments, Pers. Comm., February 2007

The standard error of the b_{Lgm}^{Hxl} value was lower than that found in data measured by the gravimetric method as discussed in Chapter 4. From Figure E-4, it could be seen that the magnitude of increases of hexanal uptake measured by the volumetric technique was significantly lower than that measured by the gravimetric method and this could explain the low variation associated with the estimated coefficients of the volumetric data.

Figure E-5 illustrates simulation results for hexanal accumulation in the package headspace for the LD2 active MAP system without tomatoes (refer to Table 6-1). This system was use as an example of how the predicted equilibrium vapour pressure in the sachet headspace was influenced by the estimated coefficients in Table E-1 in comparison to results predicted by the coefficients reported in Table 4-9. The mathematical models utilised for these simulations are found in the computational files listed in sections G.1.1 and G.1.2.

Very similar results were obtained for both (i) package headspace concentration (also showing reasonable agreement with experimental data) and (ii) equilibrium vapour concentration in sachet headspace. These results suggested that both methods estimated similar magnitudes for the reduction in the amount of adsorbed hexanal on silica gel over the storage period. This is expected because of the similar shape between the two isotherms. The sachet weight however would be underestimated if the volumetric data is used. Given minimal condensation effects and fully developed equilibrium condition, it could reasonably be assumed that hexanal uptake measured using the volumetric method should be comparable to those measured using the gravimetric method. The gravimetric sorption isotherm was extensively used in the present work because it was appeared more reliable.

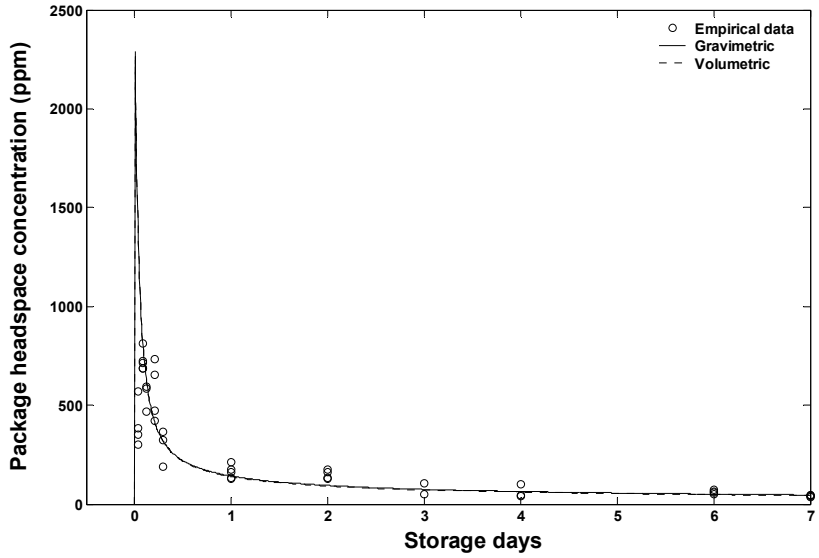

(A)

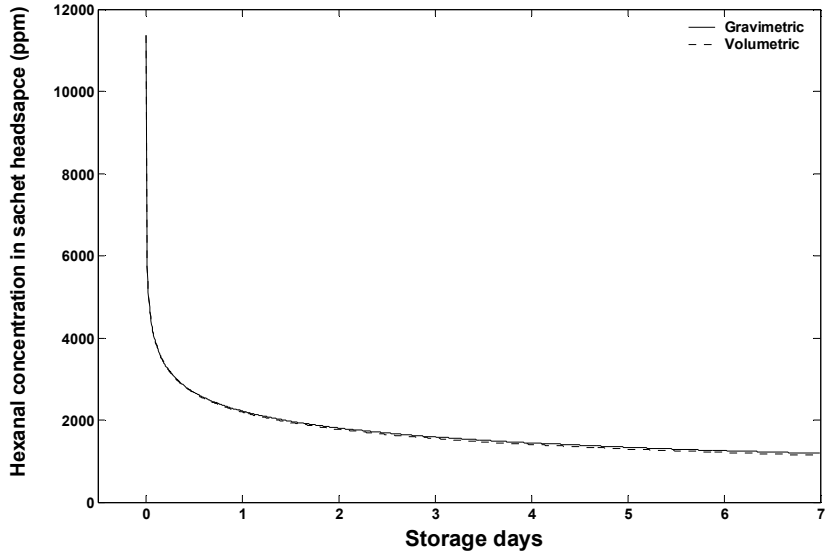

(B)

Figure E-5 Predictions of hexanal concentration in package headspace (A) and equilibrium hexanal vapour in sachet headspace (B) in a model active package (without packaged tomatoes), kept at 20ºC during 7 days, using Langmuir model coefficients which were obtained from gravimetric (solid line) and the volumetric (Autosorb-1 instrument; dotted line) sorption isotherms.

E.5 Linearisation of Langmuir model (following Ratkowsky 1990)

To enable accurate isotherm parameter fitting, the Langmuir model was linearised following the methods outlined by Ratkowsky (1990). A re-parameterisation of the Langmuir model can be expressed as Eq. E-1.

$$C_{s,bed}^{Hxl} = \frac{p/p_s}{(\theta_1 + \theta_2 (p/p_s))} \quad \textbf{(Eq. E-1)}$$

where

$$\theta_1 = \frac{1}{C_{s,max}^{Hxl} b_{Lgm}^{Hxl}} \quad \textbf{(Eq. E-2)}$$

$$\theta_2 = \frac{1}{C_{s,\max}^{Hxl}} \quad \textbf{(Eq. E-3)}$$

By rearranging Eq. E-1, a linear form can be obtained as shown in Eq. E-4.

$$\frac{p/p_s}{C_{s,bed}^{Hxl}} = \theta_1 + \theta_2 (p/p_s) \quad \textbf{(Eq. E-4)}$$

Plots of $\frac{p/p_s}{C_{s,bed}^{Hxl}}$ against p/p_s of hexanal sorption isotherm data at 10 and 20°C are shown in Figure E-6. Langmuir model coefficients estimated using linear regression following the reparameterisation proposed by Ratkowsky (1990) are summarised in Table E-2.

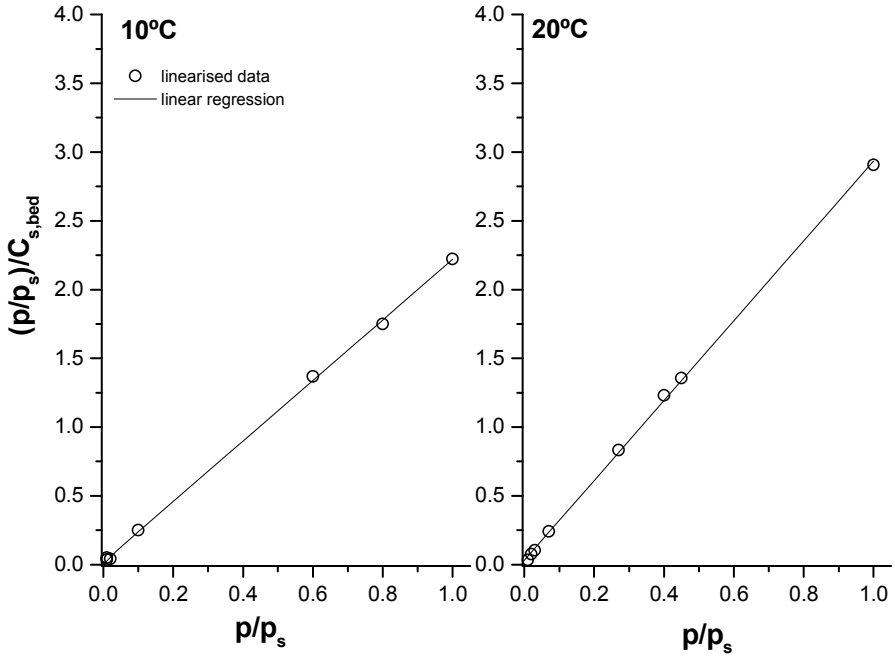

Figure E-6 Plots of $(p/p_s)/C_{s,bed}^{Hxl}$ against p/p_s for hexanal sorption isotherm data at 10 and 20°C for estimating Langmuir equation coefficients according to the reparameterisation approach proposed by Ratkowsky (1990)

Table E-2 Langmuir coefficients estimated using the reparameterisation proposed by Ratkowsky (1990)

Temperatures (ºC)	$C_{s,max}^{Hxl}$ [a]	b_{Lgm}^{Hxl} [a]	R^2 [b] (%)	n [c]
10	0.45	113.42	99	7
20	0.34	92.72	99	8

[a] Units of $C_{s,max}^{Hxl}$ and b_{Lgm}^{Hxl} are g·g^{-1} and dimensionless, respectively.

[b] R^2 is the percentage variance accounted for by the regression

[c] Number of observations

E.6 Sorption isotherms of hexanal vapour for silica gel at 10 and 20ºC (presented in molar units)

As mentioned in section 4.3.4, sorption isotherms of hexanal vapour for silica gel at 10 and 20ºC were also presented in molar units (Figure E-7) and the coefficients of the Langmuir model estimated by the nonlinear regression are shown in Table E-3.

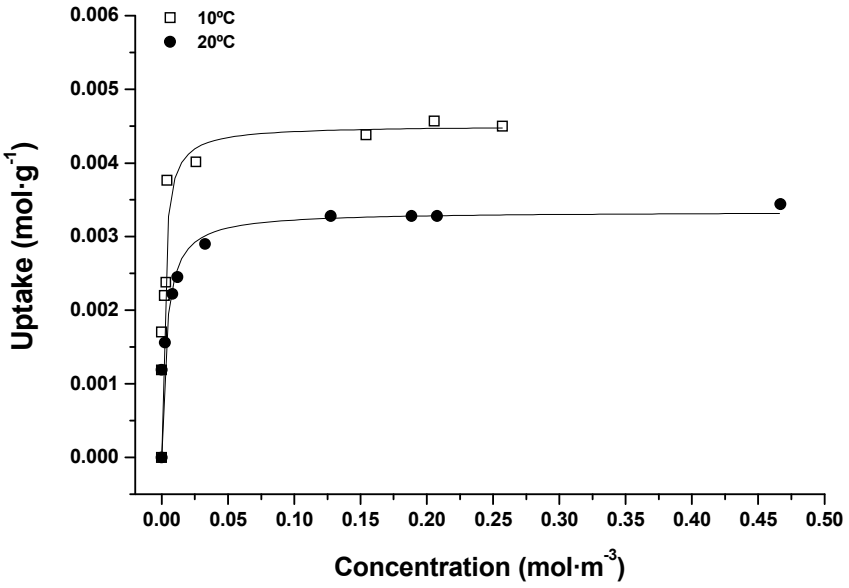

Figure E-7 Hexanal sorption isotherms for silica gel grade 40 at 10 and 20ºC, measured using a gravimetric sorption approach and presented in molar units. Solid lines were fitted using Langmuir isotherm model (Eq. 2-3).

Table E-3 Parameter estimates and standard errors (SE) from nonlinear regression analysis of hexanal sorption isotherm data for silica gel grade 40 at 10 and 20ºC (presented in molar units as illustrated in Figure E-7)

Temperature (ºC)	$C_{s,max}^{Hxl}$ (SE) [a,b]	b_{Lgm}^{Hxl} (SE)[b]	n [c]
10	0.0045 (9.53)	530 (51.9)	10
20	0.0033 (6.59)	280 (41.9)	10

[a] Standard errors (SE) is expressed as a percentage of the estimated value. The nonlinear regressions were conducted using the Nonlinear Regression package of Origin 5.0 (Microcal Software Inc.)

[b] Unit of $C_{s,max}^{Hxl}$ and b_{Lgm}^{Hxl} is mol·g^{-1} and m^3·g^{-1}, respectively.

[c] n is the number of observations.

Appendix F

FORMULATION OF GLOBAL MATHEMATICAL MODELS

F.1 Calculations of Bi values for hexanal mass transfer in sachet and package headspace

To justify the uniformity of hexanal concentration in sachet and package headspace, Bi values were estimated using Eq. 5-2 and are summarised in Table F-1.

Table F-1 Estimated Bi values for diffusion of hexanal in sachet and package atmosphere

Packaging	Films	L [a] (m)	Temperature (ºC)			
			10		20	
			k_{film}^{Hxl} [b] (m·s^{-1})	Bi [c]	k_{film}^{Hxl} [b] (m·s^{-1})	Bi [c]
Sachet	LDPE	0.002	4.62×10^{-6}	0.002	3.83×10^{-5}	0.013
	OPP	"	4.62×10^{-7}	0.0002	9.80×10^{-7}	0.0003
	Tyvek®	"	4.59×10^{-4}	0.168 [d]	1.37×10^{-3}	0.470 [d]
Package [d]	LDPE	0.009	4.62×10^{-6}	0.01	3.82×10^{-5}	0.05

[a] Because the sachet headspace was considered relatively small and the sachet was essentially flat, if there was no constraint from carrier bed which was practically loose and arranged in one layer configuration. Based on this, the characteristic length (L) of diffusion through the bed was designated as the average gel particle diameter (i.e. 1.70-3.35 mm particle) representing the conservative distance of molecular diffusion through the bed (from the bottom to the upper film). For diffusion mass transfer in the package headspace, the value of L for identifying Bi was determined following Geankoplis (1993c), as ratios of package volume to package surface area of 0.0012 m^3 and 0.125 m^2, respectively.

[b] Permeability (k_{film}^{Hxl}) was estimated as the averaged value of data presented in Figure 4-2, at determined temperatures.

[c] Bi values were calculated according to Eq. 5-2. Hexanal mass diffusivity (D_{air}^{Hxl}) in air at 10 and 20ºC was estimated using a correlation proposed by Fuller, Schettler, and Giddings (Johnson 1999) were 7.15×10^{-6} and 7.60×10^{-6} m^2·s^{-1}, respectively.

[d] As Bi values of Tyvek® sachet system were > 0.1, validity of an assumption on uniform hexanal vapour concentration in sachet headspace was considered and discussed in section 5.5.1.1.

[e] Packaging films for the active packaging systems were limited to LDPE film.

F.2 Scaling analyses

Scaling analyses (Krantz 2007) can assist decision-making in selecting which modelling approaches, (e.g. unsteady (Fick's second law) or steady-state (Fick's first law)) are best suited to simulate mass transfer processes. Scaling analysis is used here to identify the

conditions in which each modelling approach should be used for the active MAP systems of interest (discussed in Chapter 5).

F.2.1 Scaling considered at sachet film material

A conceptual model of one-dimensional mass transfer of a volatile compound across a sachet film is provided in Figure F-1. It is of interest to identify the conditions for which unsteady-state sorption of the active agent need to be considered or alternatively for which a steady-state profile across the film can be assumed. In this derivation it was assumed that there was negligible loss of volatile from the package headspace or interactions with the product. In addition permeability of the film to the volatile compound was assumed to be independent of concentration.

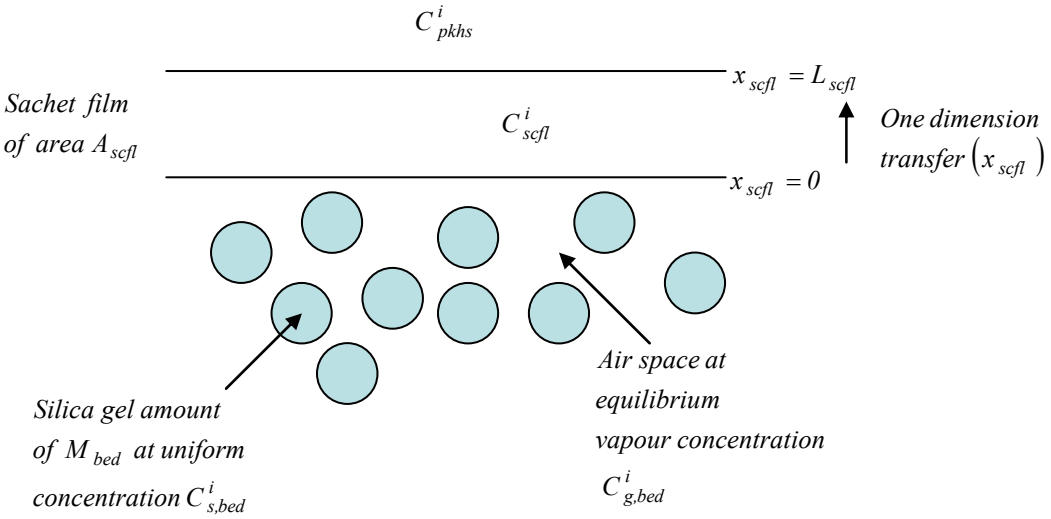

Figure F-1 Conceptual model of one-dimensional mass transfer across a sachet film

The ordinary differential equation for describing volatile accumulation in the package headspace can be expressed as Eq. F-1.

$$V_{pkg}\frac{dC^{i}_{pkhs}}{dt} = D^{i}_{scfl}A_{scfl}\left.\frac{dC^{i}_{scfl}}{dx_{scfl}}\right|_{x_{scfl}=L_{scfl}} \qquad for\ t > 0 \qquad \textbf{(Eq. F-1)}$$

where

C^{i}_{pkhs} = Concentration of active agent *i* in package headspace (mol·m^{-3})

D^{i}_{scfl} = Mass diffusivity of active agent *i* in sachet film (m^{2}·s^{-1})

C^{i}_{scfl} = Concentration of active agent *i* in sachet film (mol·m^{-3})

x_{scfl} = Position in sachet film (m)

The diffusion mass transfer within the sachet film can be modelled using Fick's second law Eq. 2-5 as shown in Eq. F-2.

$$\frac{dC^{i}_{scfl}}{dt} = D^{i}_{scfl} \frac{d^{2}C^{i}_{scfl}}{dx^{2}_{scfl}} \qquad for\ t > 0\ and\ 0 < x_{scfl} < L_{scfl} \qquad \textbf{(Eq. F-2)}$$

Given initial and boundary conditions as:

$$C^{i}_{scfl} = 0 \qquad for\ t = 0\ and\ 0 < x_{scfl} < L_{scfl} \qquad \textbf{(Eq. F-3)}$$

$$C^{i}_{scfl} = S^{i}_{scfl} \cdot C^{i}_{g,bed} \cdot RT_{pkg} \qquad for\ all\ t\ and\ x_{scfl} = 0 \qquad \textbf{(Eq. F-4)}$$

$$C^{i}_{scfl} = S^{i}_{scfl} \cdot C^{i}_{pkhs} \cdot RT_{pkg} \qquad for\ all\ t\ and\ x_{scfl} = L_{scfl} \qquad \textbf{(Eq. F-5)}$$

where

$C^{i}_{g,bed}$ = Equilibrium concentration of active agent *i* above the carrier bed ($mol \cdot m^{-3}$)

The ordinary differential equation for describing equilibrium volatile amount in the solid phase (silica gel) can be expressed as Eq. F-6.

$$M_{bed} \frac{dC^{i}_{s,bed}}{dt} = D^{i}_{scfl} A_{scfl} \left.\frac{dC^{i}_{scfl}}{dx_{scfl}}\right|_{x_{scfl}=0} \qquad for\ t > 0 \qquad \textbf{(Eq. F-6)}$$

where

$C^{i}_{s,bed}$ = Equilibrium adsorbed amount of active agent *i* on the carrier bed ($mol \cdot g^{-1}$)

In many systems the sorption isotherm can be approximated as Henry's law (Eq. F-7). Even in systems with more complicated sorption behaviour (e.g. Langmuir), over relatively small changes in adsorbed amount, this equation applies

$$C^{i}_{g,bed} = C^{i}_{s,bed} \,/\, K^{i}_{bed} \qquad \textbf{(Eq. F-7)}$$

where

K^{i}_{bed} = Henry's law coefficient ($m^{3} \cdot g^{-1}$)

By substituting Eq. F-7 in Eq. F-4, the boundary condition, which is described in term of the equilibrium amount on solid phase, can be expressed as Eq. F-8.

$$C^{i}_{scfl} = S^{i}_{scfl} \cdot \frac{C^{i}_{s,bed}}{K^{i}_{bed}} \cdot RT_{pkg} \qquad for\ all\ t\ and\ x_{scfl} = 0 \qquad \textbf{(Eq. F-8)}$$

The initial conditions for mass transfer processes across the sachet film can be expressed as Eq. F-9 and Eq. F-10.

$$C^{i}_{s,bed} = C^{i}_{s,bed,ini} \qquad at\ t = 0 \qquad \textbf{(Eq. F-9)}$$

$$C^{i}_{pkhs} = C^{i}_{pkhs,ini} \qquad at\ t = 0 \qquad \textbf{(Eq. F-10)}$$

where

$C^{i}_{s,bed,ini}$ = Initial value of equilibrium adsorbed amount of active agent *i* on the carrier bed (mol·g^{-1})

$C^{i}_{pkhs,ini}$ = Initial value of concentration of active agent *i* in package headspace (mol·m^{-3})

After defining key mass transfer processes due to the sachet film, scaling variables were then defined as summarised in Eq. F-11.

$$C^{i*}_{scfl} = \frac{C^{i}_{scfl} - C^{i}_{scfl,ref}}{C^{i}_{scfl,s}},\ dC^{i}_{scfl} = C^{i}_{scfl,s} \cdot dC^{i*}_{scfl},\ C^{i*}_{pkhs} = \frac{C^{i}_{pkhs}}{C^{i}_{pkhs,s}},\ C^{i*}_{s,bed} = \frac{C^{i}_{s,bed}}{C^{i}_{s,bed,s}}, \qquad \textbf{(Eq. F-11)}$$

$$x^{*}_{scfl} = \frac{x_{scfl}}{x_{scfl,s}},\ t^{*} = \frac{t}{t_s}$$

It should be noted that variables with '*' superscript or 's' and 'ref' subscripts are unknown variables for developing the scale. Whilst units of '*' superscripted variables are dimensionless, those of 's' and 'ref' subscripted variables are the same as units of the non-subscripted variables, for example $x_{scfl,s}$ has the same unit as x_{scfl} (hence m).

Substituting scaling variables summarised in relevant equations and in the initial and boundary conditions yields the following:

$$\frac{C^{i}_{pkhs,s} V_{pkg}}{t_s} \frac{dC^{i*}_{pkhs}}{dt^{*}} = D^{i}_{scfl} A_{scfl} \frac{C^{i}_{scfl,s}}{x_{scfl,s}} \frac{dC^{i*}_{scfl}}{dx^{*}}\Bigg|_{x^{*} = \frac{L_{scfl}}{x_s}} \qquad for\ t^{*} > 0 \qquad \textbf{(Eq. F-12)}$$

$$\frac{C^{i}_{scfl,s}}{t_s}\frac{dC^{i*}_{scfl}}{dt^*}=\frac{D^{i}_{scfl}C^{i}_{scfl,s}}{x^{2}_{scfl,s}}\frac{d^2C^{i*}_{scfl}}{dx^{*2}_{scfl}} \qquad for\ t^*>0\ and\ 0<x^*_{scfl}<\frac{L_{scfl}}{x_{scfl,s}} \qquad \textbf{(Eq. F-13)}$$

$$\frac{C^{i}_{s,bed,s}M_{bed}}{t_s}\frac{dC^{i*}_{s,bed}}{dt^*}=\frac{D^{i}_{scfl}A_{scfl}C^{i}_{scfl,s}}{x_{scfl,s}}\frac{dC^{i*}_{scfl}}{dx^*_{scfl}}\Bigg|_{x^*_{scfl}=0} \qquad for\ t^*>0 \qquad \textbf{(Eq. F-14)}$$

$$C^{i}_{scfl,s}C^{i*}_{scfl}+C^{i}_{scfl,ref}=S^{i}_{scfl}RT_{pkg}C^{i}_{pkhs,s}C^{i*}_{pkhs} \qquad at\ x^*_{scfl}=\frac{L_{scfl}}{x_{scfl,s}} \qquad \textbf{(Eq. F-15)}$$

$$C^{i}_{scfl,s}C^{i*}_{scfl}+C^{i}_{scfl,ref}=\frac{S^{i}_{scfl}RT_{pkg}C^{i}_{s,bed,s}C^{i*}_{s,bed}}{K^{i}_{bed}} \qquad at\ x^*_{scfl}=0 \qquad \textbf{(Eq. F-16)}$$

Initial conditions can be expressed as:

$$C^{i}_{s,bed,s}C^{i*}_{s,bed}=C^{i}_{s,bed,ini} \qquad at\ t^*=0 \qquad \textbf{(Eq. F-17)}$$

$$C^{i}_{pkhs,s}C^{i*}_{pkhs}=C^{i}_{pkhs,ini} \qquad at\ t^*=0 \qquad \textbf{(Eq. F-18)}$$

The initial concentration gradient of active substance across the sachet film material can be conceptually modelled as show in Figure F-2.

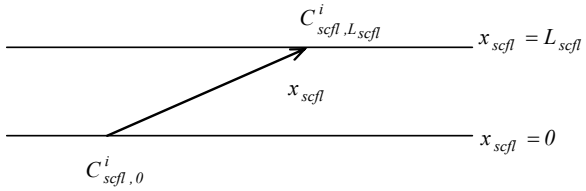

Figure F-2 Conceptual model of the concentration gradient of volatile across the sachet film

The initial form of the concentration gradient can be expressed as Eq. F-19.

$$C^{i}_{scfl}=C^{i}_{scfl,0}-\frac{x_{scfl}}{L_{scfl}}\left(C^{i}_{scfl,0}-C^{i}_{scfl,L_{scfl}}\right) \qquad at\ t=0 \qquad \textbf{(Eq. F-19)}$$

Substituting scaling variables into Eq. F-19 yields:

$$C^{i}_{scfl,s}C^{i,*}_{scfl}+C^{i}_{scfl,ref}=C^{i}_{scfl,0}-\frac{x_{scfl,s}x^*_{scfl}}{L_{scfl}}\left(C^{i}_{scfl,0}-C^{i}_{scfl,L_{scfl}}\right) \qquad at\ t^*=0 \qquad \textbf{(Eq. F-20)}$$

Eq. F-12 to Eq. F-14, were divided through by scaling variables, to yield Eq. F-21 to Eq. F-23, respectively:

$$\frac{C^{i}_{pkhs,s} V_{pkg} x_{scfl,s}}{C^{i}_{scfl,s} D^{i}_{scfl} A_{scfl} t_s} \frac{dC^{i*}_{pkhs}}{dt^*} = \left.\frac{dC^{i*}_{scfl}}{dx^*}\right|_{x^*_{scfl}=\frac{L_{scfl}}{x_{scfl,s}}} \qquad for\ t^* > 0 \qquad \textbf{(Eq. F-21)}$$

$$\frac{x^2_{scfl,s}}{D^{i}_{scfl} t_s} \frac{dC^{i*}_{scfl}}{dt^*} = \frac{d^2 C^{i*}_{scfl}}{dx^{*2}_{scfl}} \qquad for\ t^* > 0\ and\ 0 < x^*_{scfl} < \frac{L_{scfl}}{x_{scfl,s}} \qquad \textbf{(Eq. F-22)}$$

$$\frac{C^{i}_{s,bed,s}}{C^{i}_{scfl,s}} \frac{M_{bed} x_{scfl}}{D^{i}_{scfl} A_{scfl} t_s} \frac{dC^{i*}_{s,bed}}{dt^*} = \left.\frac{dC^{i*}_{scfl}}{dx^*_{scfl}}\right|_{x^*_{scfl}=0} \qquad for\ t^* > 0 \qquad \textbf{(Eq. F-23)}$$

After rearranging the dimensionless equations, the scale factors are then determined. Because x_{scfl} varies from 0 to L_{scfl}, x^*_{scfl} varies from 0 to 1. Then value of $x_{scfl,s}$ can be determined as equal to L_{scfl} as demonstrated in Eq. F-24.

$$x^*_{scfl} = 1 = \frac{L_{scfl}}{x_{scfl,s}} \text{ therefore } x_{scfl,s} = L_{scfl} \qquad \textbf{(Eq. F-24)}$$

Substituting Eq. F-24 in the dimensionless concentration gradient Eq. F-20 yields Eq. F-25.

$$C^{i}_{scfl,s} C^{i*}_{scfl} + C^{i}_{scfl,ref} = C^{i}_{scfl,0} - x^*_{scfl}\left(C^{i}_{scfl,0} - C^{i}_{scfl,L_{scfl}}\right) \qquad \textbf{(Eq. F-25)}$$

By defining $C^{i*}_{scfl} \approx 1$ at $x^*_{scfl} = 0$, then Eq. F-25 becomes Eq. F-26.

$$C^{i}_{scfl,s} + C^{i}_{scfl,ref} = C^{i}_{scfl,0} \qquad \textbf{(Eq. F-26)}$$

Similarly by defining $C^{i*}_{scfl} = 0$ at $x^*_{scfl} = 1$, Eq. F-25 becomes Eq. F-27.

$$C^{i}_{scfl,ref} = C^{i}_{scfl,L_{scfl}} \qquad \textbf{(Eq. F-27)}$$

Substituting Eq. F-27 into Eq. F-26 yields Eq. F-28.

$$C^{i}_{scfl,s} = \left(C^{i}_{scfl,0} - C^{i}_{scfl,L_{scfl}}\right) \qquad \textbf{(Eq. F-28)}$$

Considering the boundary condition at $x^{*}_{scfl} = 1$ (Eq. F-15 provided $x_{scfl,s} = L_{scfl}$), it can be defined that $C^{i*}_{scfl} = 1$ when $C^{i*}_{pkhs} = 1$. By substituting these defined values and together with Eq. F-27 and Eq. F-28 in Eq. F-15, Eq. F-29 is obtained.

$$\left(C^{i}_{scfl,0} - C^{i}_{scfl,L_{scfl}} \right) + C^{i}_{scfl,L_{scfl}} = S^{i}_{scfl} C^{i}_{pkhs,s} RT_{pkg} \qquad \textbf{(Eq. F-29)}$$

Rearranging Eq. F-29 yields Eq. F-30.

$$C^{i}_{pkhs,s} = \frac{C^{i}_{scfl,0}}{S^{i}_{scfl} RT_{pkg}} \qquad \textbf{(Eq. F-30)}$$

Considering the boundary condition at $x^{*}_{scfl} = 0$ Eq. F-16, it can be defined that $C^{i*}_{s,bed} = 1$ when $C^{i*}_{scfl} = 1$. Substituting these defined values in Eq. F-16 yields the following:

$$C^{i}_{scfl,s} + C^{i}_{scfl,ref} = \frac{S^{i}_{scfl} RT_{pkg} C^{i}_{s,bed,s}}{K^{i}_{bed}} \qquad \textbf{(Eq. F-31)}$$

Substituting Eq. F-26 in Eq. F-31 yields Eq. F-32.

$$C^{i}_{scfl,0} = \frac{S^{i}_{scfl} RT_{pkg} C^{i}_{s,bed,s}}{K^{i}_{bed}} \qquad \textbf{(Eq. F-32)}$$

By rearranging Eq. F-32, the value of $C^{i}_{s,bed,s}$ can be identified as shown in Eq. F-33.

$$C^{i}_{s,bed,s} = \frac{C^{i}_{scfl,0} K^{i}_{bed}}{S^{i}_{scfl} RT_{pkg}} \qquad \textbf{(Eq. F-33)}$$

The value of t_s can be defined as equal to t_0 (representing observation or contact time) as shown in Eq. F-34.

$$t_s = t_0 \qquad \textbf{(Eq. F-34)}$$

By substituting defined scaling factors into dimensionless equations and the initial and boundary conditions, the following equations are obtained:

- Dimensionless ODE of package headspace

$$\frac{C^{i}_{scfl,0} V_{pkg} L_{scfl}}{S^{i}_{scfl} RT_{pkg} \left(C^{i}_{scfl,0} - C^{i}_{scfl,L_{scfl}} \right) D^{i}_{scfl} A_{scfl} t_0} \frac{dC^{i*}_{pkhs}}{dt^*} = \left. \frac{dC^{i*}_{scfl}}{dx^*} \right|_{x^*_{scfl}=1} \qquad \textbf{(Eq. F-35)}$$

$for\ t^* > 0$

- Dimensionless PDE of sachet film

$$\frac{L^2_{scfl}}{D^{i}_{scfl} t_0} \frac{dC^{i*}_{scfl}}{dt^*} = \frac{d^2 C^{i*}_{scfl}}{dx^{*2}_{scfl}} \qquad for\ t^* > 0\ and\ 0 < x^*_{scfl} < 1 \qquad \textbf{(Eq. F-36)}$$

- Dimensionless ODE of silica gel

$$\frac{C^{i}_{scfl,0} K^{i}_{bed}}{S^{i}_{scfl} RT_{pkg} \left(C^{i}_{scfl,0} - C^{i}_{scfl,L_{scfl}} \right)} \frac{M_{bed} L_{scfl}}{D^{i}_{scfl} A_{scfl} t_0} \frac{dC^{i*}_{s,bed}}{dt^*} = \left. \frac{dC^{i*}_{scfl}}{dx^*_{scfl}} \right|_{x^*=0} \qquad \textbf{(Eq. F-37)}$$

$for\ t^* > 0$

- Initial conditions

For $C^{i}_{s,bed}$ at $t = 0$:

By substituting Eq. F-33 to Eq. F-17, the initial value of $C^{i}_{s,bed}$ can be expressed as Eq. F-38.

$$C^{i*}_{s,bed} = \frac{C^{i}_{s,bed,ini} S^{i}_{scfl} RT_{pkg}}{C^{i}_{scfl,0} K^{i}_{bed}} \qquad at\ t^* = 0 \qquad \textbf{(Eq. F-38)}$$

For C^{i}_{pkhs} at $t = 0$:

By substituting Eq. F-30 in Eq. F-11, the initial value of C^{i}_{pkhs} can be expressed as Eq. F-39.

$$C^{i*}_{pkhs} = \frac{C^{i}_{pkhs,ini} S^{i}_{scfl} RT_{pkg}}{C^{i}_{scfl,0}} \qquad at\ t^* = 0 \qquad \textbf{(Eq. F-39)}$$

For the initial concentration gradient (Eq. F-25) at $t = 0$: Substituting Eq. F-27 and Eq. F-28 in Eq. F-25 yields Eq. F-40.

$$\left(C^{i}_{scfl,0} - C^{i}_{scfl,L_{scfl}} \right) C^{i*}_{scfl} = \left(C^{i}_{scfl,0} - C^{i}_{scfl,L_{scfl}} \right) - x^{*}_{scfl} \left(C^{i}_{scfl,0} - C^{i}_{scfl,L_{scfl}} \right) \quad \textbf{(Eq. F-40)}$$

$$at\ t^{*} = 0$$

By further rearranging Eq. F-40 where both sides of the equation are divided by $\left(C^{i}_{scfl,0} - C^{i}_{scfl,L_{scfl}} \right)$, Eq. F-41 is obtained.

$$C^{i*}_{scfl} = 1 - x^{*}_{scfl} \quad at\ t^{*} = 0 \quad \textbf{(Eq. F-41)}$$

The summary of dimensionless models can be expressed as the following:

- Dimensionless ODE for package headspace

$$\frac{C^{i}_{scfl,0} V_{pkg} L_{scfl}}{S^{i}_{scfl} RT_{pkg} \left(C^{i}_{scfl,0} - C^{i}_{scfl,L_{scfl}} \right) D^{i}_{scfl} A_{scfl} t_{0}} \frac{dC^{i*}_{pkhs}}{dt^{*}} = \left. \frac{dC^{i*}_{scfl}}{dx^{*}} \right|_{x^{*}_{scfl}=1} \qquad for\ t^{*} > 0$$

- Dimensionless PDE for sachet film

$$\frac{L^{2}_{scfl}}{D^{i}_{scfl} t_{0}} \frac{dC^{i*}_{scfl}}{dt^{*}} = \frac{d^{2} C^{i*}_{scfl}}{dx^{*2}_{scfl}} \qquad for\ t^{*} > 0\ and\ 0 < x^{*}_{scfl} < 1$$

- Dimensionless ODE for silica gel

$$\frac{C^{i}_{scfl,0} K^{i}_{bed}}{S^{i}_{scfl} RT_{pkg} \left(C^{i}_{scfl,0} - C^{i}_{scfl,L_{scfl}} \right)} \frac{M_{bed} L_{scfl}}{D^{i}_{scfl} A_{scfl} t_{0}} \frac{dC^{i*}_{s,bed}}{dt^{*}} = \left. \frac{dC^{i*}_{scfl}}{dx^{*}_{scfl}} \right|_{x^{*}=0} \qquad for\ t^{*} > 0$$

- Dimensionless initial conditions

$$C^{i*}_{s,bed} = \frac{C^{i}_{s,bed,ini} S^{i}_{scfl} RT_{pkg}}{C^{i}_{scfl,0} K^{i}_{bed}} \qquad at\ t^{*} = 0$$

$$C^{i*}_{pkhs} = \frac{S^{i}_{scfl} RT_{pkg} C^{i}_{pkhs,ini}}{C^{i}_{scfl,0}} \qquad at\ t^{*} = 0$$

$$C^{i*}_{scfl} = 1 - x^{*}_{scfl} \qquad at\ t^{*} = 0$$

As the rate of concentration change is a function of the reciprocal of the system capacity (Levenspiel 1972), the relative rate of two systems can be determined by comparing the

reciprocal of each system capacity. Therefore (i) relative rate in sachet film and silica gel bed and (ii) relative rate in sachet film and package headspace can be expressed as Eq. F-42 and Eq. F-43, respectively.

$$\frac{dC_{scfl}^{i*} / dt^*}{dC_{s,bed}^{i*} / dt^*} = \frac{r_{scfl}}{r_{bed}} = \frac{K_{bed}^{i} M_{bed}}{L_{scfl} S_{scfl}^{i} RT_{pkg} A_{scfl}} \cdot \frac{C_{scfl,0}^{i}}{\left(C_{scfl,0}^{i} - C_{scfl,L_{scfl}}^{i} \right)} \quad \textbf{(Eq. F-42)}$$

$$\frac{dC_{scfl}^{i*} / dt^*}{dC_{pkhs}^{i*} / dt^*} = \frac{r_{scfl}}{r_{pkhs}} = \frac{V_{pkg}}{L_{scfl} S_{scfl}^{i} RT_{pkg} A_{scfl}} \cdot \frac{C_{scfl,0}^{i}}{\left(C_{scfl,0}^{i} - C_{sch,L_{scfl}}^{i} \right)} \quad \textbf{(Eq. F-43)}$$

Eq. F-42 and Eq. F-43 can be used to determine the need to model transport of volatile through the sachet film as a dynamic or equilibrium process.

As mentioned in section 5.5.1.2, ratio of carrier bed capacity to sachet film capacity (denoted as $CR_{bed/scfl}$) and ratio of package headspace capacity to that of the sachet film (denoted as $CR_{pkhs/scfl}$) can be described by Eq. F-44 and Eq. F-45, respectively.

$$CR_{bed/scfl} = \frac{K_{bed}^{i} M_{bed}}{L_{scfl} S_{scfl}^{i} RT_{pkg} A_{scfl}} \cdot \quad \textbf{(Eq. F-44)}$$

$$CR_{pkhs/scfl} = \frac{V_{pkg}}{L_{scfl} S_{scfl}^{i} RT_{pkg} A_{scfl}} \quad \textbf{(Eq. F-45)}$$

F.2.2 Scaling considered at packaging film

The importance of the dynamics of the outer packaging film absorption can be assessed using a similar approach. The conceptual model for mass transfer across the packaging film, of an active packaging system containing a controlled released sachet, is provided as in Figure F-3. In this exercise, the release of volatile into the package headspace is modelled assuming steady-state is achieved instaneously through the sachet film and the concentration in the sachet headspace is constant. No absorption or product interactions are considered. In addition permeability of the film to the volatile compound was assumed to be independent of concentration.

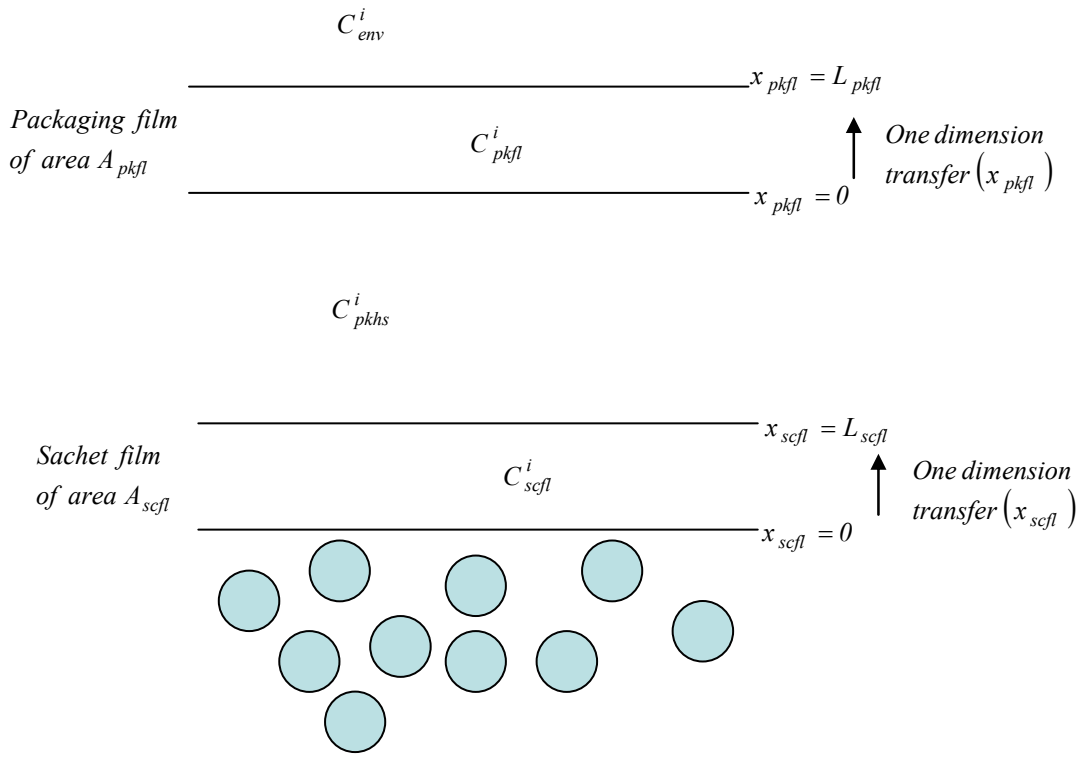

Figure F-3 Conceptual model of mass transfer across packaging film in an active packaging system

The ODE for describing 1-MCP accumulation in the package headspace can be expressed as Eq. F-46.

$$V_{pkg}\frac{dC^{i}_{pkhs}}{dt} = D^{i}_{scfl}A_{scfl}\left.\frac{dC^{i}_{scfl}}{dx_{scfl}}\right|_{x_{scfl}=L_{scfl}} - D^{i}_{pkfl}A_{pkfl}\left.\frac{dC^{i}_{pkfl}}{dx_{pkfl}}\right|_{x_{pkfl}=0}, \quad for\ t>0 \qquad \textbf{(Eq. F-46)}$$

where

C^{i}_{pkfl} = Concentration of active agent *i* in packaging film ($mol \cdot m^{-3}$)

D^{i}_{pkfl} = Mass diffusivity of active agent *i* in packaging film ($m^2 \cdot s^{-1}$)

x_{pkfl} = Position in packaging film (m)

The diffusion mass transfer within the outer packaging film can be modelled using Fick's second law as shown in Eq. F-47.

$$\frac{dC^{i}_{pkfl}}{dt} = D^{i}_{pkfl}\frac{d^2C^{i}_{pkfl}}{dx^{2}_{pkfl}} \qquad for\ t>0\ and\ 0<x_{pkfl}<L_{pkfl} \qquad \textbf{(Eq. F-47)}$$

Initial and boundary conditions can be expressed as:

$$C^{i}_{pkfl} = C^{i}_{scfl} = 0 \qquad for\ t = 0\ and\ 0 < x_{pkfl}\ (\&\ x_{scfl}) < L_{pkfl}\ (\&\ L_{scfl}) \qquad \textbf{(Eq. F-48)}$$

$$C^{i}_{scfl} = S^{i}_{scfl} \cdot C^{i}_{pkhs} \cdot RT_{pkg} \qquad for\ all\ t\ and\ x_{scfl} = L_{scfl} \qquad \textbf{(Eq. F-49)}$$

$$C^{i}_{pkfl} = S^{i}_{pkfl} \cdot C^{i}_{pkhs} \cdot RT_{pkg} \qquad for\ all\ t\ and\ x_{pkfl} = 0 \qquad \textbf{(Eq. F-50)}$$

$$C^{i}_{pkfl} = S^{i}_{pkfl} \cdot C^{i}_{env} \cdot RT_{pkg} \qquad for\ all\ t\ and\ x_{pkfl} = L_{pkfl} \qquad \textbf{(Eq. F-51)}$$

where

C^{i}_{env} = Concentration of active agent *i* in surrounding environment (mol·m^{-3})

The initial concentration gradient of 1-MCP across the packaging film material can be conceptually modelled as show in Figure F-4.

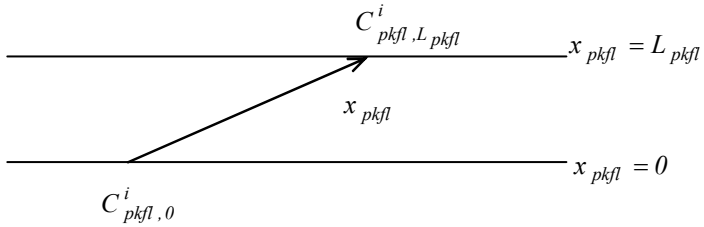

Figure F-4 Conceptual model of the initial concentration gradient of 1-MCP across the packaging film

The initial form of the concentration gradient across the packaging film material can be expressed as Eq. F-52.

$$C^{i}_{pkfl} = C^{i}_{pkfl,0} - \frac{x_{pkfl}}{L_{pkfl}}\left(C^{i}_{pkfl,0} - C^{i}_{pkfl,L_{scfl}}\right) \qquad at\ t = 0 \qquad \textbf{(Eq. F-52)}$$

where

$C^{i}_{pkfl,0}$ = Concentration of active agent *i* in packaging film at $x_{pkfl} = 0$

$C^{i}_{pkfl,L_{pkfl}}$ = Concentration of active agent *i* in packaging film at $x_{pkfl} = L_{pkfl}$

Scaling variables as defined in Eq. F-11 are also utilised in this section. Additional scaling factors are for concentration and position in the packaging film, which can be defined as:

$$C^{i*}_{pkfl} = \frac{C^{i}_{pkfl} - C^{i}_{pkfl,ref}}{C^{i}_{pkfl,s}} \quad \textbf{(Eq. F-53)}$$

$$dC^{i}_{pkfl} = C^{i}_{pkfl,s} \cdot dC^{i*}_{pkfl} \quad \textbf{(Eq. F-54)}$$

$$x^{*}_{pkfl} = \frac{x_{pkfl}}{x_{pkfl,s}} \quad \textbf{(Eq. F-55)}$$

It should be noted that D^{i}_{scfl} is assumed to be equal to D^{i}_{pkfl} (i.e. same polymer material for sachet and packaging film) and thus designated as D^{i}_{fl}. Given this assumption, following scaling parameters were applied: $dC^{i}_{scfl} = C^{i}_{pkfl,s} \cdot dC^{i*}_{scfl}$ and $x^{*}_{scfl} = x^{*}_{pkfl}$. Substituting these scaling factors in relevant equations and the initial and boundary conditions yields the following:

- Dimensionless ODE for package headspace

$$\frac{C^{i}_{pkhs,s} V_{pkg}}{t_s} \frac{dC^{i*}_{pkhs}}{dt^{*}} = \frac{D^{i}_{fl} A_{pkfl} C^{i}_{scfl,s}}{x_{pkfl,s}} \left(\frac{A_{scfl}}{A_{pkfl}} \frac{dC^{i*}_{scfl}}{dx^{*}_{pkfl}}\bigg|_{x^{*}_{scfl}=1} - \frac{dC^{i*}_{pkfl}}{dx^{*}_{pkfl}}\bigg|_{x^{*}_{pkfl}=0} \right) \quad for\ t^{*} > 0$$

(Eq. F-56)

- Dimensionless PDE for packaging film

$$\frac{C^{i}_{scfl,s}}{t_s} \frac{dC^{i*}_{pkfl}}{dt^{*}} = \frac{D^{i}_{fl} C^{i}_{pkfl,s}}{x^{2}_{pkfl,s}} \frac{d^{2} C^{i*}_{pkfl}}{dx^{*2}_{pkfl}} \qquad for\ t^{*} > 0\ and\ 0 < x^{*}_{pkfl} < \frac{L_{pkfl}}{x_{pkfl,s}} \quad \textbf{(Eq. F-57)}$$

- Dimensionless boundary conditions

$$C^{i}_{pkfl,s} C^{i*}_{pkfl} + C^{i}_{pkfl,ref} = S^{i}_{pkfl} RT_{pkg} C^{i}_{pkhs,s} C^{i*}_{pkhs} \qquad at\ x^{*}_{pkfl} = 0 \quad \textbf{(Eq. F-58)}$$

$$C^{i}_{pkfl,s} C^{i*}_{pkfl} + C^{i}_{pkfl,ref} = 0 \qquad at\ x^{*}_{pkfl} = \frac{L_{pkfl}}{x_{pkfl,s}} \quad \textbf{(Eq. F-59)}$$

- Dimensionless initial condition

$$C^{i}_{pkhs,s}\,C^{i*}_{pkhs} = C^{i}_{pkhs,ini} \qquad at\ t^{*} = 0 \qquad \textbf{(Eq. F-60)}$$

- Concentration gradient across the packaging film

$$C^{i}_{pkfl,s}\,C^{i*}_{pkfl} + C^{i}_{pkfl,ref} = C^{i}_{pkfl,0} - \frac{x_{pkfl,s}\,x^{*}_{pkfl}}{L_{pkfl}}\left(C^{i}_{pkfl,0} - C^{i}_{pkfl,L_{scfl}}\right) \quad at\ t^{*} = 0 \qquad \textbf{(Eq. F-61)}$$

- Identifying scaling factors

Because x_{pkfl} varies from 0 to L_{pkfl}, x^{*}_{pkfl} varies from 0 to 1. The value of $x_{pkfl,s}$ can be identified as equal to L_{pkfl} as demonstrated in Eq. F-62.

$$x^{*}_{pkfl} = 1 = \frac{L_{pkfl}}{x_{pkfl,s}} \text{ then } x_{pkfl,s} = L_{pkfl} \qquad \textbf{(Eq. F-62)}$$

Substituting Eq. F-62 in Eq. F-61 yields Eq. F-63.

$$C^{i}_{pkfl,s}\,C^{i*}_{pkfl} + C^{i}_{pkfl,ref} = C^{i}_{pkfl,0} - x^{*}_{pkfl}\left(C^{i}_{pkfl,0} - C^{i}_{pkfl,L_{pkfl}}\right) \qquad \textbf{(Eq. F-63)}$$

By assuming $C^{i*}_{pkfl} \approx 1 \quad at\ x^{*}_{pkfl} = 0$, then Eq. F-63 becomes Eq. F-64.

$$C^{i}_{pkfl,s} + C^{i}_{pkfl,ref} = C^{i}_{pkfl,0} \qquad \textbf{(Eq. F-64)}$$

Similarly, by assuming $C^{i*}_{pkfl} = 0 \quad at\ x^{*}_{pkfl} = 1$, Eq. F-63 becomes Eq. F-65.

$$C^{i}_{pkfl,ref} = C^{i}_{pkfl,L_{pkfl}} \qquad \textbf{(Eq. F-65)}$$

Substituting Eq. F-65 in Eq. F-64 yields Eq. F-66.

$$C^{i}_{pkfl,s} = \left(C^{i}_{pkfl,0} - C^{i}_{pkfl,L_{pkfl}}\right) \qquad \textbf{(Eq. F-66)}$$

By assuming $C^{i*}_{pkfl} = 1$ when $C^{i*}_{pkhs} = 1$ and substituting these defined values together with Eq. F-65 and Eq. F-66 in Eq. F-58, then Eq. F-67 is obtained.

$\left(C^{i}_{pkfl,0} - C^{i}_{pkfl,L_{pkfl}} \right) + C^{i}_{pkfl,Lpkfl} = S^{i}_{pkfl} C^{i}_{pkhs,s} RT_{pkg}$ or rearranging to

$$C^{i}_{pkhs,s} = \frac{C^{i}_{pkfl,0}}{S^{i}_{pkfl} RT_{pkg}} \qquad \textbf{(Eq. F-67)}$$

As the VOC concentration is presumably zero in the environment surrounding the package, it can then be assumed that $C^{i}_{pkfl,L_{pkfl}} = 0 \quad for\ t^{*} > 0$ at $x^{*}_{pkfl} = 1$. Furthermore t_s was designated as t_0 (representing observation or contact time). Substituting defined scaling factors in relevant equations and the boundary and initial conditions yields the following:

- Dimensionless ODEs for package headspace

$$\frac{C^{i}_{pkfl,0} V_{pkg} L_{pkfl}}{S^{i}_{pkfl} RT_{pkg} \left(C^{i}_{pkfl,0} - C^{i}_{pkfl,L_{pkfl}} \right) D^{i}_{pkfl} A_{pkfl} t_0} \frac{dC^{i*}_{pkhs}}{dt^{*}} = \left(\frac{A_{scfl}}{A_{pkfl}} \frac{dC^{i*}_{scfl}}{dx^{*}} \bigg|_{x^{*}_{scfl}=1} - \frac{dC^{i*}_{pkfl}}{dx^{*}} \bigg|_{x^{*}_{pkfl}=0} \right)$$

$for\ t^{*} > 0$ **(Eq. F-68)**

- Dimensionless PDEs for packaging film

$$\frac{L^{2}_{pkfl}}{D^{i}_{fl} t_0} \frac{dC^{i*}_{pkfl}}{dt^{*}} = \frac{d^{2} C^{i*}_{pkfl}}{dx^{*2}_{pkfl}} \qquad for\ t^{*} > 0 \ and\ 0 < x^{*}_{pkfl} < 1 \qquad \textbf{(Eq. F-69)}$$

- Dimensionless initial conditions

$$C^{i*}_{pkhs} = \frac{S^{i}_{pkfl} RT_{pkg} C^{i}_{pkhs,ini}}{C^{i}_{pkfl,0}} \qquad at\ t^{*} = 1 \qquad \textbf{(Eq. F-70)}$$

$$C^{i*}_{pkfl} = 1 - x^{*}_{pkfl} \qquad at\ t^{*} = 1 \qquad \textbf{(Eq. F-71)}$$

Relative rate of concentration changes in packaging film and headspace can be compared using the reciprocal of each system capacity, which is the film solubility and the package headspace volume, respectively. The relative rate can be expressed as Eq. F-72.

$$\frac{dC^{i*}_{pkfl} \,/\, dt^{*}}{dC^{i*}_{pkhs} \,/\, dt^{*}} = \frac{r_{pkfl}}{r_{pkhs}} = \frac{V_{pkhs}}{L_{pkfl} S^{i}_{pkfl} RT_{pkg} A_{pkfl}} \frac{C^{i}_{pkfl,0}}{\left(C^{i}_{pkfl,0} - C^{i}_{pkfl,L_{pkfl}} \right)} \qquad \textbf{(Eq. F-72)}$$

Eq. F-72 can be used to determine the need to model transport of volatile through the outer packaging film as a dynamic or equilibrium process. As mentioned in section 5.5.2, ratio of the capacity of the package headspace for holding adsorbent to that of the packaging film (denoted as $CR_{pkhs/pkfl}$) can be described by Eq. F-73.

$$CR_{pkhs/pkfl} = \frac{V_{pkhs}}{L_{pkfl} S^{i}_{pkfl} RT_{pkg} A_{pkfl}} \qquad \textbf{(Eq. F-73)}$$

F.3 Derivations of mathematical models for exploring the effects of capacity ratios ($CR_{pkhs/scfl}$ and $CR_{pkhs/pkfl}$; Chapter 5) on modelling 1-MCP accumulation in package headspace

The global ordinary differential equation (ODE) model for describing 1-MCP accumulation in the package headspace, according to the modes of mass transfer processes considered at (i) the sachet film and (ii) the packaging film, are derived in this section. Computational files (developed using MATLAB® language) are provided in the attached CD-ROM.

F.3.1 Modelling 1-MCP accumulation in package headspace based on 'Modes of mass transfer across sachet film material'

The mass transfer process across sachet film material can be modelled using either steady-state permeation (Fick's first law; Eq. 2-8) or transient diffusion (Fick's second law; Eq. 2-5) approachs. This investigation was carried out to understand what values of the parameters in $CR_{pkhs/scfl}$ (Eq. F-45) justify each modelling approach. A simplified system was considered for 1-MCP release from a sachet into a package head space. The key assumptions made included (i) no packaged horticultural products, (ii) film permeability is not concentration dependend (iii) no mass transfer out from the headspace (of a bag) to the surrounding environment (given $P^{MCP}_{pkfl} = 0$), and (iv) 1-MCP concentration in the sachet is always equal to its saturated value (C^{MCP}_{sat}) at 23ºC.

For 'steady-state permeation' across the sachet film, the global ODE for describing 1-MCP accumulation in package headspace can be expressed as Eq. F-74.

$$\frac{dC_{pkhs}^{MCP}}{dt}=\left(\frac{P_{scfl}^{MCP}A_{scfl}}{L_{scfl}}\left(C_{sat}^{MCP}-C_{pkhs}^{MCP}\right)-\frac{P_{pkfl}^{MCP}A_{pkfl}}{L_{pkfl}}\left(C_{pkhs}^{MCP}-C_{env}^{MCP}\right)\right)\frac{RT_{pkg}}{V_{pkg}},\ for\ t>0 \qquad \textbf{(Eq. F-74)}$$

where

P_{scfl}^{MCP} = Sachet film permeability to 1-MCP vapour (mol·m·m^{-2}·s^{-1}·Pa^{-1})

P_{pkfl}^{MCP} = Packaging film permeability to 1-MCP vapour (mol·m·m^{-2}·s^{-1}·Pa^{-1})

C_{sat}^{MCP} = 1-MCP saturated vapour concentration (mol·m^{-3})

For 'transient diffusion' mass transfer across the sachet film, diffusion in the sachet film can be described as Eq. F-75 and the global mathematical model for describing 1-MCP accumulation in package headspace can be expressed as Eq. F-76.

$$\frac{dC_{scfl}^{MCP}}{dt}=D_{scfl}^{MCP}\frac{d^2C_{scfl}^{MCP}}{dx_{scfl}^2} \qquad \textbf{(Eq. F-75)}$$

$$\frac{dC_{pkhs}^{MCP}}{dt}=\left(D_{scfl}^{MCP}A_{scfl}\left.\frac{dC_{scfl}^{MCP}}{dx_{scfl}}\right|_{x_{scfl}=L_{scfl}}-\frac{P_{pkfl}^{MCP}A_{pkfl}RT_{pkg}}{L_{pkfl}}\left(C_{pkhs}^{MCP}-C_{env}^{MCP}\right)\right)\frac{1}{V_{pkg}},\ for\ t>0 \qquad \textbf{(Eq. F-76)}$$

where

C_{scfl}^{MCP} = 1-MCP concentration in sachet film (mol·m^{-3})

D_{scfl}^{MCP} = Mass diffusivity of 1-MCP in sachet film (m^2·s^{-1})

Initial and boundary conditions for diffusions across the sachet film can be expressed as:

$$C_{scfl}^{MCP}=0 \qquad for\ t=0\ and\ 0<x_{scfl}<L_{scfl} \qquad \textbf{(Eq. F-77)}$$

$$C_{scfl}^{MCP}=S_{scfl}^{MCP}\cdot C_{sat}^{MCP}\cdot RT_{pkg} \qquad for\ all\ t\ and\ x_{scfl}=0 \qquad \textbf{(Eq. F-78)}$$

$$C_{scfl}^{MCP}=S_{scfl}^{MCP}\cdot C_{pkhs}^{MCP}\cdot RT_{pkg} \qquad for\ all\ t\ and\ x_{scfl}=L_{scfl} \qquad \textbf{(Eq. F-79)}$$

where

S_{scfl}^{MCP} = Sachet film solubility to 1-MCP (mol·m^{-3}·Pa^{-1})

The Finite Difference scheme (similar to that shown in Chapter 5) was utilised to solve the PDE model describing diffusion in the sachet film material.

F.3.2 Modelling 1-MCP accumulations in package headspace based on 'Modes of mass transfer across packaging film material'

Like for the sachet film material, the mass transfer process across the packaging film material (from headspace to surrounding environment) can be modelled using the steady-state permeation or transient diffusion (unsteady-state) approach. In a similar investigation a model was developed to identify how $CR_{pkhs/pkfl}$ (Eq. F-73) determines when each approach is more suitable. For this exercise models using each approach were developed for the simplistic scenario of 1-MCP release from a sachet into a package headspace initially free of 1-MCP. At the sachet, an assumption was made regarding steady-state permeation to describe the mass transfer across the sachet film material, to simplify model complexity.

The global ODE for describing 1-MCP accumulation in package headspace, in which the mass transfer across the packaging film is modelled using 'steady-state permeation', can be expressed as Eq. F-74.

For 'transient diffusion' across the packaging film, diffusion in the packaging film can be described as Eq. F-80 and the global model for describing 1-MCP accumulation in package headspace can be expressed as Eq. F-81.

$$\frac{dC_{pkfl}^{MCP}}{dt} = D_{pkfl}^{MCP} \frac{d^2 C_{pkfl}^{MCP}}{dx_{pkfl}^2} \qquad \textbf{(Eq. F-80)}$$

$$\frac{dC_{pkhs}^{MCP}}{dt} = \left(\frac{P_{scfl}^{MCP} A_{scfl} RT_{pkg}}{L_{scfl}} \left(C_{sat}^{MCP} - C_{pkhs}^{MCP} \right) - D_{pkfl}^{MCP} A_{pkfl} \left. \frac{dC_{pkfl}^{MCP}}{dx_{pkfl}} \right|_{x_{pkfl}=L_{pkfl}} \right) \frac{1}{V_{pkg}}, \quad for\ t>0$$

(Eq. F-81)

where

C_{pkfl}^{MCP} = 1-MCP concentration in packaging film ($mol \cdot m^{-3}$)

D_{pkfl}^{MCP} = Mass diffusivity of 1-MCP in packaging film ($m^2 \cdot s^{-1}$)

Initial and boundary conditions for diffusion across the packaging film can be expressed as:

$$C_{pkfl}^{MCP} = 0 \qquad for\ t = 0\ and\ 0 < x_{pkfl} < L_{pkfl} \qquad \textbf{(Eq. F-82)}$$

$$C_{pkfl}^{MCP} = S_{pkfl}^{MCP} \cdot C_{pkhs}^{MCP} \cdot RT_{pkg} \qquad for\ all\ t\ and\ x_{pkfl} = 0 \qquad \textbf{(Eq. F-83)}$$

$$C_{pkfl}^{MCP} = S_{pkfl}^{MCP} \cdot C_{env}^{MCP} \cdot RT_{pkg} \qquad for\ all\ t\ and\ x_{pkfl} = L_{pkfl} \qquad \textbf{(Eq. F-84)}$$

where

S_{pkfl}^{MCP} = Packaging film solubility to 1-MCP ($mol \cdot m^{-3} \cdot Pa^{-1}$)

C_{env}^{MCP} = 1-MCP concentration in environment ($mol \cdot m^{-3}$)

The Finite Difference scheme (similar to that shown in Chapter 5) is utilised to solve the PDE model describing diffusion in the packaging film material.

F.3.3 Numerical solutions for 1-MCP accumulation in package headspace investigations

MATLAB® filenames of the computational files for simulations of 1-MCP accumulation in package headspace are provided in Table F-2.

Table F-2 MATLAB® filenames for simulations of 1-MCP accumulation in package headspace

Modelling approaches				Computational files	
At sachet film		At packaging film			
Steady-state	Transient	Steady-state	Transient	Function file	Script file
√		No transfer		MCPSSsachet.m	MCPSSsachetrun.m
	√	"		MCPPDEsachet.m	MCPPDEsachetrun.m
√		√		MCPSSsachet.m	MCPSSsachetrun.m
"			√	MCPPDEpkfilm.m	MCPPDEpkfilmrun.m

F.4 Calculation of $CR_{bed/scfl}$, $CR_{pkhs/scfl}$, and $CR_{pkhs/pkfl}$ for hexanal-active MAP system

Derivations for relative rates of change in the sachet and film (both sachet and outer films) of the hexanal system were similar to those illustrated in F.2.1 and F.2.2. For the hexanal/

silica gel system the linear sorption isotherm model was approximated by the derivative of the the Langmuir equation (Eq. 2-3).

The $CR_{bed/scfl}$, $CR_{pkhs/scfl}$ and $CR_{pkhs/pkfl}$ for hexanal transfer in the active packaging systems was described as in Eq. F-85 to Eq. F-87. The estimated values of these relative capacities are summarised in Table F-3.

$$CR_{\frac{bed}{scfl}} = \frac{C_{s,max}^{Hxl} b_{Lgm}^{Hxl} M_{bed}}{L_{scfl} A_{scfl} \left(b_{Lgm}^{Hxl} C_{scfl,0}^{Hxl} + S_{scfl}^{Hxl} RT_{scfl} \right)} \quad \textbf{(Eq. F-85)}$$

$$CR_{\frac{pkhs}{scfl}} = \frac{V_{pkg}}{L_{scfl} S_{scfl}^{Hxl} A_{scfl} RT_{scfl}} \quad \textbf{(Eq. F-86)}$$

$$CR_{\frac{pkhs}{pkfl}} = \frac{V_{pkg}}{L_{pkfl} S_{pkfl}^{Hxl} A_{pkfl} RT_{pkfl}} \quad \textbf{(Eq. F-87)}$$

where

$C_{scfl,0}^{Hxl}$ = Hexanal concentration in sachet film at position $x_{scfl} = 0$ (mol·m^{-3})

S_{pkfl}^{Hxl} = Packaging film solubility to hexanal vapour (mol·m^{-3}·Pa^{-1})

Table F-3 Estimated values of $CR_{bed/scfl}$, $CR_{pkhs/scfl}$ and $CR_{pkhs/pkfl}$ for hexanal mass transfer in active packaging systems

Films	Film thickness (μm)	Film solubilities to hexanal vapour (mol·m^{-3}·Pa^{-1}) [b]		$CR_{bed/scfl}$ [c]		$CR_{pkhs/scfl}$ [d]		$CR_{pkhs/pkfl}$ [d]	
		10ºC	20ºC	10ºC	20ºC	10ºC	20ºC	10ºC	20ºC
LDPE [a]	30	0.44	0.75	208.63	45.33	12.87	7.29	0.31	0.17
OPP	20	0.25	0.74	548.85	68.91	33.87	11.08		
Tyvek	173	0.45	0.04	35.41	158.78	2.19	25.55		

[a] LDPE is the only packaging material.

[b] Values of solubilities of film *i* to hexanal vapour were estimated according to Piringer (2000) (page 270), where solubility is a ratio of the equilibrium amount of gas adsorbed to film volume and the equilibrium pressure of the gas being used.

[c] $C_{scfl,0}^{Hxl} = C_{sat}^{Hxl} \cdot S_{scfl}^{Hxl} \cdot R \cdot T_{pkg}$, where C_{sat}^{Hxl} is a saturated hexanal vapour concentration, as 0.23 and 0.46 mol·m^{-3} for 10 and 20ºC, respectively. It is worth noting that the values of $CR_{bed/scfl}$ was generally high and this suggested that rate of concentration changes in the bed was much slower than that in the sachet film.

[d] provided V_{pkg} = 0.0012 m^3, A_{scfl} = 0.003 m^2, and A_{pkfl} = 0.125 m^2, for all calculations.

Appendix G

NUMERICAL SOLUTIONS

G.1 Numerical solution for the global model describing hexanal concentration accumulation in the package headspace

The global mathematical models for predicting hexanal concentration in package headspace were solved numerically using MATLAB®. The MATLAB® code for the models is provided in both the function and script files. Whilst the former contains ODEs of key mass transfer processes of model active packaging systems for tomatoes, the latter contains model inputs and allows users to change input information to predict results of different scenarios. The model inputs shown in the script file presented later in this section refer to those of the **'LD2'** active packaging system defined in Table 6-1. The computational files are provided in the attached CD-ROM, in which filenames of a function and a script file are '**Hexanal_ActivePkgSim.m**' and '**Hexanal_ActivePkgSimrun.m**', respectively.

It should be noted that there are two colour scripts: black and green. The 'black scripts' are required for successful operation of the calculation and hence are not altered between simulations except for the model inputs. The 'green scripts' (following a '%') are comments to aid model development and understanding, and these are ignored during model implementation.

G.1.1 Function file (Hexanal_ActivePkgSim.m)

```
function odes=Hexanal_ActivePkgSim(t,Ds)
%Define global variables as following
global    Ascf;      %Sachet film surface area (m2)
global    Vpkg;      %Package volume (m3)
global    R;         %Gas constant (8.314 Pa m3/mol/K)
global    Tpkg;      %Package temperature (K)
global    Lscf;      %Sachet film thickness (m)
global    Apkg;      %Package surface area (m)
global    Lpkg;      %Packaging film thickness (m)
global    J;         %Number of the discreted spaces in packaging film due to the finite difference scheme
global    Dxpkg;     %Space step of the discretised packaging film due to the finite difference scheme (m)
global    CHxlenv;   %Hexanal concentration in surrounding environment (mol/m3)
global    bLgm;      %Langmuir equation coefficient (m3/mol)
global    CHxlbedmax; %Maximum uptake estimated by Langmuir equation (mol/g)
global    P0scf;     %Fitted pre-exponential factor for effective hexanal permeability of sachet film (mol m/m2/s/Pa)
global    bscf;      %Fitted exponential model coefficient of permeability of sachet film (m3/mol)
global    P0pkg;     %Fitted pre-exponential factor for effective hexanal permeability of packaging film (mol m/m2/s/Pa)
global    bpkg;      %Fitted exponential model coefficient of permeability of packaging film (m3/mol)
global    Mbed;      %Mass of dried silica gel in sachet (g)
```

```
global    Mtom;    %Mass of tomatoes (kg)
global    MWHxl;  %Hexanal molecular mass (g/mol)
global    HxlPsat;  %Saturated hexanal pressure at a given temperature (Pa)
global    ktomreac; %Reaction rate coefficient between hexanal and tomatoes (mol/kg/s (m3/mol)^nreac)
global    nreac;    %Order of reaction rate (dimensionless)

%Calculate new values for hexanal concentrations (dependent variables)
CHxl              =  Ds(1:J+3);       %Hexanal concentration (mol/m3)
CHxl(1)           =  CHxl(J+2);       %Hexanal concentration at node 1 of the discretised packaging film (mol/m3)
CHxl(J+1)         =  0;               %Hexanal concentration at node J+1 of the discretised packaging film (mol/m3)
CHxlbed           =  CHxl(J+3);       %Equilibrium adsorbed hexanal amount of carrier bed (mol/g)

%Vertical vector
odes      =         zeros(J+3,1);

%Calculation of equilibrium hexanal vapour concentration in sachet bed
if  CHxlbedmax <= CHxlbed
   CHxlscb =  HxlPsat/R/Tpkg;       %CHxlscb = Equilibrium hexanal vapour concentration of carrier bed (mol/m3)
else
   CHxlscb =  CHxlbed/(bLgm*(CHxlbedmax-CHxlbed));
end

%Checking the highest value of CHxlscb
if CHxlscb  >  HxlPsat/R/Tpkg
   CHxlscb =  HxlPsat/R/Tpkg;
end

%Calculating rate of hexanal uptake by tomatoes
Hxluptake  =  ktomreac*(CHxl(J+2)^nreac)*Mtom;

%Differential equations (ODEs)
odes(1)   =  0;  %Rate of changes of hexanal concentration at node 1 of packaging film (facing to package headspace)
(mol/m3/s)

for j=2:J
odes(j)   =         P0pkg*R*Tpkg*exp((CHxl(j-1)+CHxl(j))/2*bpkg)*(CHxl(j-1)-CHxl(j))/Dxpkg/Dxpkg-...
                    P0pkg*R*Tpkg*exp((CHxl(j)+CHxl(j+1))/2*bpkg)*(CHxl(j)-CHxl(j+1))/Dxpkg/Dxpkg;  %Rate of
changes of hexanal concentration at internal node j of packaging film (mol/m3/s)
end

odes(J+1)  =  0;  %Rate of changes of hexanal concentration at node J+1 of packaging film (facing to surrounding
environment) (mol/m3/s)

odes(J+2)  =   (P0scf*Ascf*R*Tpkg/(Lscf*bscf)*(exp(CHxlscb*bscf)-exp(CHxl(J+2)*bscf))...
               - (Apkg*R*Tpkg*P0pkg*exp((CHxl(1)+CHxl(2))/2*bpkg)*(CHxl(1)-CHxl(2))/Dxpkg))/Vpkg
                – (Hxluptake /Vpkg); %Rate of changes of hexanal concentration in package headspace (mol/m3/s)

odes(J+3)  =  -(P0scf*Ascf*R*Tpkg/(Lscf*bscf))*(exp(CHxlscb*bscf)-exp(CHxl(J+2)*bscf))/Mbed; %Rate of changes
of hexanal concentration (amount) on solid phase of silica gel (mol/g/s)
```

G.1.2 Script file (Hexanal_ActivePkgSimrun.m)

```
%Define global variables as following
global    Ascf;             %Sachet film surface area (m2)
global    Vpkg;             %Package volume (m3)
global    R;                %Gas constant (8.314 Pa m3/mol/K)
global    Tpkg;             %Package temperature (K)
global    Lscf;             %Sachet film thickness (m)
global    Apkg;             %Package surface area (m)
global    Lpkg;             %Packaging film thickness (m)
global    J;                %Number of the discreted spaces in packaging film due to the finite difference scheme
global    Dxpkg;            %Space step of the discretised packaging film due to the finite difference scheme (m)
global    CHxlenv;          %Hexanal concentration in surrounding environment (mol/m3)
global    bLgm;             %Langmuir equation coefficient (m3/mol)
global    CHxlbedmax;       %Maximum uptake estimated by Langmuir equation (mol/g)
```

```
global     P0scf;              %Fitted pre-exponential factor for effective hexanal permeability of sachet film (mol
m/m2/s/Pa)
global     bscf;               %Fitted exponential model coefficient of permeability of sachet film (m3/mol)
global     P0pkg;              %Fitted pre-exponential factor for effective hexanal permeability of packaging film (mol
m/m2/s/Pa)
global     bpkg;               %Fitted exponential model coefficient of permeability of packaging film (m3/mol)
global     Mbed;               %Mass of dried silica gel in sachet (g)
global     Mtom;               %Mass of tomatoes (kg)
global     MWHxl;              %Hexanal molecular mass (g/mol)
global     HxlPsat;            %Saturated hexanal pressure at a given temperature (Pa)
global     ktomreac;           %Reaction rate coefficient between hexanal and tomatoes (mol/kg/s (m3/mol)^nreac)
global     nreac;              %Order of reaction rate (dimensionless)

%System Input values
%General inputs
CHxlenv          =  0;              %Assumption
R                =  8.314;          %Gas constant
Apkg             =  0.125;          %Experimental measurement
P0pkg            =  1.97E-14;       %Experimental measurement
bpkg             =  19.65;          %Experimental measurement
Vpkg             =  0.0012;         %Experimental measurement
Lpkg             =  30*10^-6;       %Experimental measurement
Mtom             =  600*10^-3;      %Experimental measurement
MWHxl            =  100.16;         %SciFinder Scholar database

%Varied input values of 'storage temperature'
Storagetemp      =  20;             %Experimental measurement (referred to storage temperature (ºC))
Tpkg             =  273.15+Storagetemp;      %Calculation
HxlPsat          =  1137;           %Estimation following Covarrubias-Cervantes et al (2004)

%Varied input values of 'sachet content'
Mbed             =  3;              %Experimental measurement
Lscf             =  30*10^-6;       %Experimental measurement
Ascf             =  0.003;          %Experimental measurement
P0scf            =  1.97E-14;       %Experimental measurement
bscf             =  19.65;          %Experimental measurement

%Varied input values of 'coefficients of Langmuir equation'
CHxlbedmax       =  0.00334;        %Experimental measurement
bLgm             =  281.069;        %Experimental measurement

%Varied input values of 'rate of hexanal uptakes by tomatoes'
ktomreac         =  0.00009;        %Experimental measurement
nreac            =  2.64;           %Experimental measurement

%Input simulation conditions
J                =  10;             %Assumption
Dxpkg            =  Lpkg/J;         %Estimation
tPrint           =  500;            %Given time period for printing simulated results (second)
Day              =  7;              %Simulated storage day (assumption) (day)
tTotal           =  Day*24*60*60;   %Total simulation time (second)
tSpan            =  [0:tPrint:tTotal];       %Given time to evaluate the solution between initial time and total
simulation time

%Initial condition
CHxl             =  zeros(J+3,1);           %No Hexanal concentration in all nodes
CHxl(J+3)        =  CHxlbedmax;             %Assumption

%Input simulation conditions and initial conditions for changing storage temperature (e.g. from 10 to 20C) during the
storage regime
%Day              =  5;                                  %storage period of new storage temperature
%tTotal  =  Day*24*60*60;                                %Total simulation time (second)
%tSpan            =  [t(end):tPrint:tTotal+t(end)];      %t(end) as the last simulated time from the previous storage
temperature simulation
%CHxl     =  zeros(J+3,1);
%CHxl(J+2)  =  result(end,J+2);                          %using last simulated result from the previous simulation as
an initial for the new storage temperature simulation
```

```
%CHxl(J+3) =  result(end,J+3);                    %using last simulated result from the previous simulation as
an initial for the new storage temperature simulation

InitialConditions = CHxl;
%ODE calculation
[t,result] =          ode23s('Hexanal_ActivePkgSim',tSpan,InitialConditions);

%For calculation Equilibrium hexanal vapour concentration with solid phase in sachet
%CHxlbed                    =          result(:,J+3);
%CHxlscb                    =          zeros(size(CHxlbed));
%CHxlscb                    =          CHxlbed./(bLgm*(CHxlbedmax-CHxlbed));
%i                          =          find(HxlPsat /R/Tpkg <= CHxlscb);
%CHxlscb(i)                 =          HxlPsat /R/Tpkg;

%Recalculation Hexanal concentrations at node 1 and J+1
result(:,1)          =          result(:,J+2);
result(:,J+1)        =          0;

%For calculation mean value of equilibrium hexanal vapour concentration in packaging film
%CmeanFilm       =          (sum(result(:,2:J),2)+result(:,1)/2+result(:,J+1)/2)/J;

%Results
[t,result];

%Plot graph
%figure;  %plotting package headspace concentration
plot(t/24/60/60,result(:,J+2)*24372,'r');  %result(:,J+2) represents all calculated hexanal concentration in package
headspace
xlabel ('Day');
ylabel ('Concentration (ppm)');
Title ('Package headspace concentration');

%'24372' is a factor for converting concentration unit from 'mol/m3' to 'ppm (uL/L)'
%this factor was derived based on the ideal gas law as following:
%P =100000 Pa; n =1 mol; R = 8.314 Pa m3/mol/K; T  = 273.15+20 K
%calculating molar volume V = n*R*T/P and V = 0.024372491 m3
%from a calculated molar volume, concentration 1 mol/m3 equals to 24372491 uL/m3
%or ~24372 uL/L. Therefore the conversion factor at 10C is ~23541 uL/L.

%figure;  %Plotting equilibrium hexanal vapour concentration with solid phase in sachet
%plot(t/24/60/60,CHxlscb,'g');
%xlabel ('Day');
%ylabel ('Equilibrium vapour concentration (mol/m3)');
%Title ('Equilibrium hexanal vapour concentration with solid phase in sachet');

%figure;  %Plotting hexanal amount in solid phase in sachet
%plot(t/24/60/60,CHxlbed*Mbed*MWHxl,'b');
%xlabel ('Day');
%ylabel ('Amount on solid (g)');
%Title ('Equilibrium hexanal amount on solid phase in sachet');

%figure;  %Plotting equilibrium hexanal vapour concentrations with discretised nodes in film and thier mean
concentration
%plot(t/24/60/60,result(:,1:J+1)*24372,'r:');
%hold on
%plot(t/24/60/60,CmeanFilm*24372,'b');
%legend ('Concentrations at each film node', 'Mean concentration');
%legend ('boxoff');
%xlabel ('Day');
%ylabel ('Equilibrium vapour concentration (ppm)');
%Title ('Equilibrium hexanal vapour concentration with discretised nodes in packaging film');
```

G.2 MATLAB® language for the global model for predicting accumulations of O_2 and CO_2 in active MAP for tomatoes

The MATLAB® code for simulating accumulation of O_2 and CO_2 in the active packaging system as well as model inputs are provided in the attached CD-ROM. The filenames of the function and the script files are 'PassiveMAP.m' and 'PassiveMAPrun.m', respectively.

G.2.1 Function file (PassiveMAP.m)

```
function odes=PassiveMAP(t,Ds)
%Define global variables
global rO2max;          %Maximum rate of oxygen uptake by fruit (mol/s/kg),
global KmO2;            %Michaelis constant for O2 consumption (Pa)
global Mtom;            %Tomato mass (kg)
global PO2pkg;          %Packaging film permeability to oxygen (mol m/s/m2/Pa)
global PCO2pkg;         %Packaging film permeability to carbon dioxide (mol m/s/m2/Pa)
global pO2env;          %O2 partial pressure in surrounding environment (Pa)
global pCO2env;         %CO2 partial pressure in surrounding environment (Pa)
global RQ;              %Respiration quotient (dimensionless)
global Vpkg;            %Package volume (m3)
global R;               %Gas constant (8.314 Pa m3/mol/K)
global Tpkg;            %Package temperature (K)
global Lscf;            %Sachet film thickness (m)
global Apkg;            %Package surface area (m)
global Lpkg;            %Packaging film thickness (m)

%Calculate new values for number of moles of O2 and CO2 in pacakge headspace(dependent variables)
nO2pkg =Ds(1);          %number of oxygen moles in package headspace (mol)
nCO2pkg=Ds(2);          %number of carbon dioxide moles in package headspace (mol)

%Calculate new values for partial pressure of O2 and CO2 in package headspace
pO2pkg=nO2pkg*R*Tpkg/Vpkg;          %O2 partial pressure in package headspace (Pa)
pCO2pkg=nCO2pkg*R*Tpkg/Vpkg;        %CO2 partial pressure in package headspace (Pa)

%Calculation of O2 consumption rate and CO2 generation rate
rO2fr   =  rO2max*pO2pkg*Mtom/(KmO2+pO2pkg);        %O2 consumption rate (mol/s)
rCO2fr   =  RQ*rO2fr;                               %CO2 generation rate (mol/s)

%Differential equations (ODEs)
odes=zeros(2,1);
```

```
odes(1)  =  PO2pkg*Apkg/Lpkg*(pO2env-pO2pkg)-rO2fr;        %Rate of change of O2 concentrtaion in package headspace (mol/s)

odes(2)  =  rCO2fr-PCO2pkg*Apkg/Lpkg*(pCO2pkg-pCO2env);    %Rate of change of CO2 concentrtaion in package headspace (mol/s)
```

G.2.2 Script file (PassiveMAPrun.m)

```
%Define global variables
global rO2max;          %Maximum rate of oxygen uptake by fruit (mol/s/kg),
global KmO2;            %Michaelis constant for O2 consumption (Pa)
global Mtom;            %Tomato mass (kg)
global PO2pkg;          %Packaging film permeability to oxygen (mol m/s/m2/Pa)
global PCO2pkg;         %Packaging film permeability to carbon dioxide (mol m/s/m2/Pa)
global pO2env;          %O2 partial pressure in surrounding environment (Pa)
global pCO2env;         %CO2 partial pressure in surrounding environment (Pa)
global RQ;              %Respiration quotient (dimensionless)
global Vpkg;            %Package volume (m3)
global R;               %Gas constant (8.314 Pa m3/mol/K)
global Tpkg;            %Package temperature (K)
global Lscf;            %Sachet film thickness (m)
global Apkg;            %Package surface area (m)
global Lpkg;            %Packaging film thickness (m)

%Get system input variables
Lpkg    =  30*10^-6;            %Experimental measurement
Apkg    =  0.125;               %Experimental measurement
PO2pkg  =  1.46*10^-15;         %After Chen et al 2000
PCO2pkg =  4.25*10^-15;         %After Chen et al 2000
rO2max  =  0.356*10^-6;         %After Hertog et al 1998
KmO2    =  23.2*10^3;           %After Hertog et al 1998
Mtom    =  600*10^-3;           %Experimental measurement
Vpkg    =  0.0012;              %Experimental measurement
pO2env  =  21*10^3;             %After Talasila and Cameron 1997
pCO2env =  0.03*10^3;           %After Talasila and Cameron 1997
Ptot    =  10^5;                %Approximated total pressure (Pa)
RQ      =  1;                   %After Talasila and Cameron 1997
R       =  8.314;               %Gas constant
Tpkg    =  (273.15+20);         %Experimental measurement

%Initial conditions
nO2pkgin  = (21*10^3*Vpkg/(R*Tpkg));      %Initial number of oxgen moles in package headspace (Pa)
nCO2pkgin = (0.03*10^3*Vpkg/(R*Tpkg));    %Initial number of oxgen moles in package headspace (Pa)

Initialconditions = [nO2pkgin,nCO2pkgin];
```

```
%Simulation condition
tSpan  =  200;
Day    =  7;          %Storage day
tStop  =  Day*24*60*60;

%ODE calculation
[t,Ds]=ode45('PassiveMAP',[0:tSpan:tStop],Initialconditions);

%Plot graphs
plot (t/60/60/24,Ds(:,1)*R*Tpkg*100/Vpkg/Ptot,'r');      %plot O2 concentration (% v/v) in package headspace
hold on
plot (t/60/60/24,Ds(:,2)*R*Tpkg*100/Vpkg/Ptot,'b');      %plot CO2 concentration (% v/v) in package headspace
ylabel ('Concentration (%)');
xlabel ('Day');
legend ('O2','CO2');
legend ('boxoff');
```

G.2.3 Model inputs for simulations of O_2 and CO_2

Parameters	Units	Values	Sources
$P_{pkfl}^{O_2}$	mol·m·m^{-2}·s^{-1}·Pa^{-1}	1.46×10^{-15}	Chen et al (2000)
$P_{pkfl}^{CO_2}$	mol·m·m^{-2}·s^{-1}·Pa^{-1}	4.25×10^{-15}	"
A_{pkfl}	m^2	0.125	Experimentally measured
L_{pkfl}	m	30×10^{-6}	"
$p_{env}^{O_2}$	kPa	21	Talasila & Cameron (1997)
$p_{env}^{CO_2}$	kPa	0.03	Talasila & Cameron (1997)
$r_{O_2}^{max}$ (tomato)	mol·s^{-1}·kg^{-1}	0.356×10^{-6}	Hertog et al (1998)
$k_{m_{O_2}}$ (tomato)	kPa	23.2	Hertog et al (1998)
M_{tom}	kg	0.6	Experimentally measured
T_{pkg}	K	293.15	"
V_{pkg}	m^3	0.0012	"

G.3 Analytical solution for mean hexanal vapour concentration in the packaging film (PDE modelling approach)

As part of an effort to demonstrate no numerical coding errors existed in the MATLAB® solutions, the programme was checked against a number of simplified scenarios where analytical solution was possible.

An analytical solution exists for diffusion mass transfer through a thin film material with the 1st kind of boundary's condition, which is a analogous to heat conduction through an infinite slab with a fixed kind boundary's condition, i.e. replacing thermal diffusivity with diffusivity and temperature with concentration (Carslaw & Jaeger 1959). Given concentration- independent properties of the hexanal mass transfer coefficient in the film, diffusion mass transfer across the packaging film material and its initial and boundary conditions can mathematically be described as follows:

$$\frac{\partial C_{g,pkfl}^{Hxl}}{\partial t} = P_{pkfl}^{Hxl} \frac{\partial^2 C_{g,pkfl}^{Hxl}}{\partial x_{pkfl}^2} \qquad for\ t \geq 0,\ -R_{pkfl} < x_{pkfl} < +R_{pkfl} \qquad \textbf{(Eq. G-1)}$$

$$C_{g,pkfl}^{Hxl} = C_{sat}^{Hxl} \qquad for\ t \geq 0,\ at\ x_{pkfl} = -R_{pkfl}\ and\ x_{pkfl} = +R_{pkfl} \qquad \textbf{(Eq. G-2)}$$

$$C_{g,pkfl,ini}^{Hxl} = 0 \qquad for\ t = 0,\ -R_{pkfl} < x_{pkfl} < +R_{pkfl} \qquad \textbf{(Eq. G-3)}$$

where

P_{pkfl}^{Hxl} = Permeability to hexanal vapour of the packaging film ($m^2 \cdot s^{-1}$)

R_{pkfl} = Half thickness of film (m)

C_{sat}^{Hxl} = Saturated hexanal vapour concentration ($mol \cdot m^{-3}$) (i.e. 0.46 $mol \cdot m^{-3}$, at 20ºC)

$C_{g,pkfl,ini}^{Hxl}$ = Initial equilibrium concentration of hexanal vapour in packaging film ($mol \cdot m^{-3}$)

Defining the dimensionless numbers as follows:

$$F_0 = \frac{P_{pkfl}^{Hxl} \cdot t}{R_{pkfl}^2} \qquad \textbf{(Eq. G-4)}$$

$$Y_{avg} = \frac{\left(C_{g,pkfl,avg}^{Hxl} - C_{sat}^{Hxl}\right)}{\left(C_{g,pkfl,ini}^{Hxl} - C_{sat}^{Hxl}\right)} \qquad \textbf{(Eq. G-5)}$$

Series solutions for diffusion mass transfer can be expressed as:

$$Y_{avg} = \frac{8}{\pi} \sum_{m=0}^{\infty} \frac{1}{(2m+1)^2} exp\left(-(2m+1)^2 \frac{\pi^2}{4} F_0\right) \qquad \textbf{(Eq. G-6)}$$

where

Y_{avg} = Fraction unaccomplished change of concentration (dimensionless)

F_0 = Fourier number (dimensionless)

$C_{g,pkfl,avg}^{Hxl}$ = Mean equilibrium concentration of hexanal vapour in film (mol·m^{-3})

m = Term in series solution (given as 5 terms)

The mean concentration of equilibrium hexanal vapour in the packaging films from the analytical solution (m = 5) was compared with that produced by the numerical (MATLAB®) solution using the same situations as described above and the results are shown in Figure G-1. It can be seen that the mean concentration obtained by both solution methods agree well and the maximum difference for the values is < 700 ppm. A small difference is observed only at the commencement of the simulation (t = 0) where more than 5 terms are needed in the analytical solution to achieved accurate predictions, but from this point forward differences are virtually absent. The finding indicates that the term formulated to describe the mass transfer through the packaging film (thin slab) has been correctly implemented in the model.

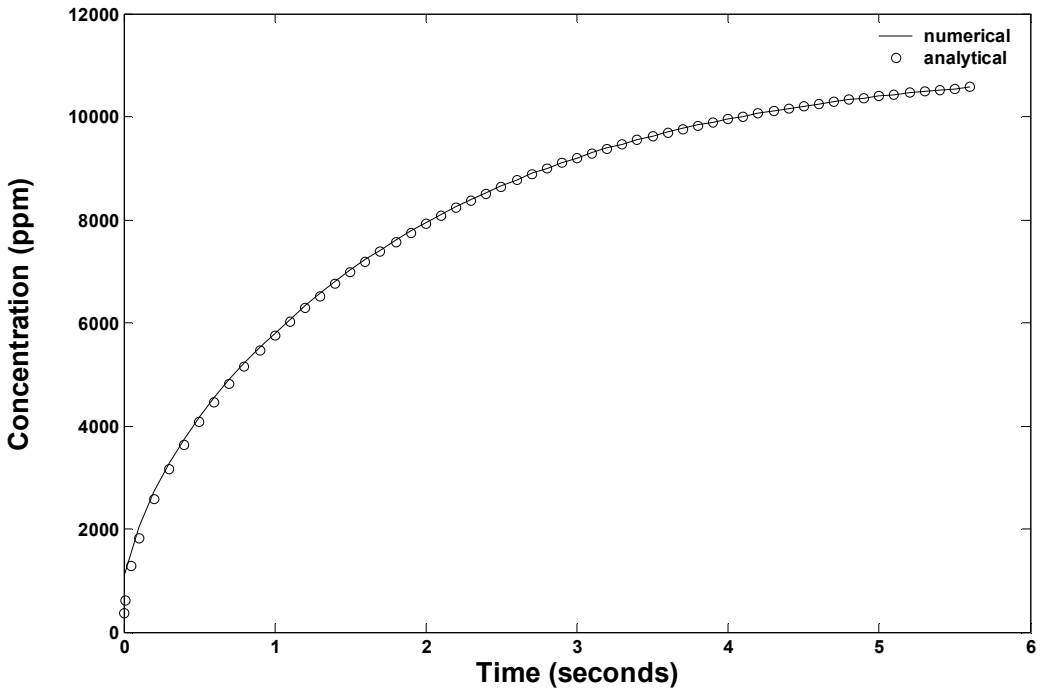

Figure G-1 Comparison of mean concentrations of equilibrium hexanal vapour in the packaging film from analytical (m = 5) and numerical solutions for diffusion mass transfer with the first kind of boundary condition.

G.4 Analytical solution for hexanal permeation across the sachet film (steady-state modelling approach)

Similar checking was performed on other parts of the model. One check was to simplify the steady-state of hexanal permeation across the sachet film as follows:

- $C_{g,bed}^{Hxl}$ is assumed to be constant and equals to the saturated vapour concentration at 20ºC (0.46 mol·m^{-3})
- no mass transfer out of package headspace to the environment
- hexanal permeability of film is independent of hexanal vapour concentration
- no packaged tomatoes in the bag

According to the assumptions made above, the ODE describing the change in headspace concentration can be described as Eq.G-7.

$$V_{pkg}\frac{dC_{pkhs}^{Hxl}}{dt}=\frac{P_{scfl}^{Hxl}A_{scfl}RT_{pkg}}{L_{scfl}}\left(C_{g,bed}^{Hxl}-C_{pkhs}^{Hxl}\right) \qquad \textbf{(Eq. G-7)}$$

Given

$$k_{scfl}=\frac{P_{scfl}^{Hxl}A_{scfl}RT_{pkg}}{L_{scfl}V_{pkg}} \qquad \textbf{(Eq. G-8)}$$

where

k_{scfl} = Constant in simplified ODE (s^{-1})

Substituting Eq. G-8 in Eq. G-7 yields Eq. G-9.

$$\frac{dC_{pkhs}^{Hxl}}{dt}=k_{scfl}\left(C_{g,bed}^{Hxl}-C_{pkhs}^{Hxl}\right) \qquad \textbf{(Eq. G-9)}$$

Rearranging Eq. G-9 gives:

$$\frac{dC_{pkhs}^{Hxl}}{\left(C_{g,bed}^{Hxl}-C_{pkhs}^{Hxl}\right)}=k_{scfl}\,dt \qquad \textbf{(Eq. G-10)}$$

Separating variables and integrating according to initial condition $t=0\,;C_{pkhs}^{Hxl}=0$, gives:

$$C_{pkhs}^{Hxl}=C_{g,bed}^{Hxl}\left(1-e^{-k_{scfl}\cdot t}\right) \qquad \textbf{(Eq. G-11)}$$

A comparison between the analytical solution and the numerical one solved by MATLAB® when these simplifications were made by setting input values in the code to appropriate values (e.g. setting package film permeability = 0). This comparison is shown in Figure G-2 and it suggests good agreement of both results (with the maximum difference < 31 ppm). A small difference was observed only at the commencement of simulation ($t = 0$), but from this point forward differences are virtually absent. This finding confirms that the term describing diffusion of hexanal across the sachet film material has been correctly implemented in the model.

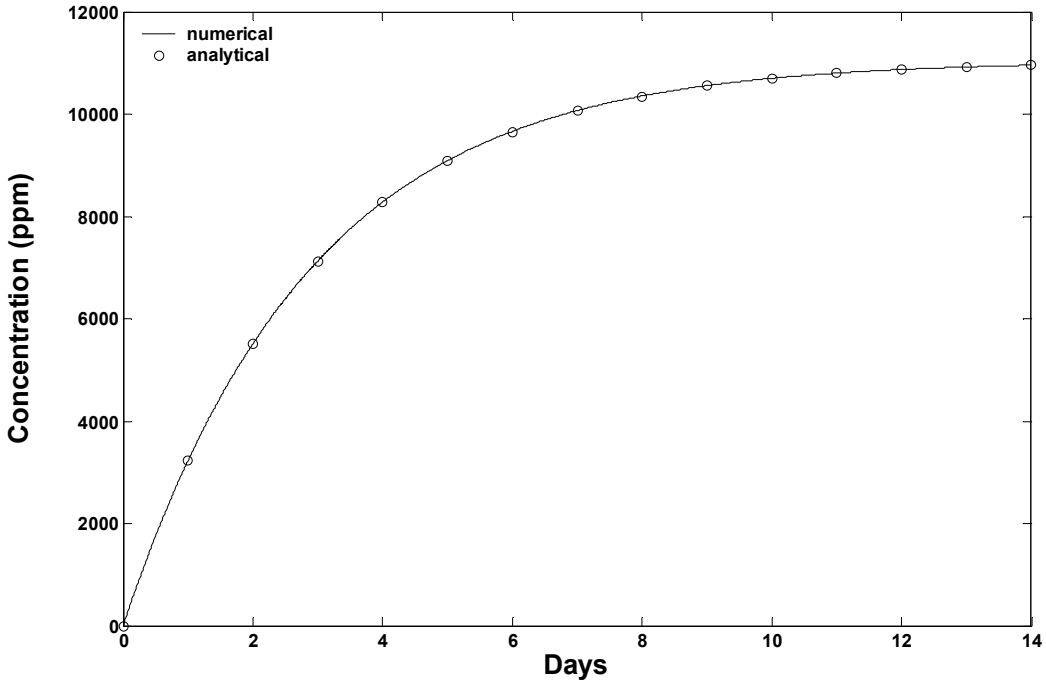

Figure G-2 Comparison of the numerical and analytical solutions for package headspace hexanal concentration, of which hexanal mass transfer across sachet film was modelled using steady-state approach

Appendix H

MODEL VALIDATIONS

H.1 Controlled release sachet preparations

Experimental procedures to prepare hexanal controlled release sachets are provided as follows:

Silica gel adsorbent samples having slightly higher than desired amounts (i.e. 5% above 1.5, 3.0 and 4.5 g) were placed in aluminium moisture cans and dried in an oven at 110ºC for ten hours. Afterward the aluminium cans were covered with aluminium lids and cooled in a desiccator for three hours at ambient condition. The cooled aluminium weighing dish were weighed (recorded as the gross weight) and dry weight of silica gel samples was obtained by subtracting the known weight of the weighing dish from the gross weight. The dry silica gel samples were then placed into individual 50 ml borosilicate flasks, and ~3-5 ml hexanal liquid (97% GC grade, Sigma-Aldrich, US) were added. Each flask was covered with a flask cap and transferred to a shaker (Orbital Incubator, Gallenkamp, Leicester, UK) for shaking at 40 rpm for at least one week and three days at 10 and 20ºC, respectively. From preliminary work, these timeframes provided maximum uptake compared to that resulting from shaking for longer periods.

After shaking, the saturated silica gel samples were transferred to a vacuum filter to remove excess hexanal liquid. The filtered silica gel sample was then transferred to an aluminium weighing dish and weighed. The weight of adsorbed hexanal was obtained by subtracting the known weight of the aluminium can and dry silica gel from the aluminium can with the saturated silica gel. It should be noted that experimental adsorbed amounts were slightly higher (on average less than 1.7-fold) than those predicted by Langmuir isotherm model (Eq. 2-3; coefficients as shown in Table 4-9) given $p/p_s \approx 1$ and these were presumably attributed to presences of thin films of excess hexanal liquid in the carrier bed (as discussed in Chatper 6). However comparable results of experimental and predicted data suggest that sorption isotherm quantified by gravimetric method is sensible. Silica gels from individual cans were individually packed and immediately sealed into a 5×6 cm sachet which was composed on one side of Tyvek®, LDPE or OPP material, and,

on the other of aluminium laminated LDPE (Al/LDPE). The Al/LDPE was a barrier to hexanal vapour and provides a one-directional mass transfer of hexanal vapour from the sachet to the package headspace (as discussed in Chapter 5).

After sealing, individual sachets were kept in a closed stainless steel cup (8 cm OD; 3 cm height; one sachet per cup) for 2-3 h prior starting experiments. The stainless steel cup provides small headspaces and minimise release of hexanal vapour.

H.2 Summary of sensitivity analyses of model validations

This section summarises the comparison of model predictions and experimental trials and the effect of each system input variable. MATLAB® files employed for following validations are those mentioned in section G.1.1 and G.1.2 of which model inputs were appropriatedly chosen.

Table H-1 Examples of model sensitivity to input variables: 4.5 g LDPE sachet loading experiment of active packages containing tomatoes (experimental data shown as ◊ symbols), with discussion made in section 6.4.1.2.

Parameters	Experimental data and model predictions
L_{pkfl} where • L_{pkfl} = 30 × 10^{-6} (control; solid line) • L_{pkfl} = 36 × 10^{-6} (dotted line) • L_{pkfl} = 24 × 10^{-6} (dashed line)	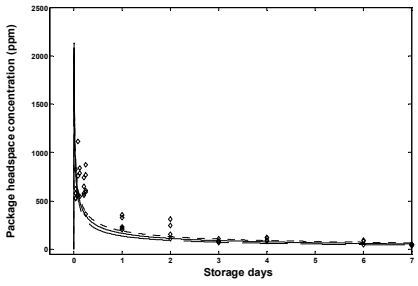
b_{Lgm}^{Hxl} where • b_{Lgm}^{Hxl} = 281.070 (control; solid line) • b_{Lgm}^{Hxl} = 394.536 (dotted line) • b_{Lgm}^{Hxl} = 167.601 (dashed line)	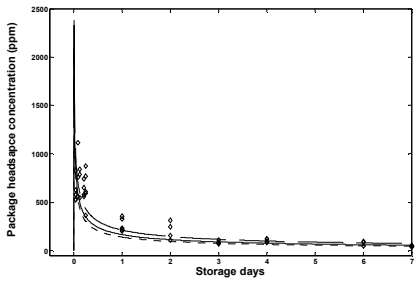

Table H-1 Examples of model sensitivity to input variables: 4.5 g LDPE sachet loading experiment of active packages containing tomatoes (experimental data shown as ◊ symbols), with discussion made in section 6.4.1.2 (continued)

Parameters	Experimental data and model predictions
$P_{LDPE,0}^{Hxl}$, b_{LDPE} (sachet film, given fixed values of these for outer packaging film) where • $P_{LDPE,0}^{Hxl} = 1.97 \times 10^{-14}$, $b_{LDPE} = 19.65$ (control; solid line) • $P_{LDPE,0}^{Hxl} = 3.12 \times 10^{-14}$, $b_{LDPE} = 22.4$ (dotted line) • $P_{LDPE,0}^{Hxl} = 8.77 \times 10^{-15}$, $b_{LDPE} = 16.85$ (dashed line)	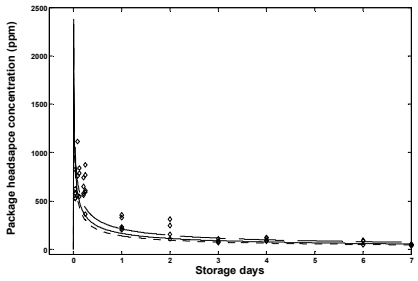
$P_{LDPE,0}^{Hxl}$, b_{LDPE} (outer packaging film, given fixed values of these permeability of sachet film) where • $P_{LDPE,0}^{Hxl} = 1.97 \times 10^{-14}$, $b_{LDPE} = 19.65$ (control; solid line) • $P_{LDPE,0}^{Hxl} = 3.12 \times 10^{-14}$, $b_{LDPE} = 22.4$ (dotted line) • $P_{LDPE,0}^{Hxl} = 8.77 \times 10^{-15}$, $b_{LDPE} = 16.85$ (dashed line)	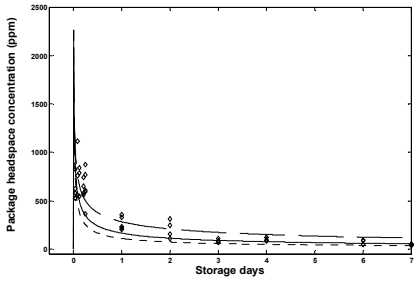
k_{reac}, n_{reac} where • $k_{reac} = 9 \times 10^{-5}$, $n_{reac} = 2.64$ (control; solid line) • $k_{reac} = 11 \times 10^{-5}$, $n_{reac} = 2.75$ (dotted line) • $k_{reac} = 8 \times 10^{-5}$, $n_{reac} = 2.53$ (dashed line)	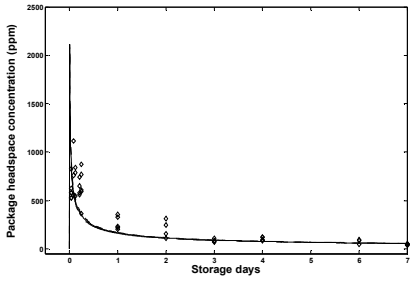

Table H-2 Examples of model sensitivity to input variables: MA condition of active packages containing tomatoes is the same as that employed in Table H-1 (experimental data of O_2 and CO_2 shown as o and ◊ symbols, respectively), with discussion made in section 6.4.1.2. Variations employed for varying values of $r_{O_2}^{max}$, $k_{m_{O_2}}$, and permeability values (both $P_{pkfl}^{O_2}$ and $P_{pkfl}^{CO_2}$) are 10%, 20%, and 10%, respectively (as utilised by in Merts 1996; Tanner 1998). Variation of package volume is as shown in Table 6-3.

Parameters	Experimental data and model predictions
$r_{O_2}^{max}$ where • $r_{O_2}^{max} = 3.56 \times 10^{-7}$ (control; solid line) • $r_{O_2}^{max} = 4.27 \times 10^{-7}$ (dotted line) • $r_{O_2}^{max} = 2.85 \times 10^{-7}$ (dashed line)	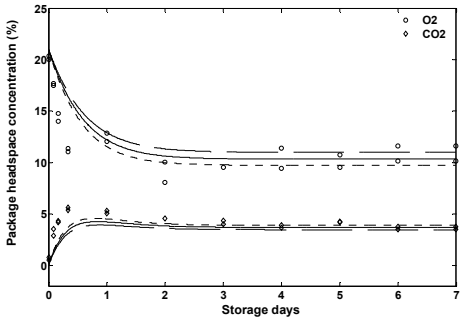
$k_{m_{O_2}}$ where • $k_{m_{O_2}} = 23.2$ (control; solid line) • $k_{m_{O_2}} = 30.16$ (dotted line) • $k_{m_{O_2}} = 16.24$ (dashed line)	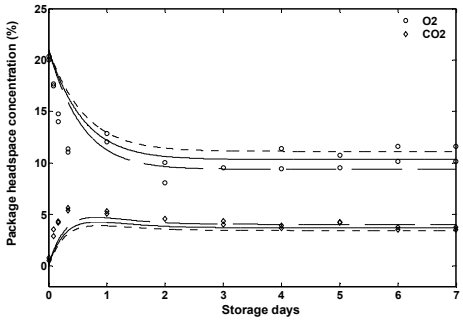
$P_{pkfl}^{O_2}$ & $P_{pkfl}^{CO_2}$ where • $P_{pkfl}^{O_2}$ & $P_{pkfl}^{CO_2}$ = 1.46×10^{-15} & 4.25×10^{-15} (control; solid line) • $P_{pkfl}^{O_2}$ & $P_{pkfl}^{CO_2}$ = 1.75×10^{-15} & 5.10×10^{-15} (dotted line) • $P_{pkfl}^{O_2}$ & $P_{pkfl}^{CO_2}$ = 1.17×10^{-15} & 3.40×10^{-15} (dashed line)	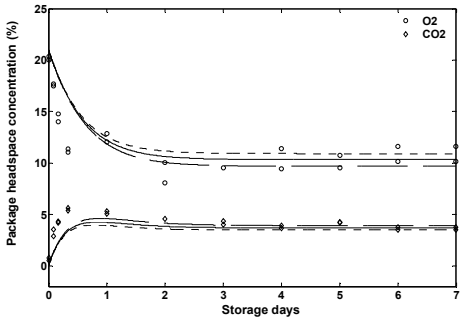
V_{pkg} where • $V_{pkg} = 0.0012$ (control; solid line) • $V_{pkg} = 0.0013$ (dotted line) • $V_{pkg} = 0.0011$ (dashed line)	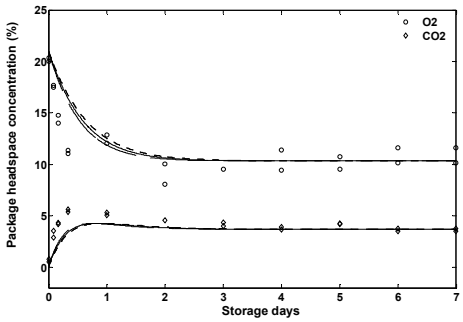

Table H-3 Examples of model sensitivity to input variables: model package LD6 (experimental data shown as o symbols), with discussion made in section 6.4.2.

Parameters	Experimental data and model predictions
L_{pkfl} where • L_{pkfl} = 30 × 10^{-6} (control; solid line) • L_{pkfl} = 36 × 10^{-6} (dotted line) • L_{pkfl} = 24 × 10^{-6} (dash line)	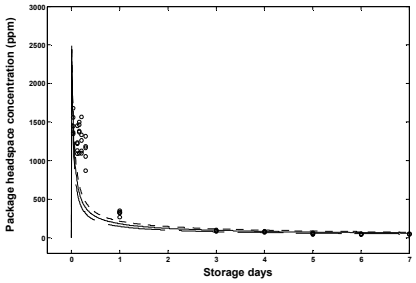
b_{Lgm}^{Hxl} where • b_{Lgm}^{Hxl} = 281.070 (control; solid line) • b_{Lgm}^{Hxl} = 394.536 (dotted line) • b_{Lgm}^{Hxl} = 167.601 (dash line)	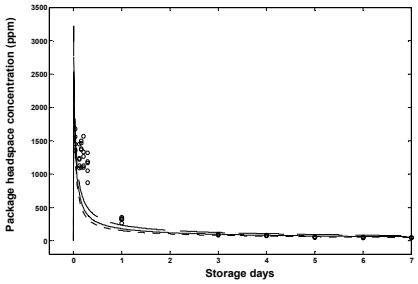
$P_{LDPE,0}^{Hxl}$, b_{LDPE} (sachet film, given fixed values of these for outer packaging film) where • $P_{LDPE,0}^{Hxl}$ = 1.97 × 10^{-14}, b_{LDPE} = 19.65 (control; solid line) • $P_{LDPE,0}^{Hxl}$ =3.12 × 10^{-14}, b_{LDPE} = 22.4 (dotted line) • $P_{LDPE,0}^{Hxl}$ = 8.77 × 10^{-15}, b_{LDPE} = 16.85 (dash line)	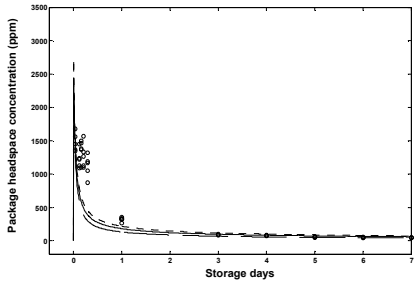
$P_{LDPE,0}^{Hxl}$, b_{LDPE} (outer packaging film, given fixed values of these for sachet film) where • $P_{LDPE,0}^{Hxl}$ = 1.97 × 10^{-14}, b_{LDPE} = 19.65 (control; solid line) • $P_{LDPE,0}^{Hxl}$ =3.12 × 10^{-14}, b_{LDPE} = 22.4 (dotted line) • $P_{LDPE,0}^{Hxl}$ = 8.77 × 10^{-15}, b_{LDPE} = 16.85 (dash line)	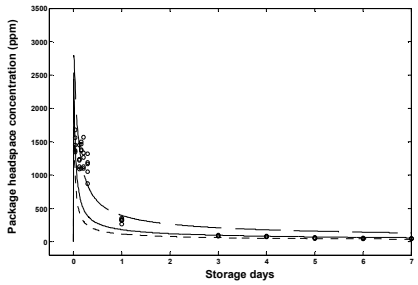

Table H-4 Examples of model sensitivity to input variables: model package containing tomatoes and OPP film as a sachet film material (experimental data shown as ◊ symbols), with discussion made in section 6.4.3.1.

Parameters	Experimental data and model predictions
L_{pkfl} where • $L_{pkfl} = 30 \times 10^{-6}$ (control; solid line) • $L_{pkfl} = 36 \times 10^{-6}$ (dotted line) • $L_{pkfl} = 24 \times 10^{-6}$ (dashed line)	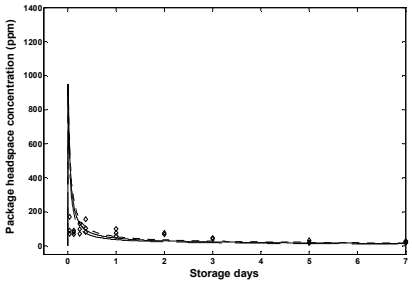
b_{Lgm}^{Hxl} where • $b_{Lgm}^{Hxl} = 281.070$ (control; solid line) • $b_{Lgm}^{Hxl} = 394.536$ (dotted line) • $b_{Lgm}^{Hxl} = 167.601$ (dashed line)	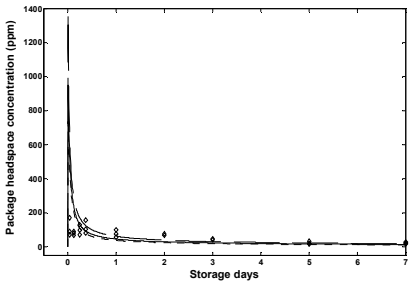
$P_{OPP,0}^{Hxl}$, b_{OPP} where • $P_{OPP,0}^{Hxl} = 9 \times 10^{-16}$, $b_{OPP} = 19.74$ (control; solid line) • $P_{OPP,0}^{Hxl} = 1.08 \times 10^{-15}$, $b_{OPP} = 21.27$ (dotted line) • $P_{OPP,0}^{Hxl} = 7.20 \times 10^{-16}$, $b_{OPP} = 18.20$ (dashed line)	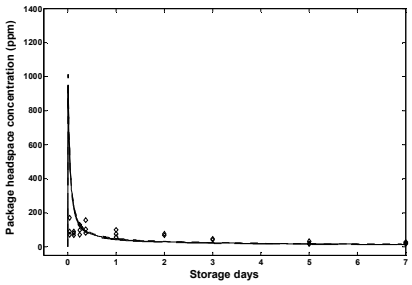
$P_{LDPE,0}^{Hxl}$, b_{LDPE} where • $P_{LDPE,0}^{Hxl} = 1.97 \times 10^{-14}$, $b_{LDPE} = 19.65$ (control; solid line) • $P_{LDPE,0}^{Hxl} = 3.12 \times 10^{-14}$, $b_{LDPE} = 22.4$ (dotted line) • $P_{LDPE,0}^{Hxl} = 8.77 \times 10^{-15}$, $b_{LDPE} = 16.85$ (dashed line)	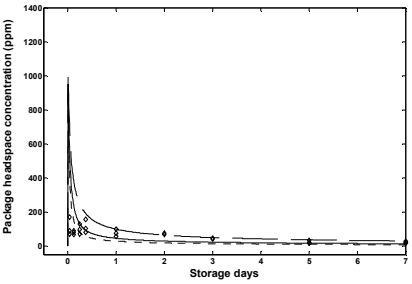
k_{reac} , n_{reac} where • $k_{reac} = 9 \times 10^{-5}$, $n_{reac} = 2.64$ (control; solid line) • $k_{reac} = 11 \times 10^{-5}$, $n_{reac} = 2.75$ (dotted line) • $k_{reac} = 8 \times 10^{-5}$, $n_{reac} = 2.53$ (dashed line)	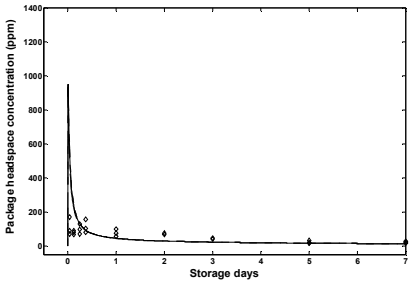

Table H-5 Examples of model sensitivity to input variables: model package containing tomatoes and Tyvek® film as a sachet film material (experimental data shown as ◊ symbols), with discussion made in section 6.4.3.2.

Parameters	Experimental data and model predictions
L_{pkfl} where • $L_{pkfl} = 30 \times 10^{-6}$ (control; solid line) • $L_{pkfl} = 36 \times 10^{-6}$ (dotted line) • $L_{pkfl} = 24 \times 10^{-6}$ (dashed line)	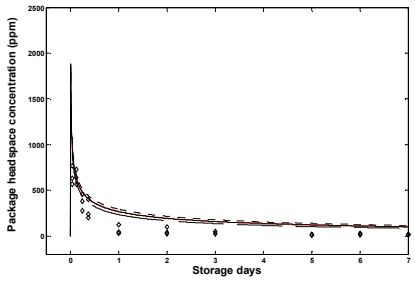
b_{Lgm}^{Hxl} where • $b_{Lgm}^{Hxl} = 281.070$ (control; solid line) • $b_{Lgm}^{Hxl} = 394.536$ (dotted line) • $b_{Lgm}^{Hxl} = 167.601$ (dashed line)	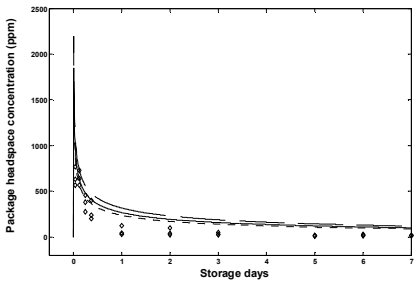
$P_{Tyvek,0}^{Hxl}$, b_{Tyvek} where • $P_{Tyvek,0}^{Hxl} = 1.97 \times 10^{-14}$, $b_{Tyvek} = 19.65$ (control; solid line) • $P_{Tyvek,0}^{Hxl} = 3.12 \times 10^{-14}$, $b_{Tyvek} = 22.4$ (dotted line) • $P_{Tyvek,0}^{Hxl} = 8.77 \times 10^{-15}$, $b_{Tyvek} = 16.85$ (dashed line)	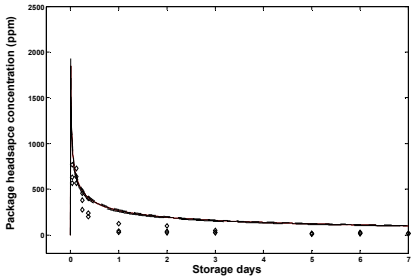
$P_{LDPE,0}^{Hxl}$, b_{LDPE} where • $P_{LDPE,0}^{Hxl} = 1.97 \times 10^{-14}$, $b_{LDPE} = 19.65$ (control; solid line) • $P_{LDPE,0}^{Hxl} = 3.12 \times 10^{-14}$, $b_{LDPE} = 22.4$ (dotted line) • $P_{LDPE,0}^{Hxl} = 8.77 \times 10^{-15}$, $b_{LDPE} = 16.85$ (dashed line)	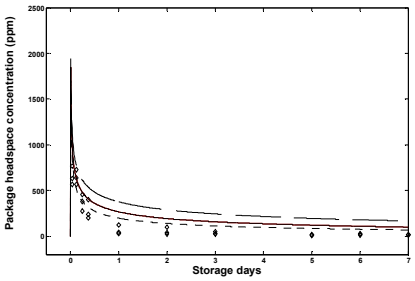
k_{reac} , n_{reac} where • $k_{reac} = 9 \times 10^{-5}$, $n_{reac} = 2.64$ (control; solid line) • $k_{reac} = 11 \times 10^{-5}$, $n_{reac} = 2.75$ (dotted line) • $k_{reac} = 8 \times 10^{-5}$, $n_{reac} = 2.53$ (dashed line)	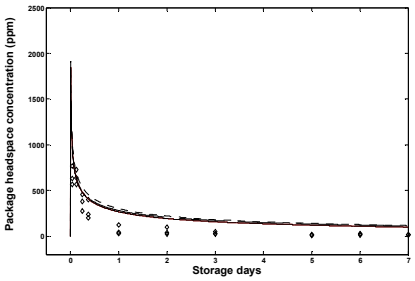

Table H-6 Examples of model sensitivity to input variables: model package containing tomatoes kept at 10°C, sachet materials were LDPE, OPP, and Tyvek® (experimental data shown as ◊ symbol) [1], with discussion made in section 6.4.4.

Variables	Experimental data and model predictions		
	LDPE sachet	**OPP sachet**	**Tyvek® sachet**
L_{pkfl} (LDPE bag)	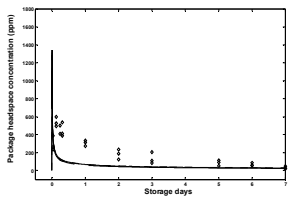	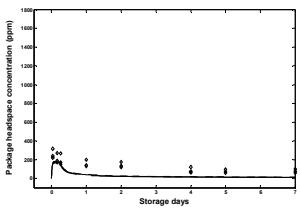	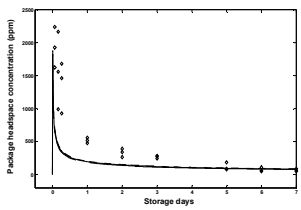
$P_{LDPE,0}^{Hxl}$, b_{LDPE} (LDPE bag)	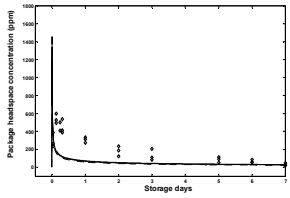	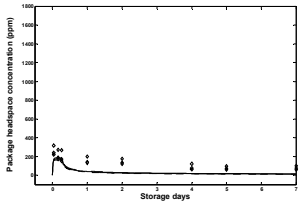	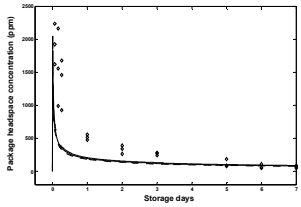
$P_{i,0}^{Hxl}$, b_i (sachet film)	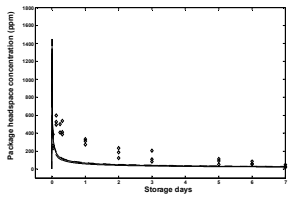	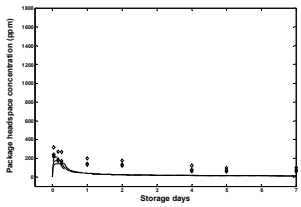	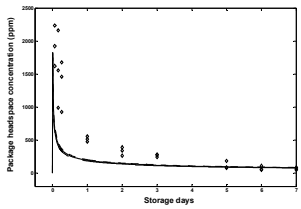
$C_{s,max}^{Hxl}$	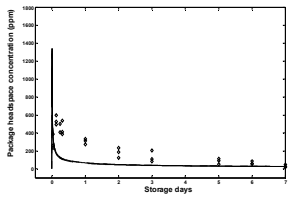	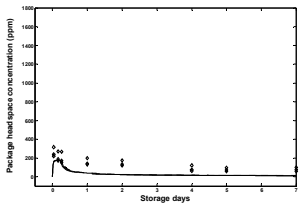	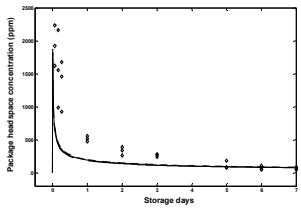
b_{Lgm}^{Hxl}	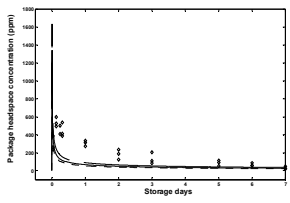	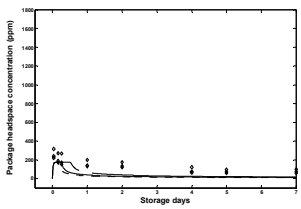	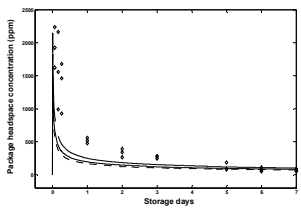
k_{reac}, n_{reac}	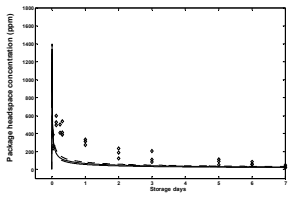	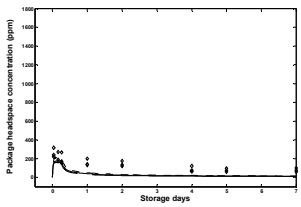	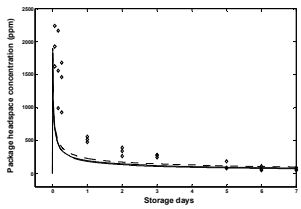

[1] Extent of variation of individual model inputs is shown in Table 6-3. Solid, dotted and dashed lines represent model predictions using original, increased, and decreased values of model inputs, respectively.

Table H-7 Examples of model sensitivity to input variables: changes of hexanal amount on silica gel (empirical data shown as o symbols). Initial hexanal adsorbed amount used in the modified global model was referred to as the effective amount. Results for discussion are made in section 6.4.5.

Parameters	Prediction bounds
$C_{s,max}^{Hxl}$ where • $C_{s,max}^{Hxl}$ = 0.00334 (control; solid line) • $C_{s,max}^{Hxl}$ = 0.00357 (dotted line) • $C_{s,max}^{Hxl}$ = 0.00311 (dashed line)	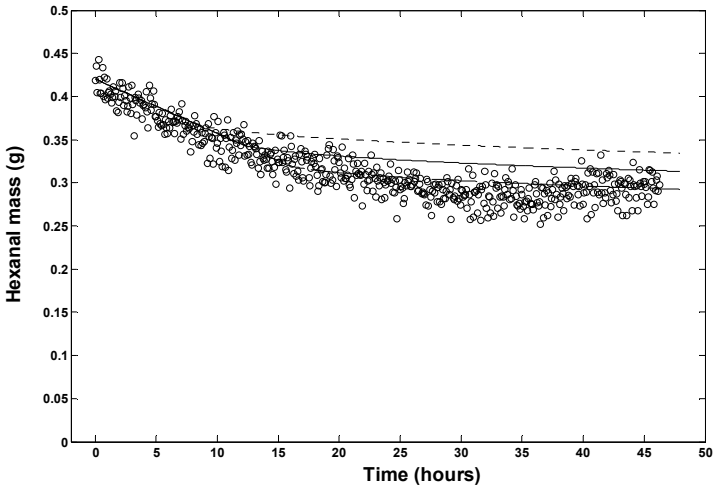
b_{Lgm}^{Hxl} where • b_{Lgm}^{Hxl} = 281.070 (control; solid line) • b_{Lgm}^{Hxl} = 394.536 (dotted line) • b_{Lgm}^{Hxl} = 167.601 (dashed line)